MICROBIAL CARBONATE RESERVOIRS AND ANALOGS FROM UTAH

Thomas C. Chidsey, Jr., David E. Eby,
Michael D. Vanden Berg, and Douglas A. Sprinkel

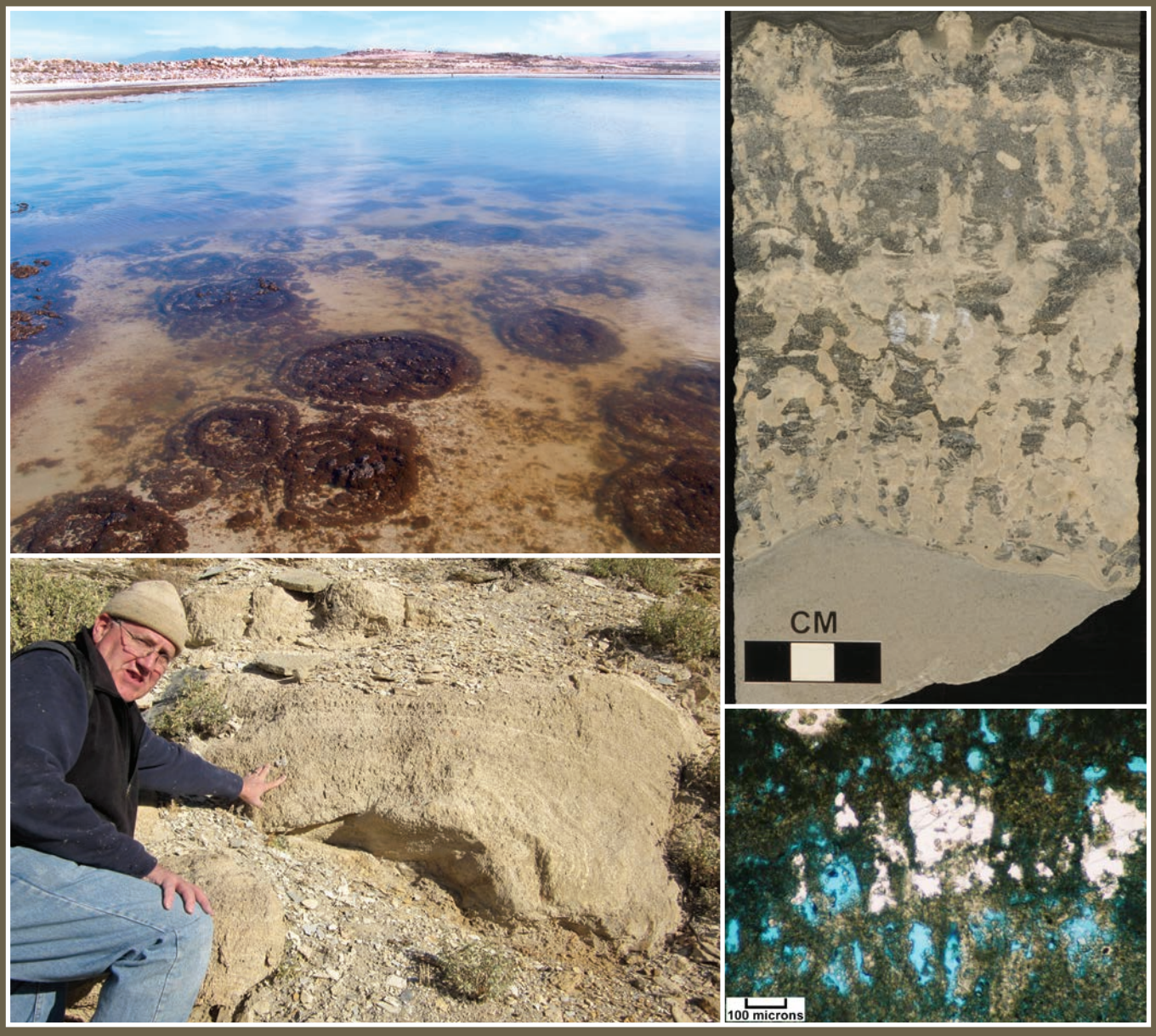

SPECIAL STUDY 168
UTAH GEOLOGICAL SURVEY
UTAH DEPARTMENT OF NATURAL RESOURCES
2021

Blank pages are intentional for printing purposes.

MICROBIAL CARBONATE RESERVOIRS AND ANALOGS FROM UTAH

by Thomas C. Chidsey, Jr.[1], David E. Eby[2],
Michael D. Vanden Berg[3], and Douglas A. Sprinkel[1]

[1] Utah Geological Survey, retired
[2] Eby Petrography & Consulting, Inc., Denver, Colorado
[3] Utah Geological Survey, Salt Lake City, Utah

Cover photo: *Top left: Holocene microbialite structures in Bridger Bay, Antelope Island, Great Salt Lake, October 2013, when the lake was nearly 1.7 meters (5.5 ft) below its historical average of 1280 meters (4200 ft). Top right: Branching microbial carbonates (stromatolites) in the lacustrine Eocene Green River Formation, Uinta Basin of eastern Utah, from the Skyline 16 reseach core. Bottom left: Large microbial (thrombolite interior and stromatolites on the margins) head within the Green River Formation, Evacuation Canyon, Uinta Basin. Bottom right: Photomicrograph from outcrop in photograph to the left showing margin of the stromatolite head with microbial laminations and primary constructional pores (in blue).*

Suggested citation:

Chidsey, T.C., Jr., Eby, D.E., Vanden Berg, M.D., and Sprinkel, D.A., 2021, Microbial carbonate reservoirs and analogs from Utah: Utah Geological Survey Special Study 168, 112 p., 14 plates, 1 appendix, https://doi.org/10.34191/SS-168.

SPECIAL STUDY 168
UTAH GEOLOGICAL SURVEY
UTAH DEPARTMENT OF NATURAL RESOURCES
2021

STATE OF UTAH
Spencer J. Cox, Governor

DEPARTMENT OF NATURAL RESOURCES
Brian C. Steed, Executive Director

UTAH GEOLOGICAL SURVEY
R. William Keach II, Director

PUBLICATIONS
contact
Natural Resources Map & Bookstore
1594 W. North Temple
Salt Lake City, UT 84116
telephone: 801-537-3320
toll-free: 1-888-UTAH MAP
website: utahmapstore.com
email: geostore@utah.gov

UTAH GEOLOGICAL SURVEY
contact
1594 W. North Temple, Suite 3110
Salt Lake City, UT 84116
telephone: 801-537-3300
website: geology.utah.gov

CONTENTS

FIGURES

PLATES

PREFACE

Microbial carbonates, created by ancient cyanobacteria, are now recognized as geologically and economically important deposits. Multiple oil discoveries have revealed the global significance of this distinctive reservoir type composed of possible microbial lacustrine carbonates like the Lower Cretaceous pre-salt reservoirs in deepwater offshore Brazil and Angola. Marine microbialite reservoirs are also important in the South Oman Salt Basin, Caspian Basin of Kazakhstan, and the Williston Basin in Montana and North Dakota. Evaluation of the various microbial fabrics and facies, associated petrophysical properties, diagenesis, and bounding surfaces are critical to understanding these reservoirs. Utah contains unique analogs of microbial hydrocarbon reservoirs in the modern hypersaline Great Salt Lake and the lacustrine Tertiary (Eocene) Green River Formation (cores and outcrop) within the Uinta Basin of northeastern Utah. In addition, Utah has numerous examples of marine microbial carbonates and associated facies that are present in subsurface analog oil field cores.

This Utah Geological Survey Special Study represents research that began in 2010. In the decade that followed, many researchers focused on microbial carbonates in various regions of the world, and several major discoveries occurred. Concepts and interpretation of these fascinating deposits have rapidly evolved and continue to do so. The Mars rover, Perseverance, began its mission in 2021 searching for ancient microbial life in the Jezero Crater. The purpose of our study was to provide a brief characterization and petrographic overview (including carbonate fabrics, pore types, and diagenetic alteration) of the diverse types of Utah microbialites and associated carbonate grains that are present within Great Salt Lake, the Green River Formation, and reservoirs (non-marine and marine) from various active oil fields in Utah's major producing provinces. They offer analogs of the characteristics, geometry, distribution, and bounding surfaces of lacustrine and marine microbial carbonates throughout the Earth and possibly beyond.

Thomas C. Chidsey, Jr., Utah Geological Survey

MICROBIAL CARBONATE RESERVOIRS AND ANALOGS FROM UTAH

by Thomas C. Chidsey, Jr., David E. Eby, Michael D. Vanden Berg, and Douglas A. Sprinkel

ABSTRACT

Multiple oil discoveries reveal the global scale and economic importance of a distinctive reservoir type composed of possible microbial lacustrine carbonates like the Lower Cretaceous pre-salt reservoirs in deepwater offshore Brazil and Angola. Marine microbialite reservoirs are also important in the Neoproterozoic to lowest Cambrian starta of the South Oman Salt Basin as well as large Paleozoic deposits including those in the Caspian Basin of Kazakhstan (e.g., Tengiz field), and the Cedar Creek Anticline fields and Ordovician Red River "B" horizontal play of the Williston Basin in Montana and North Dakota, respectively. Evaluation of the various microbial fabrics and facies, associated petrophysical properties, diagenesis, and bounding surfaces are critical to understanding these reservoirs. Utah contains unique analogs of microbial hydrocarbon reservoirs in the modern Great Salt Lake and the lacustrine Tertiary (Eocene) Green River Formation (cores and outcrop) within the Uinta Basin of northeastern Utah. Comparable characteristics of both lake environments include shallow-water ramp margins that are susceptible to rapid widespread shoreline changes, as well as compatible water chemistry and temperature ranges that were ideal for microbial growth and formation/deposition of associated carbonate grains. Thus, microbialites in Great Salt Lake and from the Green River Formation exhibit similarities in terms of the variety of microbial textures and fabrics. In addition, Utah has numerous examples of marine microbial carbonates and associated facies that are present in subsurface analog oil field cores.

Great Salt Lake is a Holocene hypersaline lake and a remnant of freshwater Pleistocene Lake Bonneville. The lake represents a carbonate "factory," forming microbialites and associated carbonate grains (hypersaline ooids, coated grains, peloids, lithified crusts) on the lake bottom and along its shores. Open constructional pores, often partially lined with cements, are common within a spectrum of microbial structures.

The Eocene Green River Formation in the Uinta Basin of eastern Utah contains excellent examples of microbial carbonates. The Uinta Basin is a major structural basin, which subsided during the early Cenozoic along the southern flank of the Uinta Mountains. Freshwater, and at times saline to hypersaline, lakes developed between the eroding Sevier highlands to the west and the rising Laramide-age uplifts to the north, east, and south. The Green River Formation, comprising up to 2000 meters (6000 ft) of lacustrine strata, accumulated in and around ancient Lake Uinta. Three major depositional facies tracts are associated with lake sedimentation: alluvial, marginal lacustrine, and open lacustrine. The marginal lacustrine environment is represented by nearshore clastics and carbonates—including microbialites. The Skyline 16 research core sampled the middle to upper Green River Formation and displays excellent examples of (1) low-relief stomatolites and thrombolites, (2) primary megascopic pores and microporosity within microbial fabrics, (3) grainstones composed of ooids, pisoids, peloids, and skeletal material with abundant interparticle and intraparticle porosity, (4) porous, lacy dolomite, and (5) some microporous cherts. Many of the Green River microbial features observed in the core are also well displayed in extensive nearby outcrops, both vertically (including depositional cycles) and horizontally. They offer a production-scale analog of the characteristics, geometry, distribution, and bounding surfaces of microbial and related lacustrine facies.

A survey of carbonate cores from active Utah oil fields also reveals a variety of microbial fabrics (of which four are previously undocumented in marine formations), associated carbonate grains, pore types, and reservoir characteristics. The reservoirs, fields, and geologic locations, respectively, are the (1) Eocene Green River Formation, West Willow Creek field, Uinta Basin, (2) Jurassic Twin Creek Limestone, Pineview field, thrust belt, (3) Triassic Moenkopi Formation, Upper Valley field, Kaiparowits Basin, (4) Pennsylvanian Paradox Formation, Greater Aneth field, Paradox Basin, and (5) Mississippian Leadville Limestone, Lisbon field, Paradox Basin.

OVERVIEW OF MICROBIAL CARBONATES: SOME BASICS

Introduction

Microbial carbonates are now recognized as geologically and economically important deposits because (1) they span a geologic history longer than any other biogenic carbonates, (2) the cyanobacteria that created them generated the oxygen for the Earth's atmosphere, (3) they formed in the past and do so today in an extremely wide range of depositional environments, and (4) reservoir rocks composed of microbialites store and produce enormous amounts of oil (Bosence and others, 2015; Grey and Awramik, 2020). Multiple oil discoveries in Lower Cretaceous lacustrine strata are composed of possible microbial carbonates in deepwater offshore basins of Brazil and Angola (pre-salt reservoirs), the super giant Carboniferous marine reservoirs of the Caspian Basin (e.g., Tengiz field), and Neoproterzoic to lowest Cambrian reservoirs of the South

Oman Salt Basin. Other large oil deposits in Williston Basin marine microbialite reservoirs occur in Paleozoic Cedar Creek Anticline fields of Montana and the recently exploited Ordovician Red River "B" horizontal play of North Dakota. Truly microbial carbonates are of global-scale economic importance in both lacustrine and marine deposits. Several oil fields within the state of Utah contain microbial carbonate facies that have previously been unrecognized. Understanding these microbialite reservoirs requires defining flow units and petrophysical rock types by their depositional macrostructures, internal microfabrics, poroperm-altering diagenesis or fractures, and the interrelationships of those attributes with reservoir performance.

Utah is exceptional in that representative analogs of microbial reservoirs occur in conventional cores, including examples from active oil fields, and are well displayed in extensive outcrops of the Tertiary (Eocene) Green River Formation in the Uinta Basin. Microbial carbonates and their associated facies are also forming today in the hypersaline Great Salt Lake, an excellent modern analog to the Green River Formation. Characteristics of both lake environments include shallow-water ramp margins that are and were susceptible to rapid widespread shoreline changes, as well as similar water chemistry and temperature ranges that were ideal for microbial growth and formation/deposition of associated carbonate grains. Thus, microbialites in Great Salt Lake and cores/outcrops from the Green River Formation exhibit many of the same textures and fabrics. In addition, one of the mission goals for the Mars rover, Perseverance, which landed on February 18, 2021, is to search for evidence of ancient microbial life in lacustrine deposits in the Jezero Crater. Microbialites in Great Salt Lake and outcrops of the Green River Formation were used to help plan sampling protocols and recognize potential microbial biosignatures by the Perseverance rover team (Yingst and others, 2020).

Finally, microbial carbonates are abundantly represented in cores from Mississippian, Pennsylvanian, Triassic, and Jurassic marine reservoirs in various Utah oil fields. These examples display many of the features, both vertically and horizontally, observed in highly productive lacustrine/marine microbial and related reservoir facies worldwide.

Purpose and Approach

The purpose of this study was to provide a brief characterization and detailed petrographic overview (including carbonate fabrics, pore types, and diagenetic alteration) of the diverse types of microbialites that are present within carbonates of modern Great Salt Lake, the Green River Formation in the Uinta Basin, and reservoirs (non-marine and marine) from various active oil fields in Utah's other major producing provinces. Our approach includes (1) field observations in and adjacent to Great Salt Lake, and at well-exposed Green River and Twin Creek Limestone (Jurassic) outcrops, (2) megascopic observations and petrographic descriptions of thin sections from the Green River Formation Skyline 16 research core and various selected oil field cores, and (3) petrographic analysis of thin sections of a spectrum of Great Salt Lake Holocene carbonates.

Microbialite Classification

The most fundamental division in all of life occurs at the cellular level. Two fundamental cell types account for all known life forms: prokaryote and eukaryote. Microbes are composed of the simpler of the two types, the prokaryotes (figure 1A). The prokaryote cells are very small and contain only a cell wall, which encases undifferentiated cytoplasm inside a membrane with only vague, poorly organized structures known as nucleoids, ribosomes, and plasmids (Madison and others, 2012).

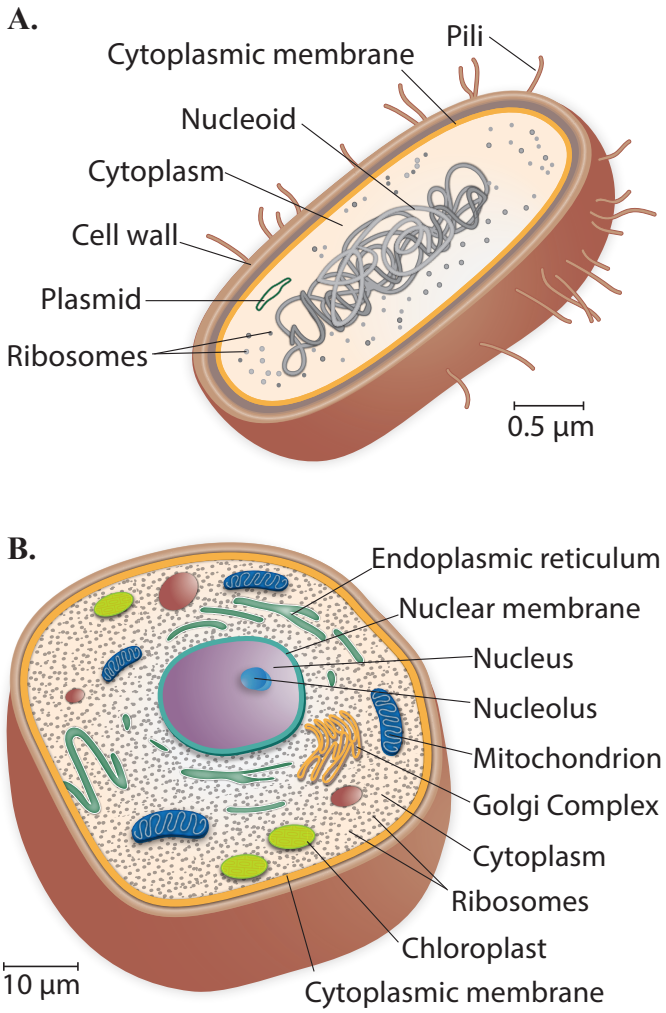

Figure 1. *Cell types for microbe versus "higher" organisms.* ***(A)*** *Generalized sketch of the key components of a prokaryotic cell. Note the very small size of this cell type (scale on the right). Nearly all microbes are composed of a prokaryotic cell.* ***(B)*** *Generalized sketch of the key components of a eukaryotic cell. Note the larger size of this cell type (scale on the left). All multi-celled "higher" organisms (i.e., plants and animals) are composed of eukaryotic cells. Modified from Madison and others (2012).*

The second larger and more complex cell type is known as the eukaryotes (figure 1B). Eukaryotic cells contain highly differentiated structures within the cell wall, including a well-defined nucleus. It is broadly accepted that prokaryotes were the more primitive of the two types and are responsible for microbial structures and fabrics within rocks (i.e., microbialites) that are the subject of this study.

Microbes (which are composed of prokaryotes) are very diverse and have been responsible for life forms within two of the three "domains" of life (Bacteria and Archea) as conceived by the evolutionary biologist Lynn Margolis (figure 2). All "higher" or "advanced" life forms, including all plants and animals (formerly termed "kingdoms"), are part of Margolis' Eukaryotes domain (Margolis, 1998; Madison and others, 2012).

Important Definitions

Two key terms convey significant meaning for studying carbonate rocks that have formed as a result of microbial (prokaryotic cell) activities.

Microbialites = Organosedimentary deposits that have accreted as a result of a benthic microbial community trapping and binding detrital sediment and/or forming the locus of mineral precipitation (Burne and Moore, 1987; Grey and Awramik, 2020) (figures 3 through 5).

MISS (Microbially Induced Sedimentary Structures) = Primary sedimentary structures formed by the interaction of microbes with sediment and physical agents of erosion, deposition, transportation, or deformation traces of microbial activity (Grey and Awramik, 2020) (figure 3). These structures commonly form microbial mats (which may be composed of bacteria, fungi, protozoans, archea, or algae), or evidence thereof, and are preserved in the sedimentary geological record (figure 6).

Microbialite Types (Classification)

Attempts to classify carbonate rocks dominated by microbialites have been plagued with a plethora of terms and classifications. From the diverse classification schemes for microbialites, we use the following five general varieties of microbialites.

1. Stromatolites = laminated, biosedimentary structures, with calcification due to the growth of cyanophytes (Riding, 2000; Grey and Awramik, 2020) (figures 7 through 9). Besides calcite mineralization, bacteria can fix aragonite, dolomite, and chert. For example, siliceous stromatolites form within a range of geothermal, chemical, and hydrodynamic settings preserving cellular structures (Handley and Campbell, 2011).

2. Thrombolites (from Greek word *thrombo* meaning a clot) = calcareous structures with a clotted microtex-

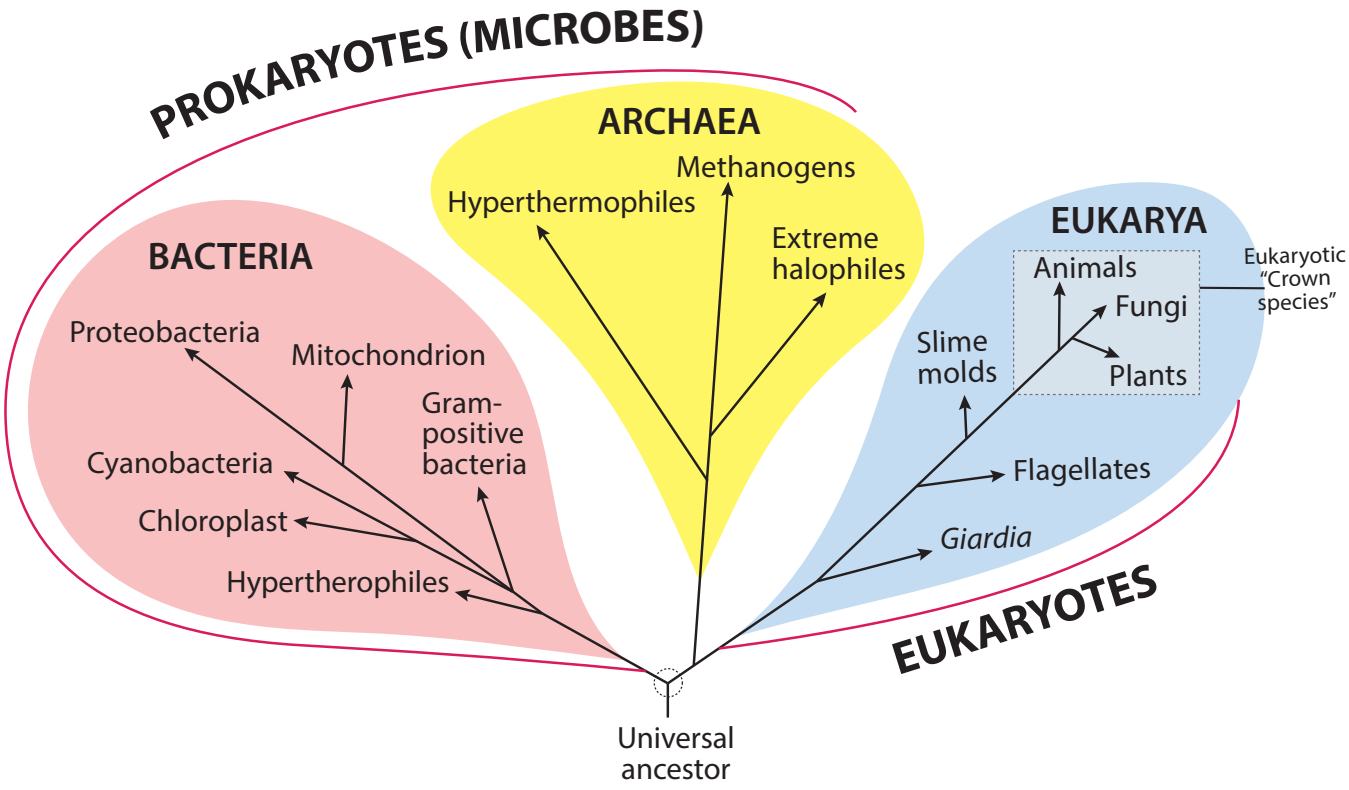

Figure 2. *Conceptual diagram of the three "domains" of life, as proposed by Lynn Margolis. Microbes (responsible for microbialites) dominate two of life's domains, Bacteria and Archaea. Modified from Madison and others (2012).*

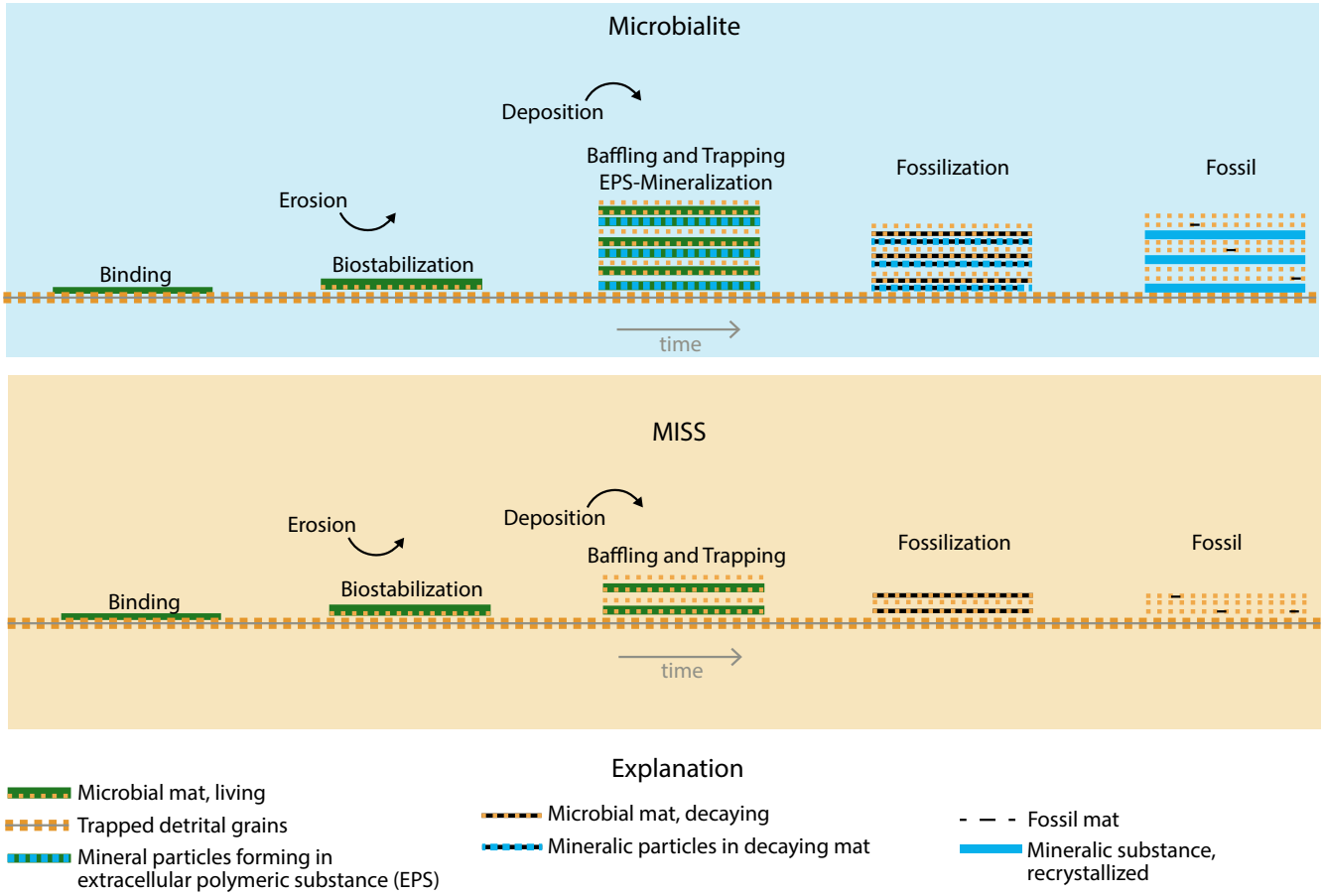

Figure 3. *Formation of microbialites versus microbially induced sedimentary structures (MISS). Modified from Noffke and Awramik (2013).*

Figure 4. *Classic example of a microbialite (stromatolitic) from the lacustrine Eocene Green River Formation. Cut and polished slab, Evacuation Creek area, Uinta Basin, eastern Utah.*

A.

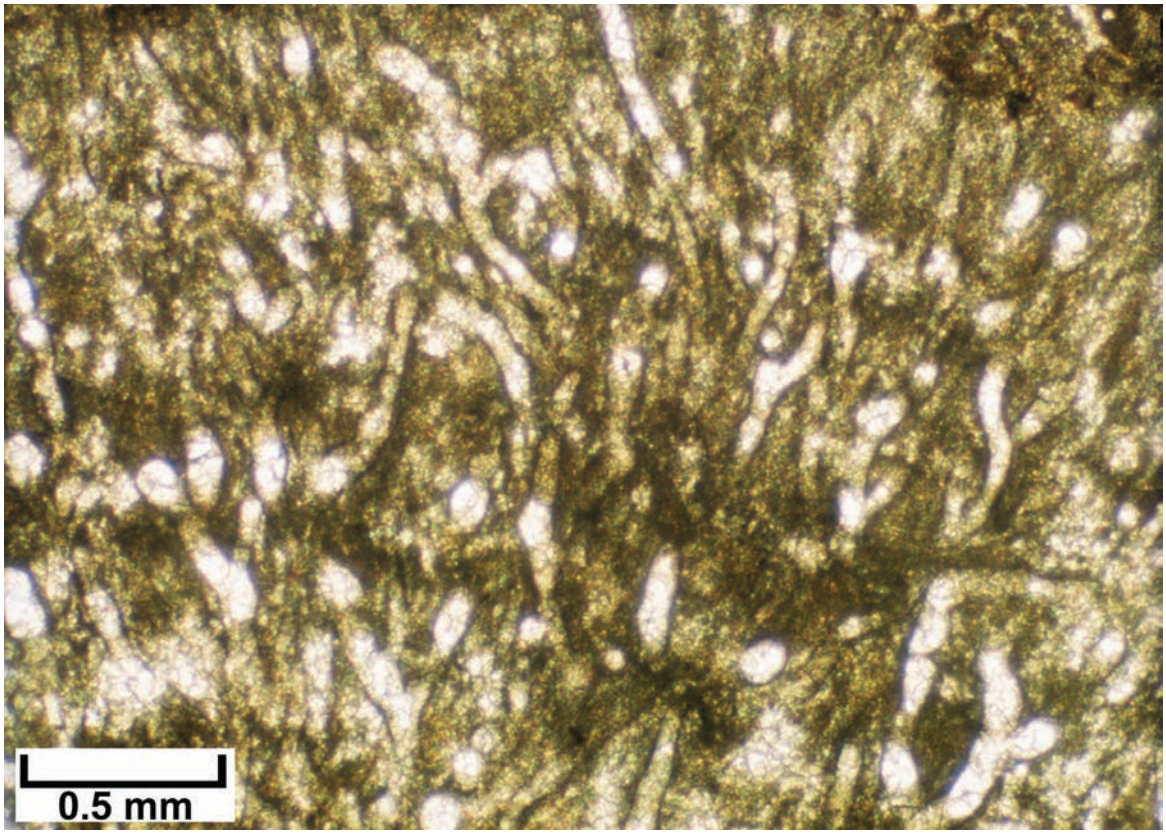

B.

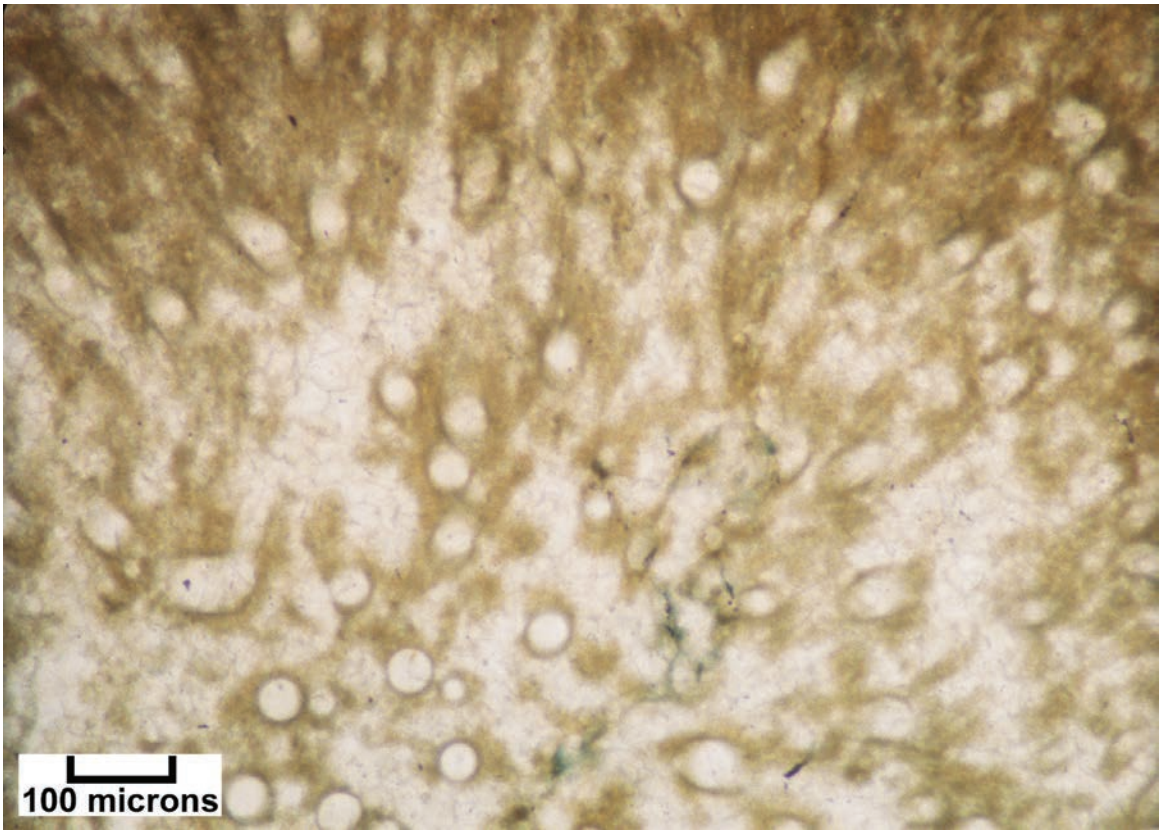

Figure 5. *Photomicrographs showing microbialite examples from the Federal No. 15-24B core, lacustrine Eocene Green River Formation, West Willow Creek field, Uinta Basin; 1459.2 meters (4787.5 ft).* ***(A)*** *Filamentous cells that curve and branch within a laminated microbial structure (plane light).* ***(B)*** *Spherical (coccoid?) cell and filamentous structures that curve and branch within a dense microbial structure (plane light with white card).*

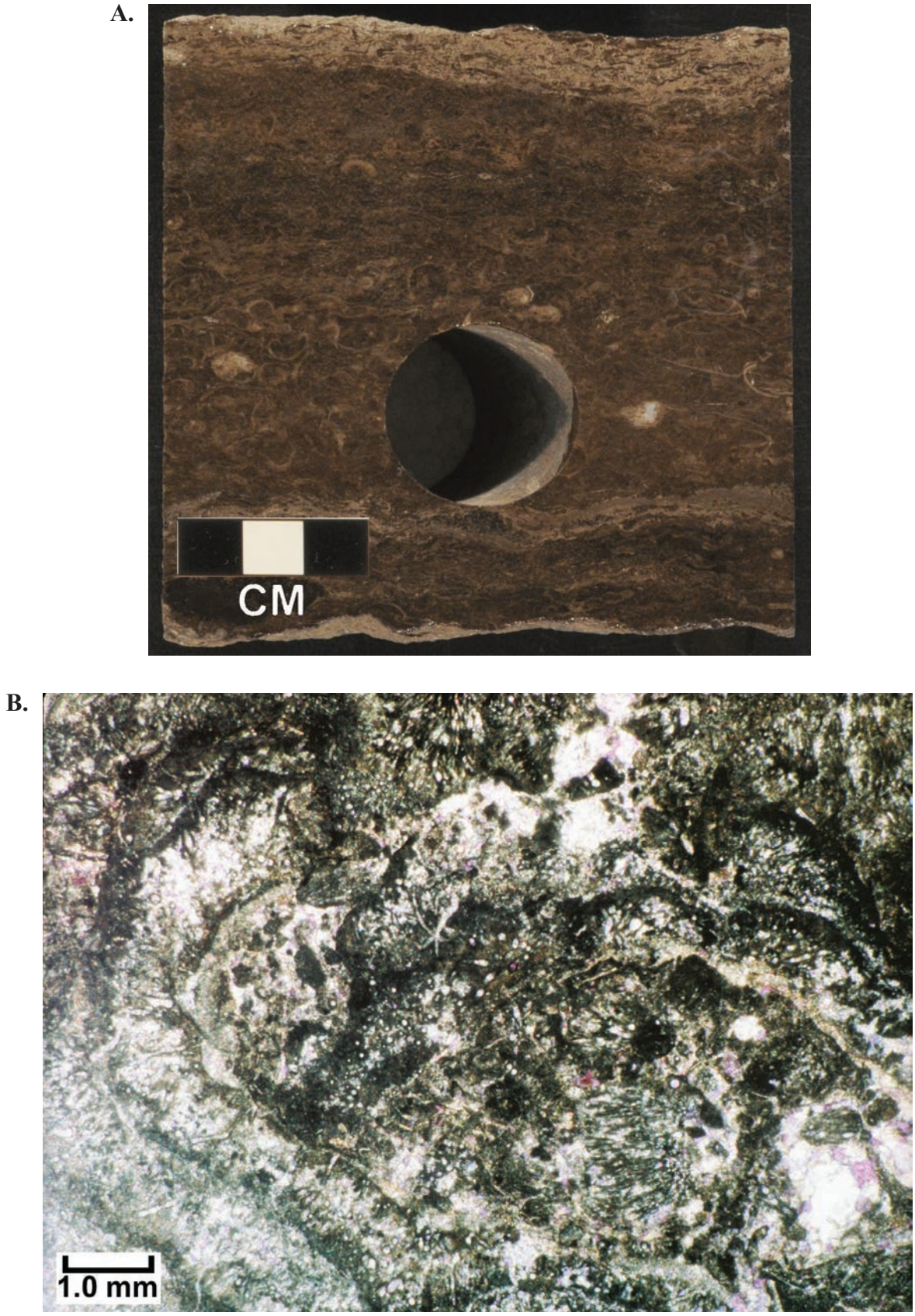

Figure 6. *Microbially induced sedimentary structures (MISS) examples in the Green River Formation from the Federal No. 15-24B core.* ***(A)*** *Conventional core segment showing vaguely laminated MISS; 1458.8 meters (4786.5 ft).* ***(B)*** *Low-magnification photomicrograph showing thin section micrograph of MISS. Microbial cellular remains and dense micritic rinds define small "heads" within a vaguely laminated interval; 1459.2 meters (4787.5 ft) (crossed nicols with accessory plate).*

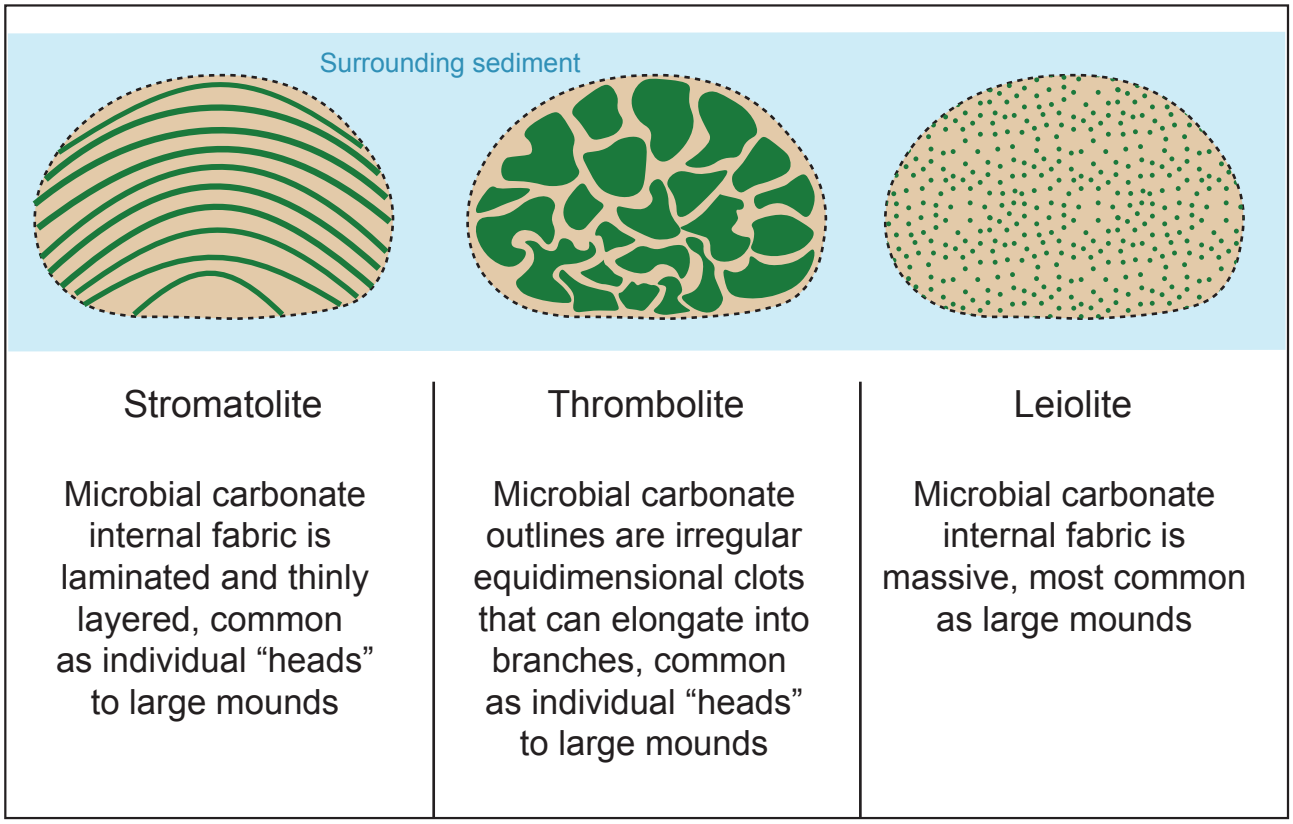

Figure 7. *Classification and general characteristics for three major types of microbialites—stromatolites, thrombolites, and leiolites. Modified from Grey and Planavsky (2009), Riding (2011), and Grey and Awramik (2020).*

ture and no internal laminae, built by cyanobacterial microbes (Aitken, 1967; Kennard and James, 1986; Grey and Awramik, 2020) (figures 7, 10, and 11).

3. Oncolites = sedimentary structures formed out of oncoids, which are layered spherical structures formed by cyanobacterial growth (figures 12 and 13). Oncolites are similar to stromatolites, but instead of forming columns or domes, they form approximately spherical structures. They are essentially mobile stromatolites in which a sedimentary fragment or shell particle often serves as a central nucleus for stratigraphic coatings. The calcium carbonate structure is precipitated by encrusting microbes.

4. Travertine/tufa = a porous or compact, dense form of limestone deposited out of solution from a mineral spring or lake, especially hot springs (Riding, 2000); however, it can also form from ambient temperature waters (Neuendorf and others, 2011). Travertine often has a fibrous or concentric appearance, frequently laminated, and exists in white, tan, and cream-colored varieties (figure 14). It is biologically and/or abiotically precipitated calcium carbonate ($CaCO_3$), predominantly calcite and aragonite (Neuendorf and others, 2011). However, increasing evidence shows that travertine is microbial in which bacteria play important roles in its formation (Chafetz and Guidry, 1999; Pentecost, 2005; Fouke, 2011; Grey and Awramik, 2020). Tufa is a variety of travertine that is a commonly "spongy" or highly porous, cool freshwater carbonate (figure 14) that often precipitates around various floral structures such as microphytic growths (e.g., algae), reeds, leaves, plant roots, and other woody tissues (Pedley, 1990; Neuendorf and others, 2011). Travertine can be laminated, clotted, or shrubby. Controversy exists between abiotic and biotic controls on tufa/travertine formation. Physico-chemical preciptation occurs when alkaline waters are supersaturated with calcite and degassing of carbon dioxide increases pH, which decreases carbonate solubility. Conversely, Pedley and others (2009) demonstrated the precipitation does not occur unless a biofilm is present, despite supersaturation with respect to calcite. Grey and Awramik (2020, p. 227) refer to tufa formed as a result of microbial activity as tufa microbialite.

5. Leiolites (from the Greek word *leios* meaning uniform or smooth) = buildups with dense, structureless microfabrics, without laminations, clots, or dendritic fabrics (figures 7 and 15). (Braga and others, 1995; Riding, 2000; Ahr, 2009; Grey and Awramik, 2020). Mud mounds are typically composed of leiolites that generally do not have much deposional porosity, but diagenesis (especially dolomitization) and fracturing can make them prolific petroleum producers (Ahr, 2009).

A.

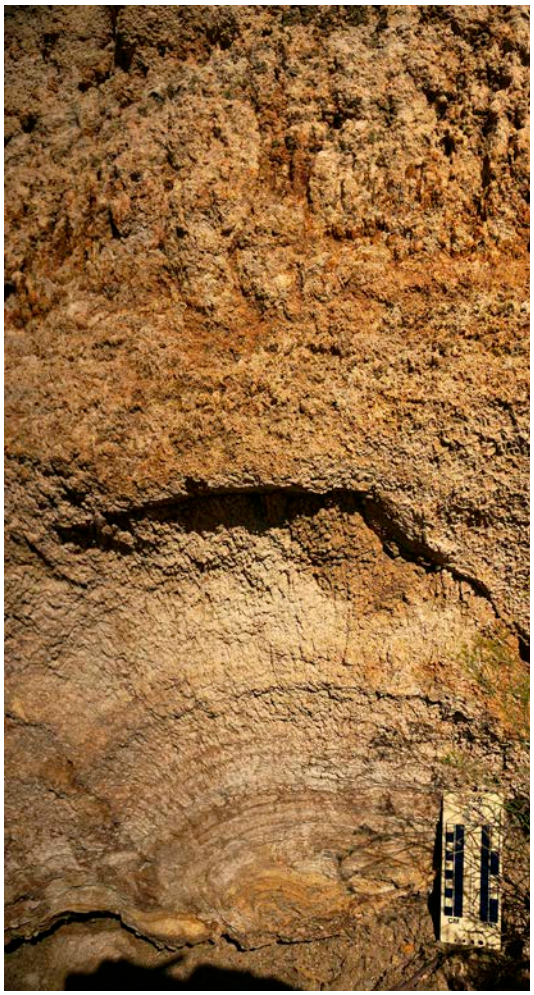

B.

C.

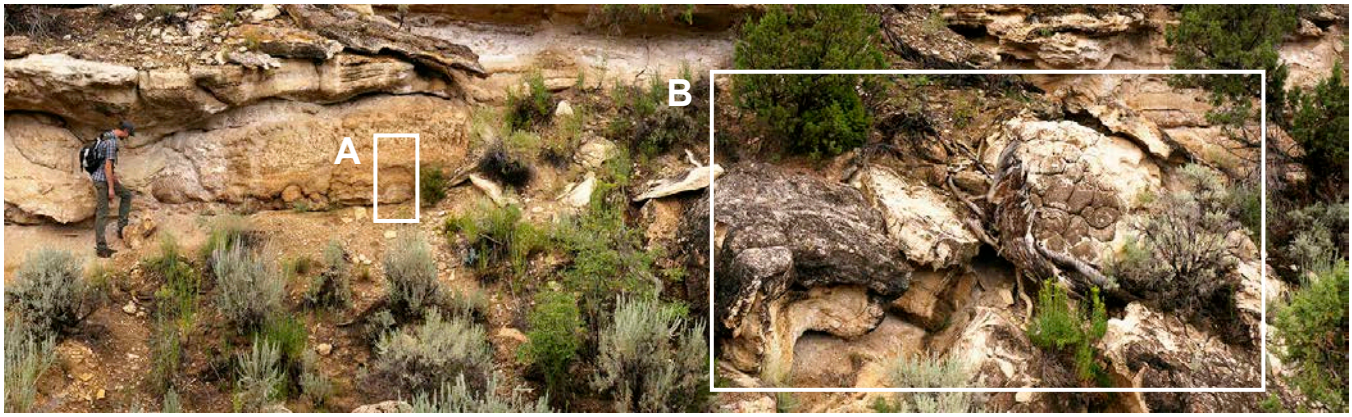

Figure 8. *Stromatolites in outcrop of the Green River Formation, Evacuation Creek area, eastern Uinta Basin.* ***(A)*** *Cross sectional view of large stromatolite domal head.* ***(B)*** *Top view of stromatolite heads.* ***(C)*** *Panorama of outcrop dominated by stromatolites. Locations of A and B indicated; person for scale.*

A.

B.

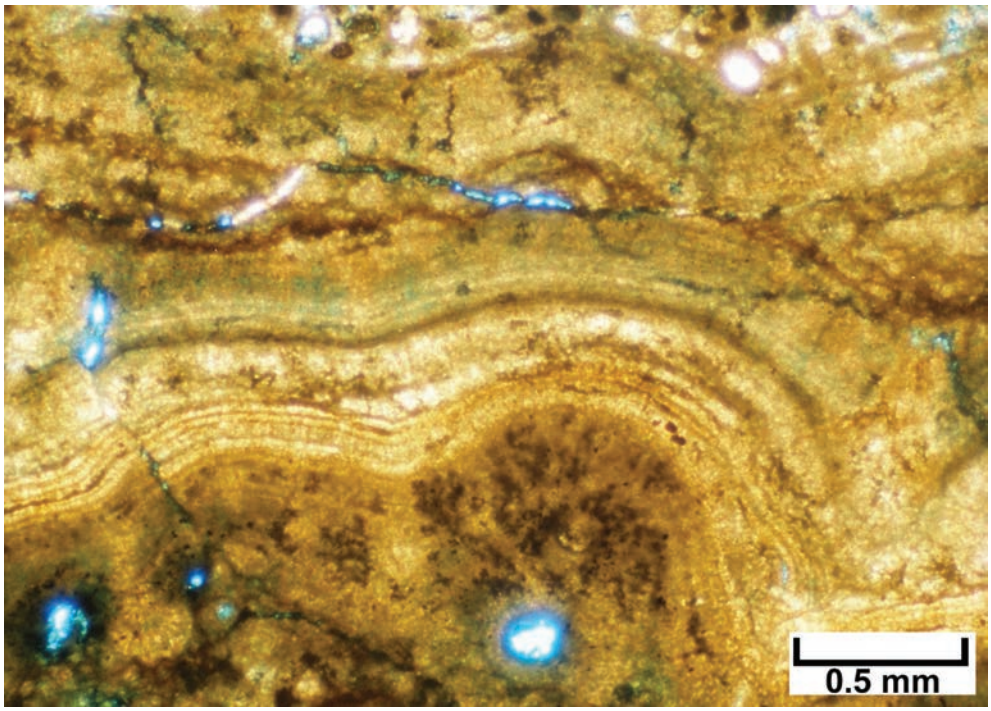

Figure 9. *Stromatolites in the subsurface of the Green River Formation, Uinta Basin.* ***(A)*** *Large stromatolite domal head; Skyline 16 research core, eastern Uinta Basin; 294.0 to 294.4 meters (964.5–966.0 ft).* ***(B)*** *Close-up photomicrograph of well-laminated, dense microbial (stromatolitic) head; Federal No. 15-24B core West Willow Creek field, 1455.2 meters (4774.5 ft) (plane light).*

Figure 10. *Large thrombolite head in outcrop of the Green River Formation, Evacuation Creek area, eastern Uinta Basin.*

A.

B.

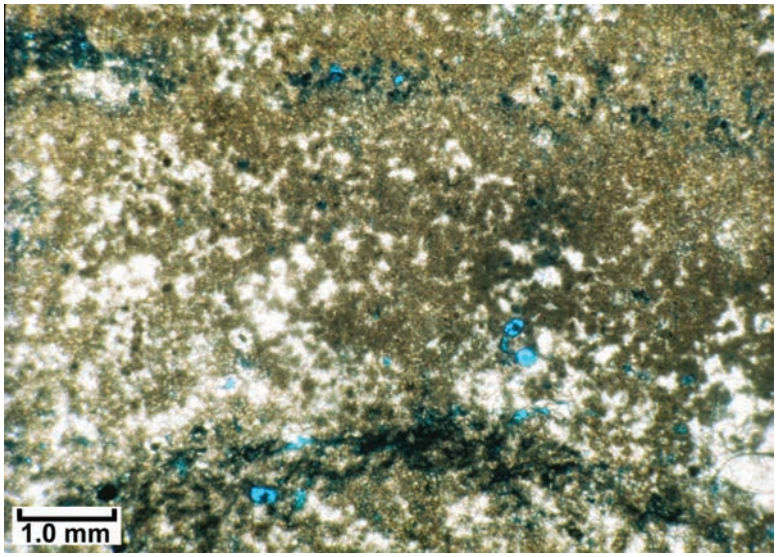

Figure 11. *Thrombolites in the Green River Formation from the Skyline 16 research core, eastern Uinta Basin.* ***(A)*** *Low-relief thrombolitic head (in the lower half of the core segment) on a layer of oncolites and draped with stromatolitic laminae and thin beds of rip-up clasts; 285.5 to 285.6 meters (936.7–937.1 ft).* ***(B)*** *Photomicrograph displaying clotted structure within the thrombolite head shown in core photograph A. The white areas between the dense microbial clots consist of sparry calcite cement; 285.6 meters (937.0 ft) (plane light).*

Figure 12. *Classic example of oncolites from the Green River Formation. Cut and polished slab, Hells Hole Canyon area, eastern Uinta Basin.*

Figure 13. *Oncolites from the Federal No. 15-24B core, 1456.7 meters (4779.5 ft), West Willow Creek field. This oncolitic rudstone is composed of large compound oncoids displaying good laminated microbial coatings; core plug analysis: porosity = 5.6%, permeability = 0.12 mD. The yellow arrow indicates the location of the photomicrographs in later figures.*

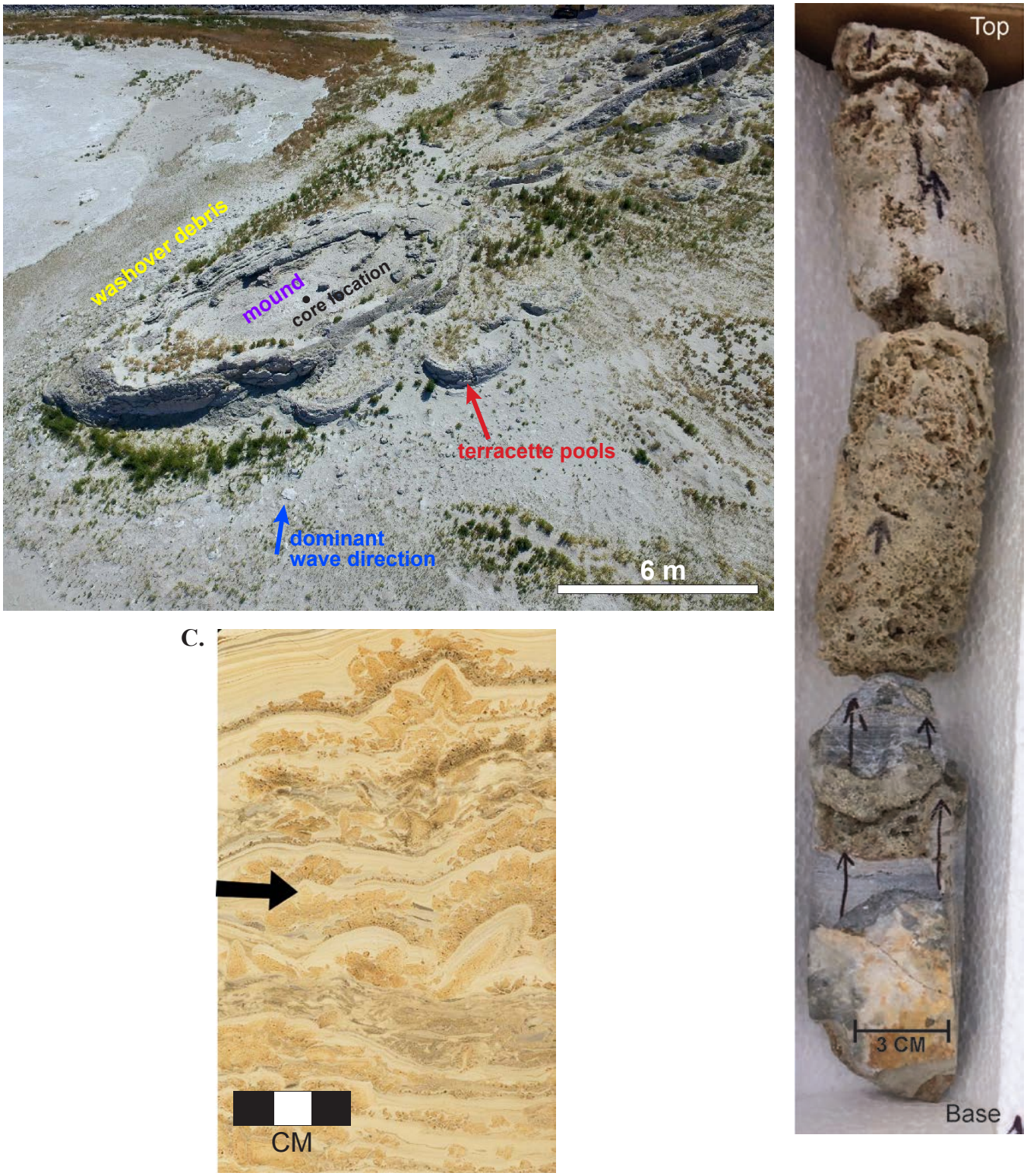

Figure 14. *Pleistocene and Eocene travertine and tufa.* ***(A)*** *Oblique aerial (drone) photograph, view south, of a Pleistocene travertine mound at Lakeside, Utah, along the western shore of Great Salt Lake. Mesothermal alkaline fluids flowed from bedrock fractures to deposit travertine drapes and mini-terracettes that formed a 30 x 15-meter (9 x 4.5 ft), 2-meter-high (0.6 ft) mound (Homewood and others, 2018, in press). Photograph by Jean-Charles Schaegis.* ***(B)*** *Vertical core (1.4 meters [4.6 ft]) taken from the top of the Lakeside travertine mound showing highly porous zones within the travertine. Mississippian Great Blue Limestone at the base. See A for core location.* ***(C)*** *Example of travertine and tufa from the Green River Formation in the Skyline 16 research core; 198.36 to 198.43 meters (650.8–651.0 ft). Travertine occurs as the light-colored, dense, laminated layers in this core segment. Tufa is present as the spongy, very porous, light brown areas. In addition, partially filled evaporite (?) crystal molds are shown. Black arrow indicates the location of photomicrographs shown in later figures.*

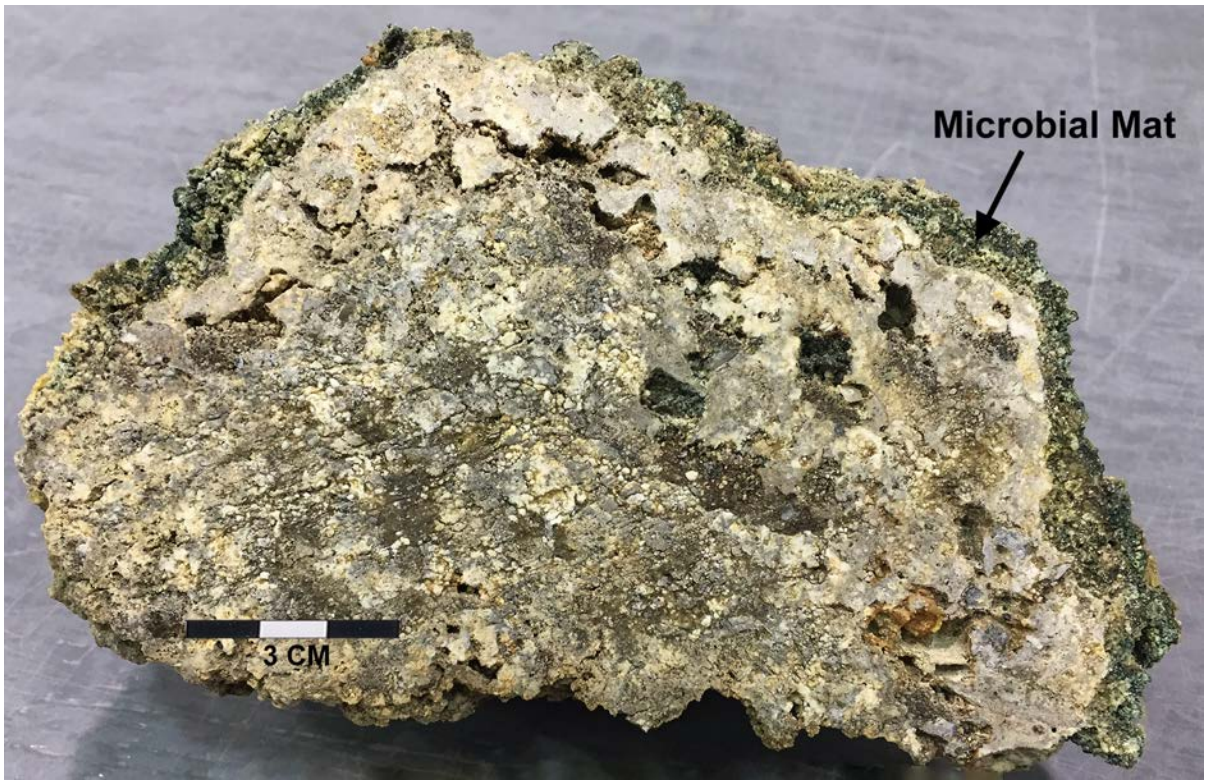

Figure 15. *Holocene microbialite showing mostly structureless, leiolite-like interior and a thin, outer microbial mat layer. Slab from Bridger Bay, Antelope Island, Great Salt Lake.*

Porosity Development within Microbialites

Reservoir quality in microbialites is highly dependent on the construction and preservation of porosity within the matrix of microbial structures (porosity types used in this study are from Murray [1960] and Choquette and Pray [1970]). Petrographic analyses of thin sections illustrate various porosity styles within stromatolites (figure 16A), thrombolites (figure 16B), and tufa (figure 16C). Stromatolites typically have less porosity than the thrombolites. Primary porosity may be well-preserved megascopic pores produced from constructional processes and fabrics. Constructional pores (also called constructional vugs) are produced by formation of a rigid or semi-rigid framework of tubules attributed to microbial construction (Murray, 1960). Constructional pores often formed during the growth of mudstone microbial mounds; vugs can be stromatactis or cavities in the mudstone (Ahr, 2008; Ahr and others, 2011). These pore types resemble fenestral, moldic, and small vuggy pores previously occupied by organic matter. The pores in the constructional framework may be open or filled with sediment or later with cement (Murray, 1960). Microposity (micro-intercrystalline porosity) is also common.

In most carbonate intervals containing microbialites, there are associated facies and diagenetic alteration that are not purely microbial in origin, but which also can have important preserved porosity for fluid storage and transmissibility. Among the most common are oolites, pisolites, and peloidal/skeletal calcarenite (grainstone/packstone) that contain excellent preserved interparticle pore space. Peloids also display both interparticle and intraparticle pore space. Microposity including open microfractures are also present in peloids, pisolites, and other grains.

Early dolomite has been observed in some microbial facies. These dolomites, both Holocene and ancient, can have excellent intercrystalline porosity (Gebelein and Hoffman, 1971; Saller and Henderson, 1998; Saller, 2004). Well-connected pores between individual dolomite crystals represent unrecognized potential reservoirs. Almost all the microbialites and associated grainstones in the Green River Formation are dolomitized.

GREAT SALT LAKE: A HOLOCENE LACUSTRINE MICROBIAL ENVIRONMENT

Great Salt Lake in northern Utah (figures 17 and 18) is an excellent locale to study modern microbial formation serving as a modern analog to the lacustrine (Lake Uinta) Eocene Green River Formation in the shoreline changes, as well as comparable water chemistry and temperature ideal for microbialite growth and formation/deposition of associated carbonate grains (Chidsey and others, 2015; Vanden Berg, 2019). Microbial mats, microbialites, and associated carbonate grains (hypersaline ooids [ooids with large-scale, radially oriented ara-

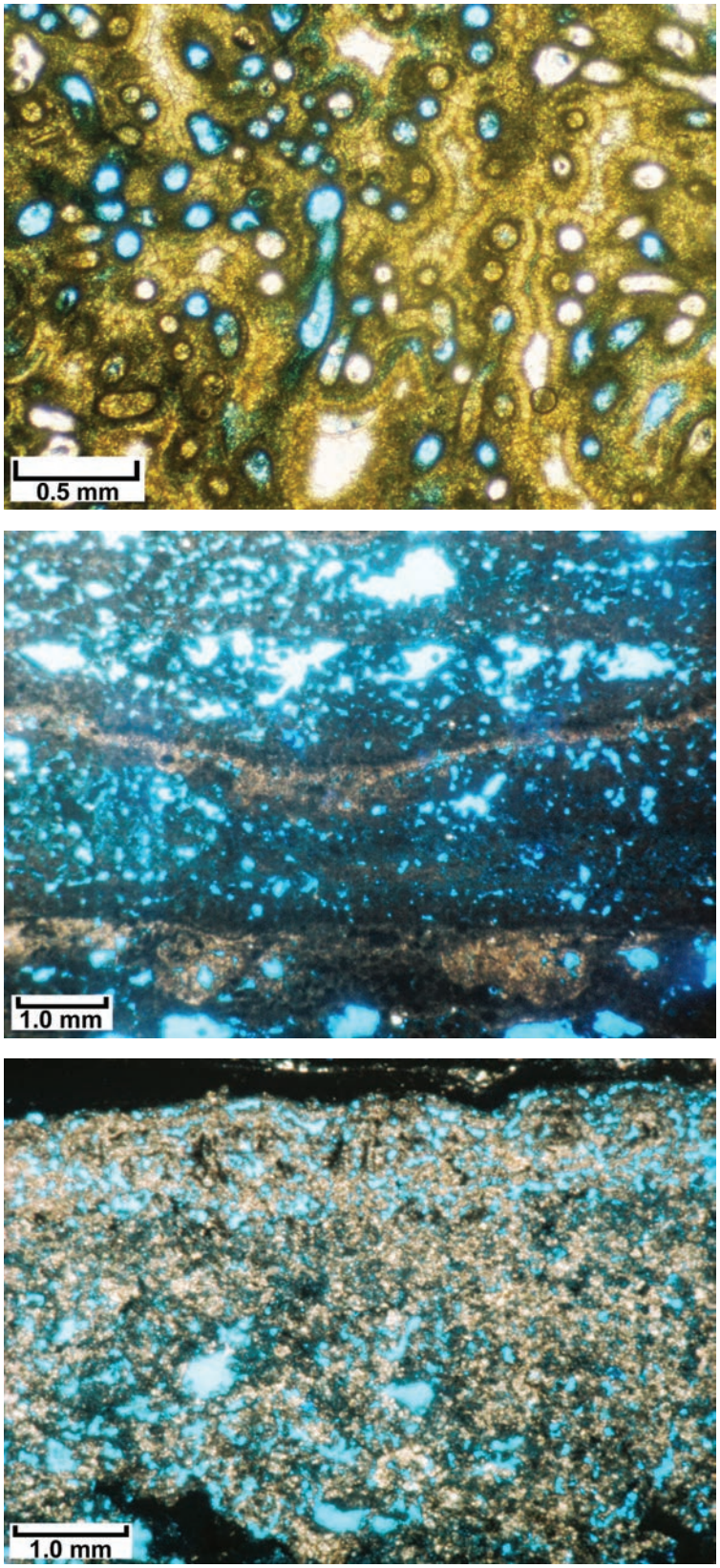

Figure 16. *Porosity within Green River Formation microbialites.* ***(A)*** *Photomicrograph of a stromatolitic boundstone with preserved constructional pores (in blue). Note early isopachous fibrous cements lining pores; Federal No. 15-24B core, 1454.8 meters (4773.3 ft), West Willow Creek field (plane light).* ***(B)*** *Photomicrograph showing excellent preserved primary porosity within a thrombolitic interval. Megascopic pores are intimately associated with clotted constructional fabrics. Note also the small primary vugs; Skyline 16 research core, 305.5 meters (1002.2 ft) (plane light).* ***(C)*** *Photomicrograph showing extensive porosity within a delicate lacy tufa fabric composed of crystalline dolomite growing within open voids; Skyline 16 research core; 198.3 meters (650.5 ft) (plane light), see figure 14C for core photograph.*

gonite fabrics], coated grains, peloids, and lithified crusts) are widespread and easily accessible when the lake level is low for examination in and around Great Salt Lake. In particular, microbialites are readily accessible at Rozel Point, in the northern part of the lake, and at Bridger Bay at the northern end of Antelope Island, in the south arm of the lake (figure 17).

The depositional environments of Great Salt Lake represent a remarkable Holocene carbonate "factory." During its Holocene history the lake has been ideally suited for microbialites to develop, chiefly from the cyanobacteria genus *Aphanothece* (Eardley 1938; Pedone and Folk, 1996; Lindsay and others, 2017; Baxter, 2018; Baxter and Butler, 2020, and references therein; Kanik and others, 2020), and for the production of hypersaline ooids. The high salinity in the lake is hostile to most plants and algae that would compete for nutrients and space; organisms that would normally browse on or burrow into microbial mats are also absent. The extensive shallow margins of the lake allow good sunlight penetration, possibly further promoting microbial growth.

Figure 17. *Satellite image of Great Salt Lake (NASA #STS047-097-021, September 1992). Rozel Point close-up (inset top left), Google Earth image taken May 2010. Bridger Bay close-up (inset bottom left), Google Earth image taken July 2010.*

Figure 18. *Great Salt Lake; view to the south of the north arm from Rozel Point.*

General Geology and Lake Characteristics

Great Salt Lake is the remnant of the freshwater, Pleistocene-age Lake Bonneville that covered 52,000 square kilometers (20,000 mi^2) of northwestern Utah as well as small parts of northeastern Nevada and southeastern Idaho. Lake Bonneville existed from about 30,000 to 13,000 years ago (Oviatt, 2015). Lake Bonneville and other large pluvial lakes in the Great Basin region of the western U.S. formed during glacial maxima; the Wasatch Range and Uinta Mountains east of Great Salt Lake were extensively glaciated at this time. While oscillating due to climatic changes, Lake Bonneville gradually increased in size and depth. At its maximum, the lake was nearly 300 meters (1000 ft) deep in the area occupied by the present Great Salt Lake (Hintze and Kowallis, 2009). Shortly after reaching its highstand elevation about 18,000 years ago, Lake Bonneville breached its threshold near Red Rock Pass in southeastern Idaho, causing a catastrophic flood into the Snake River Plain (Gilbert, 1890; Oviatt, 2015). Following the flood, the lake stabilized for 2000 to 3000 years at the Provo shoreline level until changes in climatic conditions drove the lake to levels comparable to modern Great Salt Lake by about 13,000 years ago (Godsey and others, 2011; Oviatt, 2015). This marked the end of the Bonneville lake cycle. Following a brief rise in lake level referred to as the Gilbert episode that peaked about 11,600 years ago (Oviatt, 2014), a warmer and drier climate further reduced the lake's size, leaving behind present-day, hypersaline Great Salt Lake.

Great Salt Lake is the 33rd largest lake in the world by area (and the largest fresh or saltwater lake in the United States after the Great Lakes). It averages 121 kilometers (75 mi) long and 56 kilometers (35 mi) wide, covering 4190 square kilometers (1620 mi^2), and fills the lowest depression in the Utah part of the Great Basin. The surface elevation of the lake averages 1280 meters (4200 ft) above sea level, and the lake level fluctuates an average of 0.3 to 0.6 meters (1–2 feet) annually. However, years of drought led to a near-historical low lake level of 1277.7 meters (4192.0 ft) in 2020 (U.S. Geological Survey, 2020).

The maximum depth of Great Salt Lake is about 10 meters (33 feet). The volume of water fluctuates depending on the variation of precipitation and evaporation. The volume of water also varies during the year—increasing in spring and early summer due to snowmelt in the nearby mountains, decreasing in late summer and fall. Generally, Great Salt Lake contains about 19,000 cubic hectometers (15,400,000 ac-ft) of water. Water sources include four main rivers (the Bear, Weber, Ogden, and Jordan Rivers) and small streams (66%), direct precipitation into the lake (31%), and groundwater (3%) (Gwynn, 1996).

The Great Basin, including the depression occupied by Great Salt Lake, is internally drained—there is no outlet to the sea. Thus, water loss is primarily due to evaporation; 3600 cubic hectometers (2,900,000 ac-ft) of water evaporates annually (Gwynn, 1996). From 1953 to 1959, the Southern Pacific Transportation Company constructed a boulder/gravel-filled railroad causeway (currently used by Union Pacific trains) across the lake, creating north and south arms (figure 17). As none of the four major rivers enter the north arm, it became much saltier. The salinity of the north arm is 24% to 26% (near

its salt-saturation point), whereas the salinity of the south arm is 12% to 14%. The average composition of dissolved salts in Great Salt Lake water by dry weight percent is: chloride = 54.5%, sodium = 32.8%, sulfate = 7.2%, magnesium = 3.3%, potassium = 2%, calcium = 0.2% (Gwynn, 1996). However, in December 2016 the causeway was breached by Union Pacific (now the owner of the rail line). The salinity in the south arm is expected to increase by 1% whereas the north arm should remain the same (Andrew Rupke, Utah Geological Survey, verbal communication, 2017).

Microbial muds and microbial mats (which may be composed of bacteria, fungi, protozoans, or algae) are exposed during seasonal or draught-caused low lake levels. Microbial mud and mats can generally be distinguished from the non-microbial muds by pinkish colors caused from coatings of photosynthetic halophilic bacteria (Collister and Schamel, 2002). Mud is transported to the lake by the processes of erosion. These it is deposited and often mixes with microbial communities. Lake mud is typically organic rich (sapropelic) containing halophilic (salt-loving) cyanobacteria and green algae, fecal pellets from brine shrimp (*Artemia franciscana*), ooids (discussed below), silt or fine-grained quartz sand, and minor amounts of decayed terrestrial plant material (Collister and Schamel, 2002).

Halite precipitates in the saltier north arm at certain times of the year. Gypsum (selenite) crystals grow in the mud along the shore of Great Salt Lake (figure 19) as well as in dikes constructed for brine evaporation ponds.

Applicable Previous Studies

Scientists from around the world have come to Utah to study the unique ecology, biology, and sedimentary geology of Great Salt Lake. Most geological studies have focused on lake levels over time and the deltaic deposits associated with Lake Bonneville, but several studies have detailed the microbialite formation within the lake. Eardley (1938) provid-

Figure 19. *Typical gypsum (selenite) crystals growing in the organic-rich mud along the shore of Great Salt Lake. Inset – close-up view of a large gypsum crystal recovered from Great Salt Lake sediments.*

ed the earliest definitive work on the "bioherms" and associated deposits in Great Salt Lake including the importance of bacteria in their formation. These features have since been included in many studies and guides. For example, Carozzi (1962a) and Post (1980) described the "bioherms" and the precipitation of calcium carbonate by "blue-green algae," whereas Halley (1976) researched the textural variations within Great Salt Lake "bioherms." The formation of aragonite cement by nannobacteria in the lake's bioherms was determined by Pedone and Folk (1996) and Baxter and others (2005), and Lindsay and others (2017) considered the living microbial communities in Great Salt Lake, their abilities to survive in a hypersaline environment, and the effects of north arm versus south arm salinity on carbonate precipitation. Lindsay and others (2017) concluded that biotic aragonite precipitation and microbialite formation now occurring in the south arm was from a limited diversity of cyanobacteria—mainly the photoautotroph *Euhalothece*. Baskin (2014) attempted to characterize the distribution, depth, size, shape, and spacing of Great Salt Lake microbialites. Chidsey and others (2015) and Della Porta (2015) described Great Salt Lake microbialite characteristics and associated facies. Vanden Berg (2019) described the basic morphology of Great Salt Lake microbial structures and how local environmental conditions, as well as periods of exposure and erosion, contribute to growth location, grouping, shape, size, orientation, and internal structure. Several other research groups have explored other important aspects including mineral precipitation mechanisms (Bouton and others, 2016a; Pace and others, 2016), biogeochemistry/microbiology (Lindsay and others, 2017; Baxter, 2018; Baxter and Butler, 2020; Kanik and others, 2020), and possible age of formation and paleoenvironmental record (Newell and others, 2017; Vennin and others, 2019). Homewood and others (2018, in press) studied a well-lithified Pleistocene travertine mound and associated microbialites near Lakeside on the western shore of the lake (figures 14 and 17). Detailed mapping along the shoreline in the Buffalo Point area near the northwest end of Antelope Island south of Bridger Bay (figure 17) by Bouton and others (2016b), showed lobe-shaped microbial colonization on a conglomerate substrate formed by late Pleistocene-age gravity flows, although microbialites form on all hard substrates.

The study of Great Salt Lake oolites is more extensive than that of the microbialites. Early descriptions by Matthews (1930), Eardley (1938), and Carozzi (1962b) recognized the radial crystalline fabric of these ooids. Much debate followed as to whether the radial fabric was primary or diagenetic, the latter being the result of recrystallization of aragonite to calcite or aragonite to aragonite (Pedone and Norgauer, 2002). Ultimately, modern petrographic techniques proved the radial crystalline fabrics of the oolites are primary and the composition is aragonite (Kahle, 1974; Sandberg, 1975; Halley, 1977). The petrography, as well as the geochemistry, of Great Salt Lake oolites was further studied by Pedone and Norgauer (2002) and Paradis (2019).

Great Salt Lake Microbialites and Associated Carbonate Grains

The surface of the lakebed is mostly composed of ooid sand and mud, underlain by clay. However, areas of slightly higher topography on the lakebed have created a preferred location for microbial growth. There may also be a link between microbialites and groundwater flow similar to findings in the rock of the Green River Formation (Awramik and Buckheim, 2015; Vanden Berg, 2019); "freshwater" (most likely brackish) springs are common along exposed parts of the lake during low lake levels. Vanden Berg (2019) also suggested that Great Salt Lake microbialites formed rapidly during large-scale lake level transgression and that they are relatively old (about 6 ka) rather than modern. Wave energy, salinity variations, water depth, water temperature, and duration of submersion affect the types, shape, and size of the microbialites.

The first part of this study focuses on the petrographic characterization of microbial structures from two distinct areas: (1) partially lithified microbialites and associated lake-margin carbonate grains in Bridger Bay at the north end of Antelope Island in the south arm of Great Salt Lake; and (2) relict microbialite or travertine structures associated with probable springs near Rozel Point in the salt-saturated north arm (figure 17).

Overall, the spatial distribution of the microbialites and their association with various carbonate grains provides information that can be applied to the study of ancient microbial development, such as within the Eocene Green River Formation. The analysis of pore structures in Holocene microbialites and carbonate grains provides formation clues to ancient equivalents and could help determine spatial characteristics of potential reservoir units.

Bridger Bay, Antelope Island

The shallow, sheltered waters of Bridger Bay on the northwestern tip of Antelope Island (figure 17) support extensive microbialite formation (figures 20 and 21), especially in the north-northwest part of the bay near Egg Island. Thin, dark brown to green, living microbial mats cover the surfaces of carbonate/lithified microbialites (averaging 5 to 12 centimeters [2–5 in] thick (figure 20A).

In Bridger Bay, the microbialites tend to form distinct, low-profile circular domes, ranging in diameter from less than 0.5 meters up to 2 meters (1.6–6.5 ft) (figure 20B), and giving the appearance of domal stromatolites; however, their internal composition is mostly structureless, lacking preserved, distinct internal laminations (i.e., leiolite-like fabrics[?], figure 15) (Vanden Berg, 2019). These features are composed of a mostly featureless (faintly laminated near the surface [stromatolites?]) outer crust about 10 to 20 centimeters (4–8 in.) thick, which covers unconsolidated to partially lithified captured carbonate grains (e.g., oolitic sands and pellets) and

organic-rich lime mud, but sometimes up to 10% lithics (figure 20A) (Vanden Berg, 2019). Along the windward side of Bridger Bay's northern spit, the microbial communities are much larger, 3 to 4 meters (10–13 ft) in diameter and 4 meters (13 ft) tall (Vanden Berg, 2019).

In general, the microbial domes are more abundant and spaced closer together in shallow water of Bridger Bay and become less abundant, taller (12 to 26 centimeters [4.8–10.2 in]) and spread out as water depth increases. In addition, the mats and domes display a curvilinear to trend that can be parallel to shore in some places and perpendicular to shore in others, but always perpendicular to wave direction (parallel to the waves themselves) (Vanden Berg, 2019). When submerged, the outer surface of these domal structures is covered with brown-green microbial pustules, the "microbial mat." As water level drops and wave energy increases, the mats are eroded off the top of the microbial domes and are redeposited between the domes (figure 20C) and as thin, shallow shoals on or near the beach (figure 21). When the microbialite structures are exposed for extended periods of time (as little as a few days to weeks), the microbial mats begin to bleach white.

In nearshore areas now exposed due to the near-historical low lake levels, the microbialites often display ring-like structures (figure 20D). These microbial rings develop as a result of exposure and erosion of the fully submerged domal structures desribed above. As the lake level falls and water table drops with a cooresponding decrease in pore pressue, the mostly unconsolidated clay and ooids composing the interiors of the domes compacts causing the outer poorly lithified crust to collapse creating raised outer rings (Vanden Berg, 2019). The collapsed central part of the domes further disintegrates with prolonged exposure and wave action during storms or brief periods of inundation washes away the broken material leaving behind only the raised outer rings.

Photomicrographs show these pustular grains, or microbial "popcorn," representing a combination of organic microbial mat and precipitated carbonate minerals (figure 22) have "lumpy" or "bumpy" textures composed of very abundant, well-defined spherulitic aragonite or calcite structures within the microbial fabrics. These lithified fragments typically contain open, internal, primary constructional pores. Filamentous strands and incipient acicular cements may bridge the pores.

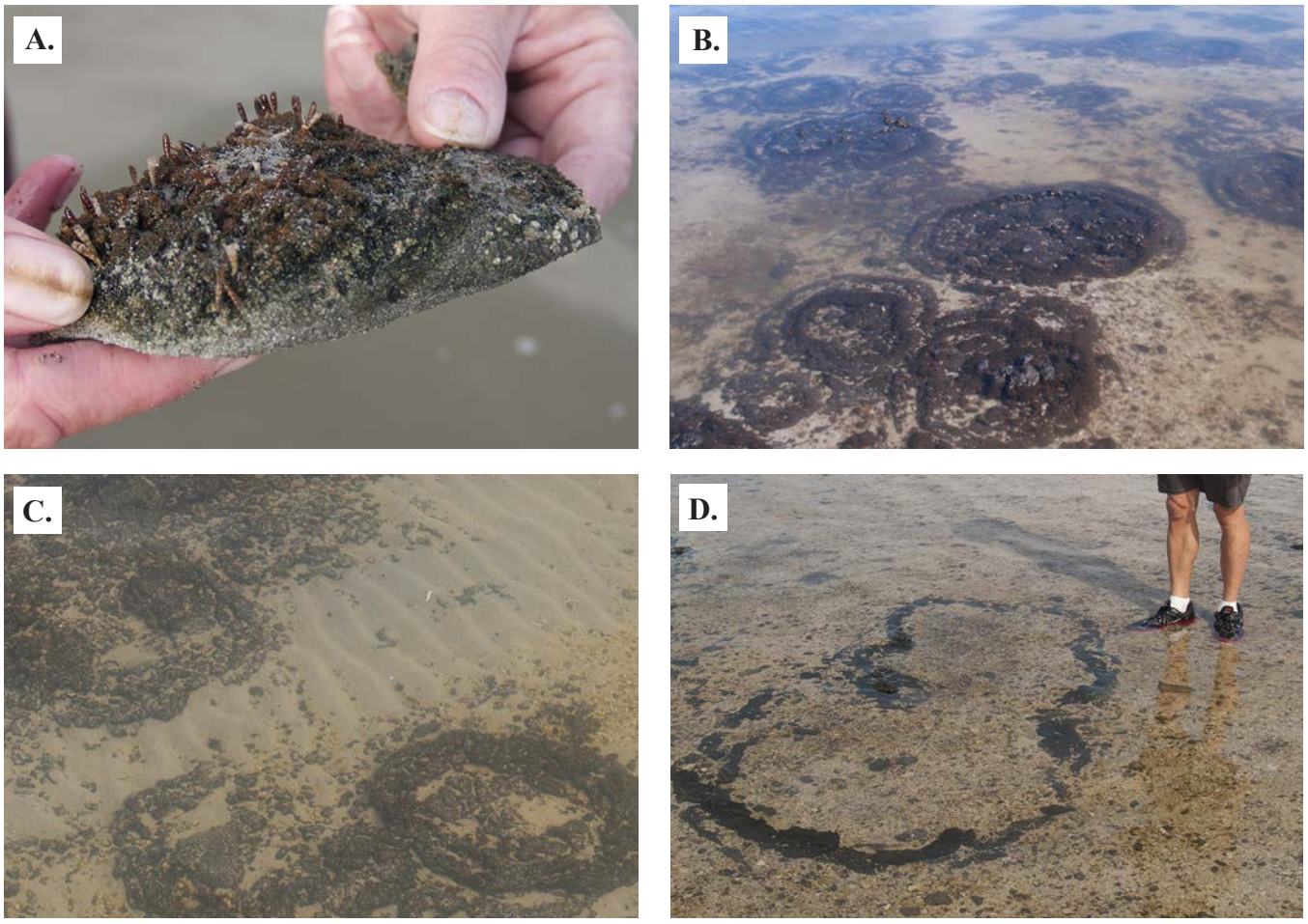

Figure 20. *Examples of Great Salt Lake Holocene microbial carbonates and associated grains, Bridger Bay, Antelope Island.* ***(A)*** *Living and growing (hand specimen) microbial mat; small vertical tubes are brine fly larval casings.* ***(B)*** *Circular Holocene microbialites exposed during low lake level.* ***(C)*** *Unlithified oolitic sand and mud between circular microbialites; note the presence of wave ripples.* ***(D)*** *Circular rim of a collapsed microbialite dome (similar to B and C), wave action most likely eroded away the interior of the structure.*

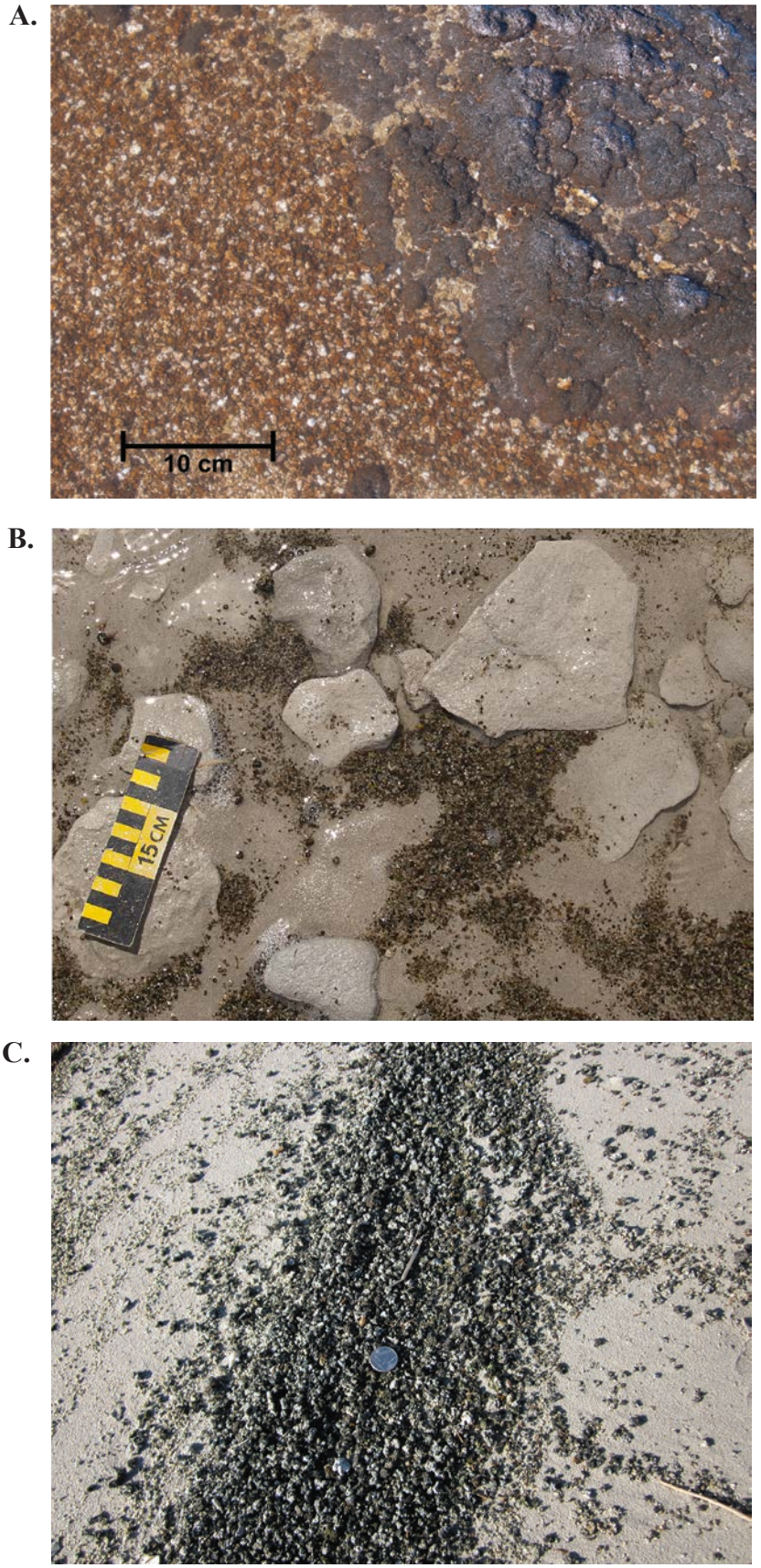

Figure 21. *Pustular microbialite deposits, Bridger Bay, Antelope Island.* ***(A)*** *Pustular grains (small pieces of microbial mats) or "microbial popcorn" eroded from the tops of microbialite domes and redeposited.* ***(B)*** *Eroded and bleached microbialite forming oolitic grainstones/"beachrock;" notice brown pustular grains.* ***(C)*** *Close-up of pustular microbial deposits (coin for scale) along the northwestern beach of Antelope Island.*

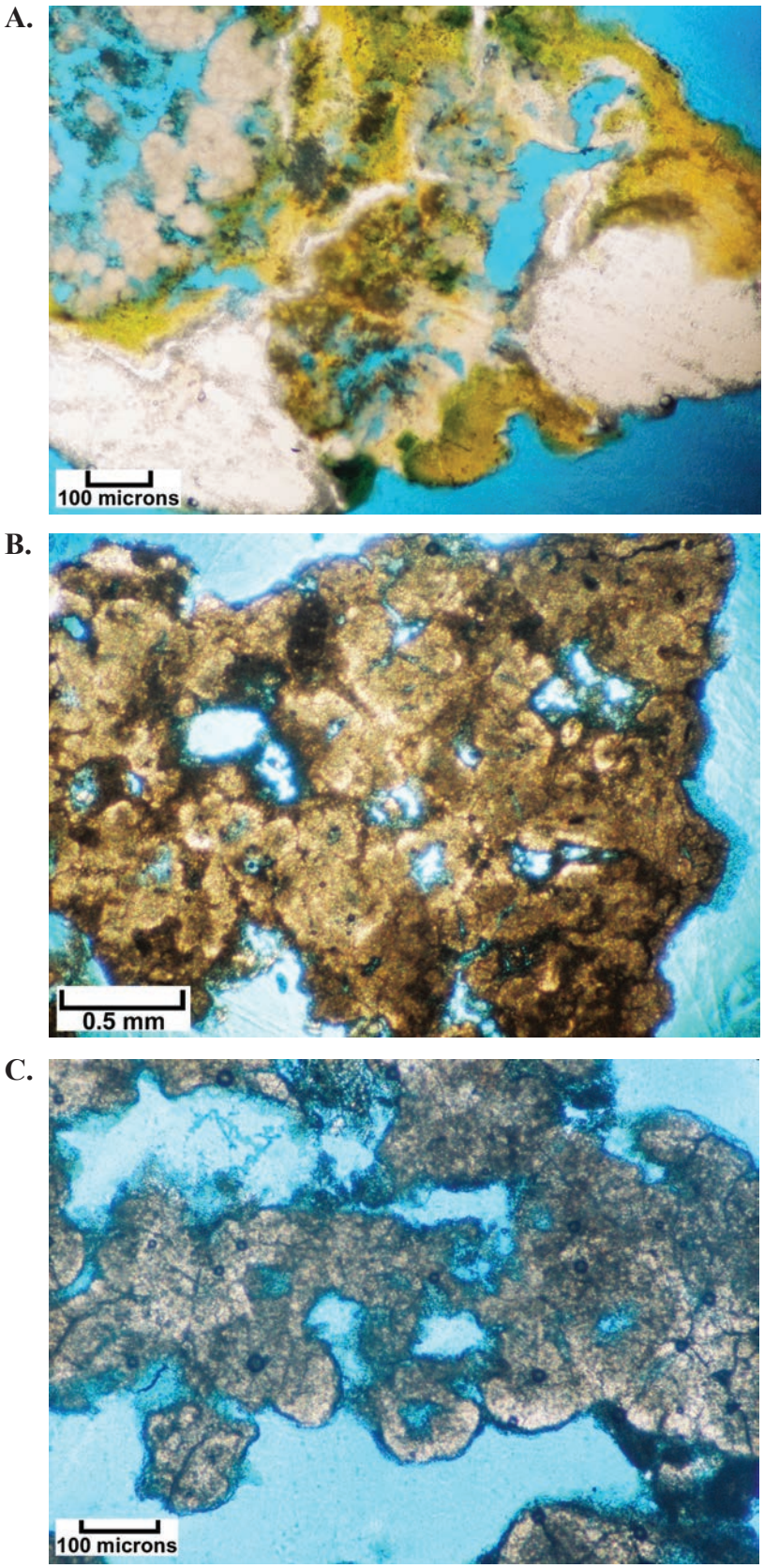

Figure 22. *Petrography (photomicrographs) of pustular grains ("microbial popcorn"), Bridger Bay, Antelope Island.* ***(A)*** *Small lithified pustule grains incorporating two silicate grains (in white) into honey-brown organic crust. Note the numerous small spherulitic structures in light brown (plane light with white card).* ***(B)*** *View of the internal "lumpy" or "bumpy" texture of a well-lithified microbialite fragment. Precipitated aragonite or calcite spherules and coalesced spherules are surrounded by pore spaces that superficially resemble interparticle pores between detrital grains (pores in blue; plane light).* ***(C)*** *Overview of well-defined spherulitic structures within a microbialite fabric (plane light).*

In thin section, most preserved pores between the in situ precipitated spherules superficially resemble interparticle pores between carbonate grains (figure 22B).

Carbonate grains and beach lag deposits are associated with Great Salt Lake microbialites. These include ooids, coated grains, pellets, peloids, and intraclasts. The intraclasts are composed of oolitic and pelletal packstone, and coated microbial and volcanic fragments. Hypersaline ooids form extensive beaches and dunes on Antelope Island (figure 23) and around much of Great Salt Lake. Oolitic sands are typically medium to well sorted (figure 24A). Petrographically, these ooids frequently have early radial recrystallization (figures 24B and 24C), cerebroid margins (figures 24B, 24D, and 24E) (Carozzi, 1962b), and breakage across the entire grain and recoating of broken ooids (regenerated ooids; figure 24E). Cerebroid ooids have irregular, embayed cortex margins due to the syndepositional radial recrystallization within the ooid (figure 24D). Radial recrystallization in ooids may occur as cortex bands covered by tangential oolitic coatings (figure 24C). Regenerated ooids may display meniscus cements at grain contacts (figure 24F). Nuclei include quartz grains, well-rounded peloids (some with micro-pyrite; figure 24G), broken ooid fragments, chert grains, igneous (volcanic?) rock fragments, and micro-

Figure 23. *Hypersaline ooids, Antelope Island.* ***(A)*** *Complex of microbial and associated oolitic beach deposits along Bridger Bay.* ***(B)*** *Close-up of beach deposits consisting of ooids and coated grains.*

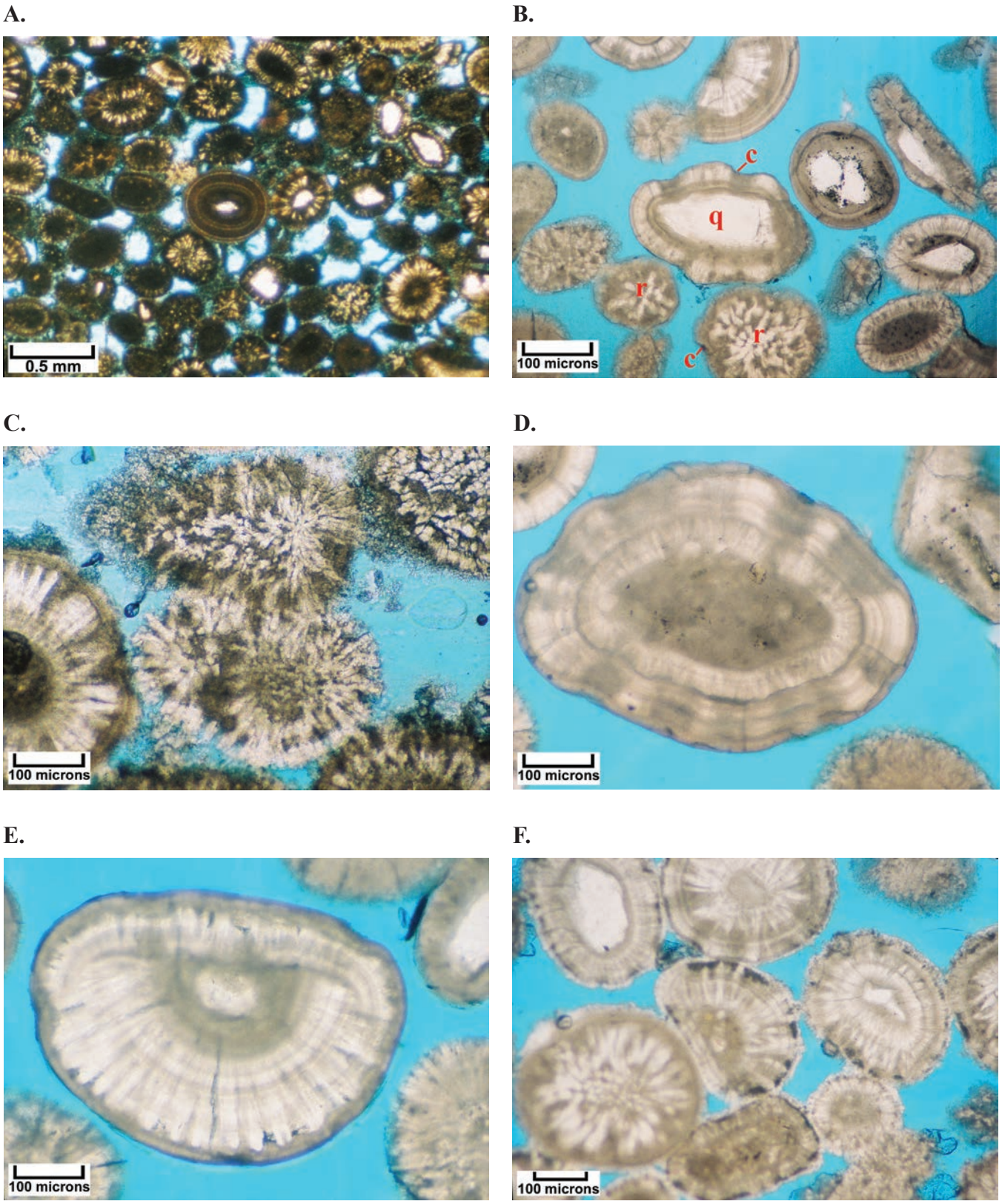

Figure 24. *Photomicrographs of carbonate grains and cements, Antelope Island.* ***(A)*** *Overview of medium- to well-sorted hypersaline oolitic sands. Note the abundance of interparticle micrite cement (plane light).* ***(B)*** *Sample of loose (unconsolidated) ooids displaying various characteristics such as radial recrystallization (r), "cerebroid" margins (c), and regeneration. Note ooid with quartz nucleus (q) near center of the image (plane light with white card).* ***(C)*** *Typical ooids displaying extensive syndepositional radial recrystallization and rough, irregular grain margins and partial micritization (plane light).* ***(D)*** *Ooid with embayed or cerebroid margins (plane light with white card).* ***(E)*** *Regenerated ooid in which a broken ooid has been surrounded by oolitic cortex coatings (plane light).* ***(F)*** *Regenerated ooids and meniscus cements at grain contacts (plane light with white card).*

G.

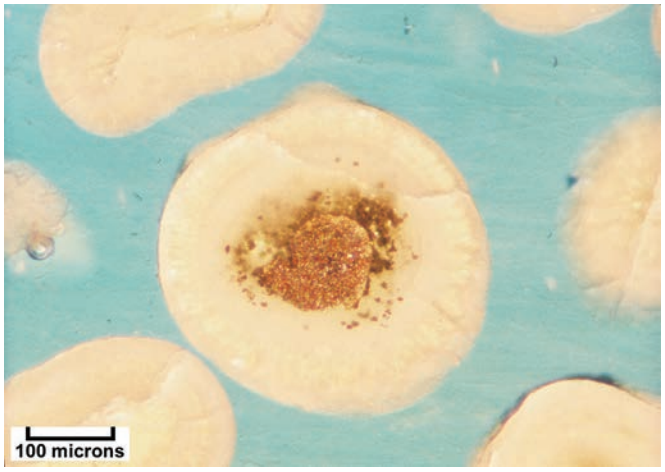

H.

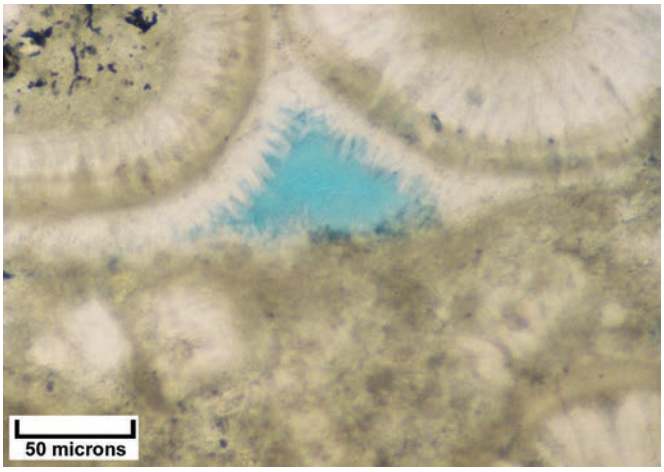

Figure 24 continued. *Photomicrographs of carbonate grains and cements, Antelope Island.* ***(G)*** *Single ooid with a brassy pyritic nucleus (plane light with white card).* ***(H)*** *Ooid contacts that are lithified by isopachous rims of acicular radial cements lining larger pores as well as micritic cements that fill smaller pores (plane light with white card).*

bialite fragments. Kahle (1974), Halley (1976), and Pedone and Norgauer (2002) described in detail these radial fabrics and their role in the syndepositional breakage and regeneration of ooids on the shorelines of Great Salt Lake. The petrography of the early ooid fabrics in Great Salt Lake could be useful in distinguishing hypersaline or non-marine ooids from marine ooids in ancient rocks. Finally, Paradis (2019) used radiocarbon chronology to show slow radial growth of ooids from Bridger Bay (and the south arm) and which could provide high-resolution records of Holocene stable isotope history and lake level change. Futhermore, relict DNA in ooid nuclei pertain to biogenicity (e.g., brine shrimp gut microbiota contain similar DNA), which can be used to analyze the relationship between microbial communities and ooids (Paradis, 2019).

Wave energy in Bridger Bay breaks up and redeposits cemented oolitic fragments, creating an oolitic grainstone/rudstone beachrock (figure 21B). The oolitic grainstone cements include (1) micritic cement (precipitated from Great Salt Lake water either microbially or inorganically), (2) isopachous microfibrous cement (from phreatic Salt Lake brines [inorganic]), (3) acicular patchy cement of unknown origin, and (4) radially bladed cement that inherits the crystal orientation and morphology of the radial recrystallized bundles within certain ooids (figure 24H). These cements are apparently all aragonite, and some may have formed rapidly with the assistance of nanobacteria (Pedone and Folk, 1996; Pedone and Norgauer, 2002).

Rozel Point

The water in the north arm of Great Salt Lake has reached salt saturation due to the construction of the railroad causeway bisecting the lake. One of the results was that the microbes that formed microbialites in the north arm could not survive in such a highly saline environment. Remains of microbialites occur near the shore at Rozel Point, west of the Promontory Mountains (figure 25). The microorganisms that formed these microbialites are no longer present and the domes are desiccated and eroded. Wave action and the episodic precipitation of halite crystals within the pores of the weathered microbialites have hastened their erosion (figure 25E). A continuous pavement of carbonate extends perpendicular to the shoreline (figure 25C) and locally contains the remains of desiccated circular microbialites, similar to the circular structures at Bridger Bay (figure 25D).

Many of the structures at Rozel Point (possibly associated with lake-margin springs) consist of pustular thrombolitic textures in their interiors, becoming more layered and laminated near their surface (figure 25B). Primary constructional pores are commonly associated with the microbial heads or tufa (figures 25B, 26A, and 26B); large open pores and vugs are often lined or nearly completely filled with acicular radial cements (figures 26C and 26D). Beach deposits consist of hypersaline ooids, coated grains, and intraclasts composed of oolites, pellet grainstones, and coated microbial and rock fragments. Beachrock clasts can be well lithified and composed of pellets surrounded by dense microfibrous cements (figure 26E). Some ooids are asymmetrical with compound nuclei of angular microbialite (figure 26F); other nuclei may consist of peloids or igneous rock fragments (figures 26G and 26H).

The microbialite material closer to shore and at lower elevations consists of eroded and dessicated microbialites similar to those at Bridger Bay (figures 25C through 25E). The material farther from shore and at higher elevations could be remnants of Pleistocene microbialtes similar to those found at Lakeside near the western side of the lake (figure 17). However, some of the higher-elevation material (broken and disturbed) is from spring mounds.

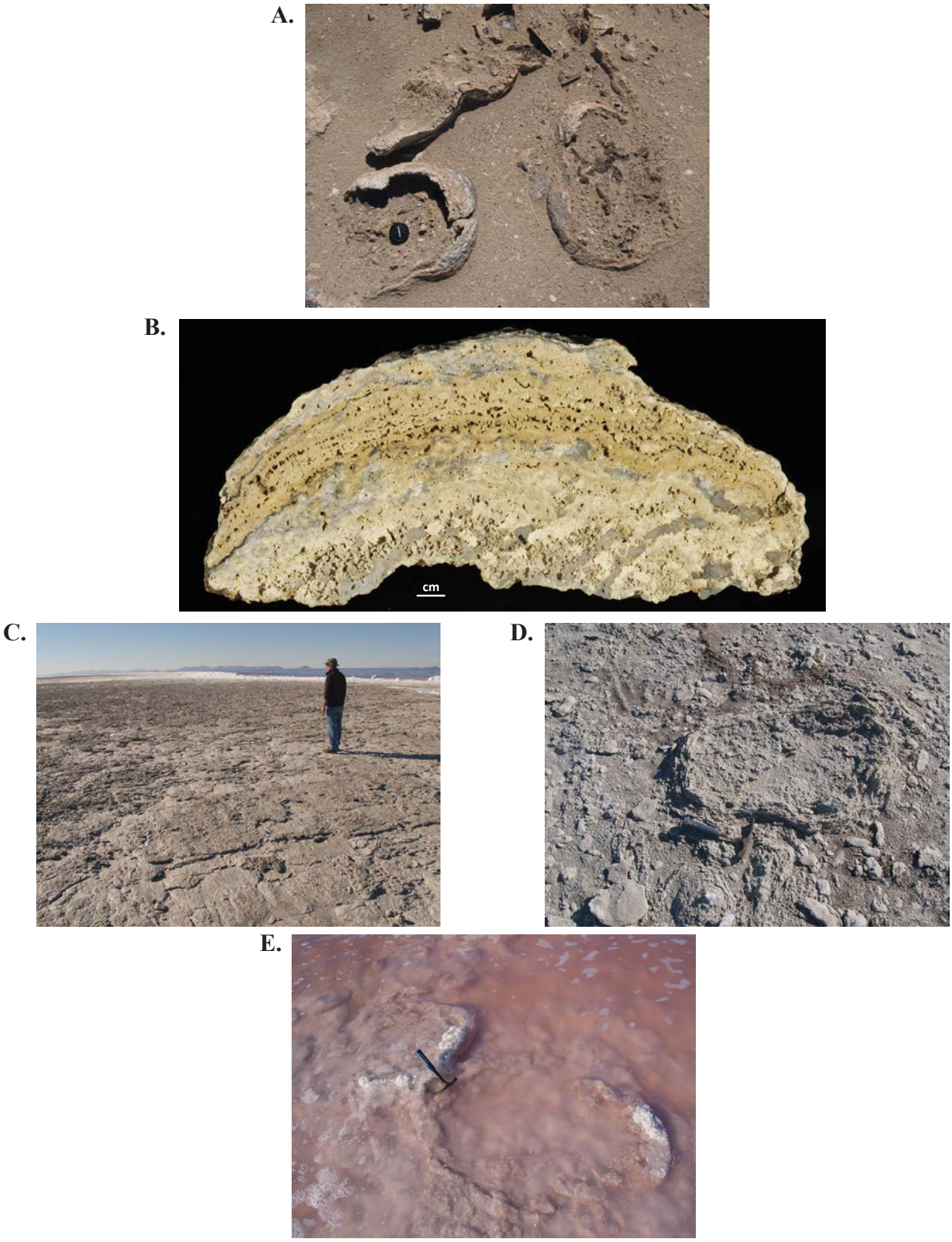

Figure 25. *Examples of Great Salt Lake relict Holocene microbialites and associated grains, Rozel Point.* ***(A)*** *Remains of relict domal (degraded) microbialite structures within oolitic sand. Black camera lens cap for scale (6 centimeters in diameter).* ***(B)*** *Close-up of sliced microbialite displaying well-developed laminations and abundant constructional pores.* ***(C)*** *Lithified relict microbial pavement/hardground, similar to the microbialites in Bridger Bay, but the Rozel Point deposits are desiccated and eroded.* ***(D)*** *Eroded remains of a circular relict microbialite dome within the hardground. Hammer for scale.* ***(E)*** *Circular relict microbialite dome encrusted with halite. Hammer for scale. The pink coating is caused by photosynthetic halophylic bacteria (Collister and Schamel, 2003).*

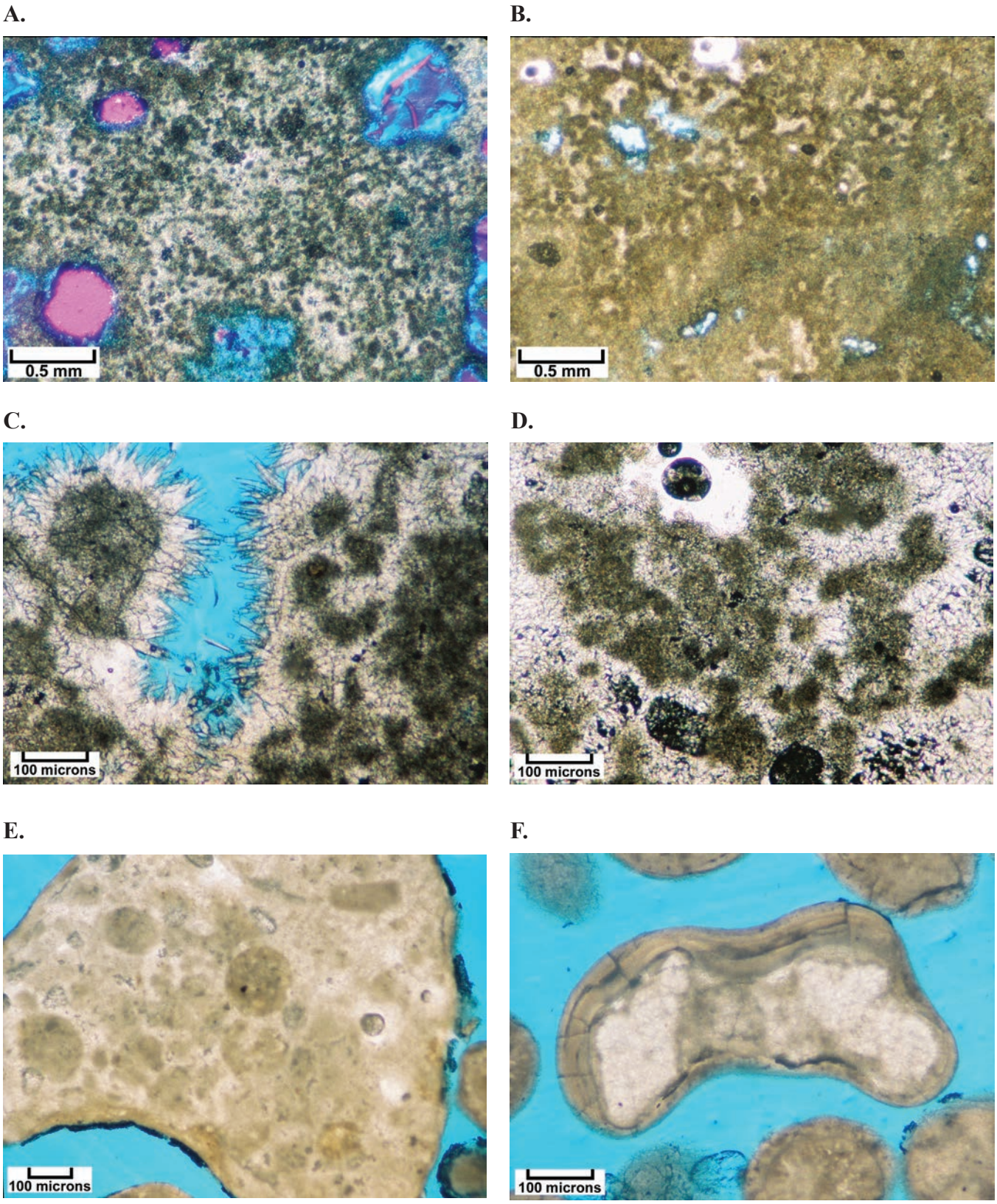

Figure 26. *Photomicrographs of relict Holocene microbialites and associated carbonate grains and cements, Rozel Point.* ***(A)*** *Close-up view of clotted microbialite dome interior including primary constructional pores (crossed nicols with gypsum plate).* ***(B)*** *A different view of clotted microbialite dome interior and open constructional pores (plane light).* ***(C)*** *Close-up view of constructional pores within a microbialite dome; pores are completely lined with radial acicular cements (plane light).* ***(D)*** *Tightly cemented microbialite pores filled with acicular crystals (plane light).* ***(E)*** *Well-lithified beachrock clast composed of peloids surrounded by dense microfibrous cements (plane light).* ***(F)*** *Asymmetrical ooid with a compound nucleus consisting of two angular microbialite fragments (in white) (plane light).*

G.

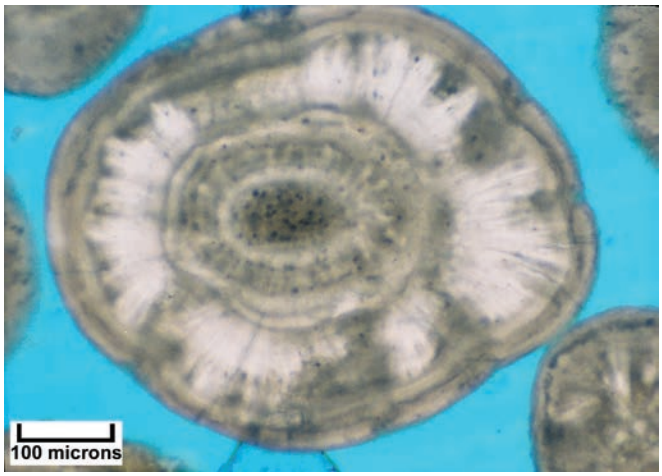

H.

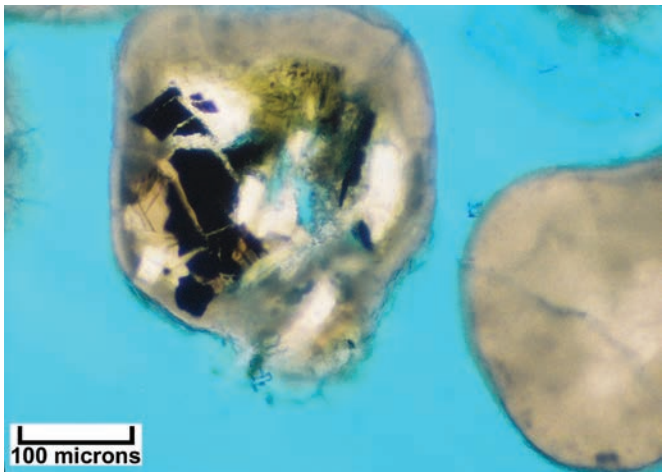

Figure 26 continued. *Photomicrographs of relict Holocene microbialites and associated carbonate grains and cements, Rozel Point.* ***(G)*** *Cerebroid ooid displaying radial recrystallized cortex bands (in white) coated by tangential oolitic coatings. Note the irregular or 'bumpy" grain outline and the peloidal nucleus (plane light with white card).* ***(H)*** *Ooid with asymmetrical cortex coatings around a nucleus composed of an igneous rock fragment (plane light with white card).*

Travertine/tufa deposits, composed primarily of barite, are well displayed at Rozel Point and are associated with active springs (figure 27). They attest to the possible relationship between groundwater and the development of microbialites around Great Salt Lake.

Synopsis and Discussion

Great Salt Lake contains excellent examples of Pleistocene to Holocene microbial carbonates and associated carbonate grains in a hypersaline lacustrine setting. The high salinity, wave energy, temperature, water depth, etc., have been ideal for microbial and carbonate grain formation from thousands of years ago to the present. The type, shape, and size of microbialites varies with wave energy and other lake conditions. The shallow ramp margins of the lake and the resulting widespread shoreline shifts have contributed to the extensive distribution of Great Salt Lake microbialites and oolites. Thus, in addition to the specific sites we have described, there are many other similar microbialite localities in and around the lake that warrant detailed study—both geologic and biologic—to better understand microbialite growth, characteristics, types, and environmental conditions. Finally, as we will show, microbialites in the lacustrine Green River Formation, as well as in marine rocks from producing oil fields, exhibit many similarities to those in Great Salt Lake.

UTAH'S "BEST" MICROBIALITES IN CORE AND OUTCROP – EOCENE GREEN RIVER FORMATION

The Green River Formation in the Uinta Basin, both in core and outcrop, has Utah's "best" microbialite occurrences that provide excellent opportunities to study the fundamentals of lacustrine depositional settings, lacustrine sediment cycles, diagenetic alteration, and reservoir-quality carbonates. The Green River carbonates that we have studied in the Skyline 16 research core and at several superb outcrops (four described in this paper) in the Uinta Basin (figure 28) are non-marine lacustrine sediments that could be similar to the possible giant microbialite, Lower Cretaceous reservoirs in the offshore pre-salt Brazilian basins and Kwanza Basin of offshore Angola (Carminatti and others, 2008, 2009; Nakano and others, 2009; Wright and Barnett, 2015; Saller and others, 2016). Besides serving as analogs for worldwide microbialite reservoirs, they may also have resource potential. Green River microbialites are an important part of at least one conventional oil field within the Uinta Basin—West Willow Creek field (figure 29) (Osmond, 2000).

Geologic Overview of the Uinta Basin

The Uinta Basin is the most prolific petroleum province in Utah. It is a major is a major structural basin, which subsided during the early Cenozoic along the southern flank of the Uinta Mountains. Lake deposits filled the basin between the eroding Sevier highlands to the west and the rising Laramide Uinta Mountains, Uncompahgre uplift, and San Rafael Swell to the north, east, and south, respectively, during Eocene time. Lake Uinta formed within Utah's Uinta Basin and Colorado's Piceance Creek Basin (figure 29). At times of low water level, the Douglas Creek arch separating the two basins was exposed, creating two distinct lakes.

The Green River Formation consists of as much as 2000 meters (6000 ft) of sedimentary strata (figures 28, 30, and 31; Hintze and Kowallis, 2009; Sprinkel, 2009, 2018) and contains three major depositional facies associated with Lake Uinta sedimen-

A.

B.

Figure 27. *Travertine/tufa deposit, Rozel Point.* ***(A)*** *Small travertine/tufa deposit and active associated spring.* ***(B)*** *Closer view of spring and associated tufa/travertine deposits.*

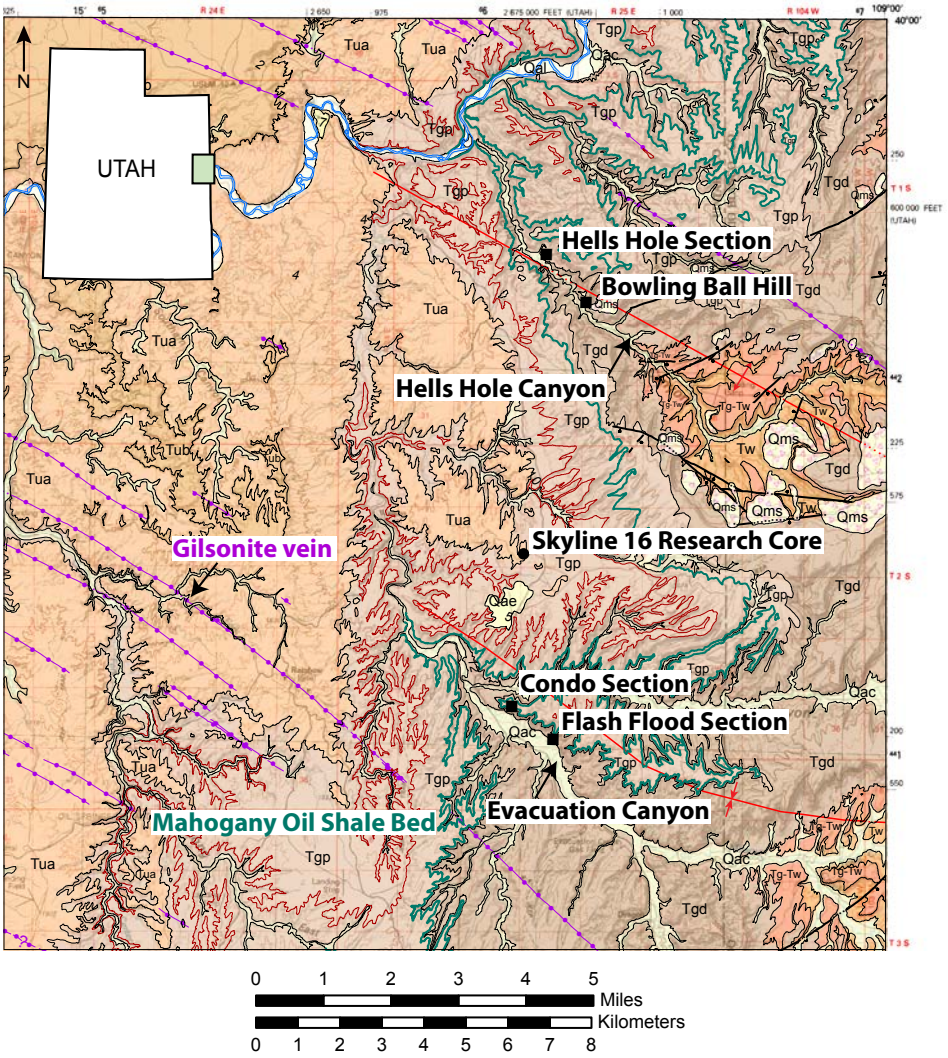

Stratigraphic Column

System	Symbol	Formation	Thickness (meters) (not to scale)	Lithology	Notes
Quaternary	Q	Unconsolidated deposits	less than 50		Qal - stream alluvium, Qms - alluvial fan deposits, Qac - alluvium/colluvium, Qae - alluvium/eolian
Tertiary	Tub	Member B of Uinta Formation	30–225		Contains gilsonite deposits
	Tua	Member A of Uinta Formation	60–180		
	Tgp	Parachute Creek Member of Green River Formation	247–950		Tuffaceous bed B Horse Bench Sandstone Bed Mahogany oil shale zone
	Tgd	Douglas Creek Member of Green River Formation	45–520		Uinta Mountains continue to uplift and erode; creation of Lake Uinta as the Uinta Basin continues to subside; contains oil shale and oil reserves Long Point Bed
	Tg-Tw	Green River-Wasatch Formations transition zone	60–220		
	Tw	Wasatch Formation	280–830		Uinta Mountains continue to uplift and erode, locally exposing the Uinta Mountain Group; subsidence of Uinta Basin; gas reservoir in Uinta Basin

Figure 28. *Geological map of a part of the eastern Uinta Basin showing the locations of selected outcrop sections described in this study (black squares) as well as the Skyline 16 research well. Modified from Sprinkel (2009).*

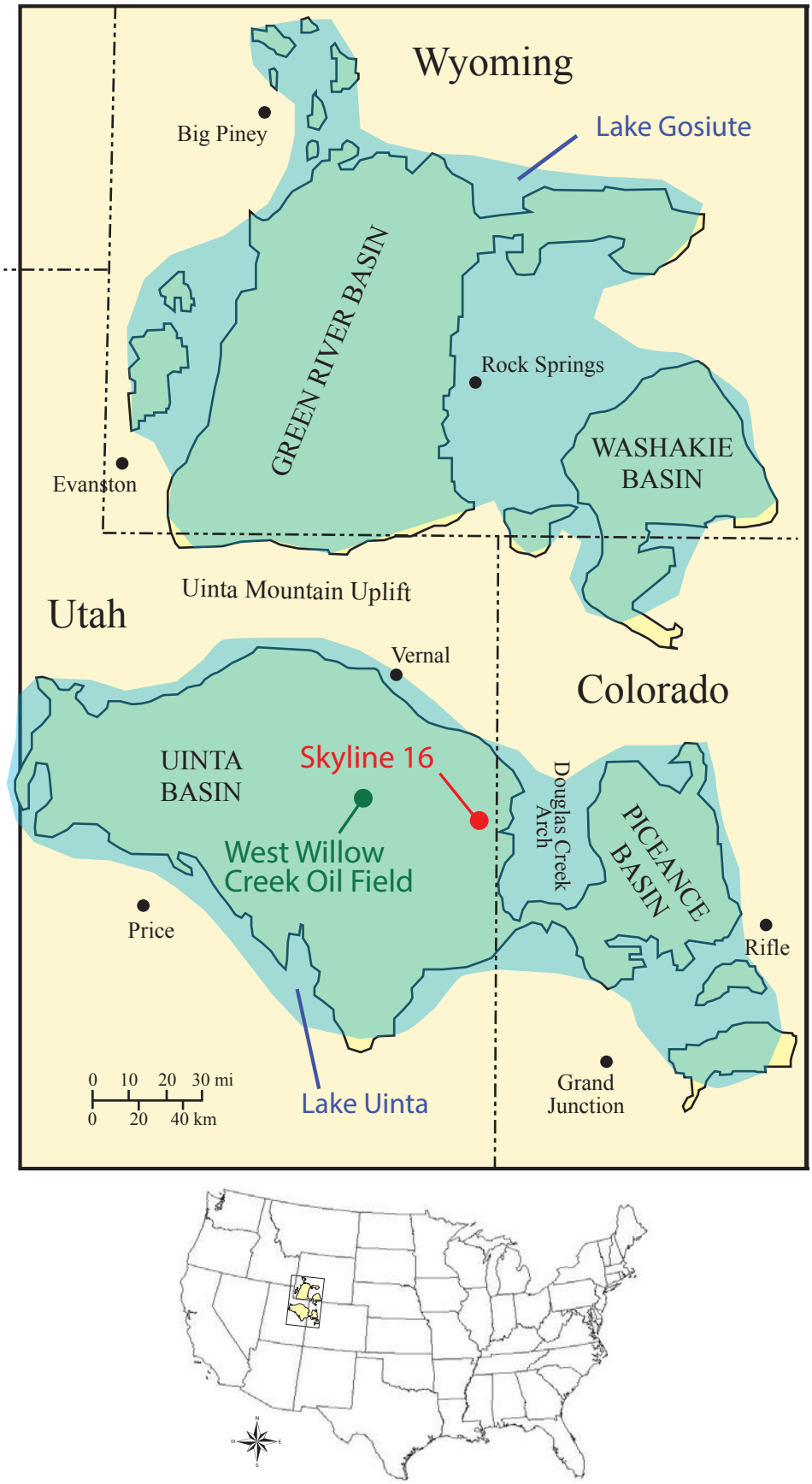

Figure 29. *Ancient Eocene lake basins of the Rocky Mountain West. Lake Gosiute occupied the Green River and Washakie Basins in Wyoming, while Lake Uinta filled the Uinta and Piceance Creek Basins in Utah and Colorado. Note the locations of the Skyline 16 research core and West Willow Creek oil field. Modified from Vanden Berg (2011).*

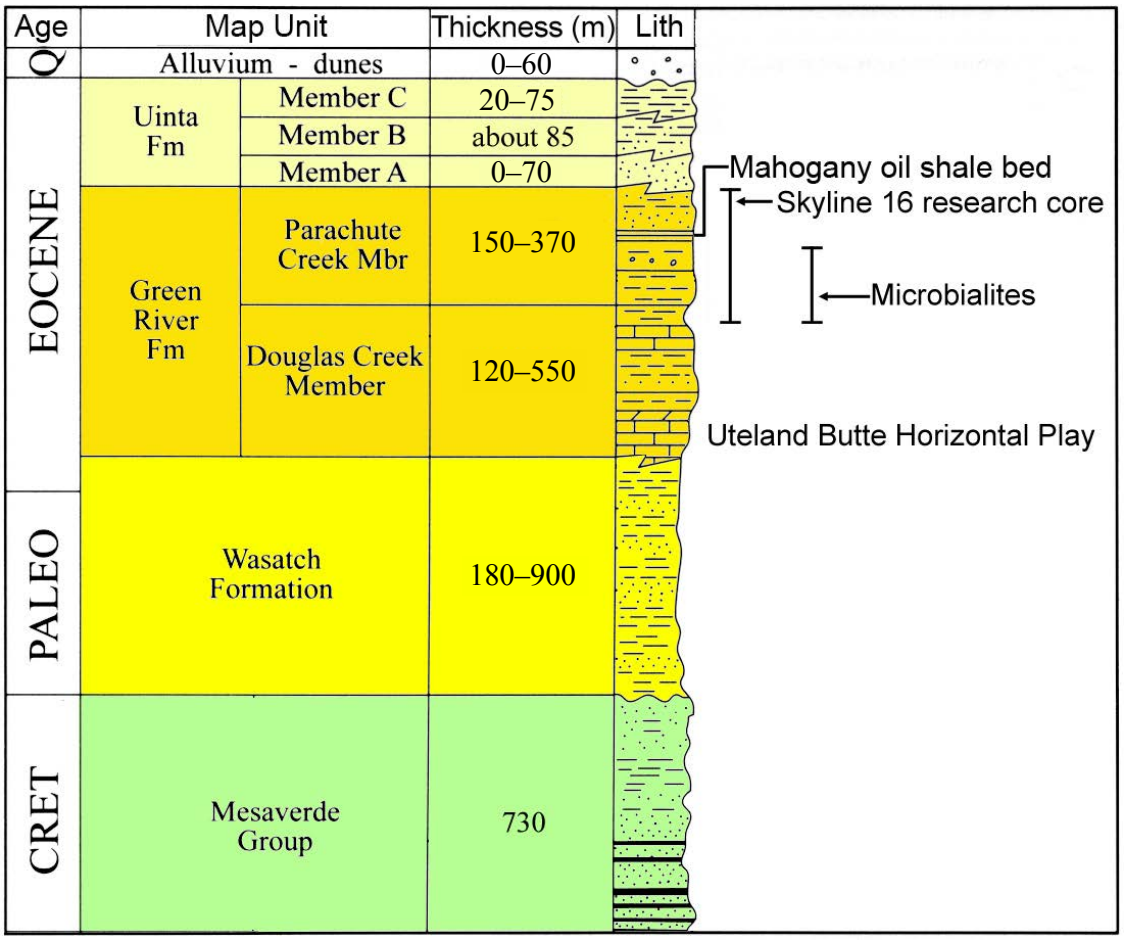

Figure 30. *Stratigraphic column, eastern Uinta Basin. Note the stratigraphic position of the entire Skyline 16 cored interval (left bar) and the interval in which microbialites and associated carbonate facies occur (right bar). In addition, the location of the famous Mahogany oil shale bed is also shown. Modified from Hintze and Kowallis (2009).*

tation: alluvial, marginal lacustrine, and open lacustrine (Fouch, 1975; Ryder and others, 1976). A generalized basin and regional-scale depositional setting model for Lake Uinta compares lake-level highstands, when carbonate deposition was widespread (figure 32A), to lowstands, when siliciclastic alluvial, fluvial, and eolian sediments were more common (figure 32B). The marginal lacustrine facies, where most of the hydrocarbon-producing reservoirs occur, consist of fluvial-deltaic, interdeltaic, and carbonate flat deposits, including microbial carbonates. The open lacustrine facies is represented by nearshore and deeper water offshore muds, including the famous Mahogany oil shale zone, which represents Lake Uinta's highest water level (U.S. Geological Survey Oil Shale Assessment Team, 2010; Tänavsuu-Milkeviciene and Sarg, 2012).

The Uinta Basin is asymmetrical to the north, paralleling the east-west-trending Uinta Mountains. The northern flank dips 10° to 35° into the basin and is bounded by a large north-dipping, basement-involved thrust fault. The southern flank gently dips between 4° and 6° north-northwest. The Green River Formation is well exposed in canyons along the southern and eastern margins of the basin providing exceptional three-dimensional access to the rocks (figure 28).

Applicable Previous Studies

Bradley (1929) was one of the first researchers to recognize the abundant microbialites (in particular, stromatolites) and several associated carbonate grains in the Green River Formation. Other early researchers (e.g., Ryder and others, 1976; Surdam and Wray, 1976) also used the generic term *stromatolite*, derived from "blue-green algae" (later identified as cyanobacteria), without any additional detailed descriptions or specific discussions of microbialites. Platt and Wright (1991) classified the Uinta Basin during Green River deposition as a foreland basin with low-gradient ramp margins with "bioherms" and stromatolites. Remy (1992) described the C marker bed in the Green River section in Nine Mile Canyon, south-central Uinta Basin, as containing large domal and tube-type stromatolites and oncolites.

Recent studies have focused attention more specifically on the Green River Formation microbialites in Wyoming's Greater Green River Basin (Lake Gosiute). Leggitt and others (2007) discussed paleoenvironments associated with the caddisfly-dominated microbial mounds of the Tipton Member of the Green River in southwest Wyoming, whereas Miller (2011)

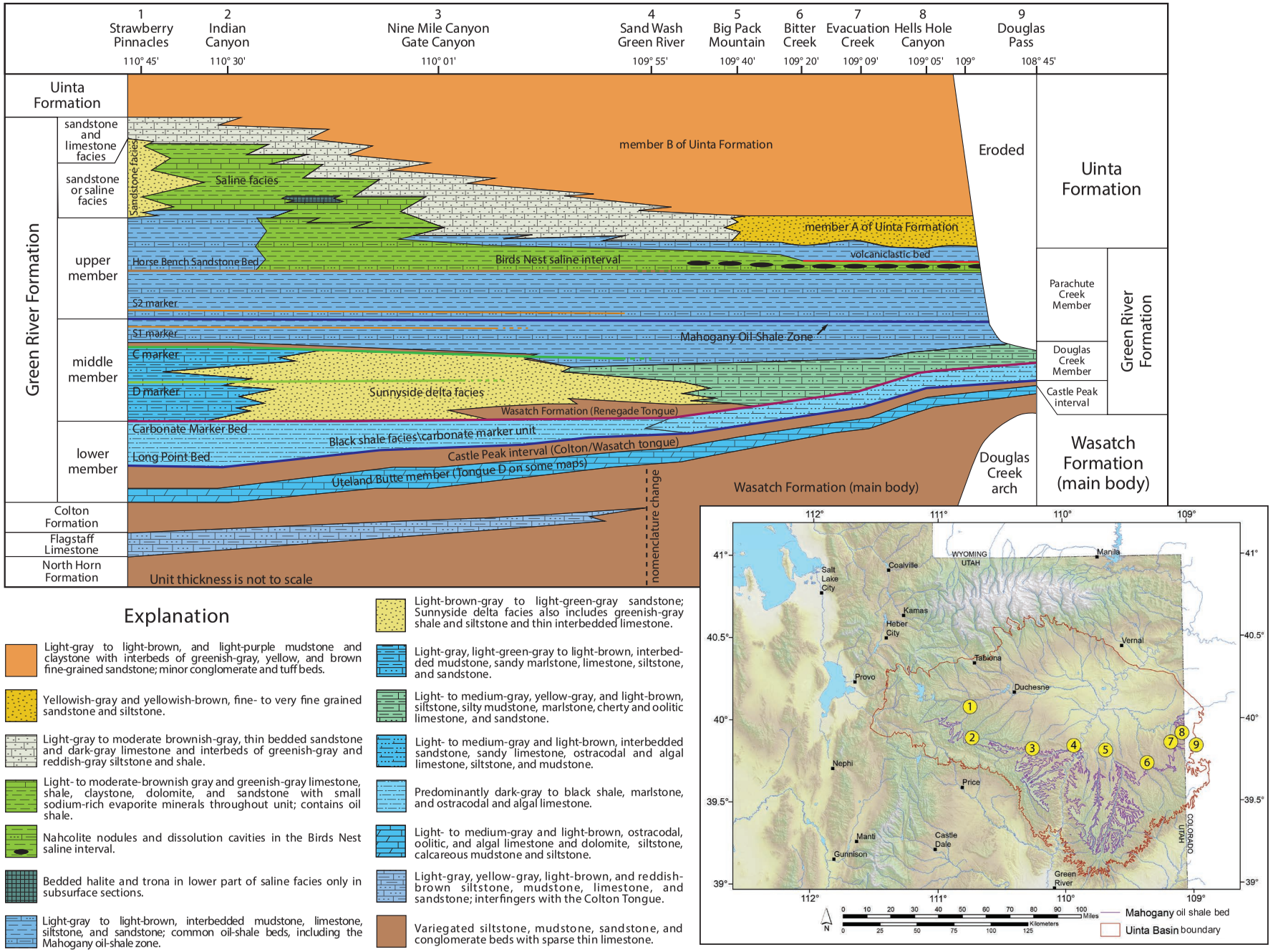

Figure 31. *General stratigraphy and major marker beds of the Green River Formation in the Uinta Basin. After Sprinkel (2018), modified from Töro and Pratt (2015) using Cashion (1967), Fouch and others (1994), Johnson and others (1988, 2010), Morgan and others (2003), Smith and others (2008), Tänavsuu-Milkeviciene and Sarg (2012), and Vanden Berg and others (2013).*

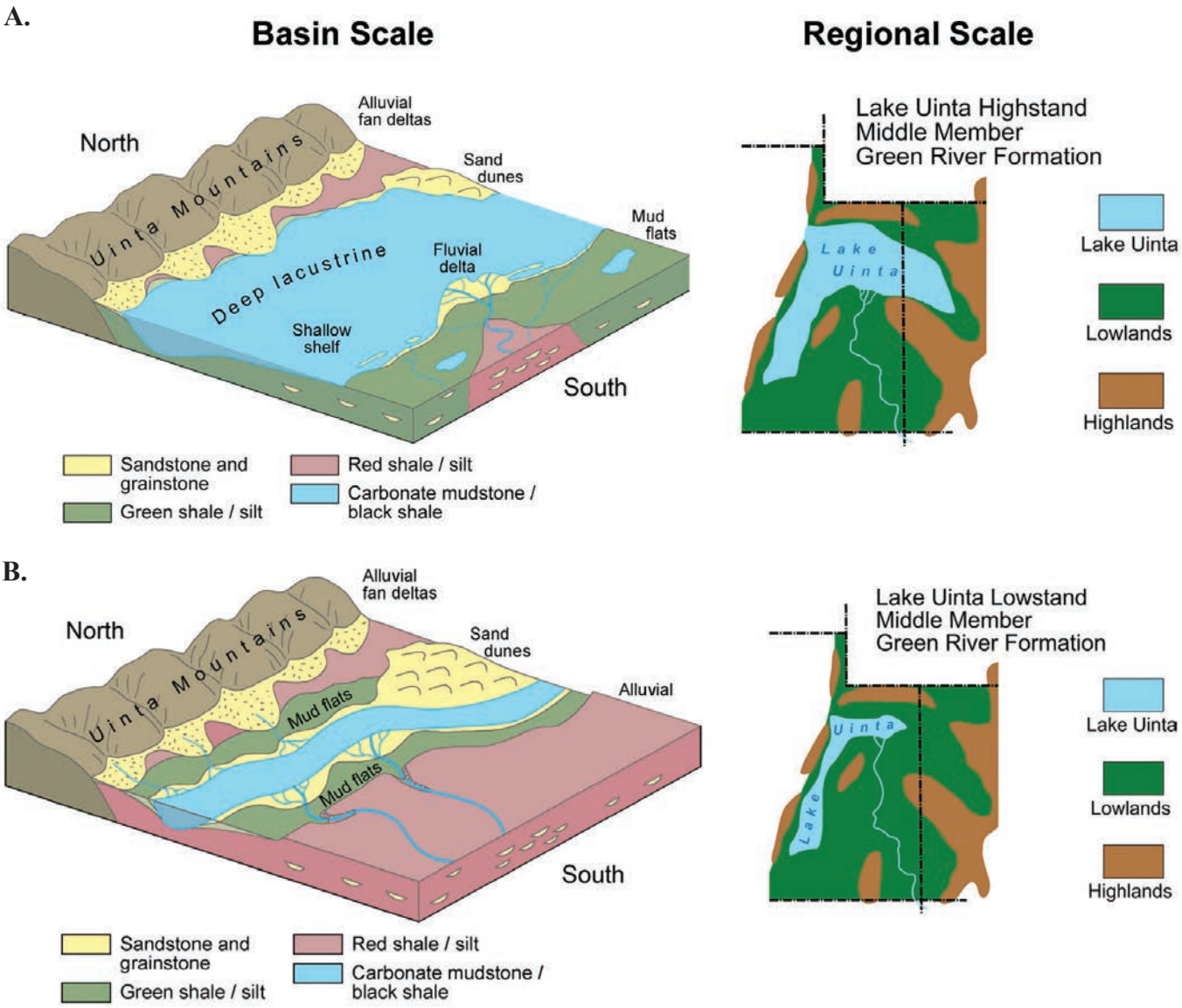

Figure 32. *Generalized basin and regional scale depositional setting for Lake Uinta:* ***(A)*** *High-lake levels, and* ***(B)*** *Low-lake levels. The Uinta Mountains were the source for the sediments in the northern part of the lake while sediments in the southern part of the lake were sourced from the much larger Four Corners area. From Morgan and others (2003).*

described branching in stromatolites and their biogenicity, also in the Tipton Member. Buchheim and others (2010, 2012) presented basic descriptions, stratigraphic architecture, sequence stratigraphy, and a depositional model for microbialite "bioherms" in the northwestern part of the Greater Green River Basin, whereas Buchheim and Awramik (2012) generally described the basic facies associations containing Green River microbialites to predict lacustrine microbialite distribution. In addition, Sarg and others (2013) described how microbial lithofacies and other carbonate rocks correlate to the evolution of Lake Uinta in the western Piceance Creek Basin of Colorado. Sarg and others (2013) also discussed syndepositional to burial diagenesis and its effect on the porosity of microbialite layers. Awramik and Buchheim (2013) and Buchheim and Awramik (2013) presented findings comparing the Green River microbialites to the South Atlantic pre-salt carbonate reservoirs. Swierenga and others (2015) described the depositional history and lateral variability of Green River microbial carbonates along an obliquely basinward transect, from shoreline to nearshore facies, of outcrops in Nine Mile Canyon of the south-central part of the Uinta Basin. Finally, Borer (2016) described the Green River algal (microbial) boundstone and grainstone carbonate facies in the northeast part of the Uinta Basin in outcrops at Raven Ridge along the border with Colorado, and in cores from Redwash oil field. The boundstones are composed of isolated or laterally continuous, laminated to thrombolitic, dome-shaped and spheroidal microbial heads representing shoal-crest, foreshore, or offshore depostional environments. The grainstones, and packstones, consist of ooids, peloids, and ostracods representing a shoal front/back to offshore storm-bed depositional environment (Borer, 2016).

Skyline 16 Research Core

The 300-meter-long (1000 ft) Skyline 16 research core, taken in 2010, recovered the upper part of the Douglas Creek Member and nearly all of the Parachute Creek Member of the middle to upper Green River Formation (figure 33 and plate 1) (Vanden Berg and Birgenheier, 2016). The original purpose of the Skyline 16 was to obtain a core through the Mahogany and other oil shale beds. Fortunately, the core also penetrated multiple intervals of microbialites and associated carbonate grains. Located in the easternmost part of the Uinta Basin, the Skyline 16 well (section 10, T. 11 S., R. 25 E., Salt Lake Base Line & Meridian [SLBL&M], Uintah County, Utah) is about 4 kilometers (2.5 mi) north and 6 kilometers (3.7 mi) south of excellent Green River outcrops in Evacuation Creek (proximal) and Hells Hole Canyon (distal), both of which display similar lacustrine facies, cycles, and microbial fabrics (megascopically and petrographically), as well as associated grain types, observed in the Skyline 16 core (medial) located between these outcrop sites (figure 28).

A suite of 13 thin sections was prepared for several of the microbialite and associated facies in the Skyline 16 research core. Together, thin section photomicrographs and close-up core photographs show a remarkable array of fabrics, textures, and preserved porosity types that are likely to be encountered in possible microbialite reservoirs like those hosted in Lower Cretaceous pre-salt carbonates in offshore Brazil and Angola. It is important to note that in the Skyline 16 core, microbialites and grainstones make up less than 10% of the interval where they occur, but they probably account for most of the megascopic (visible) porosity in this lacustrine system.

General Core Evaluation

The continuous core (figure 33 and plate 1; see the appendix for core box photographs) was located near the eastern part of the ancient lake, along the western flank of the Douglas Creek Arch (figure 29). The lower two-thirds of Skyline 16 core records an overall Lake Uinta transition from "shallow" to "deep" lake, with the Mahogany zone representing the highest lake level (U.S. Geological Survey Oil Shale Assessment Team, 2010; Tänavsuu-Milkeviciene and Sarg, 2012). In addition, the core records smaller-scale littoral to profundal deposition in distinct 1- to 2-meter (3–6 ft) cycles (figure 33 and plate 1) indicative of a shallow ramp environment, similar to present-day Great Salt Lake shorelines and which produced the same results—the susceptibility to rapid, widespread shoreline changes. In general, the Douglas Creek part at the base of the core is dominated by shallowing-upward sequences of gray mudstone, siltstone, and sandstone gradually transitioning to well-developed microbial carbonate intervals, topped by a flooding surface and a rapid transition back to profundal facies. The lower Parachute Creek Member, in particular the R-4 and R-5 zones (referring to the rich/lean oil shale nomenclature used in the oil shale of Donnell and Blair [1970] and Cashion and Donnell [1972]), records fully carbonate-dominated deepening-upward sequences, with profundal dark brown, organic-rich carbonate mudstone at the top of the cycle and light tan, dolomitic microbial carbonate in the middle of the cycle (figure 33 and plate 1). Deepening-upward sequences can be observed in outrops of the Douglas Creek Member of the Green River Formation along Nine Mile Canyon in the south-cental Uinta Basin (Morgan, 2003; Swierenga and others, 2015). Green River microbialites in southwestern Wyoming grow during transgressions (Stanley M. Awramik, University of California Santa Barbara, verbal communication, 2018). Carbonate grainstones composed of ooids, coated grains, pisoids, peloids, and carbonate rip-up clasts often precede the microbial growth.

Microbialites and Associated Grains

Reservoir quality in lacustrine carbonate microbialites can be highly dependent on the construction and preservation of porosity within the matrix of microbial structures and associated sediments (e.g., Osmond, 2000; Parcell, 2002; Ahr and others, 2011; Wasson and others, 2012). The Skyline 16 research core provides excellent examples of both megascopic pores and microporosity in different microbialite types and associated grainstones.

Stromatolites observed in the Skyline 16 core typically grew on substrates composed of beach deposits consisting of ooids, pisolites, oncoids, ostracods, and/or carbonate rip-up clasts, indicating a deepening cycle rather than a shallowing cycle. The synoptic relief of stromatolitic domal heads diminishes upwards with oolitic and peloidal sediments filling the spaces in between the domes (figure 9A). Branching digitate stromatolites are also common and grew on a substrate of peloidal dolomite mud having apparent erosional relief (figure 34A), although the effects of differential erosion and compaction cannot be ruled out. Low-relief stromatolites are commonly interbedded with ooids, peloids, and stromatolitic rip-up clasts (figure 34B). Primary porosity is preserved within the stromatolitic intervals (figures 34C through 34F). Megascopic pores are the result of constructional growth processes associated with both tubular and pustular microfabrics (figure 34E). Considerable microporosity, determined petrographically, also occurs within the very fine grained or dense stromatolitic carbonates (figure 34F).

Thrombolites occur as low-relief shrubby heads associated with oolitic and intraclastic (rip-up clasts) grainstone (figure 11A). Most thrombolites are draped with stromatolitic laminae. Areas between the dense microbial clots are white sparry calcite cement (figure 11B). The thrombolites in the Skyline 16 core typically preserve greater amounts of megascopic porosity than the stromatolites (compare figures 16B and 35A with figure 34C through 34E). Megascopic pores are intimately associated with clotted constructional fabrics and the pores often touch one another,

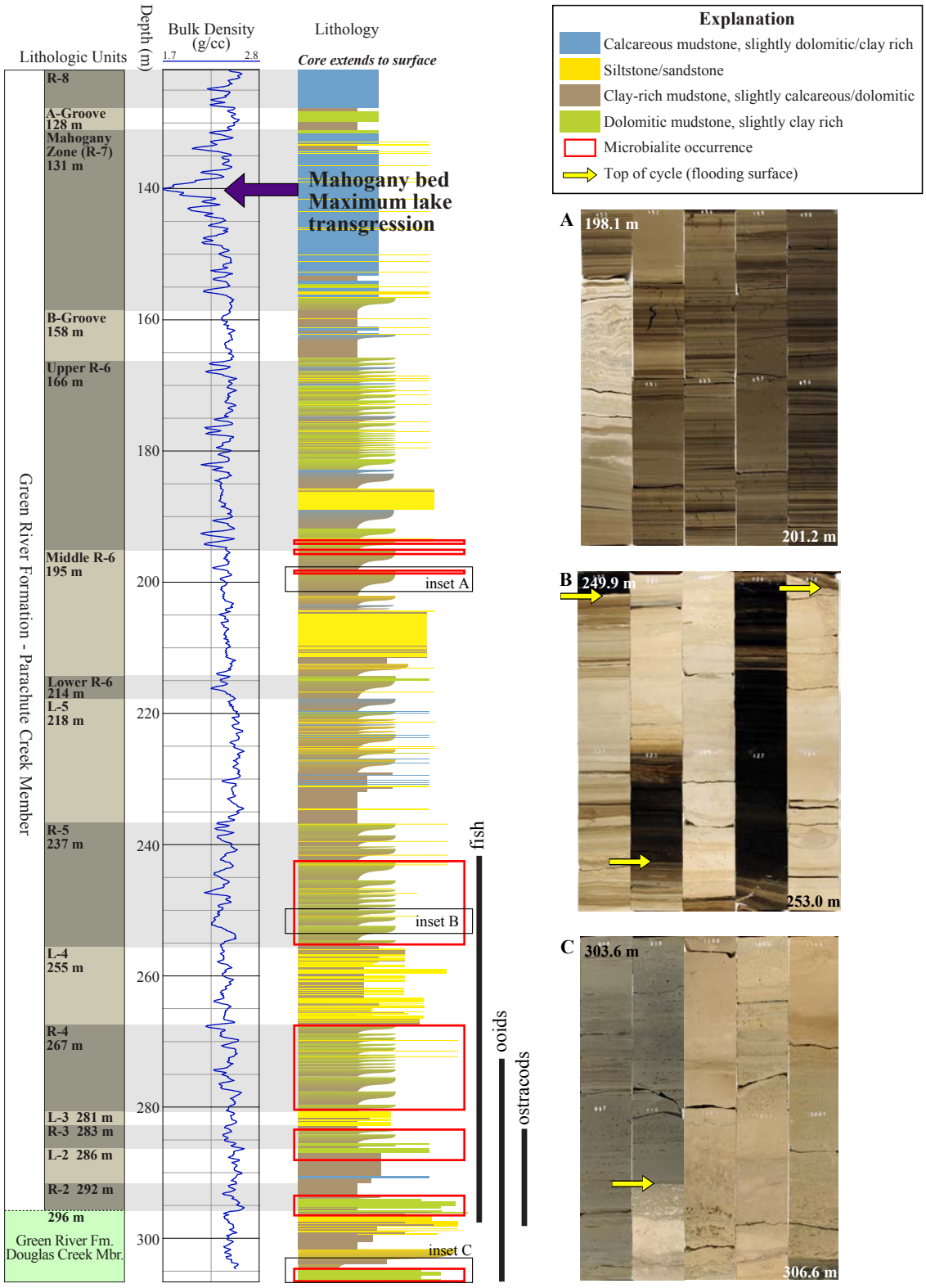

Figure 33. *Graphical description of Skyline 16 research core showing the location of microbialite deposition (also see plate 1). Lithologic units refer to rich (R) and lean (L) oil shale stratigraphic nomenclature as first described by Donnell and Blair (1970) and Cashion and Donnell (1972). Bulk density inversely correlates with overall organic richness. The richest interval is the Mahogany zone, in which the very organic-rich Mahogany bed is interpreted as the lake's maximum transgression in the Uinta Basin (U.S. Geological Survey Oil Shale Assessment Team, 2010; Tänavsuu-Milkeviciene and Sarg, 2012).* ***(A)*** *Final occurrence of microbialites (whitish beds) in the R-6 oil shale zone, which is mostly profundal facies.* ***(B)*** *Typical deepening-upward carbonate cycle (dark organic-rich carbonate mud transitioning to organic-lean, light tan, microbial carbonate) found in the R-4 and R-5 oil shale zones of the Parachute Creek Member. Yellow arrows indicate top of cycle.* ***(C)*** *Typical deepening-upward siliciclastic/carbonate cycle (organic-lean, gray mud to silts transitioning to light tan microbial carbonate) found in the Douglas Creek Member.*

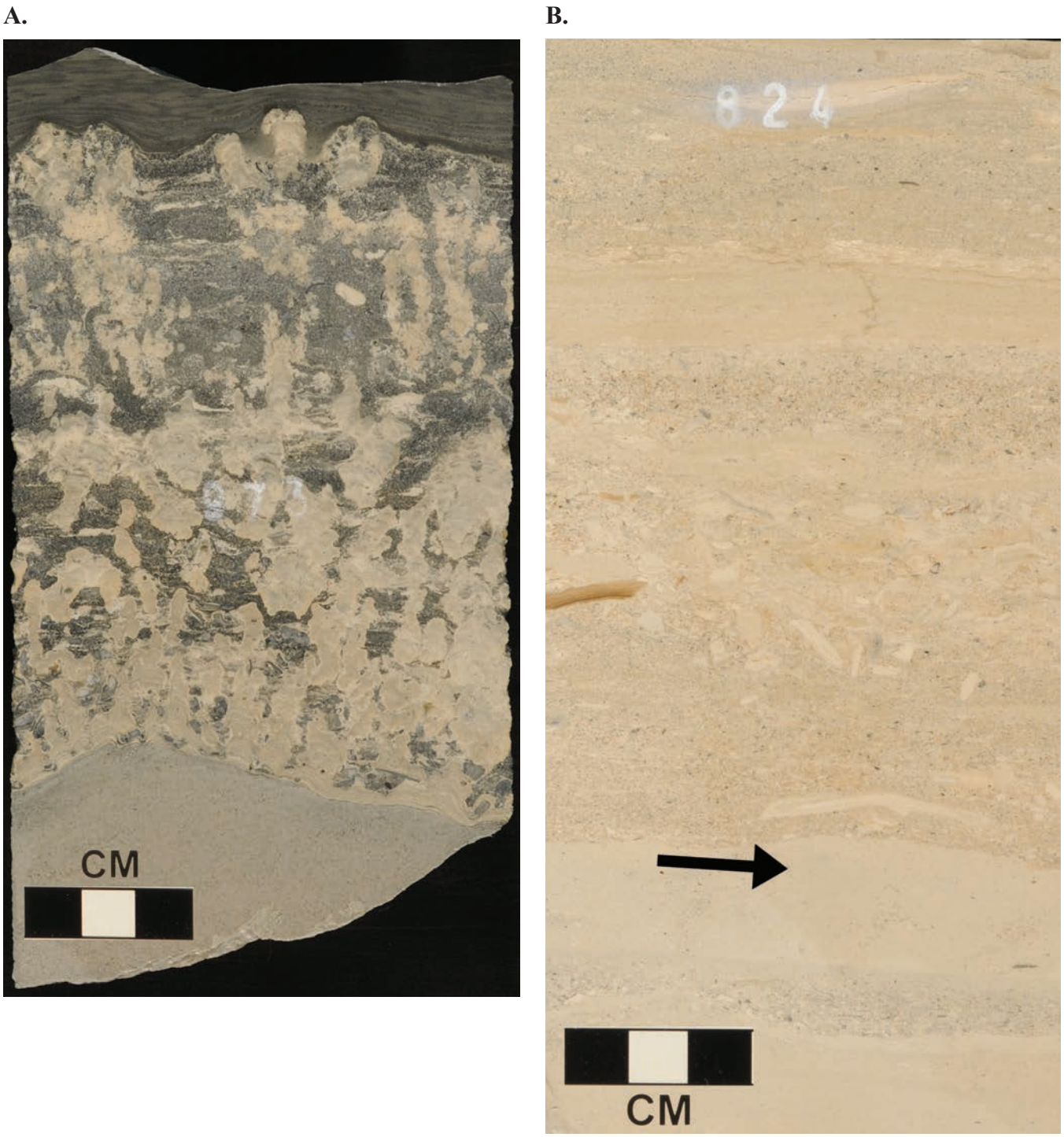

Figure 34. *Stromatolites from the Skyline 16 research core.* ***(A)*** *Branching digitate stromatolites that grew on a substrate of gray silt and mud. Layers of gray silt and ooids fill the space between the microbial "digits;" 296.5 to 296.6 meters (972.8–973.3 ft).* ***(B)*** *Low-relief stromatolites interbedded with ooids, peloids, and stromatolitic rip-up clasts. Porosity within microbialite fabrics consists of preserved primary megascopic and microporosity. Black arrow indicates the location of photomicrographs in E and F; 251.1 to 251.3 meters (824.0–824.5 ft).*

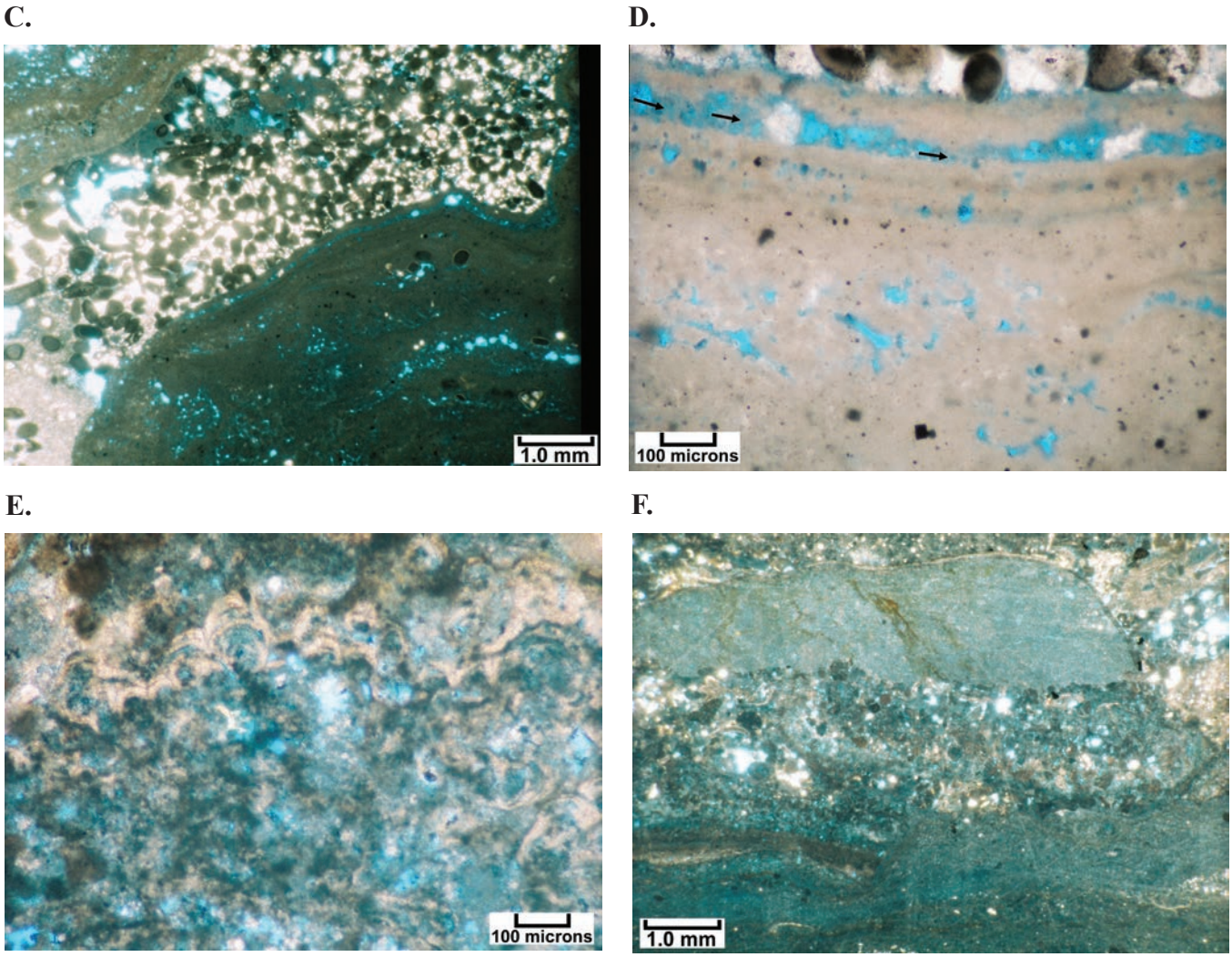

Figure 34 continued. *Stromatolites from the Skyline 16 research core.* ***(C)*** *Photomicrograph of stromatolitic laminae within small digitate heads seen in core photograph A. Note vague internal microbial laminations and the porosity (in blue) within the head. Quartz silt (in white) and ooids fill the space between the heads; 296.6 meters (973.0 ft) (plane light).* ***(D)*** *Photomicrograph of highly magnified view of the margin of a digitate stromatolite head shown in core photograph A. Note the well-defined laminae as well as the preservation of filamentous cell remains in the porous areas between the laminae (black arrows); 296.6 meters (973.0 ft) (plane light with white card).* ***(E)*** *Photomicrograph of preserved primary porosity, as seen megascopically in the lower section of core photograph B, within a stromatolitic interval resulting from constructional processes associated with tubular cells and pustular microfabrics; 251.3 meters (824.5 ft) (plane light).* ***(F)*** *Photomicrograph showing considerable microposity within very fine grained carbonates associated with a stromatolitic interval; 251.3 meters (824.4 ft) (plane light).*

suggesting some pore connectivity (figure 16B). Small primary vugs are also present and could be related to primary or early microbial precipitation.

Oncolite-rich layers commonly are overlain by thrombolites and stromatolites (figure 11A) or have sharp contacts with laminated, dark gray shale (figure 35B). The interiors of individual oncoids have a clotted texture (with spherical cell structures) overlain with dense laminated margins (figure 35C). Ooids and coated grains often occur between the oncoids.

Other associated grainstones, composed of oolites and pisolites, as well as peloidal and skeletal grains, occur below microbial intervals (figures 36 and 37). In addition, microbialites are typically capped by oolitic grainstones marked by a sharp contact (flooding surface) with laminated organic-rich carbonate mud (figures 36A and 36B). Many lightly cemented oolitic grainstones preserve excellent interparticle porosity (figures 36C and 37A), whereas individual ooids/pisoids often contain partially open microfractures ("septarian cracks") (figures 37B through 37E). Other grainstone beds consist of thin-shelled, articulated and single valve ostracods, which also have excellent interparticle and intraparticle pore space (figure 37F).

The Skyline 16 research core has lacy irregular microbial layers with small molds or vugs (figure 14C). Porous dolomites are seen as the orangish lacy patterns on the core surface. Thin sections show numerous lozenge-shaped molds retaining the shape

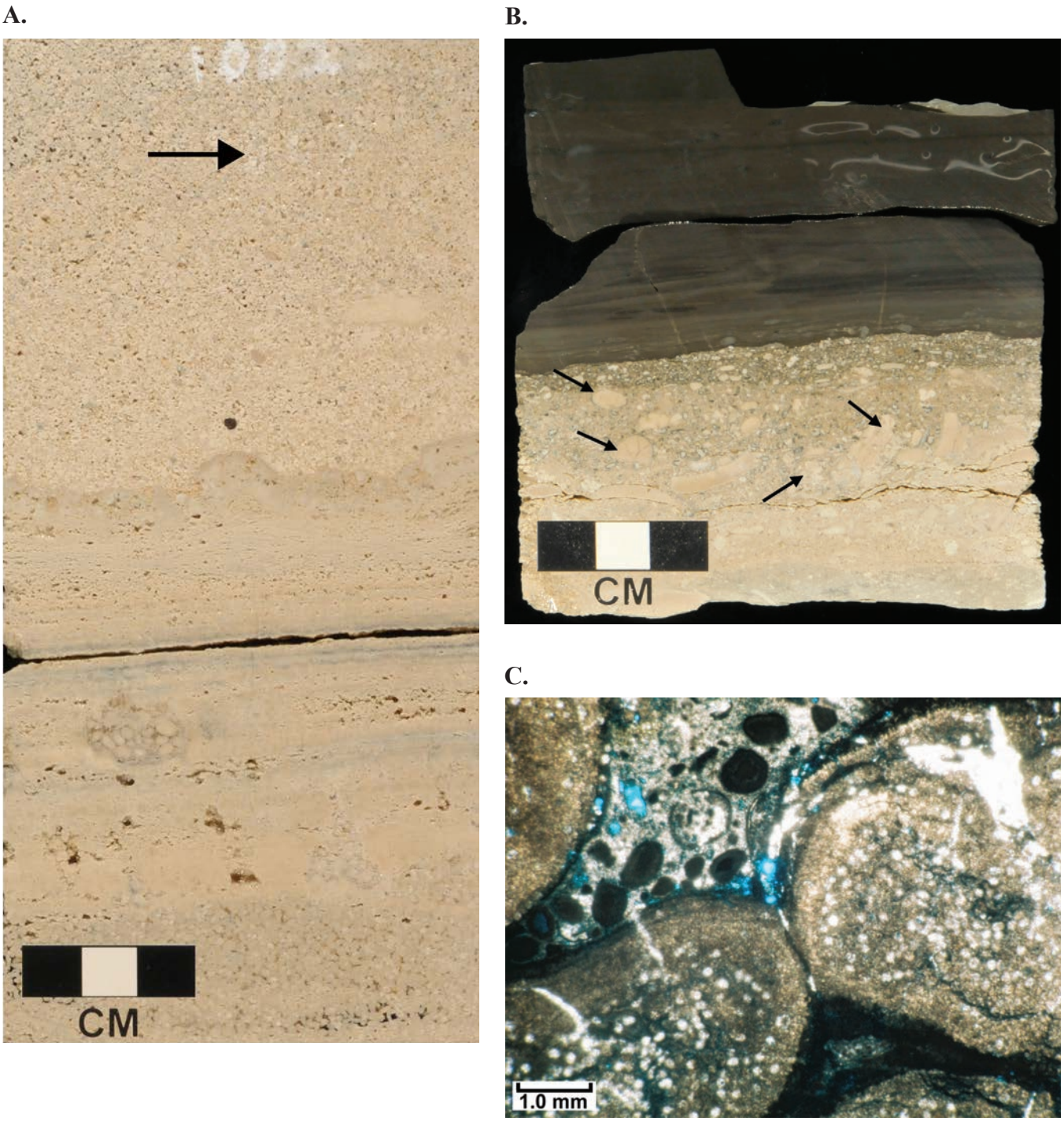

Figure 35. *Thrombolites and oncolites from the Skyline 16 research core.* ***(A)*** *Porous thrombolites associated with ooids; small primary vugs are also present. The black arrow indicates the location of photomicrograph shown on figure 16B; 305.4 to 305.5 meters (1002.0–1002.5 ft).* ***(B)*** *Oncoid-rich carbonate layer overlain (with sharp contact) by laminated, dark gray shale. Black arrows point to some individual oncoids; 283.4 to 283.5 meters (929.7–930.0 ft).* ***(C)*** *Photomicrograph showing a cross section through portions of several oncoids, as seen in the lowest section of core photograph shown on figure 11A. Note the clotted texture and well-preserved cellular pores (some of which are filled with white calcite spar) within the oncoid interiors as well as dense laminated margins; 285.6 meters (937.0 ft) (plane light).*

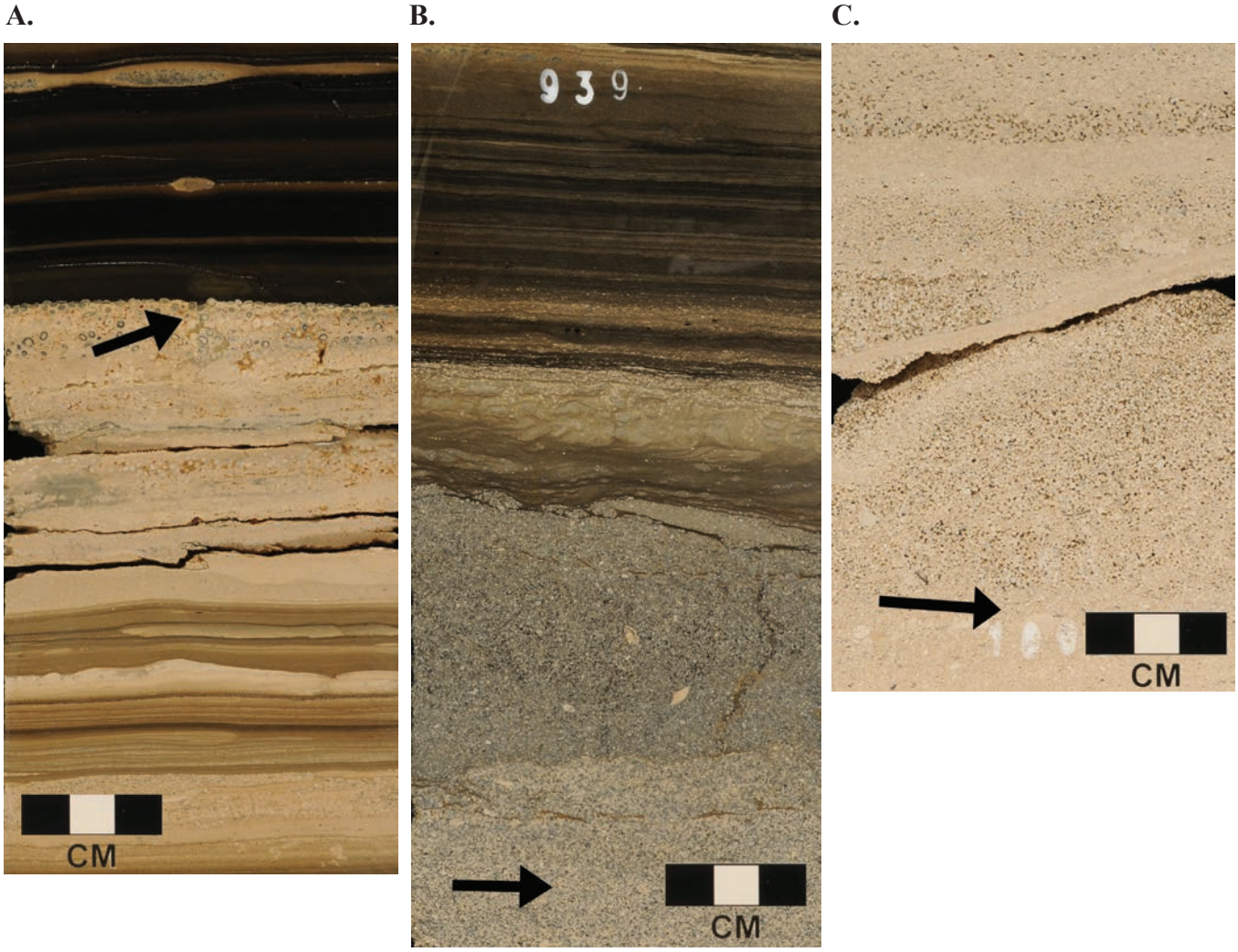

Figure 36. *Typical carbonate grainstones from the Skyline 16 research core.* ***(A)*** *Grainstone beds capped with a thin pisolitic bed and a very sharp contact with laminated, organic-rich carbonate mud; 273.8 to 273.9 meters (898.2–898.7 ft). Black arrow indicates the location of photomicrograph shown in figure 37C and 37D.* ***(B)*** *The lower half of this core segment shows a very porous peloidal/skeletal grainstone (in light to medium gray) overlain by a sharp erosional contact; 286.2 to 286.4 meters (939.0–939.6 ft). Black arrow indicates the location of photomicrograph shown in figure 37F.* ***(C)*** *Porous oolitic grainstone; 305.6 to 305.7 meters (1002.6–1003.0 ft). Primary interparticle porosity is visible within the coarser beds. Black arrow indicates the location of photomicrograph in figures 37A and 37B.*

of possible evaporite crystals, which were covered with dense carbonate mud (figures 38A through 38C). The crystal molds are partially filled with microporous, lacy calcareous fabrics (figure 38D). Clay drapes formed along possible evaporite crystal growth faces (figure 38A). Also occurring in this section are clusters of small dolomite crystal rhombs, many of which are hollow (figures 38E). Excellent well-connected pores occur between individual dolomite crystals and dolomite crystal clusters (figure 38F). Disrupted sediments are also associated with possible evaporite mineral dissolution and sediment collapse (haloturbation) (figure 39A). These intervals are commonly dolomitized and contain good matrix porosity (figure 39B). In the deeper subsurface of the Uinta Basin, these diagenetic fabrics may represent unrecognized reservoir potential.

Finally, the lower section of the Skyline 16 core contains intervals of silica/chert replacement (figure 40). The origin of the silica and the mechanism of its emplacement are currently unknown. Similar facies exist in several of the pre-salt Brazilian reservoirs. Here, considerable drilling and coring problems or "hazards" are caused by silicification of carbonate facies in the pre-salt reservoirs (figure 41) (e.g., Peixoto Filho and de Souza Neto, 2010).

Outcrop Studies

Four spectacular informally named outcrops were studied in the eastern Uinta Basin (south of Vernal, Utah; see figure 28 for locations) to determine the distribution and lateral continuity of microbialites and related carbonate facies that were encountered in the Skyline 16 research core. Measured sections (Rosenberg and others, 2015) at two of the four localities were utilized to place the microbialites and other carbonate facies into the depositional context of the lake history. In addition,

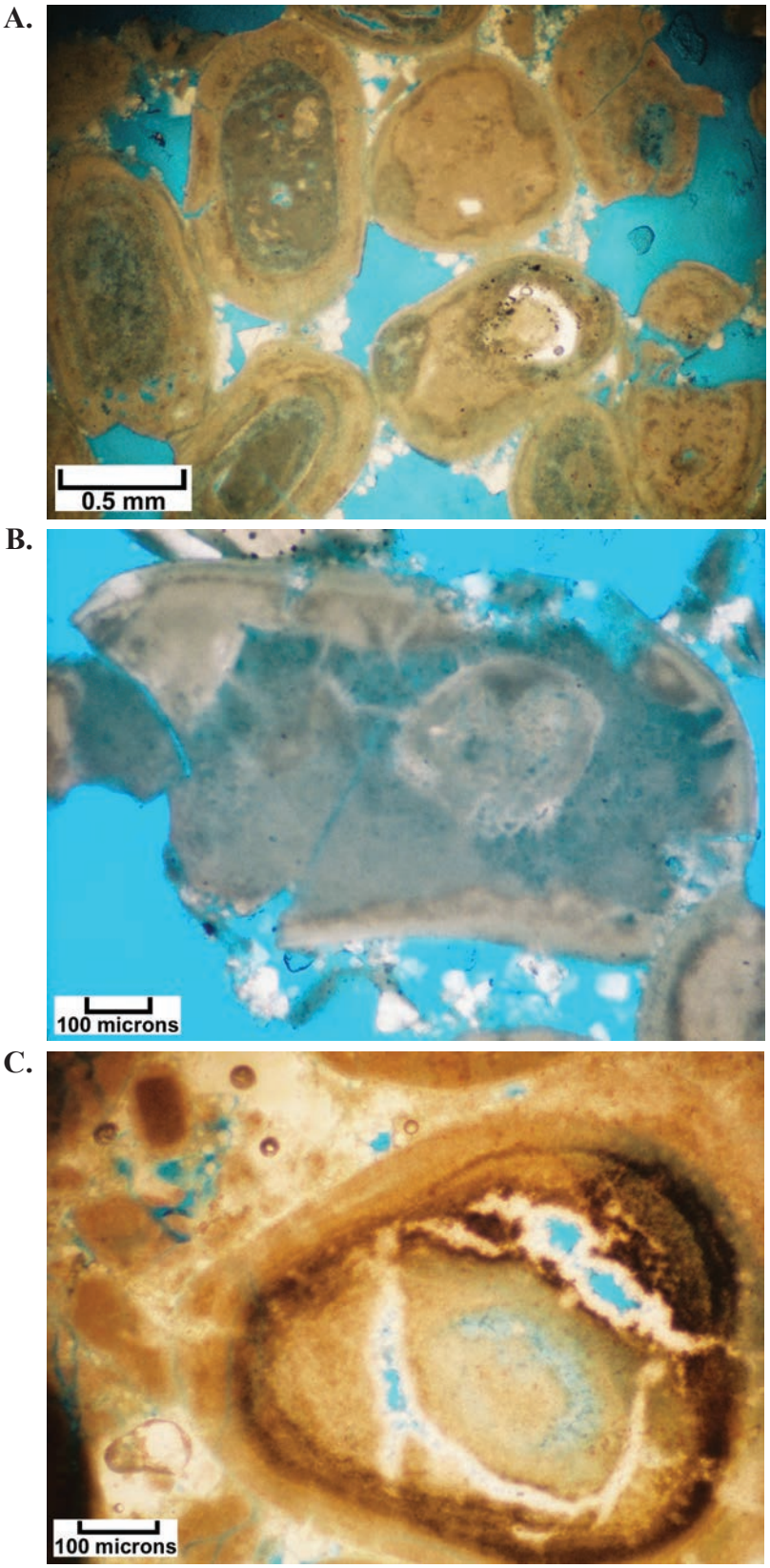

Figure 37. *Photomicrographs of carbonate grainstones from the Skyline 16 research core shown in figure 36 core photographs.* ***(A)*** *Excellent preserved interparticle porosity (blue) between very lightly cemented ooids. Note the small amounts of sparry calcite cement crystals (in white) lithifying these oolites; 305.7 meters (1003.0 ft) (plane light with white card).* ***(B)*** *Highly magnified view of impressive microporosity (dark blue) within a coated grain. This microporous composite grain is part of a very porous oolitic bed; 305.7 meters (1003.0 ft) (plane light with white card).* ***(C)*** *Close-up view of an individual pisoid. Note the partially open microfractures ("septarian cracks") as well as some preserved pores between grains; 273.8 meters (898.4 ft) (plane light with white card).*

D.

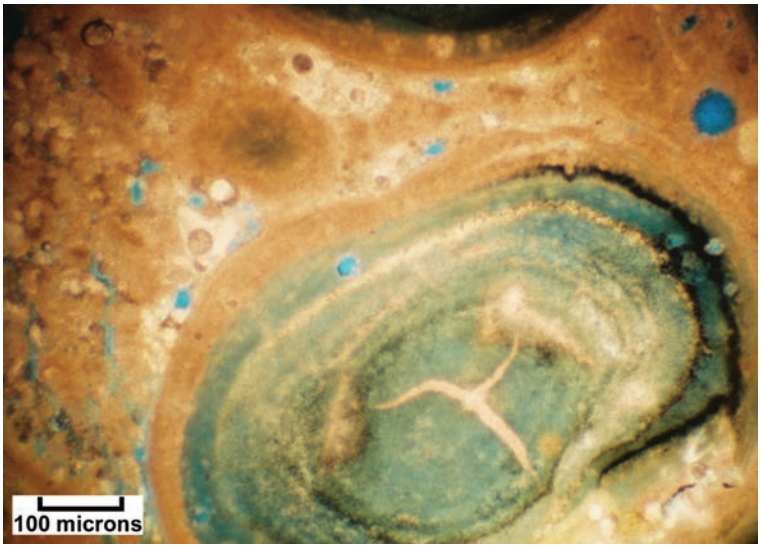

E.

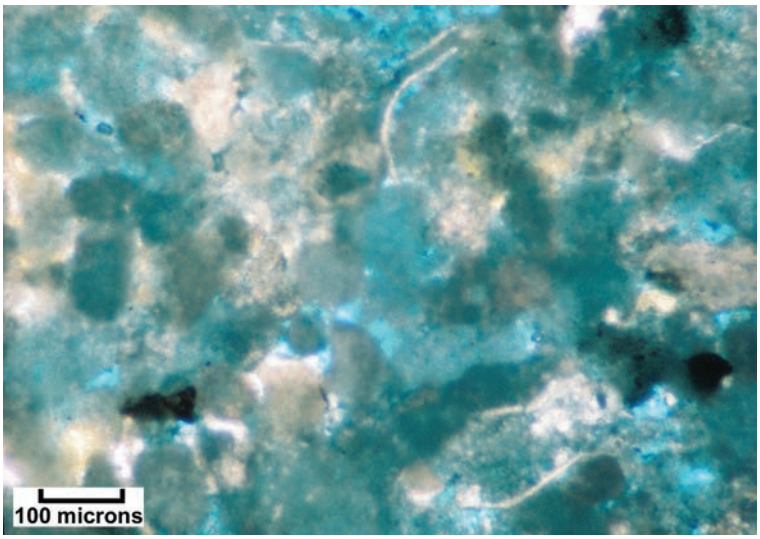

F.

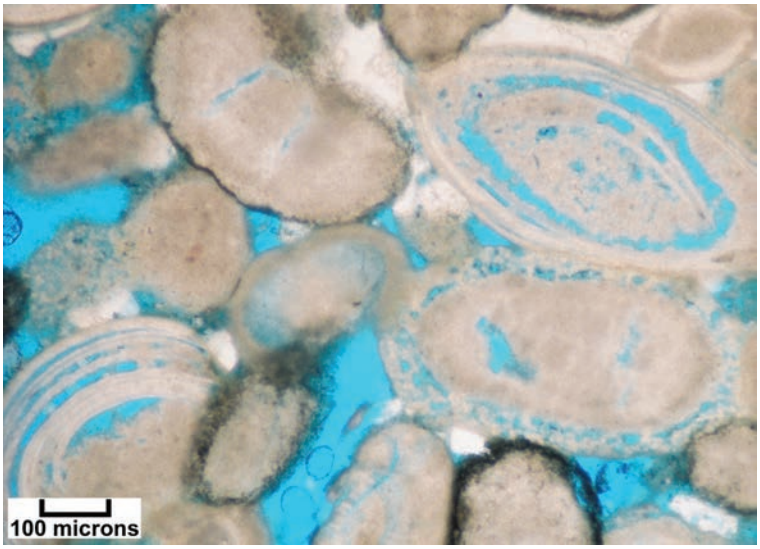

Figure 37 continued. *Photomicrographs of carbonate grainstones from the Skyline 16 research core shown in figure 36 core photographs.* ***(D)*** *View of a pisoid exhibiting significant internal microporosity (in light blue); 273.8 meters (898.4 ft) (plane light with white card).* ***(E)*** *Very significant preserved interparticle porosity (light blue) and peloidal microporosity (dark blue) are displayed in this sample that represents an interbed with stromatolites shown in figure 34B. Thin ostracod shells are also present; 251.3 meters (824.4 ft) (plane light).* ***(F)*** *Abundant preserved interparticle and intraparticle pore space is displayed in this peloidal/skeletal (ostracodal) grainstone; 286.3 meters (939.5 ft) (plane light with white card).*

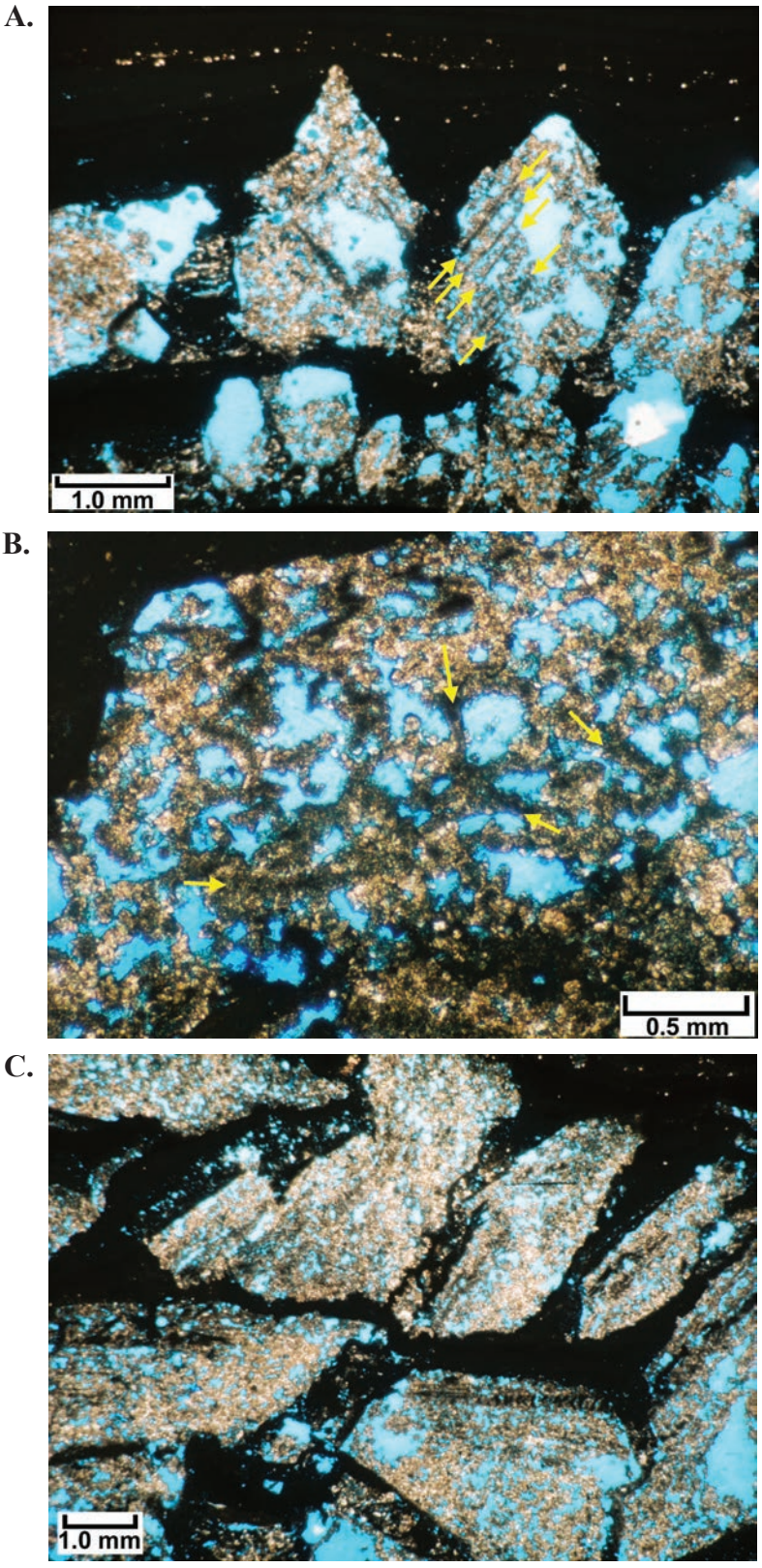

Figure 38. *Photomicrographs of possible evaporite crystal dissolution associated with microporous, lacy fabric growth from the Skyline 16 research core; see figure 14C for core photograph and approximate location of photomicrographs.* ***(A)*** *A cluster of small evaporite (?) crystal molds (from the core segment in figure 14C) that are preserved in growth position, surrounded by dense carbonate mud. The molds are partially filled and bridged with a microporous, lacy fabric (in light brown). Note preserved clay drapes that form along evaporite (?) crystal growth faces (see pairs of yellow arrows); 198.3 meters (650.7 ft) (plane light).* ***(B)*** *Interconnected lacy fabric in which filamentous cellular remains are preserved in dark brown (see yellow arrows); 198.3 meters (650.7 ft) (plane light).* ***(C)*** *Several lozenge-shaped molds occur between dense black sediments. Abundant dolomite has precipitated within these molds (see E and F); 198.2 meters (650.5 ft) (plane light).*

D.

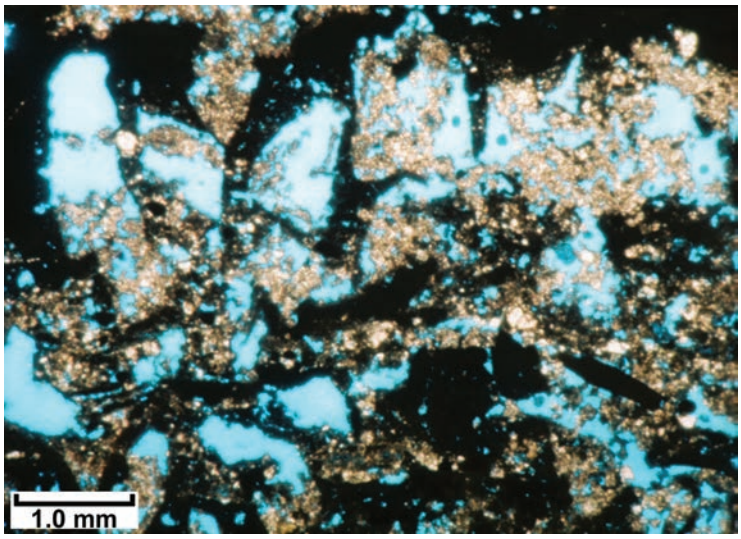

E.

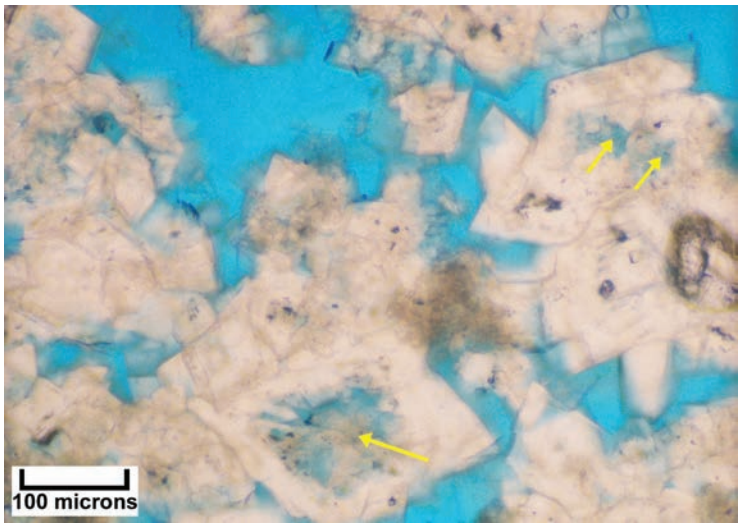

F.

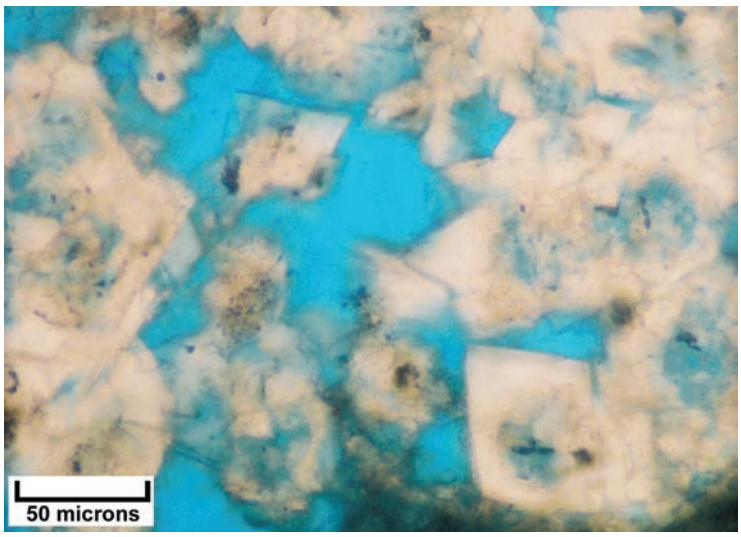

Figure 38 continued. *Photomicrographs of possible evaporite crystal dissolution associated with microporous, lacy fabric growth from the Skyline 16 research core; see figure 14C for core photograph and approximate location of photomicrographs.* ***(D)*** *Numerous molds retaining the shape of evaporite crystals can be seen between dense black sediments. Clusters of small dolomite crystals have precipitated within some of these molds (see E and F); 198.3 meters (650.7 ft) (plane light).* ***(E)*** *Porosity between clusters of dolomite crystals. Note also the presence of hollow dolomite rhombs (see yellow arrows); 198.3 meters (650.7) ft) (plane light with white card).* ***(F)*** *Well-connected pores are present between individual dolomite crystals and small crystal clusters associated with large evaporite (?) molds; 198.2 meters (650.5 ft) (plane light with white card).*

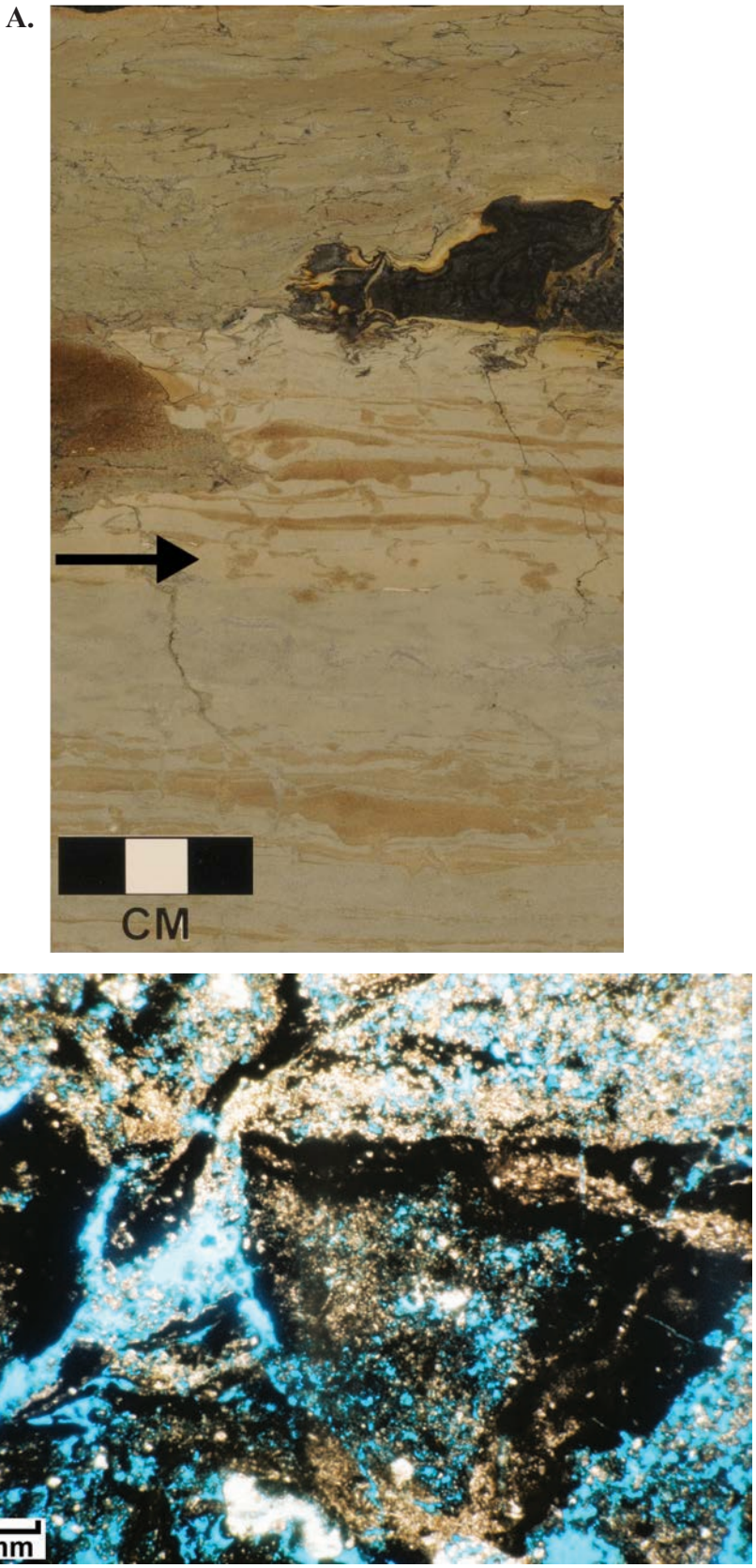

Figure 39. *Porosity associated with evaporite dissolution in the Skyline 16 research core.* ***(A)*** *Disrupted sediments associated with possible evaporite mineral dissolution and sediment collapse are shown here in a representative core segment. Porosity associated with dolomitization is present in the orangish patches. Black arrow indicates the location of photomicrograph shown in B; 240.6 to 240.8 meters (789.5–790.0 ft).* ***(B)*** *Photomicrograph showing good visible matrix porosity is associated with dissolution of evaporite minerals and associated possible collapse (haloturbation) of the sediment matrix (black and white areas here); 240.8 meters (789.5 ft) (plane light).*

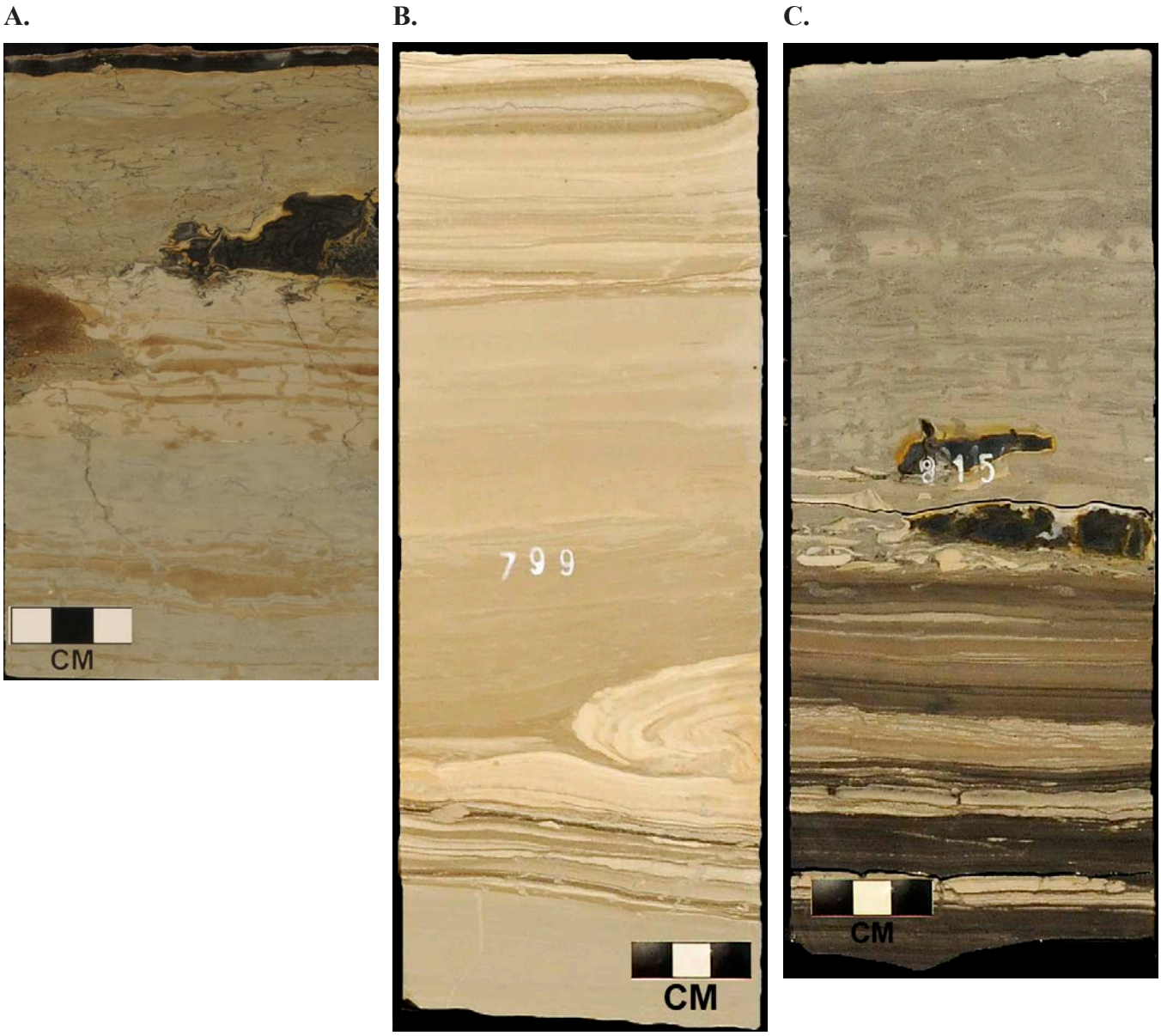

Figure 40. *Chert in the Skyline 16 research core.* ***(A)*** *Porous stromatolitic interval with small domal heads, desiccation cracks (partially filled with quartz silt grains), and dark gray chert; 240.6 meters (789.5 ft).* ***(B)*** *Stromatolitic laminae with no significant relief at the top of the core; light-colored chert nodule has replaced microbial laminae; 243.3 meters (798.5 ft). Note bulbous head in the lower part.* ***(C)*** *Small, high-relief stromatolitic heads and rip-up clasts. Some dark-colored chert nodules; 248.4 meters (815.0 ft).*

the positions of microbialites and associated carbonates in the Skyline 16 core could be accurately located to study lateral and vertical variations of these potential oil reservoir analogs.

Condo Section

The Condo measured section (figures 28 and 42A, plate 2) in this very accessible exposure in Evacuation Canyon consists of about 135 meters (445 ft) of the Parachute Creek Member of the Green River Formation. In general, shale and its organic content increases up section indicating increasing water depths of Lake Uinta. A thick, very fine grained sandstone, deposited in a distal mouth bar complex sourced from the southeast flowing to the northwest, interrupts the microbial sequence. Microbialites and associated facies are most heavily concentrated in the lower part of the Parachute Creek Member. This interval can be easily correlated into the Skyline 16 research core (taken about 5 kilometers [3 mi] to the northwest); siltstones in the core correlate with the distal mouth bar complex described above. Shale beds often overlie thin, small microbial heads and represent episodic deepening events or parasequence boundaries. This outcrop includes excellent exposures of the classic kerogen-rich shales of the Mahogany bed (figure 42B).

Among the microbialites at the Condo section are stromatolites and thrombolites (figures 43A through 43C). Stromatolites may be bedded and continuous laterally for tens of me-

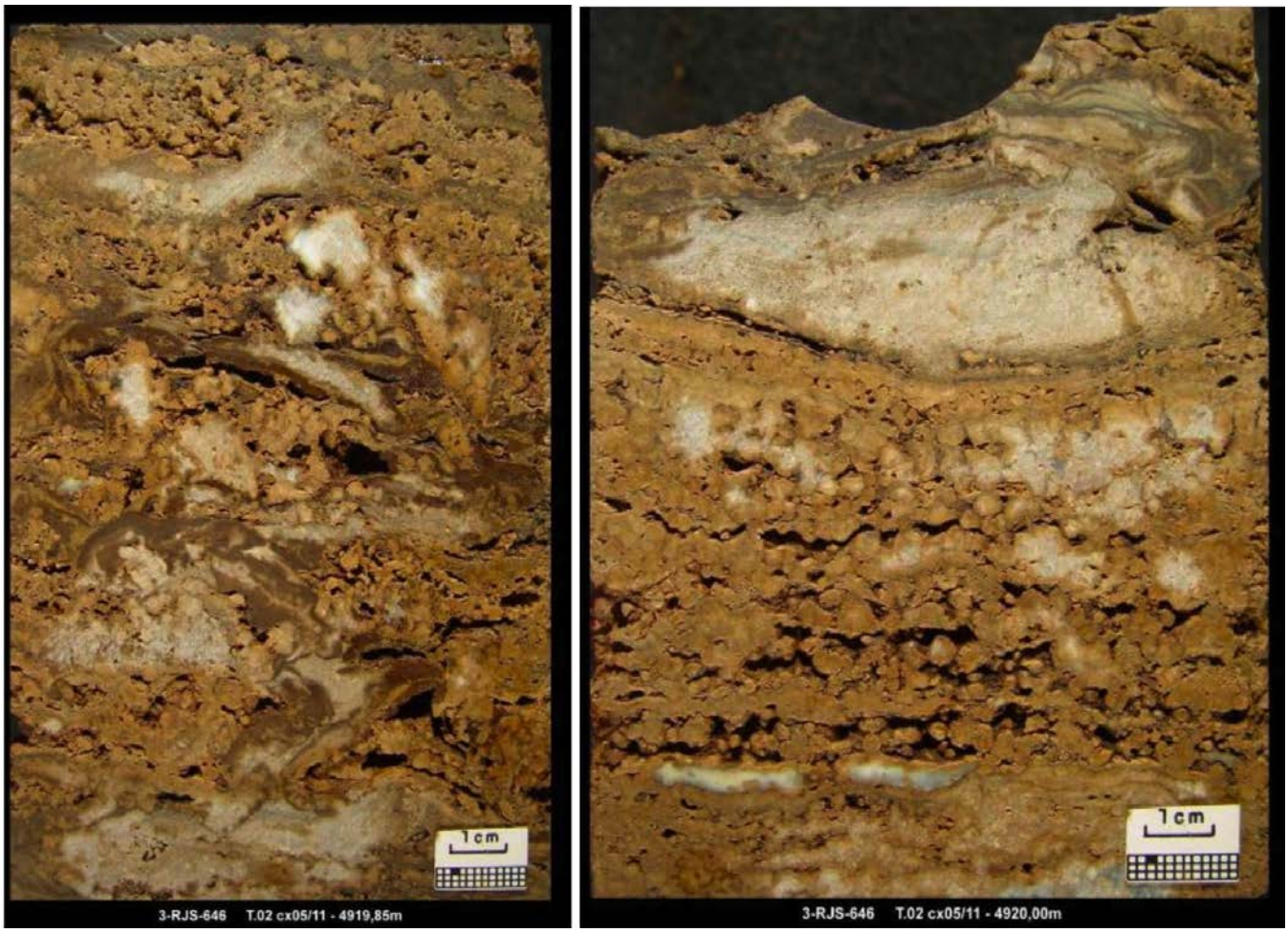

Figure 41. *Core photographs from the supergiant Lula (formerly Tupi) field reservoir within Early Cretaceous pre-salt Brazilian microbialite reservoir rocks (in brown) in which silica nodules (in white) create significant drilling and coring problems (see Peixoto Filho and de Souza Neto, 2010). See figure 40 for examples of siliceous nodules in the Skyline 16 research core and figure 45C for silicified outcrop in Green River Formation.*

ters whereas others have small domal heads grading upward into branching digitate forms. Excellent porosity is preserved as part of the laminated and clotted fabrics controlled by different microbial communities (figures 43D through 43I). In stromatolites, primary porosity is well developed between constructional microbial filaments (figures 43D through 43G). Thrombolites are also laterally extensive, especially near the base of the section, and domal with synoptic relief. Thrombolites contain large, open pores (vugs) resulting from microbial construction (figures 43H and 43I).

These facies have excellent reservoir potential and were deposited during relatively shallow lake levels. In addition, superb exposures of large casts after bottom-growth evaporite crystals (figures 43J through 43L) can be traced over significant lateral distances. Some examples wrap around or appear to encrust small microbial heads. These features are very similar to those presumed to be evaporite crystal molds observed in thin sections from the Skyline 16 research core (figures 38A, 38C, and 38D).

Flash Flood Section

The Flash Flood measured section (figures 28 and 44A, plate 3) exposed in Evacuation Canyon consists of about 180 meters (591 ft) of the Parachute Creek Member of the Green River Formation. Microbialite intervals are concentrated mostly in the lower half of the section. Like the nearby Condo section, this outcrop also includes excellent exposures of oil shale of the Mahogany bed. Note the multiple packages of alluvial and fluvial sandstone that punctuate the carbonate and claystone lacustrine deposits as shown on the graphic measured section (figure 44A, plate 3). The additional section exposed here provides an opportunity to see the older microbialite-rich R-4 interval, which can also be tied accurately into the Skyline 16 research core. Stromatolitic beds at several levels, indicating cyclic deposition, can be traced for considerable distances laterally within the R-4 (figures 44B and 44C). Excellent visible porosity within many of these stomatolitic beds can be easily observed in outcrop (figure 44D).

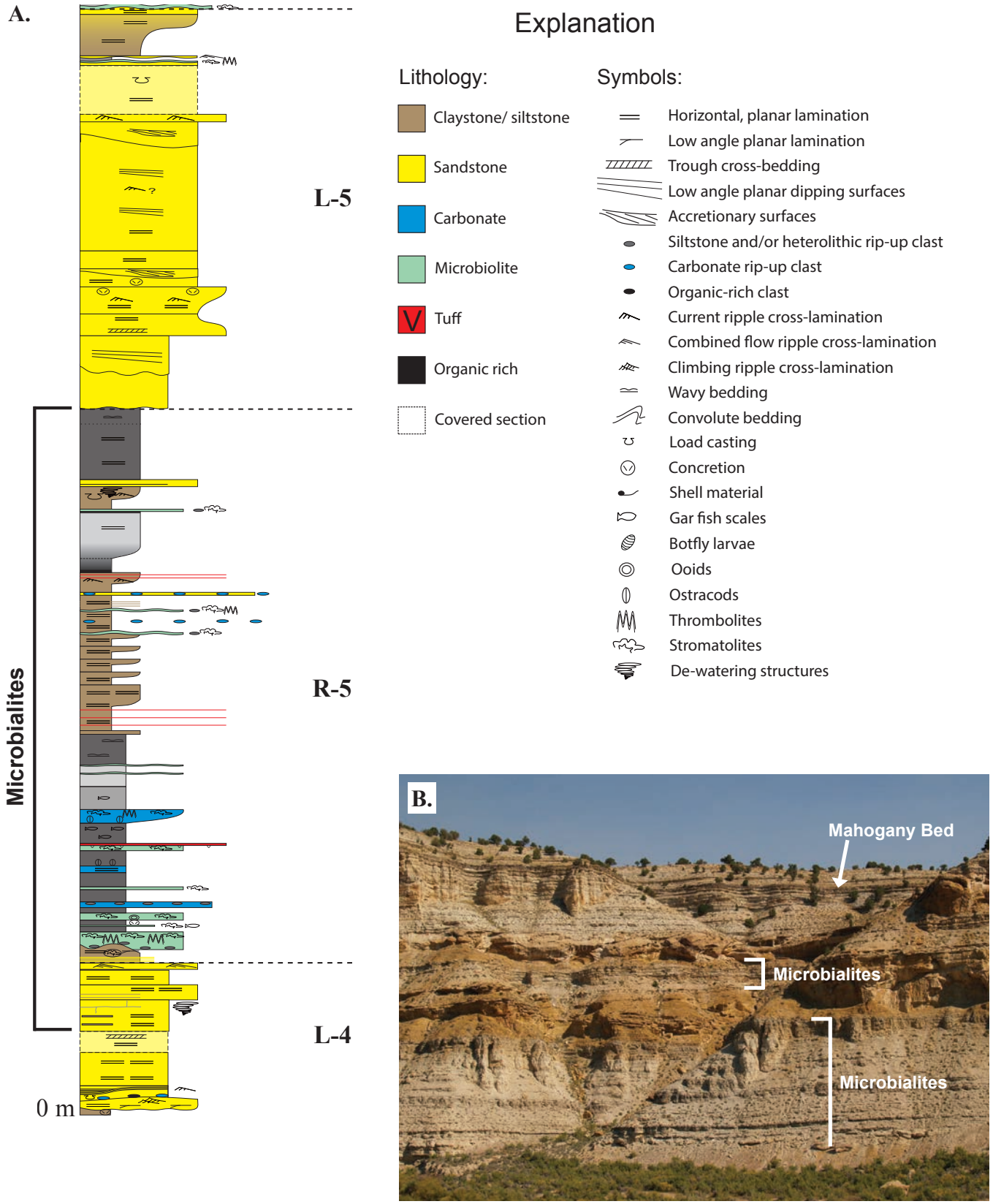

Figure 42. *Green River Formation in the Condo section, Evacuation Creek.* ***(A)*** *Measured Condo section in graphical format (see figure 28 for location map and plate 2 for detailed section description). Microbialites and associated carbonate facies are shown in blue/green. Microbialite intervals are concentrated mostly in the lower part of this 135-meter (445 ft) section. This interval can be correlated with the R-5 interval in the Skyline 16 research core. Modified from Rosenberg (2013) and Rosenberg and others (2015).* ***(B)*** *View of the entire Condo section taken from the base of the outcrop. Note the general vertical distribution of the microbialite-rich interval as well as the Mahogany oil shale bed.*

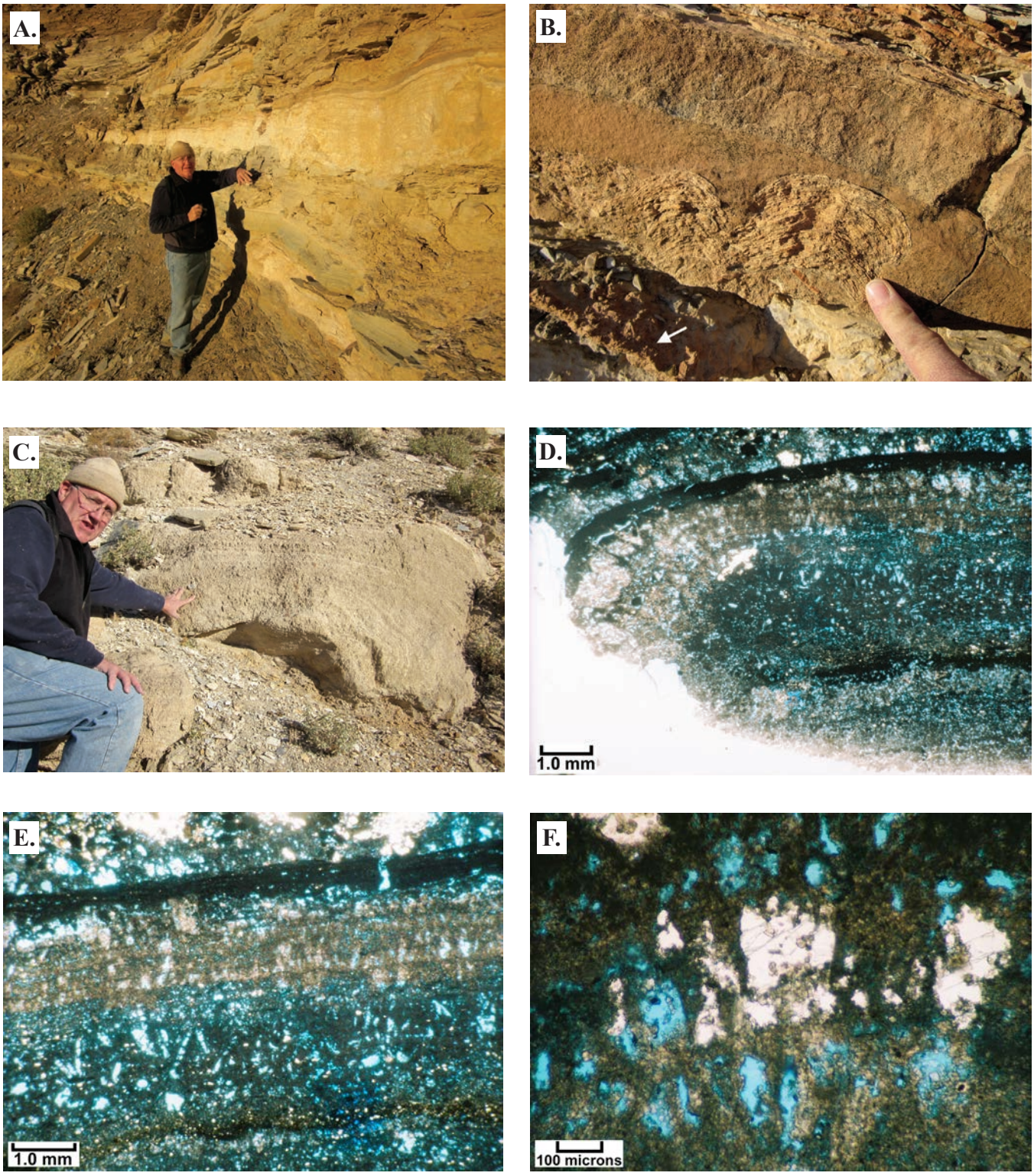

Figure 43. *Microbialite and evaporite examples in the Condo section.* ***(A)*** *Continuous beds of stromatolites (lower R-6 oil shale zone).* ***(B)*** *Small domal stromatolite heads (adjacent to the finger) that grade upward into even smaller branching stromatolites (lower R-6 oil shale zone). This stromatolitc bed has grown over densely packed evaporite (gypsum?) crystal casts (white arrow).* ***(C)*** *A meter-scale thrombolite head (right side of photo). Note the steep margin of this domal structure (R-5 oil shale zone).* ***(D)*** *Photomicrograph of the margin of a stromatolite head. Note the well-developed laminations as well as the abundant preserved primary pores (in blue) between microbial filaments (plane light).* ***(E)*** *Photomicrograph showing closer view of stromatolitic laminae with well-developed porosity (in blue) between constructional microbial filaments (plane light).* ***(F)*** *Photomicrograph of highly magnified microbial filaments within stromatolitic laminae protecting primary pores (in blue). Calcified evaporite crystals are present in the white patches (plane light).*

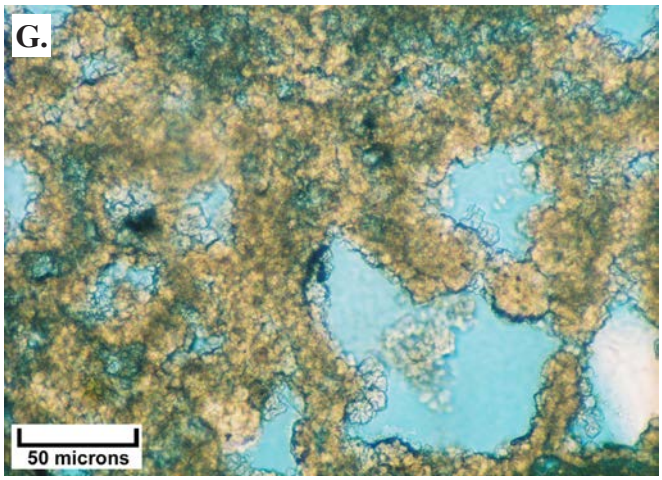

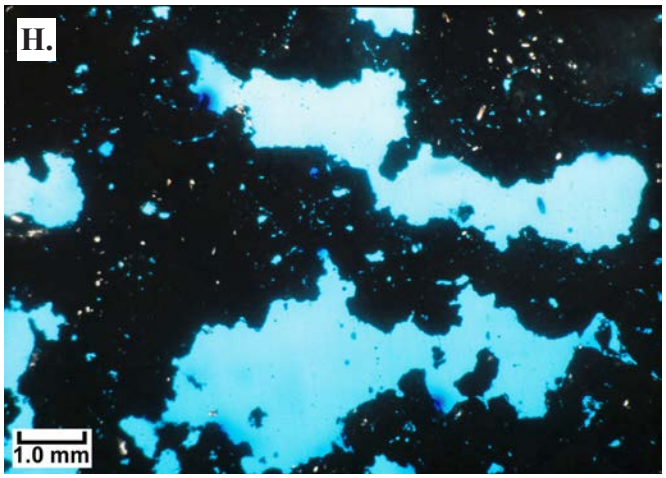

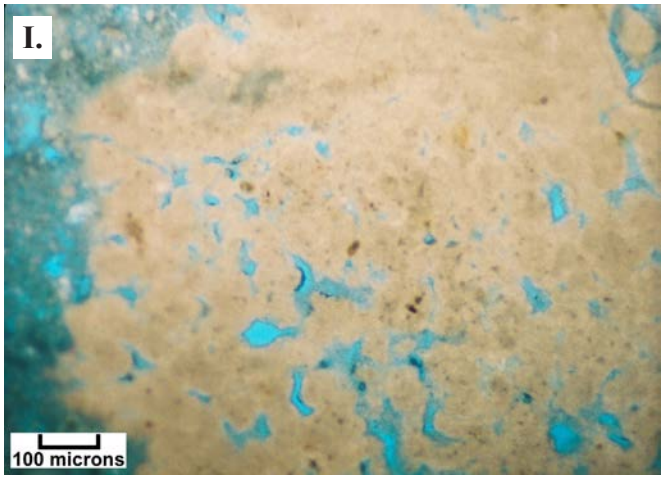

Figure 43 continued. *Microbialite and evaporite examples in the Condo section.* ***(G)*** *Photomicrograph showing interlocking microbial filaments preserved by the precipitation of small dolomite crystals. Note the open pores (in blue) encased by the dolomitized filaments (plane light).* ***(H)*** *Photomicrograph at low magnification of the clotted microfabric (in black) of a thrombolitic head like the one shown in C. Note the large open pores (vugs; in blue) that are the preserved as part of the microbial construction of this thrombolite (plane light).* ***(I)*** *Photomicrograph at high magnification of the clotted microfabric (in light brown) of a thrombolitic head like the one shown in C. Note the open pores (in blue) that are an important result of thrombolitic growth (plane light with white card).* ***(J)*** *Close-up photograph of evaporite crystal casts shown in B (lower R-6 oil shale zone).* ***(K)*** *Outcrop view of similar evaporite crystal molds seen in the Skyline 16 research core. Note the crystal-like structure on the stromatolite dome.* ***(L)*** *Plan view of stromatolite similar to outcrop photograph in K. Notice the crystal molds are only located on the dome of the stromatolite.*

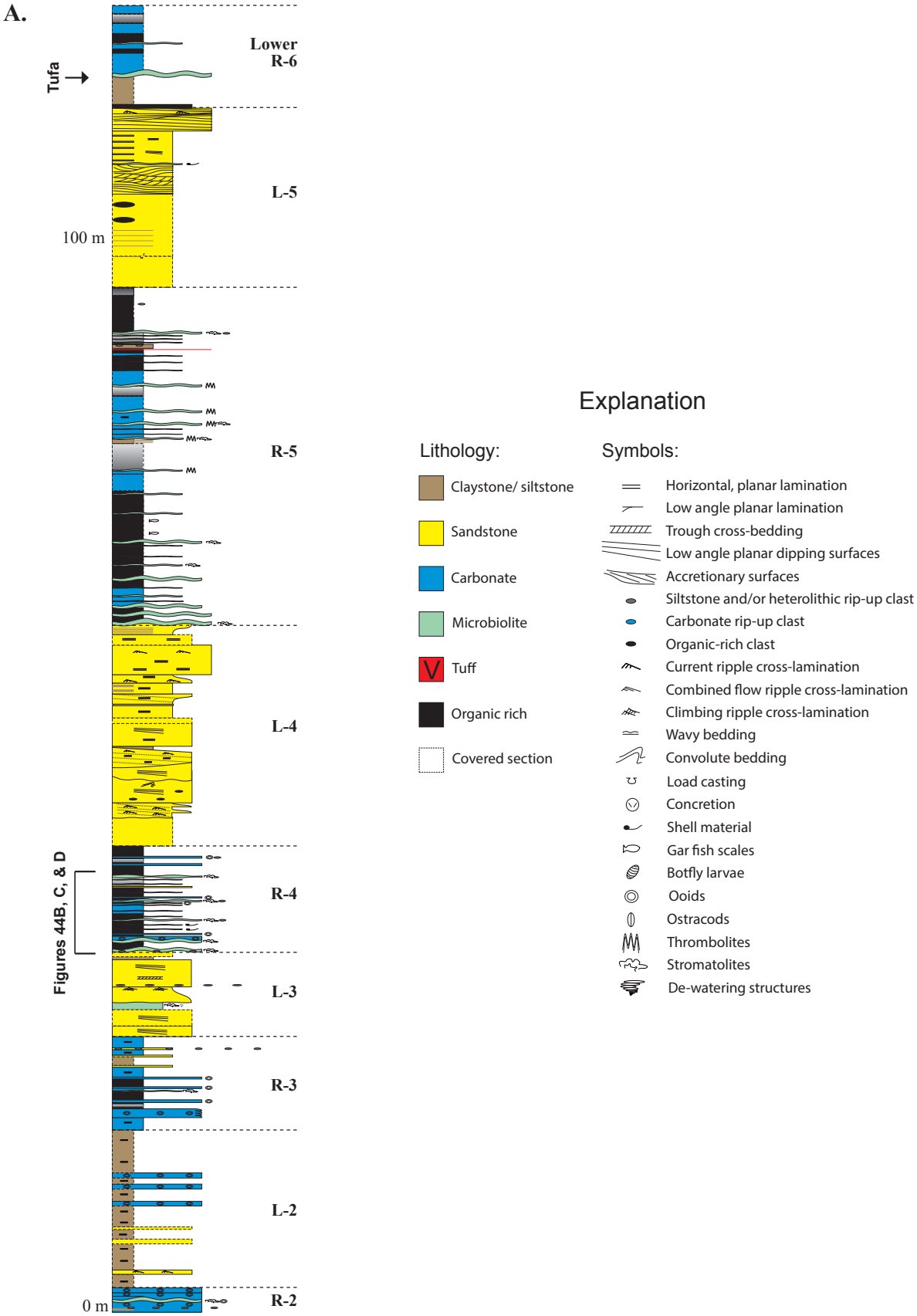

Figure 44. *Green River Formation in the Flash Flood section, Evacuation Creek.* ***(A)*** *Measured Flash Flood section in graphical format (see figure 28 for location map and plate 3 for detailed section description). Microbialites and associated carbonate facies are shown in blue/green. Microbialite intervals are concentrated mostly in the lower half of this 180-meter (591 ft) section (especially in the R-4 and R-5 intervals). Modified from Rosenberg (2013) and Rosenberg and others (2015).*

B.

C.

D.

Figure 44 continued. *Green River Formation in the Flash Flood section, Evacuation Creek.* ***(B)*** *View of a part of the Flash Flood section in which microbialites (in white) and associated carbonate facies are present.* ***(C)*** *Outcrop view of representative thin, continuous stromatolite beds in the light brown colors (below hand).* ***(D)*** *Single stromatolite head in the Flash Flood section. Note the porous laminated microbialite head that has changed orientation and relative relief from bottom to top.*

Bowling Ball Hill Section

Exposures at Bowling Ball Hill in Hells Hole Canyon (figure 28) provide a close look at a distinctive bed of dolomitized and silicified stromatolites in which the three-dimensional aspects of high-relief, domal, and coalesced heads can be examined (figure 45A and 45B). In addition, bedded and cross-bedded sheets of oolitic grainstone as well as pisolitic and oncolitic rudstone are very well exposed (figure 45C). Oncoids are typically surrounded by ostracods and microbial fabrics (figure 46A). Articulated ostracods and carbonate mud provide the sediment fill between many of the microbialite heads and oncoids (figure 46B). Many of the nuclei of pisoids are broken ooids or single large ostracod valves (figures 46C and 46D), which are also present in Great Salt Lake shoreline sediments (figure 24E). Some beds are dolomitized, but still contain preserved filamentous or tubular microbial structures (figures 46E and 46F). Interestingly, these calcarenites are heavily silicified (figures 45C and 45D). Silicified rip-up clasts composed of massive to laminated microbialite fabrics are also present at Bowling Ball Hill (figure 46G). It is likely that these clasts were derived from eroded and/or exposed thrombolitic and stromatolitic heads. As noted earlier, significant drilling problems are caused by replacement silicification of microbilites and associated facies.

Samples from the "Bowling Ball" microbialite zone exposed at Bowling Ball Hill provide important insights into the type of pore systems and reservoir quality that can be expected in subsurface microbialite reservoirs. Examples include preserved interparticle pores (figures 46A and 46C), intraparticle pores (associated with ostracod limestones; figure 46B), and pores between filamentous microstructures within stromatolites (figures 46E, 46F, and 46H). Both megascopic pores and microporosity (figure 46I) are common within the stromatolitic heads.

Hells Hole Section

Exposures at the Hells Hole section (figure 28) in Hells Hole Canyon provide another good opportunity to look at microbialite-rich and associated grainstone/rudstone facies intervals in the lower part of the Parachute Creek Member (figure 47A). Microbialites are most common within the carbonate facies in the lower part of this section. The Mahogany bed is present near the top of the section. The thrombolites and stromatolites in microbialite beds display excellent preserved matrix porosity associated with their growth forms and microbial communities (figure 47B); some beds are dolomitic (figure 47C) and may also contain good porosity. In addition, this section has easy access to small-scale cycles composed of mudstones to rudstones (oncolitic and pisolitic) to microbialites (thrombolitic and stromatolitic) to grainstones (oolitic and peloidal). This locality is also very good to examine contacts between deepening-upward cycles as well as the bounding surfaces associated with each facies within a cycle (figure 47D), similar to the Skyline 16 research core.

Synopsis and Discussion

Analysis of recently acquired Green River Formation samples in the Skyline 16 research core reveals a tremendous variety of microbial fabrics and related features. The overall section consists of medium gray siltstone, claystone, and calcareous mudstone to light brown dolomitic mudstone with dark brown, clay-rich and black, organic-rich zones. Alluvial and fluvial sandstones are also present. Within the dolomitic and limy mudstone, porous microbialites, including stromatolites with bulbous heads and thrombolites, are well displayed. Grainstones composed of ooids, coated grains, pisolites, and peloids often overlie the microbialites. The grainstones and microbialites exhibit excellent storage capacity consisting of micro-intercrystalline, interparticle, intraparticle, and moldic pore types. Outcrops of the Green River Formation in the eastern part of the Uinta Basin also display many of the features observed in core, both vertically (including depositional cycles) and horizontally. They offer a production-scale analog of the characteristics, geometry, distribution, and bounding surfaces of microbial and related lacustrine facies.

The relatively shallow-water lake-margin, carbonate-flat environment of ancient Lake Uinta was an ideal site in terms of water chemistry, temperature, and depth for microbial growth along with oolite, oncolite, and peloid formation, as observed in the Skyline 16 research core. Similar to Great Salt Lake, the salinity of Lake Uinta must have been at times fairly high (15% to 16%) to sustain microbial growth and carbonate grain formation. However, the shallow ramp, seen in Great Salt Lake and as evidenced by Green River Formation deposits, created susceptibility to rapid widespread shoreline changes and resulted in regional-scale cyclicity. The position of microbialites and other marginal lacustrine deposits changed as the lake shoreline shifted in response to lake-level fluctuations and sediment input. Vertical facies transitions appear as overall deepening-upward cycles in the Douglas Creek Member (Swierenga and others, 2015). For example, Morgan (2003) identified two depositional sequences along Nine Mile Canyon from bottom up: carbonate–green shale–sandstone–green shale, then the cycle is repeated again. These conditions were not conducive to thick accumulations of reservoir-quality microbialite buildups. Instead, deposits are dominated by 1- to 2-meter (3–6 ft) deepening-upward sequences that have only several tens of centimeters of porous microbialite formation, which are interbedded with impermeable profundal shales, but could be great horizontal drilling targets if they were buried. In addition, the thrombolites observed in the Skyline 16 core typically preserve greater amounts of megascopic porosity than the stromatolites.

As seen at Bridger Bay, Great Salt Lake carbonate muds and unconsolidated ooids often provide an adequate substrate for microbial mat formation, but in other cases, as is more com-

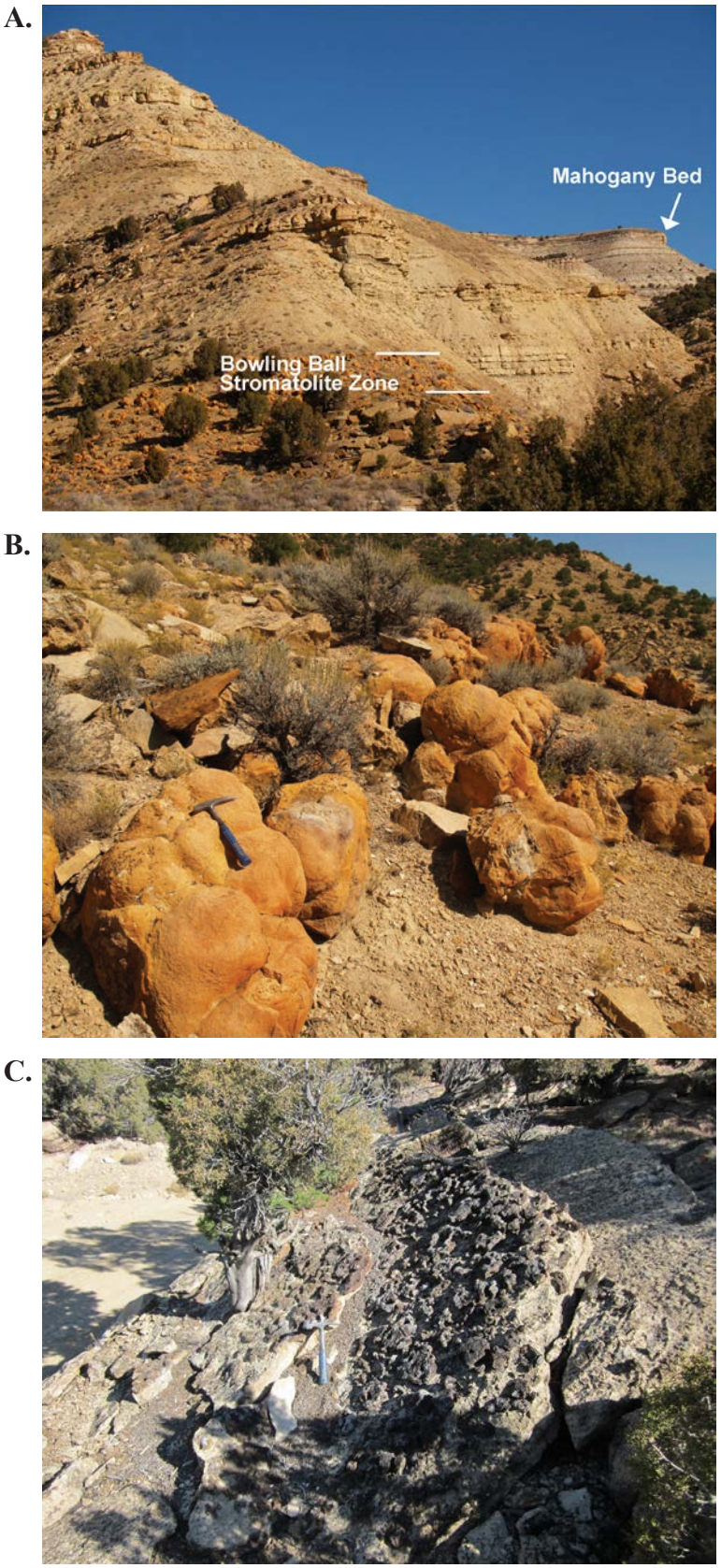

Figure 45. *Green River Formation at Bowling Ball Hill, Hells Hole Canyon (see figure 28 for location map).* ***(A)*** *View of Bowling Ball Hill. Note the location of the dolomitized "Bowling Ball" stromatolite zone in the lower foreground as well as the Mahogany bed in the middle right.* ***(B)*** *Ground view of the large rubble blocks from the "Bowling Ball" zone composed of multiple meter-scale coalesced stromatolite heads.* ***(C)*** *Inclined bedding plane surfaces of partially silicified oolite/pisolite beds that are associated with microbialite facies on Bowling Ball Hill.*

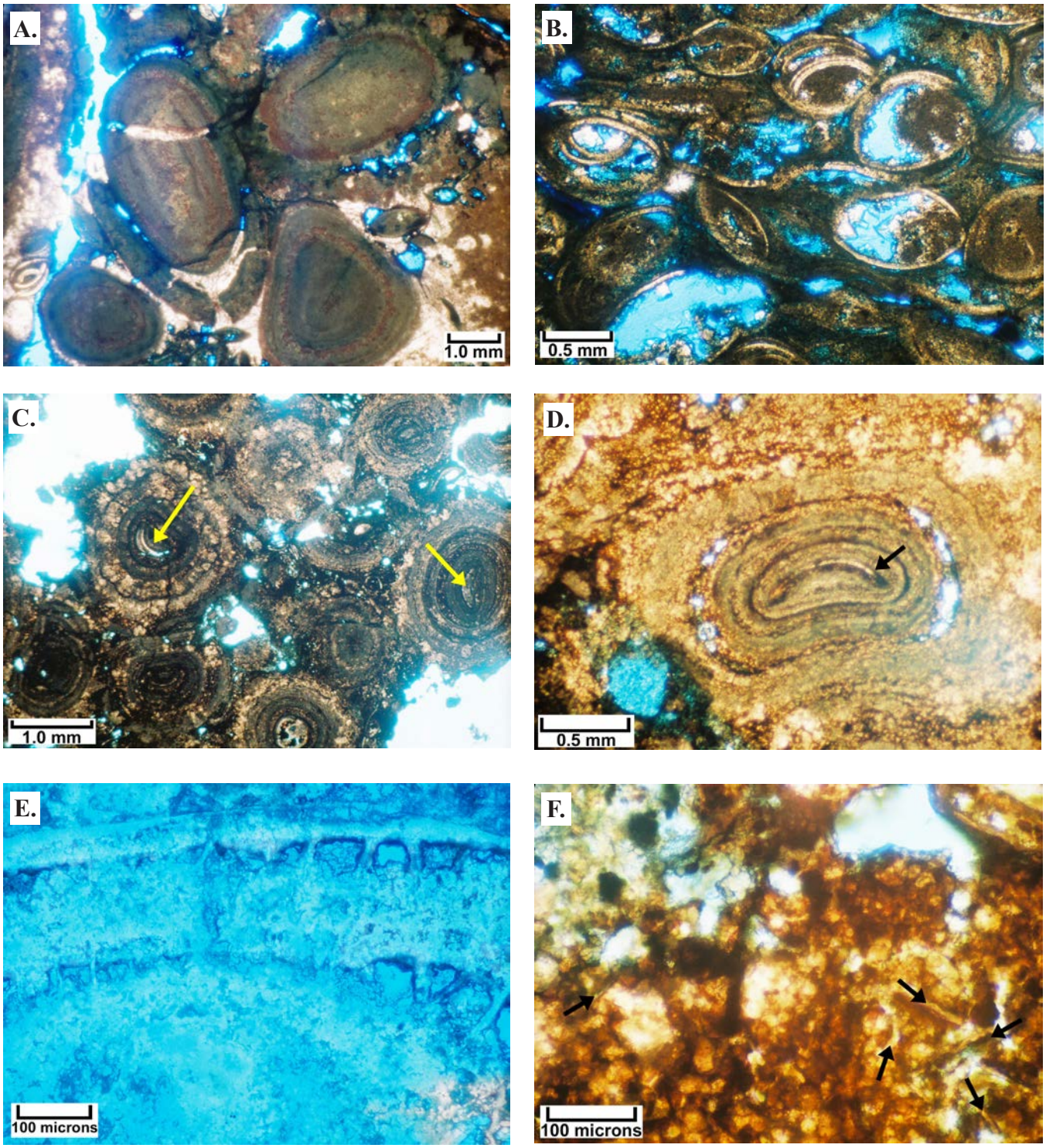

Figure 46. *Photomicrographs of microbialites and associated grainstone/rudstone facies at Bowling Ball Hill.* ***(A)*** *Grouping of several small oncoids from a microbial bed. Note the rounded margins but irregular shape of individual oncoids and the excellent interparticle porosity. Ostracods and clotted microbial fabrics surround these oncoids, especially along the right margins of this photomicrograph (plane light).* ***(B)*** *Articulated ostracods and carbonate mud provide the sediment fill between many of the microbialite heads and oncoids. Note the intraparticle porosity and geopetal fills containing peloids within some of the cavities formed by paired ostracod shells (plane light).* ***(C)*** *Small pisoids and interparticle porosity from carbonate facies associated with microbialite beds. Many of the nuclei (see yellow arrows) of these pisoids are broken ooids (plane light).* ***(D)*** *Cross section of a typical pisoid associated with microbialite beds. Note that this particular large grain contains a single ostracod valve (see black arrow) as the nucleus (plane light).* ***(E)*** *Highly magnified view of the microbial microstructure of a representative oncoid. Note the tubular and filamentous elements of this porous, dolomitized microfabric (plane light with white card).* ***(F)*** *Highly magnified image from within a representative pisoid from grainstone/rudstone facies associated with microbialite beds. Note the "ghosts" of filamentous or tubular (microbial) structures (see black arrows) within these dolomitized grains. Preserved pores are light blue (plane light).*

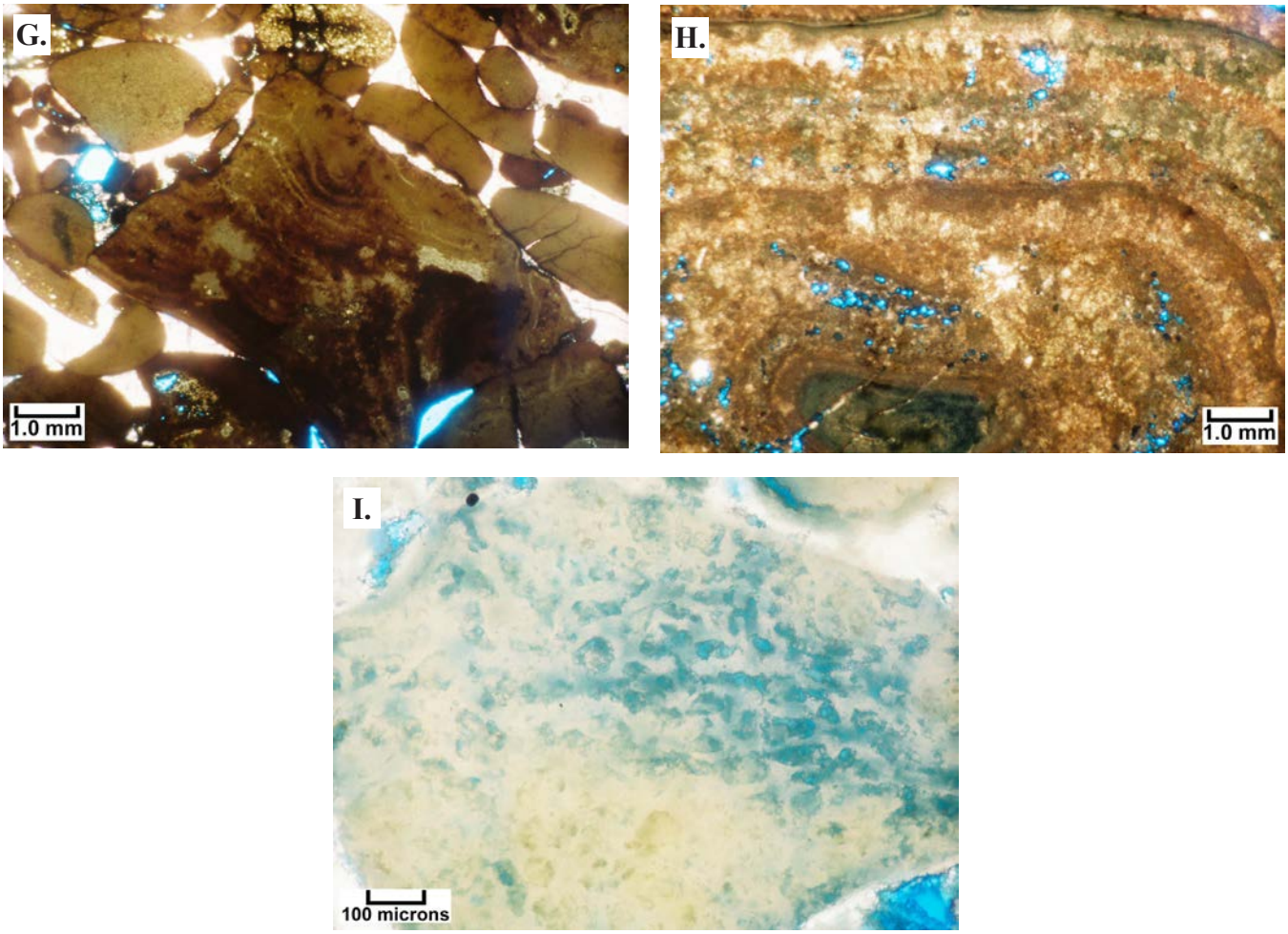

Figure 46 continued. *Photomicrographs of microbialites and associated grainstone/rudstone facies at Bowling Ball Hill.* ***(G)*** *Silicified rip-up clasts in this low-magnification image are composed of massive to laminated microbialite fabrics. It is likely that these clasts were derived from eroded and/or exposed thrombolitic and stromatolitic heads (plane light).* ***(H)*** *Cross section through a representative oncoid from a microbial bed. Note the patches of good porosity (in blue) preserved within some of the cortex bands in this oncoid. Remnants of some of the filamentous microfabrics can also be seen (plane light).* ***(I)*** *Porous (in blue) microfabric preserved within a dolomitized thrombolitic head (plane light with white card).*

mon in the Skyline 16 core, microbialites grew on accumulations of carbonate rip-up material. Currents along the lake margins would supply nutrients for these microbial communities, as well as keep the area relatively free of suffocating mud (Osmond, 2000). These currents also were critical in keeping primary interparticle and intraparticle microbial constructional pores open and mud free.

MICROBIAL CARBONATE RESERVOIRS IN UTAH OIL FIELDS

A survey of carbonate cores publicly available at the Utah Core Research Center (UCRC) in Salt Lake City, Utah, from active Utah oil fields reveals a variety of microbial fabrics (of which four are previously undocumented in marine formations), associated carbonate grains, pore types, and reservoir characteristics comparable to those observed in Great Salt Lake, the Skyline 16 core, and Green River Formation outcrops. The reservoirs, fields, and geologic locations, respectively, are the (1) Eocene Green River Formation, West Willow Creek field, Uinta Basin, (2) Jurassic Twin Creek Limestone, Pineview field, thrust belt in northern Utah, (3) Triassic Moenkopi Formation, Upper Valley field, Kaiparowits Basin in south-central Utah, (4) Pennsylvanian Paradox Formation, Greater Aneth field, Paradox Basin in southeastern Utah, and (5) Mississippian Leadville Limestone, Lisbon field, also in the Paradox Basin; the latter four are marine reservoirs.

Like their lacustrine counterparts, marine microbial carbonates display a wide variety of stromatolitic and thrombolitic growth forms, and possible leolites in mud mounds; associated carbonate grains include ooids, peloids, and oncoids. Porosity has developed in many of the microbial fabrics: intercrystalline, dissolution, interparticle, and extensive microporosity. Microbial dolomite/dolomitization has enhanced porosity and permeability development. Marine microbial carbonates could also become the drilling targets for new po-

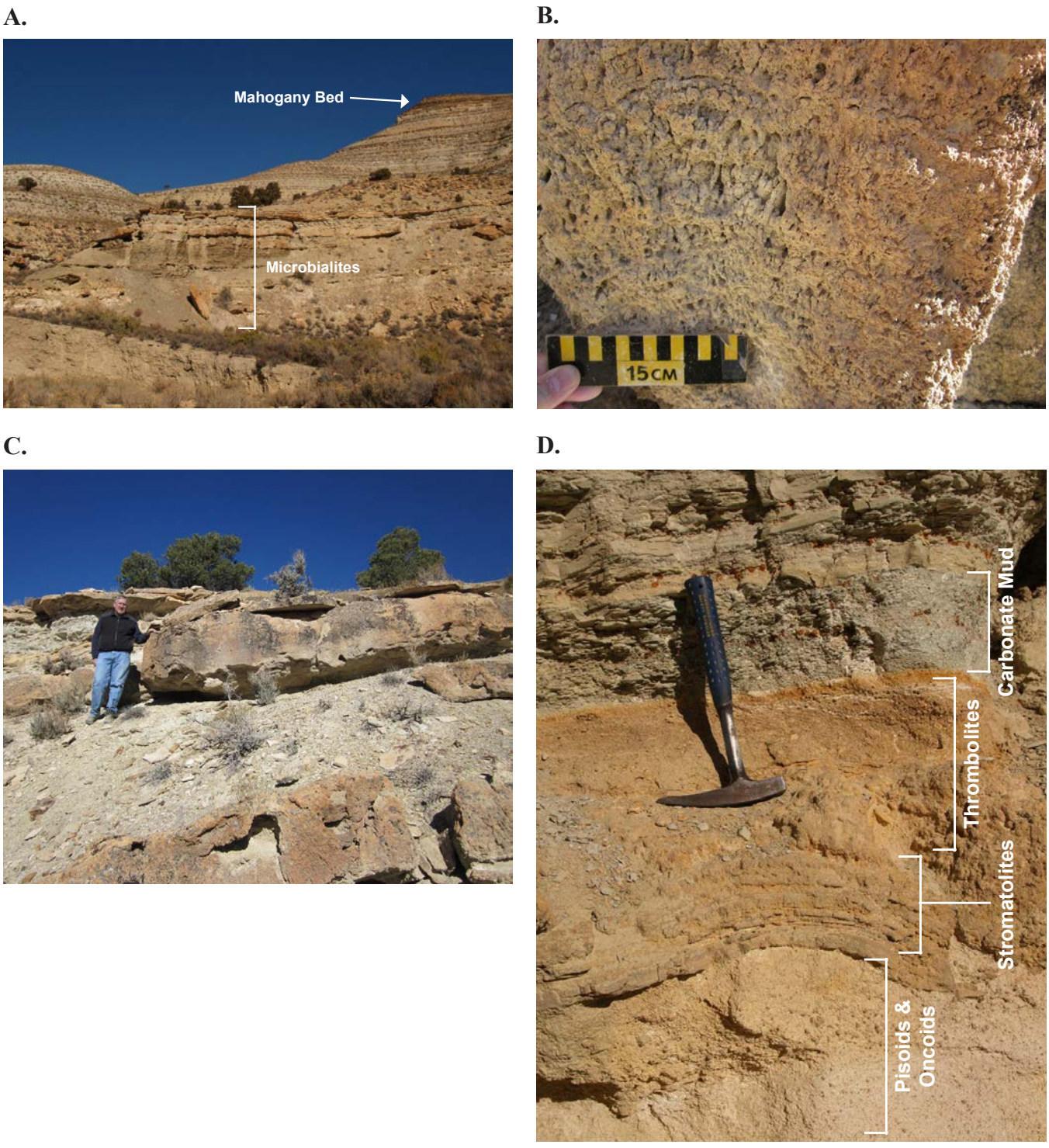

Figure 47. *Microbialites and associated grainstone/rudstone facies at Hells Hole Canyon (see figure 28 for location map).* ***(A)*** *View of the entire Hells Hole section, taken from the base of the outcrop.* ***(B)*** *Outcrop surface of a dominantly thrombolitic bed. Note the well-preserved megascopic pore system that was controlled by the growth habit of the original microbial fabric.* ***(C)*** *View of two dolomitic thrombolite beds (in orange), one at the base of this view and the other (1.5 meters [5 ft] thick) at the level of the scale person.* ***(D)*** *A typical microbialite interval and associated facies. The light tan interval near the base is composed of pisoids and oncoids (as a grainstone/rudstone). The tan beds beneath the hammer are stromatolitic, whereas a thrombolite dominates the area to the right of the hammer.*

tential hydrocarbon plays in Utah and the Rocky Mountain region. The UCRC cores serve as production-scale analogs for comparison of marine microbialites to the more common lacustrine microbial reservoirs. This offers the opportunity to better identify marine microbialites and their hydrocarbon potential in the Rockies and elsewhere in the world.

Eocene Green River Formation Microbial Carbonates at West Willow Creek Oil Field, Uinta Basin

West Willow Creek oil field is located in the center of the Uinta Basin (figures 29 and 48) and produces oil from a microbial mound interval (the "E_2 carbonate bed" of Osmond [2000], figure 49) at the transition of the Castle Peak interval to the black shale facies unit making it within the Long Point Bed of the lower Green River Formation (figures 28 and 31). Although small in size and having only limited production, it is the only conventional field actively producing from a microbial carbonate buildup in the Uinta Basin. However, other lacustrine carbonate intervals, some possibly microbial, are currently being evaluated for horizontal drilling by numerous petroleum companies.

Field Overview

The productive "E_2 carbonate bed" in the Uinta Basin is a microbial interval that was deposited in a nearshore, shallow-water, lacustrine environment. The carbonate buildup/mound, combined with an updip structural pinchout, created the trapping mechanism for West Willow Creek field (figures 50 and 51) (Osmond, 2000). The reservoir seal consists of overlying black, very finely laminated shale. The source for the oil is organic-rich shale and marlstone beds within the Green River Formation.

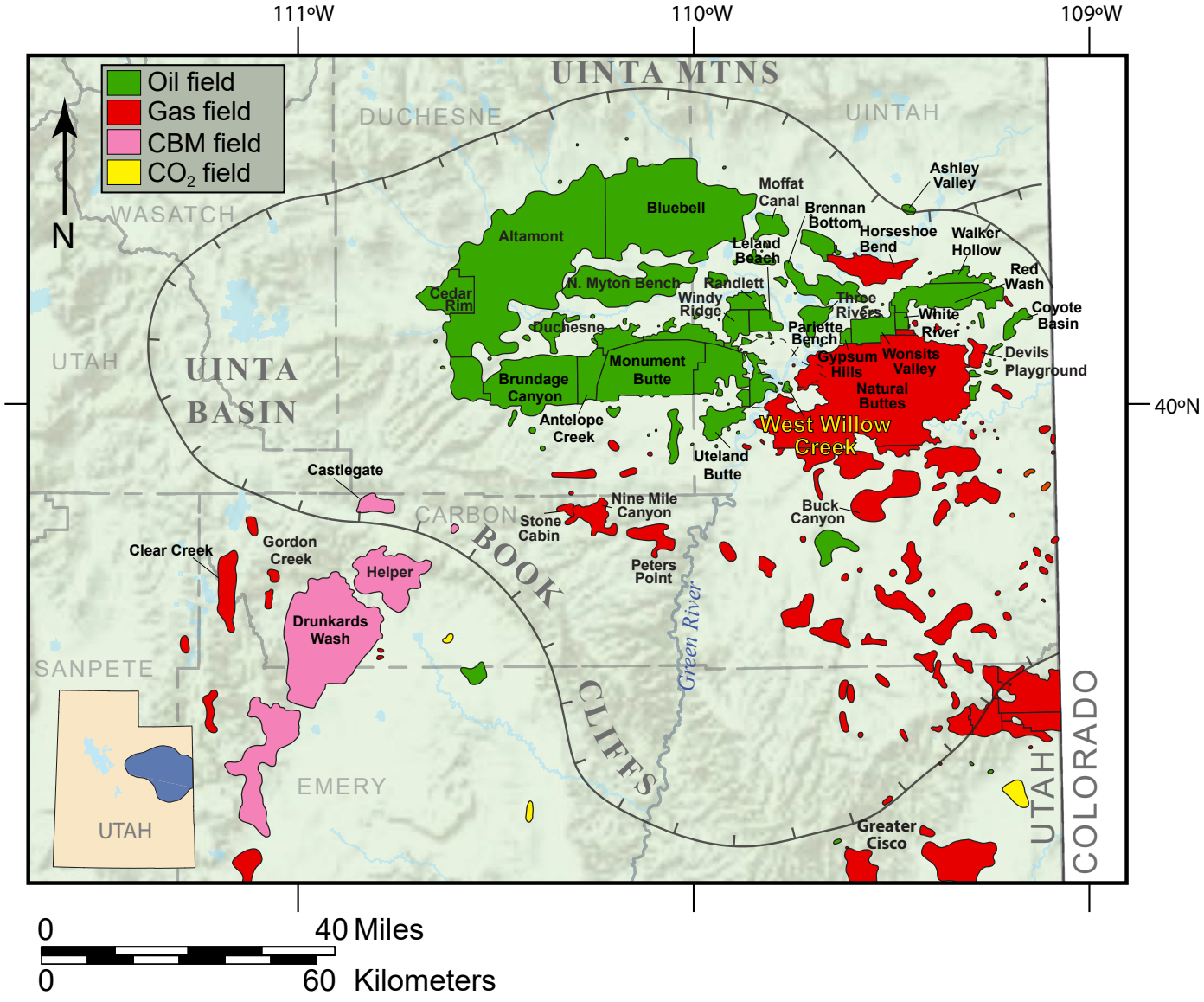

Figure 48. *Oil and gas fields in the Uinta Basin, Utah and Colorado; West Willow Creek field highlighted. Modified from Wood and Chidsey, 2015.*

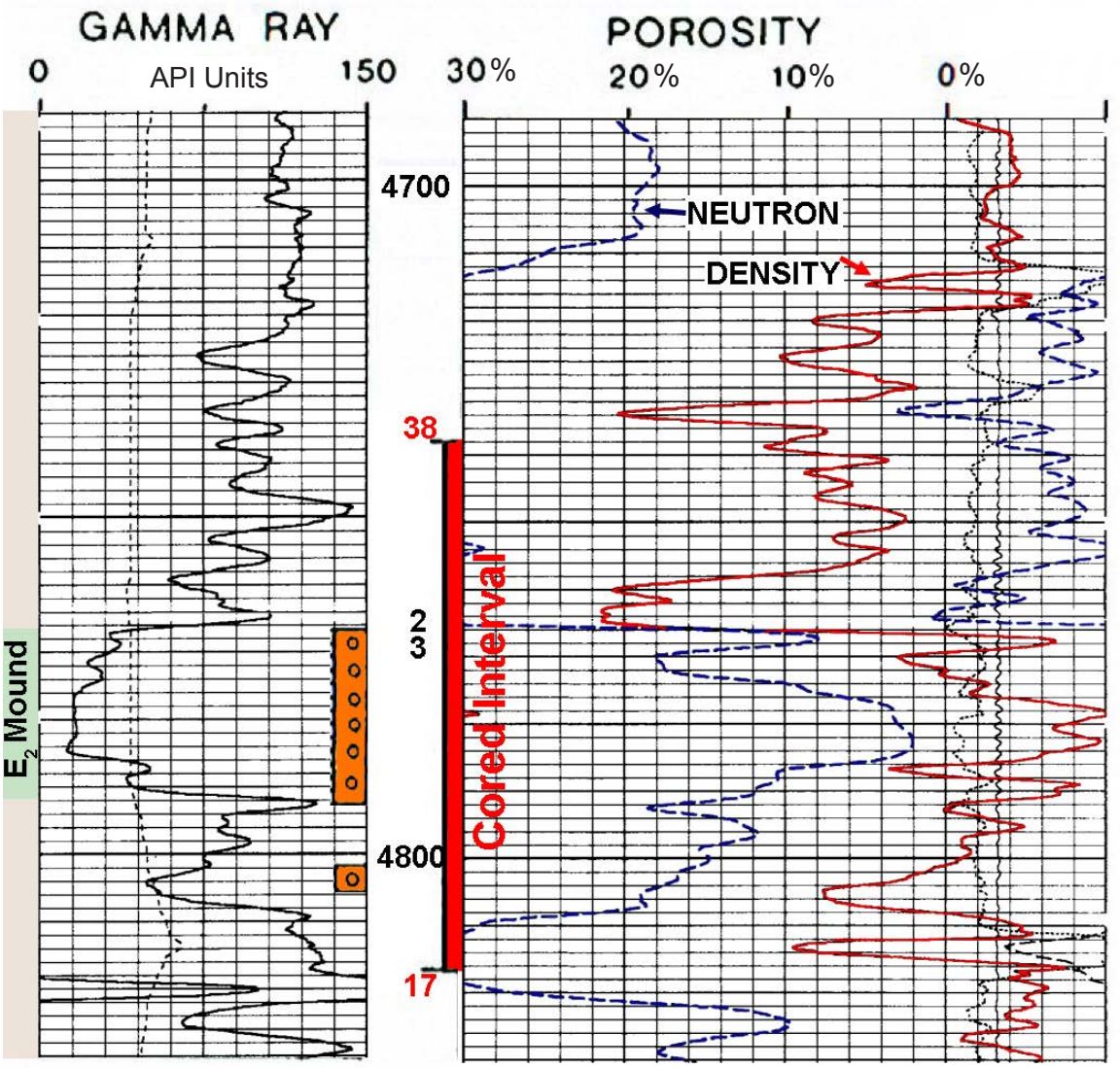

Figure 49. *The productive "E_2 carbonate bed" in lower Green River Formation displayed on the compensated neutron-formation density and gamma-ray log, Federal No. 15-24B well, West Willow Creek field, Uintah County, Utah. The red bar on the right displays cored interval; the perforated interval is indicated by circles on the outside left of the center column. Cumulative production (the well was abandoned in 2007): 15,639 BO, 5025 thousand cubic feet of gas, and 8674 barrels of water (Osmond, 2000).*

West Willow Creek field was discovered in November 1981 with the completion of the Mapco Inc. No. 7-25B well (SW1/4NE1/4 section 25, T. 9 S., R. 19 E., SLBL&M, Uintah County), which had an initial potential flow (IPF) of 21 barrels of oil per day (BOPD) and 5 barrels of water per day (BWPD). The field currently has five producing wells and three abandoned producers. Cumulative production as of March 1, 2021, was 1,166,563 barrels of oil (BO) and 12.3 billion cubic feet of gas (BCFG) (Utah Division of Oil, Gas and Mining, 2021a). Estimated original oil in place (OOIP) is 8 million BO and estimated original gas in place is 3.0 BCFG (Osmond, 2000). A secondary enhanced oil recovery program for pressure maintenance (reinjection of casing head gas into the gas cap) began in 1994 (Utah Division of Oil, Gas and Mining, 1994). The program was discontinued in 1997 because of premature gas cap breakthrough in structurally lower producing oil wells (Osmond, 2000).

The net pay thickness of the E_2 bed ranges from 3 to 12 meters (10–40 ft) (gross pay ranges from 8 to 30 meters [25–100 ft]) over a 2.3-square-kilometer (0.9 mi^2) area, whereas the geometry of the mound covers a total area of about 5 square kilometers (2 mi^2) (figure 50). The hydrocarbon column is 60 meters (200 ft) and porosity ranges from 8% to 18% in interparticle, intraparticle, shelter, intercrystalline, vuggy, and microporosity pore networks; permeability varies between from 0 to 4.1 millidarcies (mD) (Osmond, 2000).

General Core Evaluation

A core was recovered from the "E_2 carbonate bed" in the Federal No. 15-24B well (SW1/4SE1/4 section 24, T. 9 S., R. 19 E., SLBL&M; see figure 50 for well location and the appendix for core photographs) at West Willow Creek field. The 15-24B well produced 15,639 BO and 5025 thousand cubic feet of gas

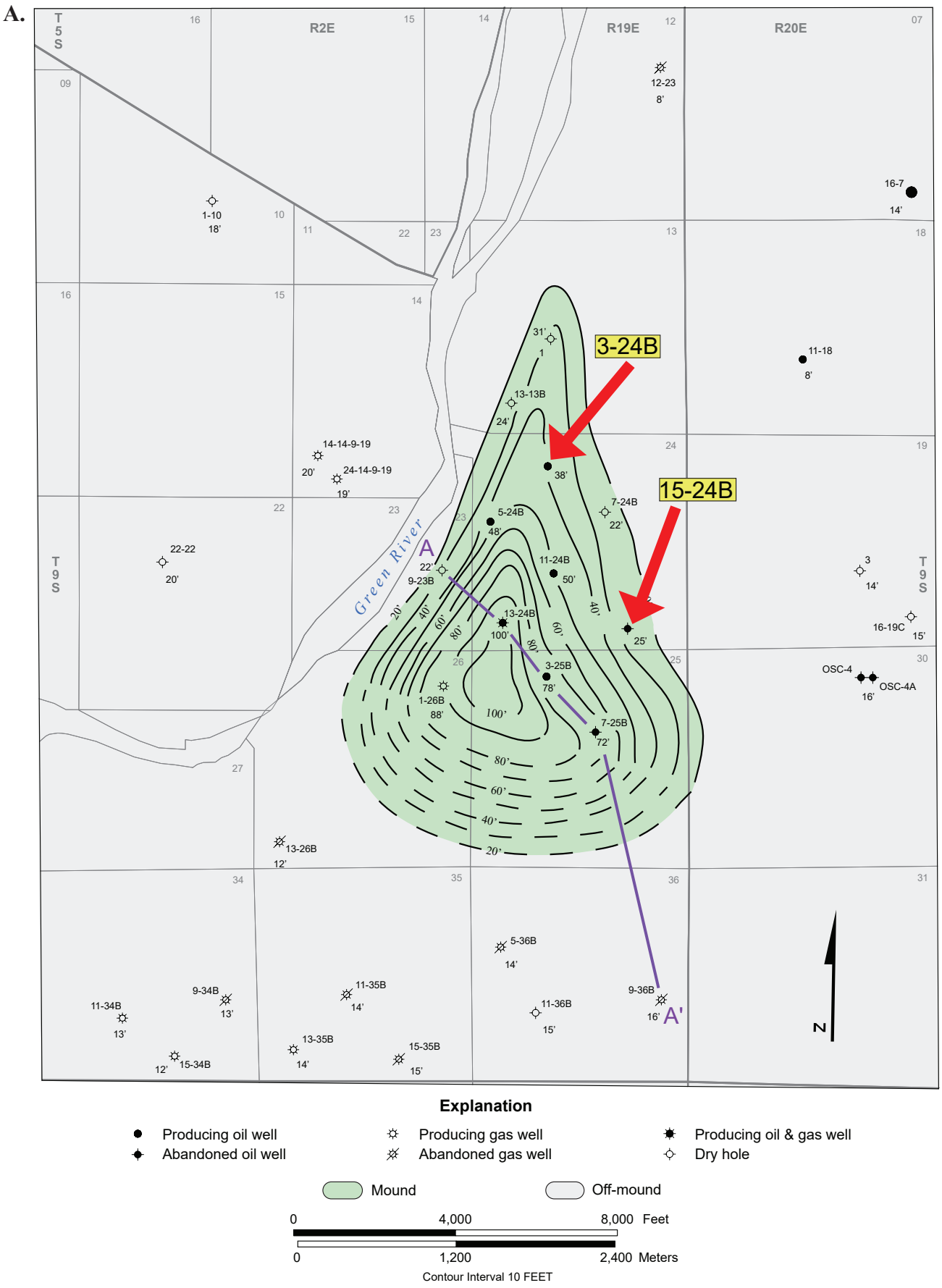

Figure 50. *West Willow Creek oil field.* ***(A)*** *Isopach map of the E_2 carbonate bed, lower Green River Formation.*

B.

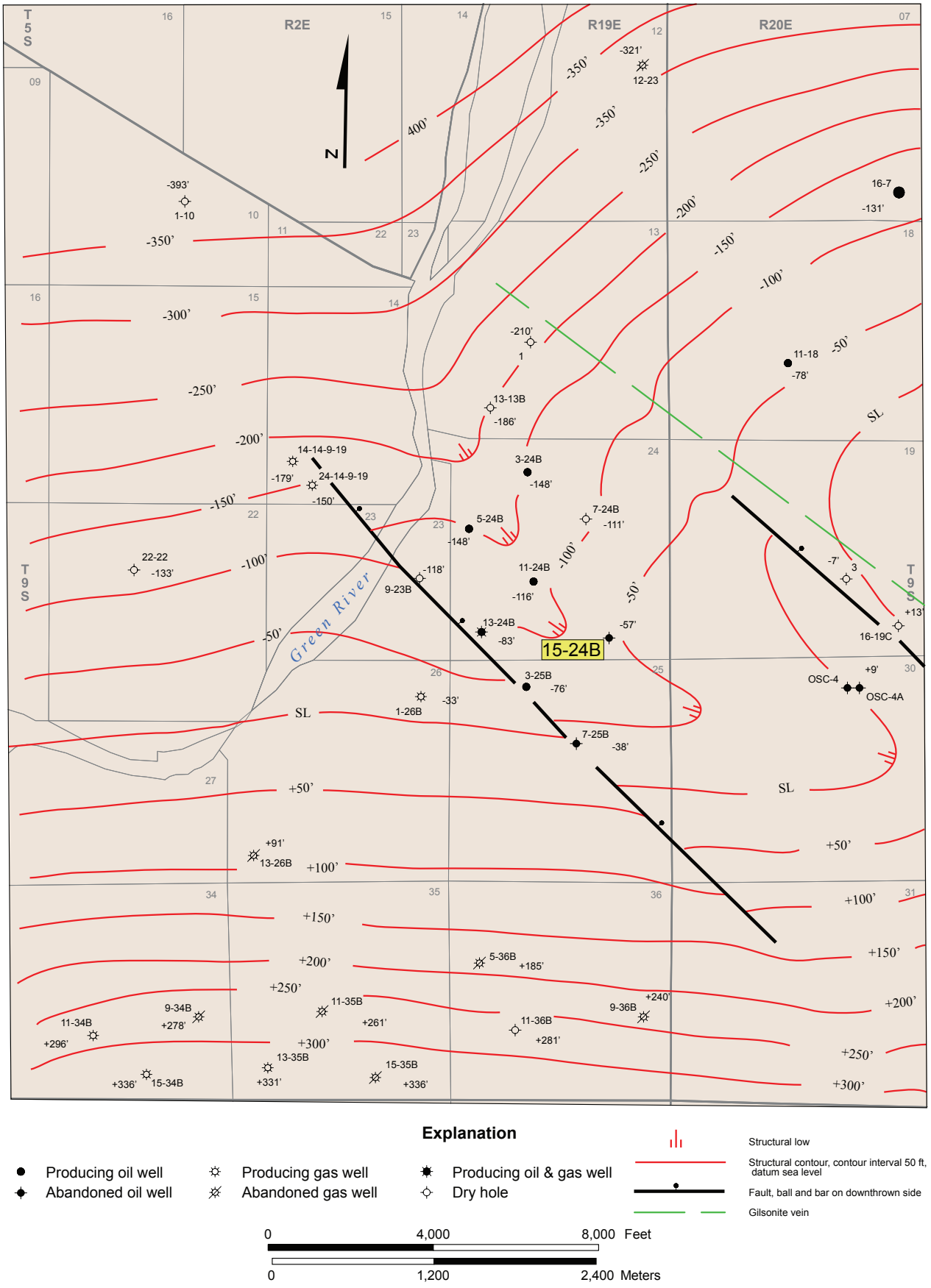

Figure 50 continued. *West Willow Creek oil field.* ***(B)*** *Structure contour map at the base of the E_2 carbonate bed. Note location of the Federal No. 15-24B well. Cross section A–A' is shown on figure 51. Modified from Osmond (2000).*

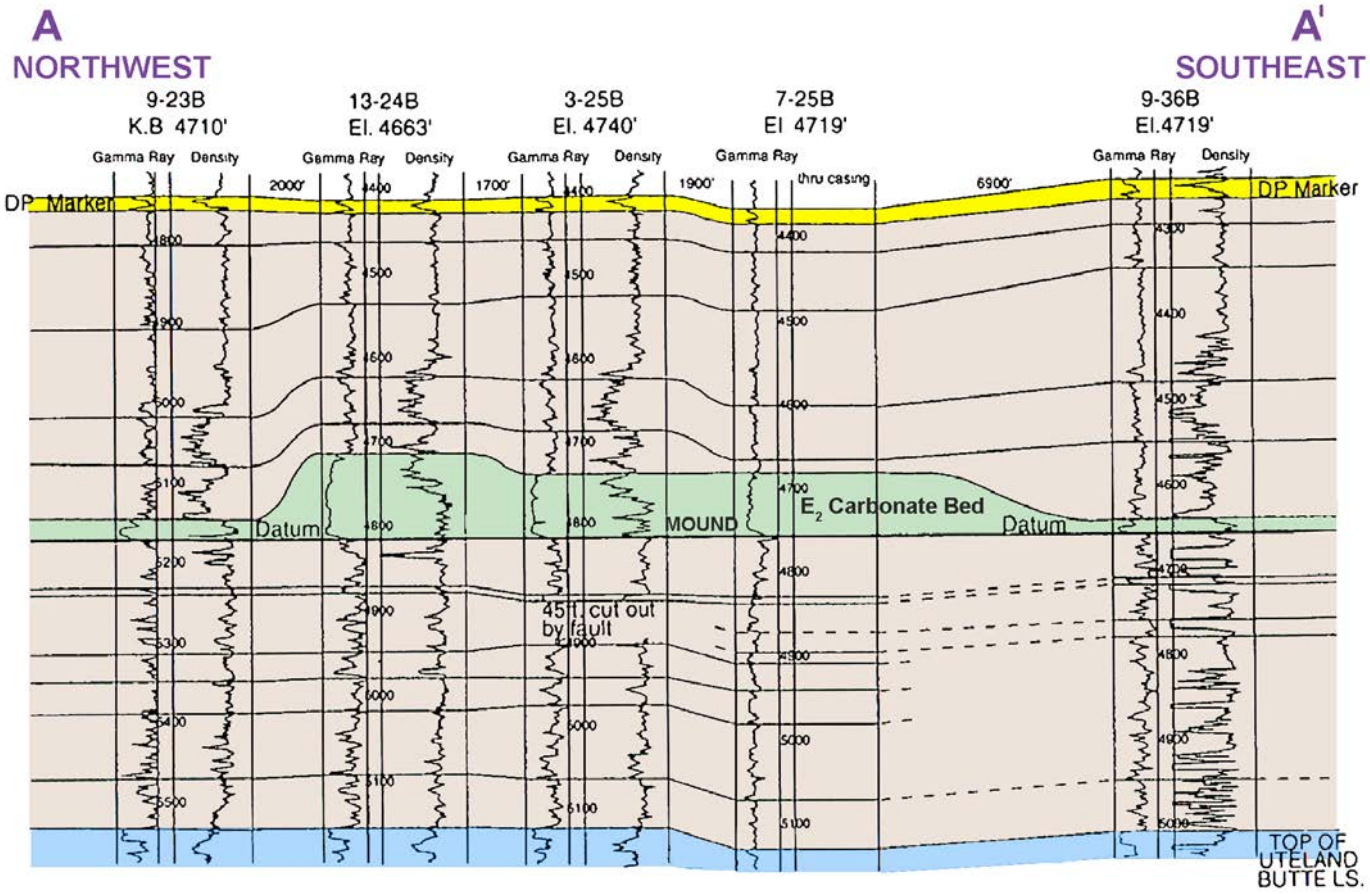

Figure 51. *Stratigraphic cross section through the E_2 carbonate bed. Line of section shown on figure 50. Modified from Osmond (2000).*

(MCFG) before it was abandoned in 2007 (Utah Division of Oil, Gas and Mining well records). The core was described and tied to wireline well logs by Osmond (2000) and Bereskin and others (2004) (plates 4 and 5). Specifically, Osmond (2000) summarized the major characteristics of the 15-24B core including lithology, fossils, sedimentary structures (primarily oncolites), fractures, and oil staining. The lower part of the core consists of a series of 2- to 4-meter-thick (7–13 ft) shale and siltstone beds with a very thin coal (1.3 centimeters [0.5 in.]). The middle consists of <1–4-meter-thick (3–13 ft), finely crystalline oncolitic dolomite units with abundant gastropods and minor stromatolites. The upper section is composed of <1-meter-thick (3 ft) oncolitic and ostracodal limestone beds capped by black fissile shale. Osmond (2000) only documented the occurrence of the stromatolites; no petrographic work was conducted as part of the study.

In addition, Osmond's (2000) study includes petrophysical data, pore types, diagenetic history, and environmental interpretations of another core from the West Willow Creek 3-24B well (NE1/4NW1/4 section 24, T. 9 S., R. 19 E., SLBL&M; see figure 50 for well location) 1300 meters (4265 ft) north of the 15-24B well. (The current location of this core is unknown; Osmond's description was from verbal communications with those who had examined the core and an industry petrographic report.) The 3-24B core was reported to contain a 2-meter-thick (6 ft) stromatolitic boundstone and associated coated grain/oolitic grainstone overlying oncolitic and oolitic packstone deposited in lacustrine upper and lower shoreface environments, respectively (Osmond, 2000). Based on analysis of a single core plug from the 3-24B, porosity is high at 25% having a variety of pore networks such as interparticle, intraparticle, and microporosity. The permeability is low (89 mD) for this porosity indicating that there are few interconnected pores. Diagenetic events began with compaction followed by pore-filling calcite, minor dissolution, dolomitization, and precipitation of minor pyrite, silica, and phosphatic material (Osmond, 2000).

Bereskin and others (2004) provided a similar, but graphical description of the 15-24B core showing both finely crystalline to microcrystalline dolomite and limestone. Ooids, pisoids, ostracods, and gastropods, interpreted as deposited in carbonate shoals, are major constituents of the limestone beds. The Bereskin and others (2004) study did include petrographic analysis of a limited number of thin sections. Microbial fabrics were described as algal stromatolites and microstromatolites deposited in a lake-margin carbonate flat. Dolomitized algal material from the carbonate buildup shows good porosity, whereas the tubules attributed to algal construction contain small intercrystalline pores with very low permeabilities (single mD).

Microbialites and Associated Grains

Our research builds on past studies, providing a detailed petrographic description of the microbial fabrics, associated carbonate grains, and pore types of the Green River Formation in the West Willow Creek 15-24B core. Carbonate fabrics observed in core include stromatolitic and thrombolitic boundstones and rudstones and associated peloidal, oolitic, and ostracodal grainstones. Microbialite heads often consist of stromatolitic crusts with internal thrombolitic fabrics. Radial, micritic, filamentous, and tubular microtextures abound, along with excellent preservation of hollow filamentous and branching cells. Stromatolitic and thrombolitic microbialites contain well-preserved primary interparticle and intraparticle (intracellular) porosity. Associated grainstones between laminated microbial fabrics are composed of peloids, ooids, and ostracods, with good to excellent interparticle porosity. Oncolites also are a significant component of the microbial system and contain microporosity along and around microtubules within the oncoid cortex layers.

Stromatolites within the 15-24B core consist of digitate heads or columns displaying synoptic relief and sharp margins (figure 52A), with abundant articulated ostracods between the columns. Internally, these stromatolitic heads have distinct cellular structures with open pores (figure 52B). Significant preserved interparticle and intraparticle pore space occurs in this facies, although very coarse calcite spar occludes some of the porosity. Fibrous, early isopachous cements line some of the intraparticle and interparticle pores within these structures (figure 16A), whereas microscopic pyrite appears to line some of the intraparticle pores. Some stromatolites have a laminated fabric with small hemispherical heads that have grown on top of, or trapped, grains composed of early peloids (semi-lithified and rigid), ooids, and ostracods (figures 52C and 52D). Good to excellent primary interparticle porosity occurs within trapped and interbedded grainstones. Figure 53A displays a complex microbialite head composed mostly of stromatolites having some thrombolitic interior characteristics. Radial, micritic, and tubular micro-tectures abound along with excellent preservation of hollow filamentous and branching cells (figures 53B and 53C). Patches of microporosity are present around some of the filamentous areas.

Thrombolites within the core are often dark colored with variable vertical synoptic relief up to 20 centimeters (7.9 in.) (figure 54A). They have sharp, laminated margins with interiors composed of clotted and cellular structures (figures 54B and 54C). Thrombolites also can have more laminated (stromatolitic) crusts, together forming small heads or fingers (figure 54D). Small oncolites, early peloids, ooids (some broken and regenerated), as well as ostracods, are found in layers between thrombolitic heads (figure 54B). Good matrix porosity (completely oil stained in the core), interparticle and intraparticle, is preserved within the heads and the intervening grainstones. Pores are typically lined with isopachous cements (figure 54E) or plugged by later calcite spar. Excellent interparticle porosity and perhaps better pore throat connections also occur between early peloids and ooids deposited between thrombolitic heads (figure 54F). The porosity (10.2%) and permeability (0.62 mD) obtained from core plug analysis appear to come from the thrombolitic head (figure 54D) where the clotted thrombolite texture may have good porosity but lower permeability, i.e., fewer interconnected pore throats.

The 15-24B core also includes a well-defined oncolitic rudstone composed of large compound oncoids that have good internal laminated microbial coatings (figure 13). Laminae are defined by alternating dark micritic/organic layers with thicker, light-colored intervals containing detrital carbonate sediment (figure 55A). Oncoids also have well-preserved internal tubules and filamentous cells. Patches of microporosity are well developed within the oncolites, especially in the dark layers and surrounding the microtubules (figure 55).

Synopsis and Discussion

Evidence of a comparable feature to the West Willow Creek oil field microbial mound is found on the western shore of Great Salt Lake near Lakeside, where well-lithified Pleistocene microbialites and a travertine mound were identified by Homewood and others (2018, in press). The West Willow Creek microbial mound reservoir developed during the transgression of the Long Point Bed forming on shallow carbonate flats near the southern shore of Lake Uinta created during the very low lake-level cycle at the end of Castle Peak regression. The growth of the West Willow Creek mound and the similar Willow Creek mound (11 kilometers [6.8 mi] to the southeast), a non-productive microbial buildup also in the E_2 carbonate bed, was able to keep pace with the eventual rising lake level; the Willow Creek mound has porosity in the upper part but does not contain oil. The rate of lake expansion may have been slower than other oscillations, which could account for these unusually thick (up to 35 meters [115 ft]) mounds in comparison to other much thinner, more continuous, microbialites elsewhere in the basin (Osmond, 2000). There is no known evidence of a bathymetric or structural anomaly that would explain why the two Willow Creek mounds developed at these locations (Osmond, 2000).

Lake conditions were also conducive for microbialite, ooid, peloid, and especially oncoid development at this location; ostracods and turretellid gastropods flourished. However, we have not identified microbialites associated with the Long Point Bed anywhere else in the basin (on outcrop or core). This begs the question – Could hydrothermal fluids have fed microbes in travertine adding a biogenetic component (filaments?) to the mound? Thus, the stromatolites formed during the transgression (Long Point Bed) into the deeper black shale facies (figure 31). The Federal No. 15-24B core shows a general deepening cycle from beach (sandstone) to offshore oncoids, to stromatolites, to mud (plates 4 and 5) (Bereskin and others 2004). Sandstone and siltstone of a subaerially exposed

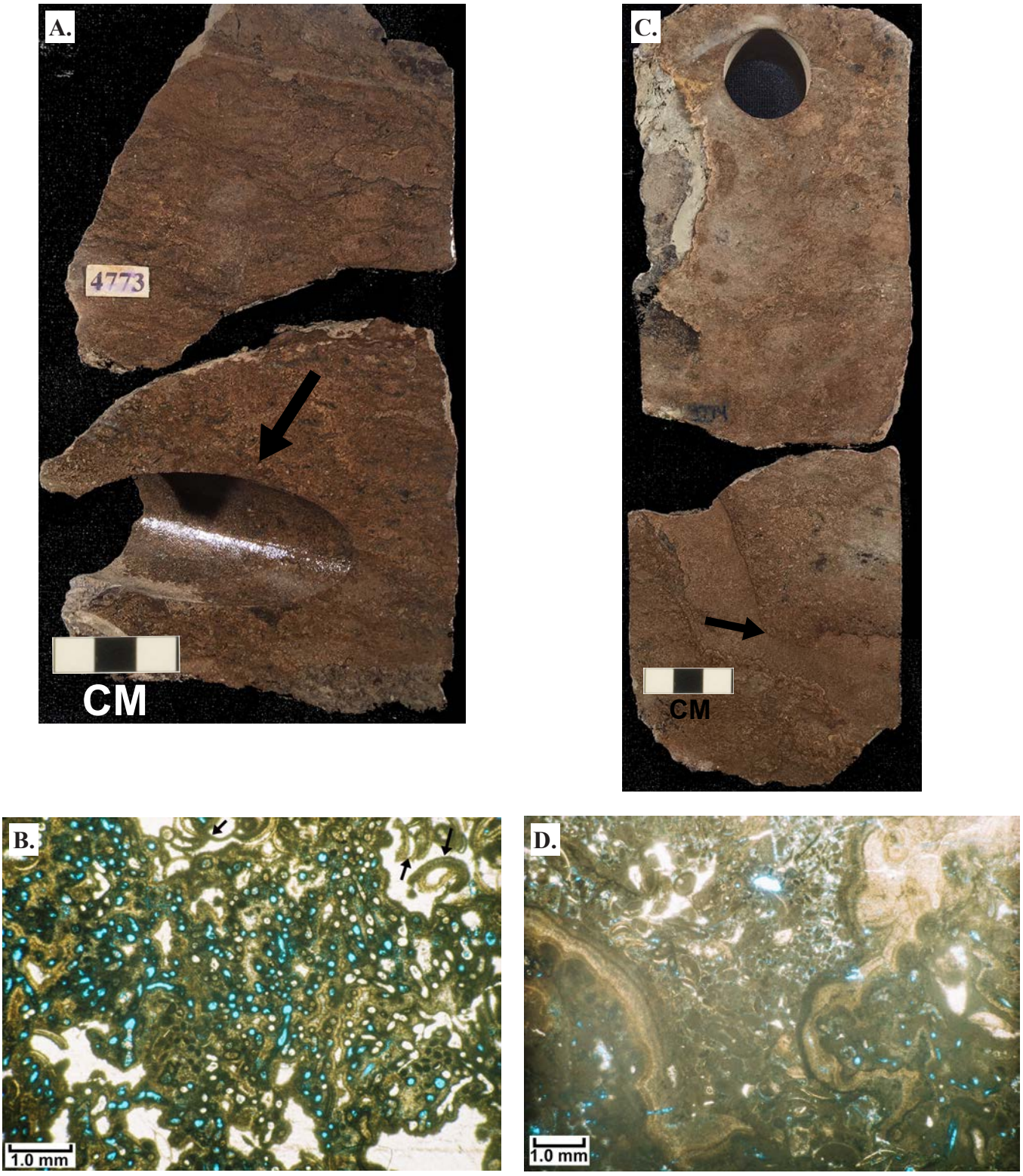

Figure 52. *Stromatolites from the Federal No. 15-24B core, West Willow Creek field.* ***(A)*** *Microbialite consisting of digitate stromatolitic heads or columns displaying relief and sharp margins, 1454.8 meters (4773.3 ft); core plug analysis: porosity = 15.6%, permeability = 4.1 mD. Black arrow indicates the location of photomicrographs shown in B and figure 16A.* ***(B)*** *Photomicrograph overview of microdigitate microbialite head with internal cellular structures and circular pores (plane light). Calcite spar occurs between and within some microbialite structures. Ostracods occur in spaces between heads (see black arrows). Porosity in blue.* ***(C)*** *Laminated (stromatolitic) microbialite fabric with small hemispherical "heads" on top of a substrate of peloids, ooids, and ostracods, 1455.2 meters (4774.5 ft); core plug analysis: porosity = 7.4%, permeability = 1.0 mD. Black arrow indicates the location of photomicrographs in D and figure 9B.* ***(D)*** *Photomicrograph of portions of two hemispherical stromatolitic domes covering peloidal/ostracodal grainstones (plane light). Minor late, coarse calcite cement plugs some of the interparticle pores.*

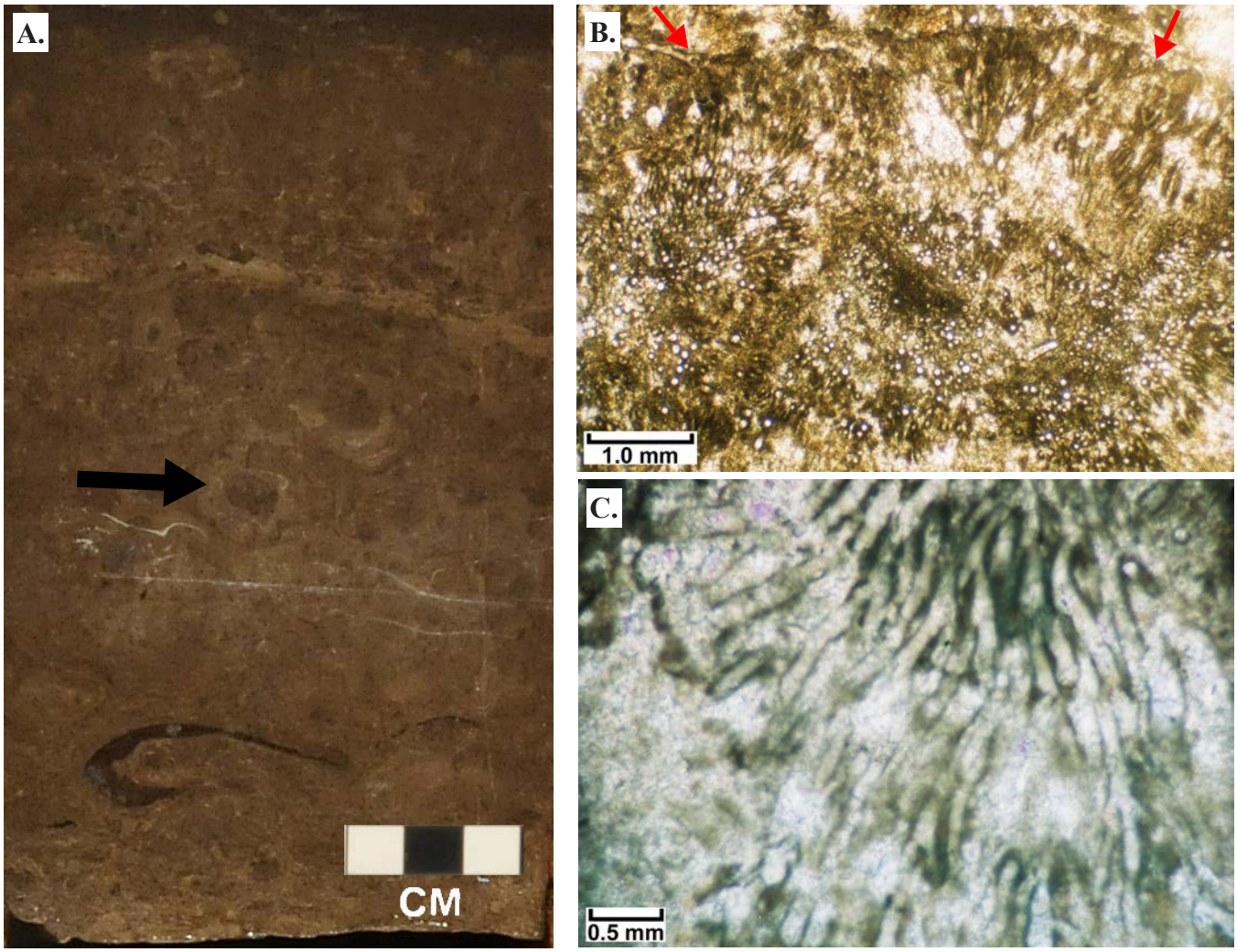

Figure 53. *Complex microbialite head from the Federal No. 15-24B core, West Willow Creek field.* ***(A)*** *Section of core showing mostly stromatolites with some thrombolitic interior characteristics, 1459.2 meters (4787.5 ft); core plug analysis: porosity = 0.4%, permeability = 0.02 mD. Black arrow indicates the location of photomicrographs shown in B and C.* ***(B)*** *Photomicrograph displaying a cross section of a radiating, pustular stromatolite "head." Note tubular and cellular microstructures. Red arrows point to top surface of the "head" (crossed nicols with accessory plate).* ***(C)*** *Radiating tubular or filamentous microstructure surrounded by sparry cement (plane light).*

sand flat formed the substrate for the microbialite buildups. Ooids, oncoids, and gastropods filled in the spaces between microbial heads. The upper part of the buildup is dominated by peloids, gastropods, ostracods, and thin stromatolites developed under deepening conditions (farther offshore). These grainstone and microbialite deposits, as well as the fine carbonate muds near the top of the mound, experienced early dolomitization (Osmond, 2000; Bereskin and others 2004), resulting in intercrystalline porosity and microporosity. Therefore, the best reservoir quality occurs in the dolomitized upper part of the mound. When Lake Uinta experienced a major rapid deepening and expansion, the West Willow Creek area was flooded.

Additional microbial mounds in the E_2 carbonate bed and other intervals are likely in the Green River Formation but remain to be discovered in the Uinta Basin. Osmond (2000) reported several possible smaller mound buildups, both in terms of thickness and areal extent, which have been identified on wireline well logs. Microbialites and associated carbonates are now recognized for their hydrocarbon potential based on West Willow Creek field and represent significant untested targets within the Uinta Basin. However, the typical thin, regional microbialites that developed along the southern shore of Lake Uinta, like those found in the Skyline 16 research core and nearby outcrops, were not buried deep enough to be reservoirs.

Finally, microbialites in Great Salt Lake and cores from the Green River Formation in the Uinta Basin (West Willow Creek field and Skyline 16 research core) exhibit similarities in terms of the variety of microbial textures and fabrics. However, although there are several possible causes for the thicker mounds in the basin, including the possible role of groundwater fluids, the mechanism of their formation is not completely understood.

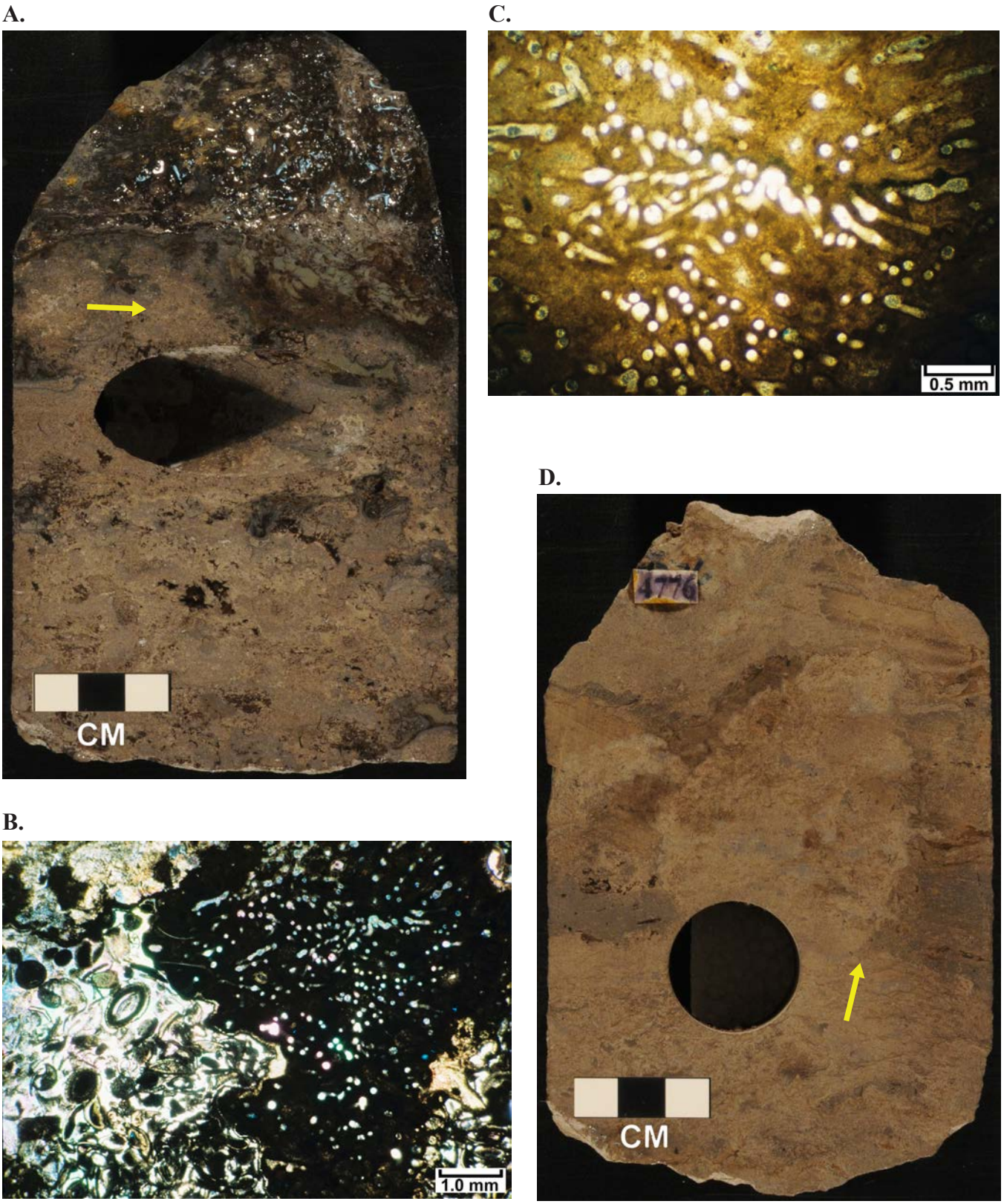

Figure 54. *Thrombolites from the Federal No. 15-24B core, West Willow Creek field.* ***(A)*** *Thrombolitic microbialite displaying significant vertical synoptic relief, 1454.3 meters (4771.5 ft); core plug analysis: porosity = 1.9%, permeability = 0.03 mD. The yellow arrow indicates the location of the photomicrographs in B and C.* ***(B)*** *Photomicrograph of steep-sided margin of a massive thrombolitic head with ostracods filling the cavity between the margins of the head (plane light).* ***(C)*** *Photomicrograph of tubular or filamentous textures within the same thrombolitic head (plane light).* ***(D)*** *Clotted (thrombolitic) fabric with laminated (stromatolitic) crusts that together form small heads and "fingers," 1455.8 m (4776.4 ft); core plug analysis: porosity = 10.2%, permeability = 0.62 mD. The yellow arrow indicates the location of the photomicrographs in E and F.*

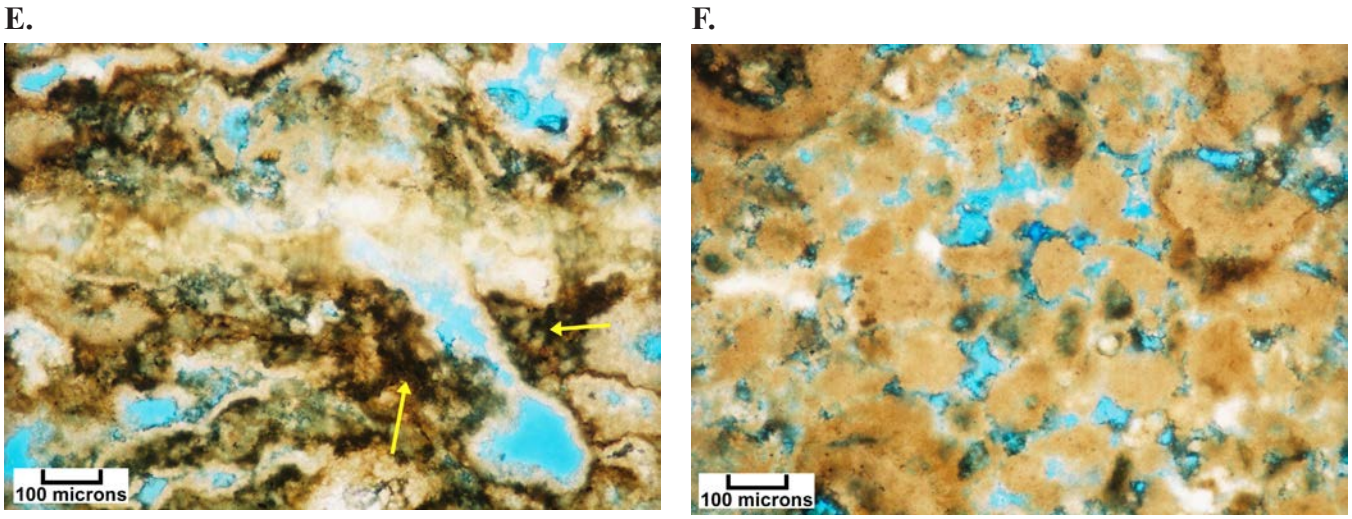

Figure 54 continued. *Thrombolites from the Federal No. 15-24B core, West Willow Creek field.* ***(E)*** *Photomicrograph close-up of clotted (thrombolitic) texture (see yellow arrows) with layers of good matrix porosity lined with isopachous cements (plane light with white card).* ***(F)*** *Photomicrograph showing excellent interparticle porosity between peloids and ooids, which occur between thrombolitic "heads" (plane light with white card).*

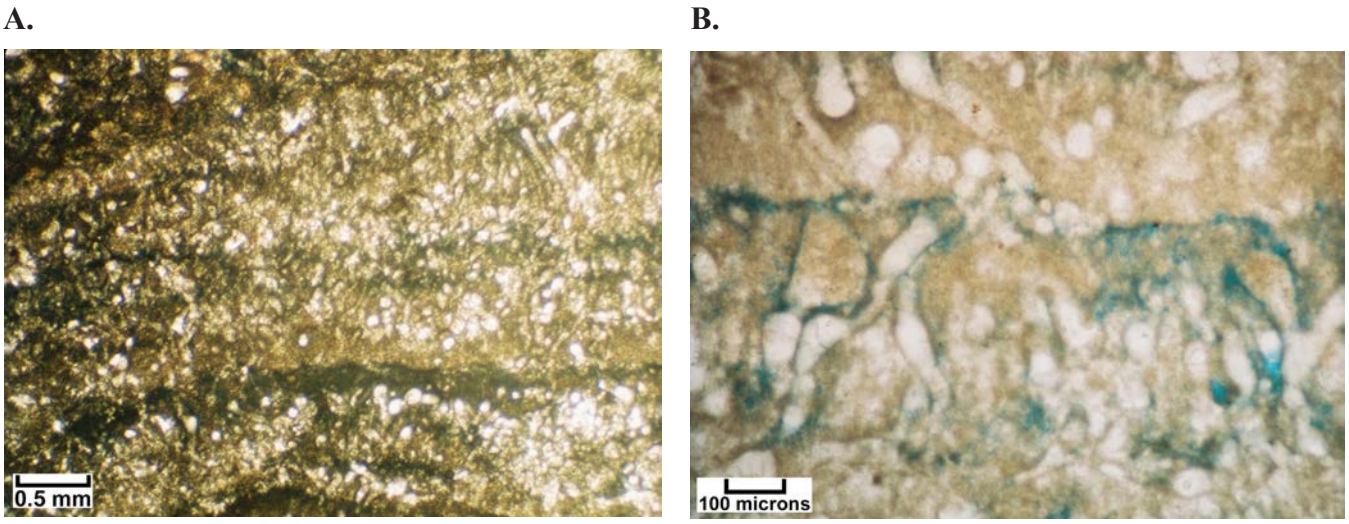

Figure 55. *Photomicrographs of oncolites from the Federal No. 15-24B core, 1456.7 meters (4779.5 ft), West Willow Creek field; see figure 13 for core photograph and locations of A and B.* ***(A)*** *Multiple dark/light layer couplets within an oncoid. Note the abundance of tubules and filaments within the thicker light layers. Microporosity occurs in the dark layers (plane light).* ***(B)*** *Microporosity (in blue) developed along and around microtubules within an oncoid cortex (plane light with white card).*

Jurassic Twin Creek Limestone Microbial Carbonates at Pineview Oil Field, Thrust Belt

The marine Middle Jurassic Twin Creek Limestone in the Utah/Wyoming thrust belt has produced over 16 million BO and 112 BCFG (Utah Division of Oil, Gas and Mining, 2021a; Wyoming Oil and Gas Conservation Comission, 2021). The Twin Creek, along with the Upper Triassic–Lower Jurassic Nugget Sandstone, is a major producer at Pineview field in northern Utah (figure 56). It was deposited in a shallow-water embayment south of the main body of a Middle Jurassic sea (figure 57). Examination of carbonate cores from Pineview, and fields from other regions in Utah described in the subsequent sections of this report, reveals a variety of previously undocumented marine microbial fabrics and associated carbonate grains, pore types, and reservoir characteristics. Like their lacustrine counterparts, these marine rocks display stromatolitic and thrombolitic growth forms, and possible leolites in mud mounds. Associated carbonate grains include ooids, peloids, and oncoids. Shark Bay on the west coast of Australia represents a modern analog where marine microbialites have been actively growing for 2000 to 3000 years in a subtidal environment (figure 58). These marine stromatolites are distinct buildups, separated by clean carbonate sand, where a living microbial mat layer colonizes its surface (Noffke and Awramik, 2013).

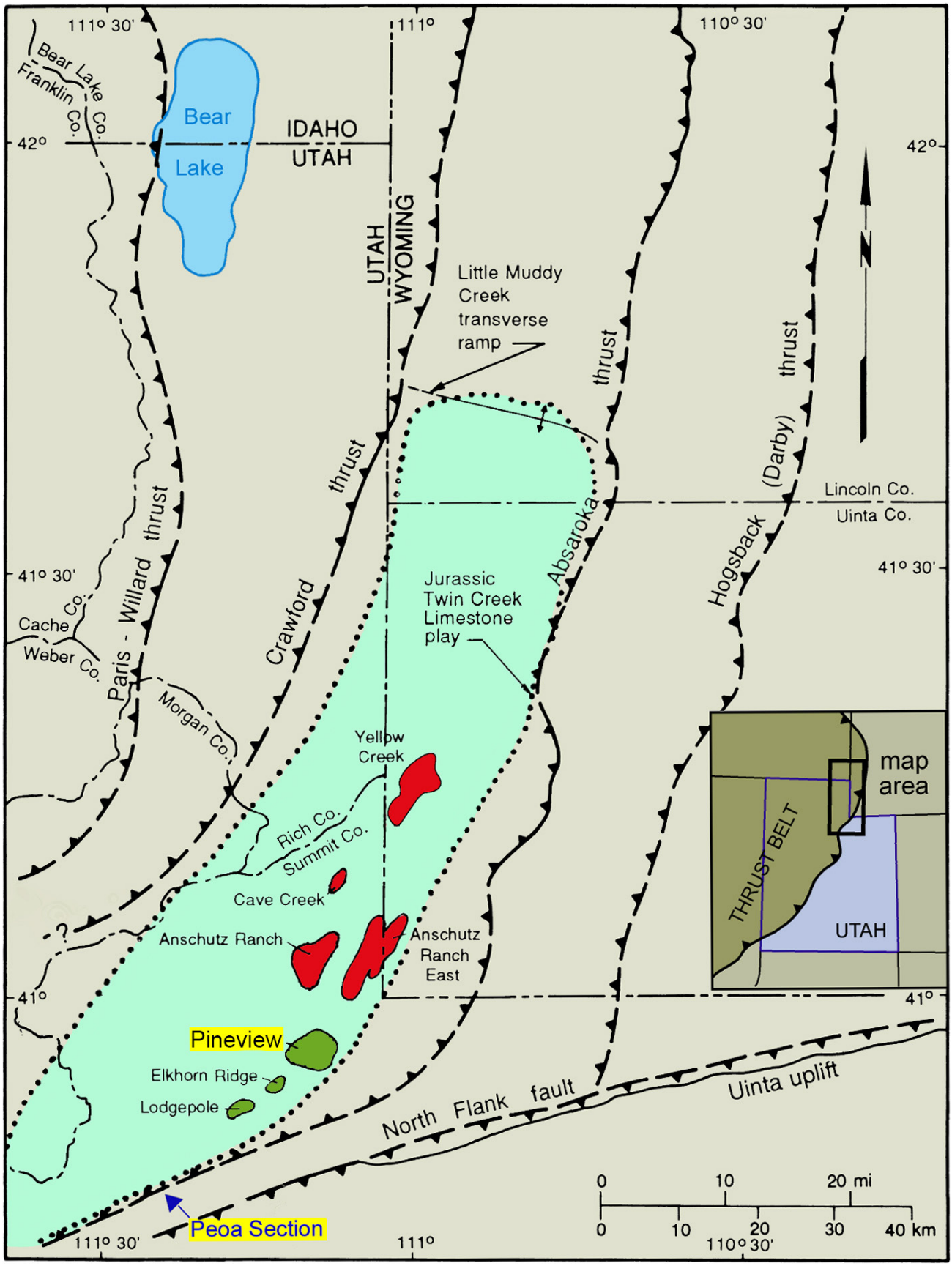

Figure 56. *Location of reservoirs that produce oil (green) and gas and condensate (red) from the Jurassic Twin Creek Limestone, Utah and Wyoming; major thrust faults are dashed where approximate (teeth indicate hanging wall). The Twin Creek Limestone thrust belt play area is dotted. Modified from Sprinkel and Chidsey (1993). The Peoa outcrop analog location is also indicated.*

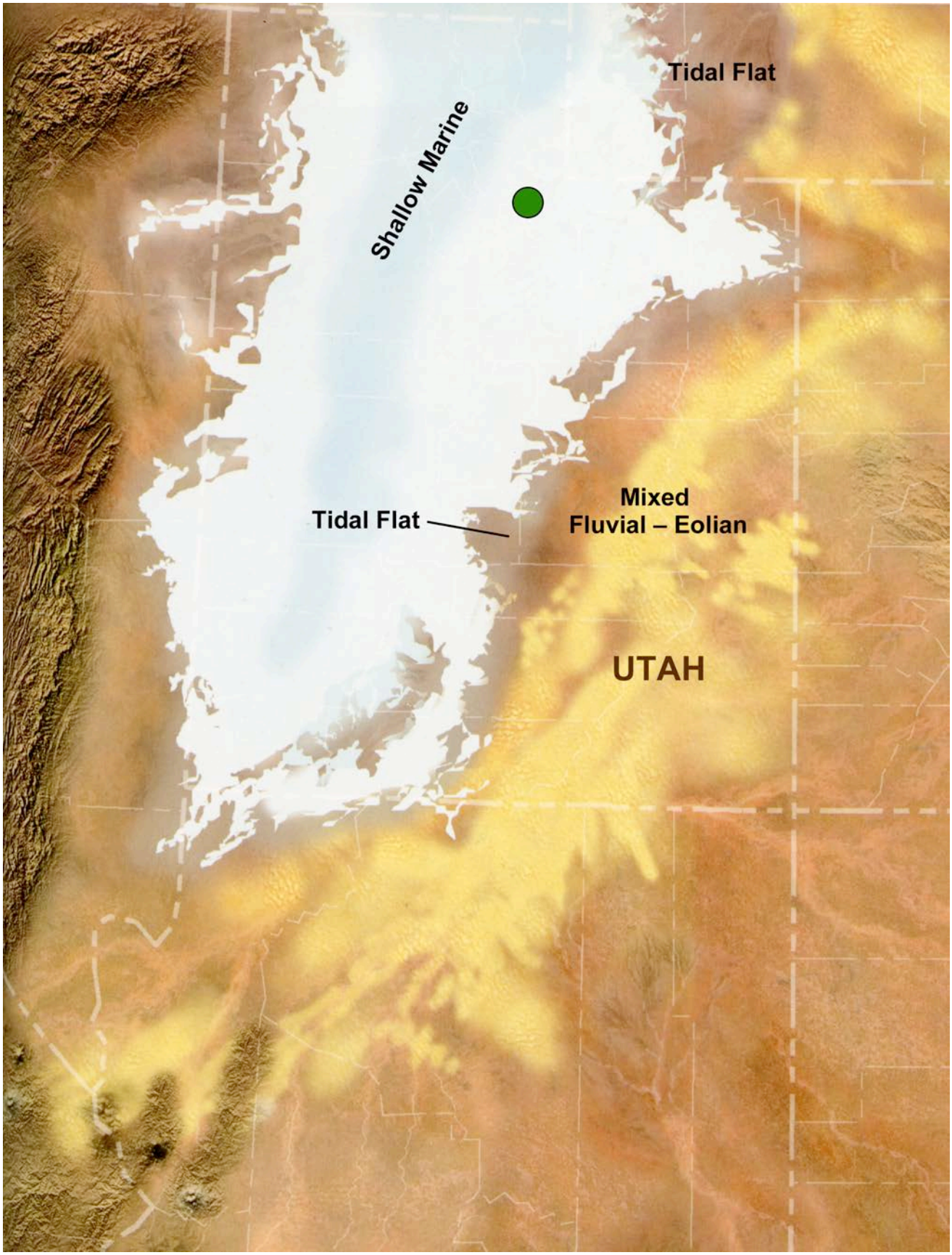

Figure 57. *Generalized paleogeography during the Middle Jurassic showing the invasion of the shallow marine sea from the north (Utah's position during Middle Jurassic). The green dot represents the approximate position of Pineview field, Summit County, Utah (not palinspastically restored). Modified from Blakey and Ranney (2008).*

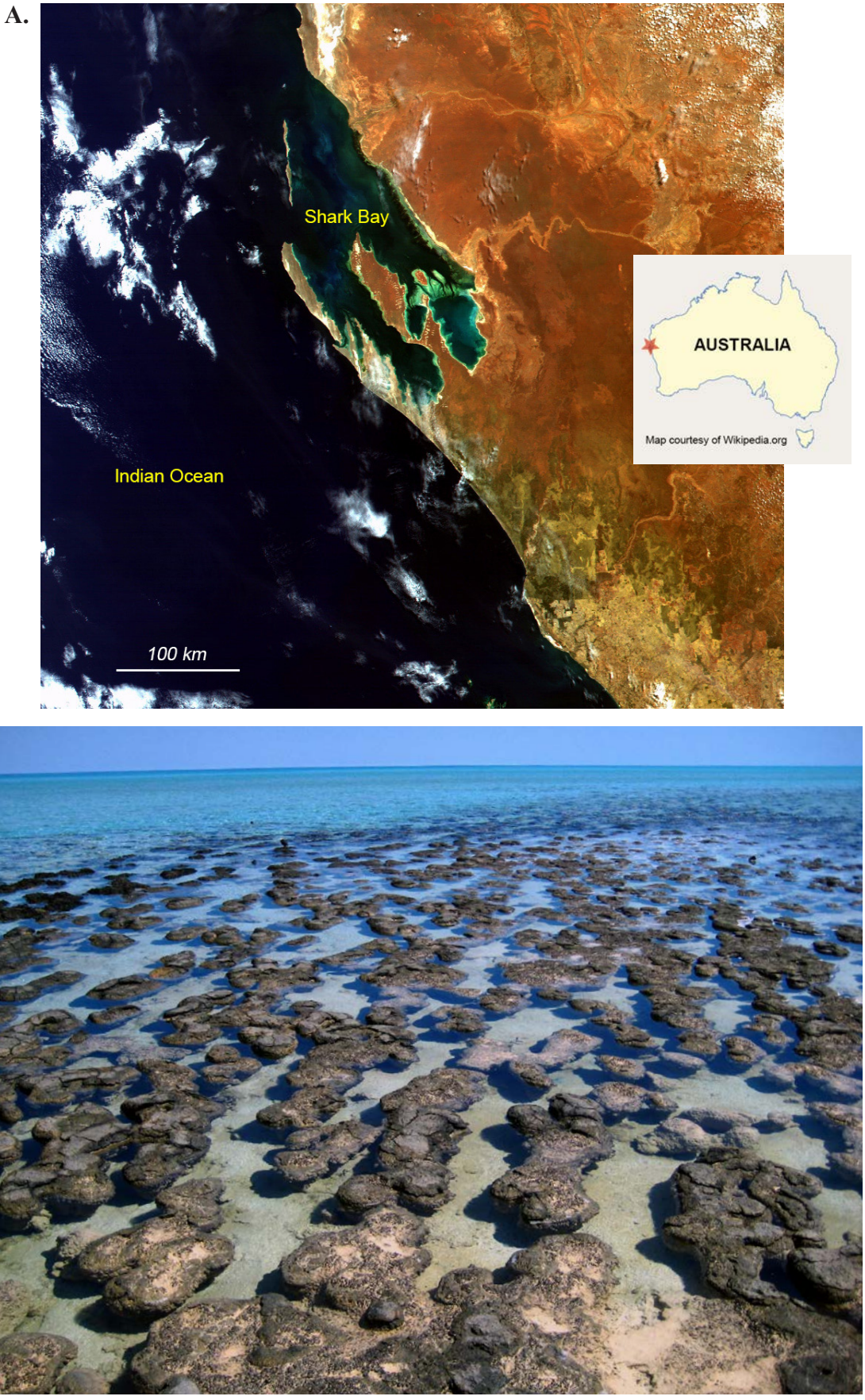

Figure 58. *Shark Bay, Australia.* ***(A)*** *Satellite image of the west coast of Australia and location of Shark Bay. MODIS image courtesy of NASA.* ***(B)*** *Actively growing marine stromatolites separated by carbonate sands. Photograph courtesy of jazzmarazz.com.*

Field Overview

The trap for Pineview and other thrust belt fields formed as a subsidiary closure along a major ramp anticline (figures 59 and 60), where the low-porosity Twin Creek Limestone is extensively fractured. Thus, productive members (five out of the seven) of the Twin Creek (figure 61, plate 6) have little to no primary porosity but exhibit secondary porosity in the form of fracturing. Natural and open fractures provide good permeability pathways within these very low porosity rocks. Seals, barriers, and baffles consist of argillaceous and clastic beds, and non-fractured units within the Twin Creek that overlie the reservoir rocks. Hydrocarbons in the Twin Creek reservoirs were generated from organic-rich subthrust Cretaceous marine shale (Mowry Shale).

Pineview field (Twin Creek Formation) was discovered in 1975 with completion of the American Quasar Petroleum Union Pacific No. 3-1 well (NW1/4NW1/4 section 3, T. 2 N., R. 7 E., SLBL&M, Summit County). The Twin Creek had an IPF of 576 BOPD and 420 MCFGPD. The original reservoir field pressure was 4200 psi (Cook and Dunleavy, 1996). The field currently has 3 producing (or shut-in) and 16 abandoned Twin Creek producers. Cumulative production as of March 1, 2021, was 9,305,008 BO and 11.7 BCFG (Utah Division of Oil, Gas and Mining, 2021a, 2021b). Estimated ultimate recovery is 12.2 million BO and 14.9 BCFG (Cook and Dunleavy, 1996). A horizontal drilling program conducted in the 1990s had limited success.

The net pay thickness of the Twin Creek Limestone reservoir at Pineview field is 60 meters (200 ft) over an 840-hectare (2080 acre) area; gross pay is 250 meters (830 ft) (Sprinkel and Chidsey, 1993). The hydrocarbon column is 340 meters (1100 ft). Porosity averages 2% to 10% in dissolution and fracture pore networks; permeability varies between 4 and 30 mD. The drive mechanism is solution gas; original water saturation was 15% to 35%. The bottom-hole temperature

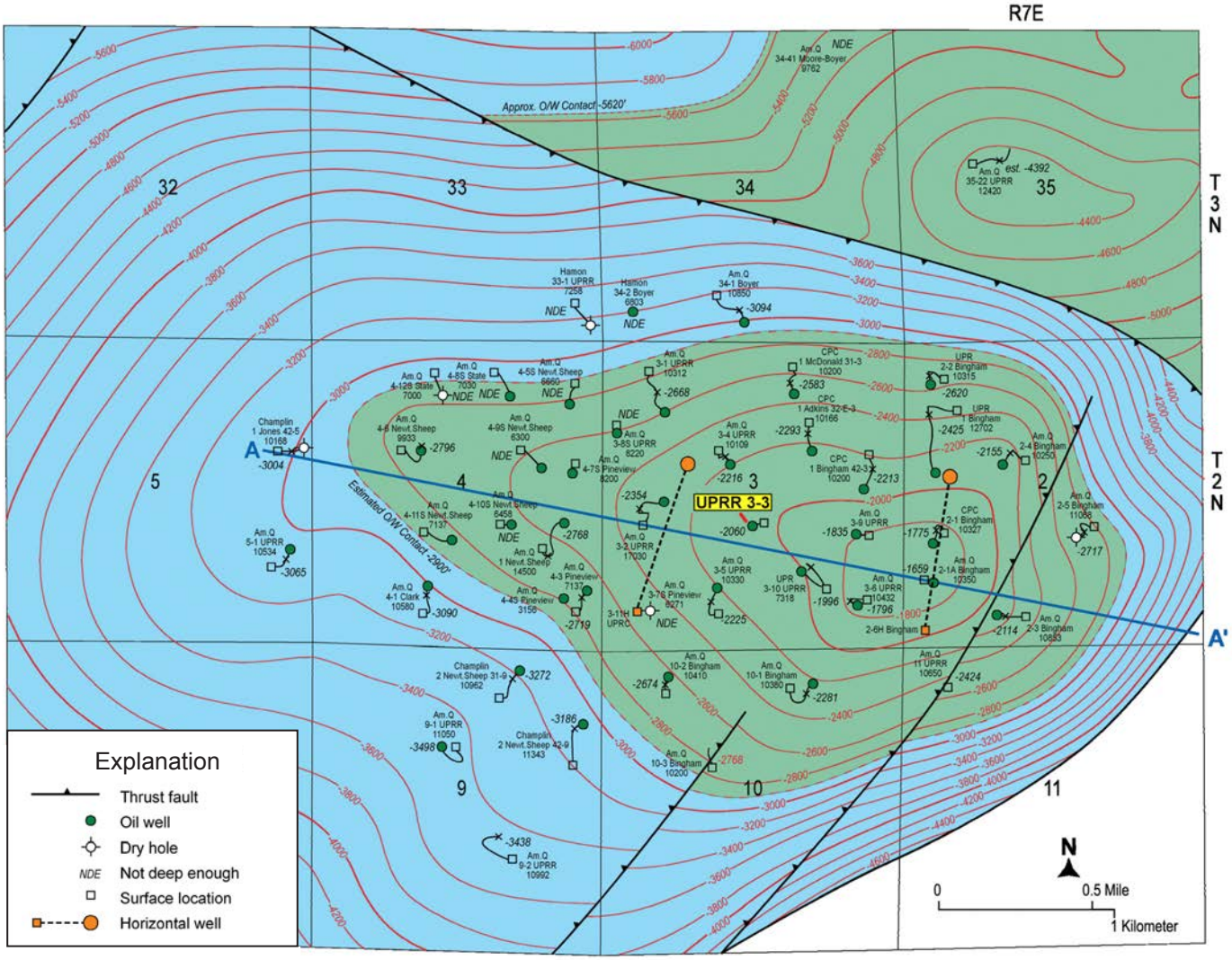

Figure 59. *Structure on top of Watton Canyon Member of the Twin Creek Limestone, Pineview field; see figure 56 for location of Pineview field. Contour interval = 200 feet, datum = mean sea level. Note the location of the UPRR No. 3-3 well. Cross section A–A' shown on figure 60. Modified from the Utah Division of Oil, Gas and Mining (1997a).*

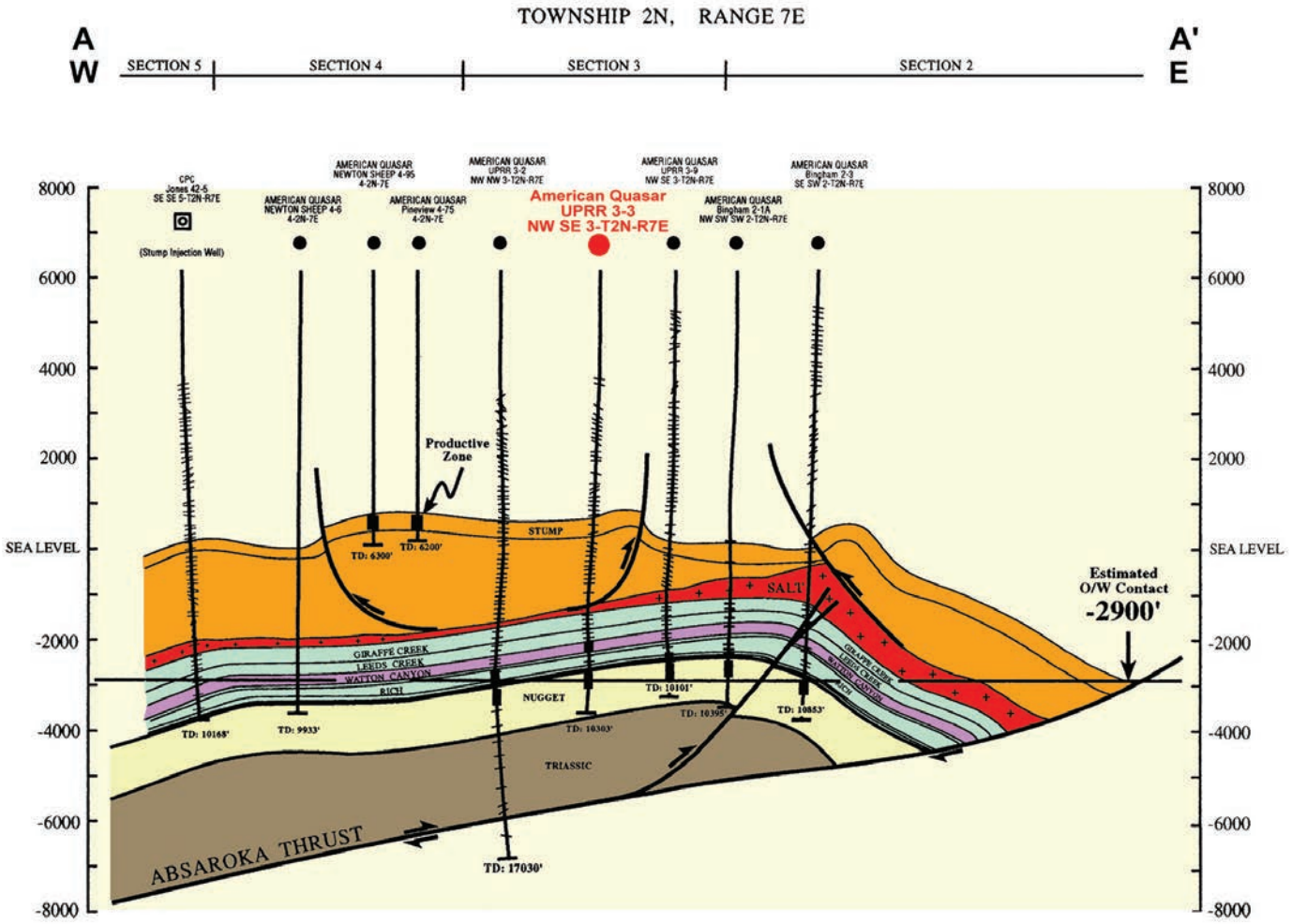

Figure 60. *Detailed east-west structural cross section through Pineview field. Line of section shown on figure 59; note the location of the UPRR No. 3-3 well. The Watton Canyon Member of the Twin Creek Limestone shown in purple. Dipmeter projections shown on some wellbores. After Utah Division of Oil, Gas and Mining (1997b).*

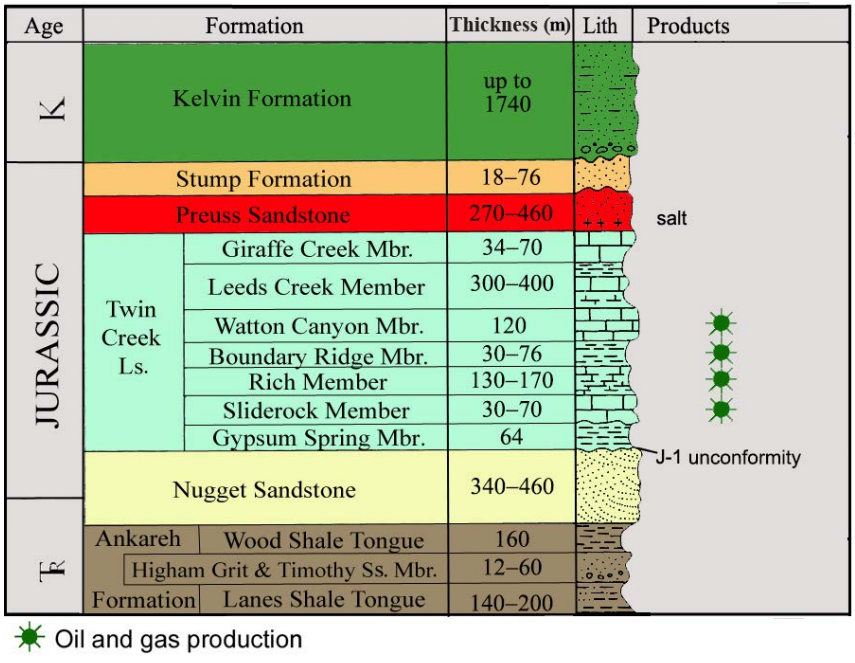

Figure 61. *Stratigraphic column of part of the Mesozoic section, including members of the Jurassic Twin Creek Limestone, exposed in Weber Canyon 35 kilometers (22 mi) west-northwest of Pineview field. Modified from Hintze and Kowallis (2009).*

(BHT) averages 99°C (210°F) (Blazzard, 1979; Petroleum Information, 1984; Sprinkel and Chidsey, 1993; Cook and Dunleavy, 1996).

Fractures display a complex history of opening, calcite filling, and dissolution. Representative thin sections show nearly parallel, subvertical and subhorizontal swarms of calcite- or anhyhdrite-filled microfractures. Visible porosity occurs as isolated dissolution pores and partially open microfractures. Both bed-parallel and bed-normal stylolites are common. Replacement dolomite, microporosity, pyrite, and late calcite, and possibly emplacement of bitumen were controlled by fractures or stylolites.

General Core Evaluation

We described a core from the UPRR No. 3-3 well (NW1/4SE1/4 section 3, T. 2 N., R. 7 E., SLBL&M; plates 6 through 8 and the appendix), Pineview field. The core also tied to wireline well logs. The 3-3 well produced 315,581 BO and 0.65 BCFG from commingled Twin Creek Limestone and the underlying Nugget Sandstone before it was abandoned in 1992 (Utah Division of Oil, Gas and Mining well records). There are cores from, in ascending order, the Sliderock, Rich, Boundary Ridge, and Watton Canyon Members (plate 6). Microbialites are present only in the Rich and Watton Canyon. However, neither of these cores represent the perforated, productive zones in the well.

A general analysis of Twin Creek cores from the UPRR No. 3-3 well revealed complex heterogeneity due to a variety of carbonate lithofacies, textures, structures, and diagenesis (fracturing and stylolitization). Lithofacies include open marine, low- to high-energy middle shelf, terrestrial siliciclastics, marine sabkha, inner shelf lagoon, oolitic shoals, tubular tempestites, and microbial mats/tidal flat. Carbonate fabrics consist of laminated mudstone, wackestone, packstone, grainstone/rudstone, and thrombolite boundstone with beds of siltstone and shale. These units may contain variable amounts of peloids, oolites/oncolites, soft pellets, and skeletal grains (including crinoids, bryozoans, brachiopods, benthic forams, and bivalves). Sedimentary structures include mud cracks, ripples, cross-beds, burrows, and anhydrite nodules. Mudstone is the dominant fabric for stylolite and fracture development.

The lower part of the Rich Member core (plate 7) consists of silty carbonate mudstone whereas the upper part is mainly boundstones, grainstones, and dolomitic to anyhdritic shale beds near the top of the core, which is close to the top of the member. The middle and upper parts of the section (plate 7) also have some dolomitic mudstone, boundstone, and grainstone units. A few zones contain ostracods. Porosity varies from 1% to 6% depending on the presence of open fractures; permeability is variable but 10 mD or lower. The Rich was deposited in a variety of environments including tidal flat, supratidal to sabkha, salinity-restricted inner shelf, and low-energy peritidal.

The lower one-third of the Watton Canyon Member core (plate 8) consists of nonfossiliferous wackestone and packstone with one thin silty interval; a thin grainstone occurs at the base of the core. The rest of the core is a rather homogenous section of mudstones and wackestones containing some crinoids. No dolomite is present, only limestone. Anhydritic zones are also absent. Porosity is consistently less than 2%; like the Rich Member below, permeability is variable but less than 10 mD. There are a few isolated moldic pores but fractures are the dominant contributor to the limited porosity development. The Watton Canyon was deposited in a quiet-water, inner shelf lagoon. The grainstone unit at the bottom of the core represents a higher energy, middle shelf environment.

Microbialites and Associated Grains

Microbialites in the upper Rich Member core are typically thrombolitic boundstones (figure 62). They may be mixed with pockets of grainstone composed of ooids or display possible solution-collapse breccia (figure 62A). Thrombolites in this section of the core represent microbial buildups in a salinity-restricted inner shelf. Porosity, mainly created by fractures, ranges from 1.4% to 5.1% and permeability is 0.08 to 4.5 mD, based on core-plug analysis; pores are often plugged with anhydrite. Microbial mudstones also display low-relief, laminated stromatolite structures (figure 63), which grew in supratidal to sabkha settings. This facies has the most potential for the development of microporosity during dissolution related to burial diagenesis. Figure 64A shows an oolitic grainstone from the lower part of the core bounded by laminated structures representing microbial mats. The ooids within this interval display syndepositional breakage and “cerebroid” margins (figures 64B and 64C). Broken ooids are common in modern Great Salt Lake hypersaline carbonate sediments. Porosity is less than 1.5% and permeability is 0.01 mD, based on core-plug analysis. These microbialites and ooids probably formed within a hypersaline lagoon. Other intervals in the lower part of the core show microbial microlaminations alternating with laminated and rippled siltstones. This section was probably deposited in a silt and lime mud tidal flat with intermittent exposure.

Microbialites in the upper Watton Canyon Member are found near the bottom of the core. They are represented by subtle, millimeter-scale microbial laminations in lime mudstone (figure 65). No fossils are present. These micobialites were likely thin mats, with little if any relief, that grew in a quiet-water, inner shelf lagoon. Based on core-plug analysis, the minor amount of matrix porosity (1.4%) present was created by fractures and permeability is essentially nonexistent (0.01 mD). A higher energy, middle shelf environment is indicated at the very bottom of the core by a thin bed of ooids within a massive lime mudstone exhibiting microbial laminae (figure 66). The contact between the oolitic grainstone and the microbial laminations is sharp. Scattered rounded quartz silt grains are found throughout the zone.

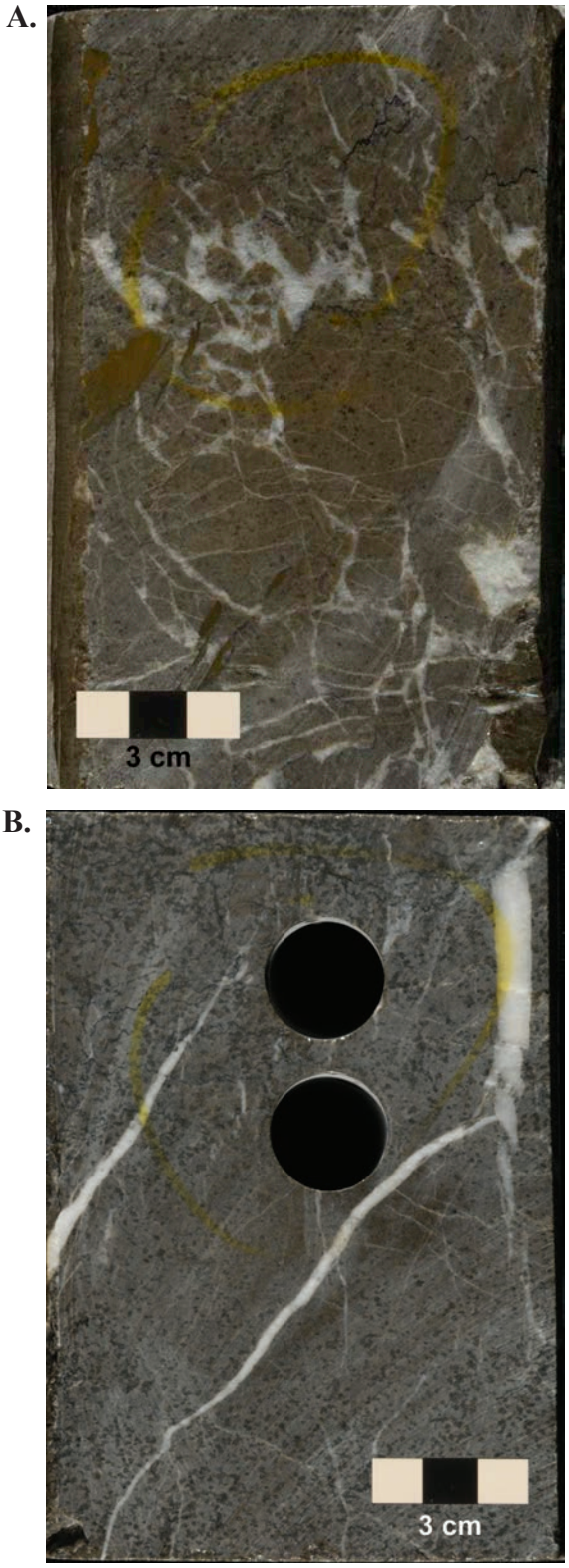

Figure 62. *Microbialites from the Rich Member of the Twin Creek Formation, UPRR No. 3-3 core.* ***(A)*** *Boundstone/oolitic grainstone displaying a thrombolitic fabric, 2738.2 meters (8983.5 ft); core plug analysis: porosity = 1.4%, permeability = 0.08 mD. Note that anhydrite (white) has filled any possible pore space.* ***(B)*** *Microbial boundstone that displays a thrombolitic texture, 2740.2 meters (8990.0 ft); core plug analysis: porosity = 5.1%, permeability = 4.5 mD. Note the mineralized vertical and oblique fractures (in white). See figure 59 for location of the UPRR No. 3-3 well.*

Figure 63. *Microbial mudstone displaying laminated stromatolite structures, Rich Member, UPRR No. 3-3 core, 2741.2 meters (8993.6 ft); core plug analysis: porosity = 2.7%, permeability = 0.22 mD. Note the displacive and replacive white anhydrite nodules as well as vertical fractures healed with anhydrite.*

Outcrop Analog – Twin Creek Limestone Section Near Peoa, Utah

An excellent outcrop analog of the Twin Creek Limestone reservoir is found along State Route 32 about 15 kilometers (9 mi) southwest of Pineview field near the town of Peoa, Utah, on the Absaroka thrust plate (?) (figure 67). All seven formal members are recognized in this outcrop (figure 61, plate 6), and Imlay (1967) and Bruce (1988) provided detailed descriptions, regional correlation, fossils, and depositional environments of these members. The Twin Creek section at Peoa was measured and described by Sprinkel and Doelling (in preparation; plate 9). The outcrop generally strikes parallel to the leading edge of the Absaroka thrust (east-northeast) and the North Flank fault of the Uinta uplift, with beds dipping more than 70° north-northwest. The Peoa section displays the same reservoir heterogeneity characteristics that affect production in the Twin Creek productive fields.

As in the UPRR No. 3-3 core from Pineview field, we recognized microbialites in the Rich and Watton Canyon Members of the Twin Creek Limestone in the Peoa outcrop. The intervening Boundary Ridge Member contains beds of oolitic limestone like those also in the UPRR No. 3-3 core. The following are general descriptions of the lithology, sedimentary structures, and microbialites and associated carbonate grains from these three Twin Creek members found in the Peoa section.

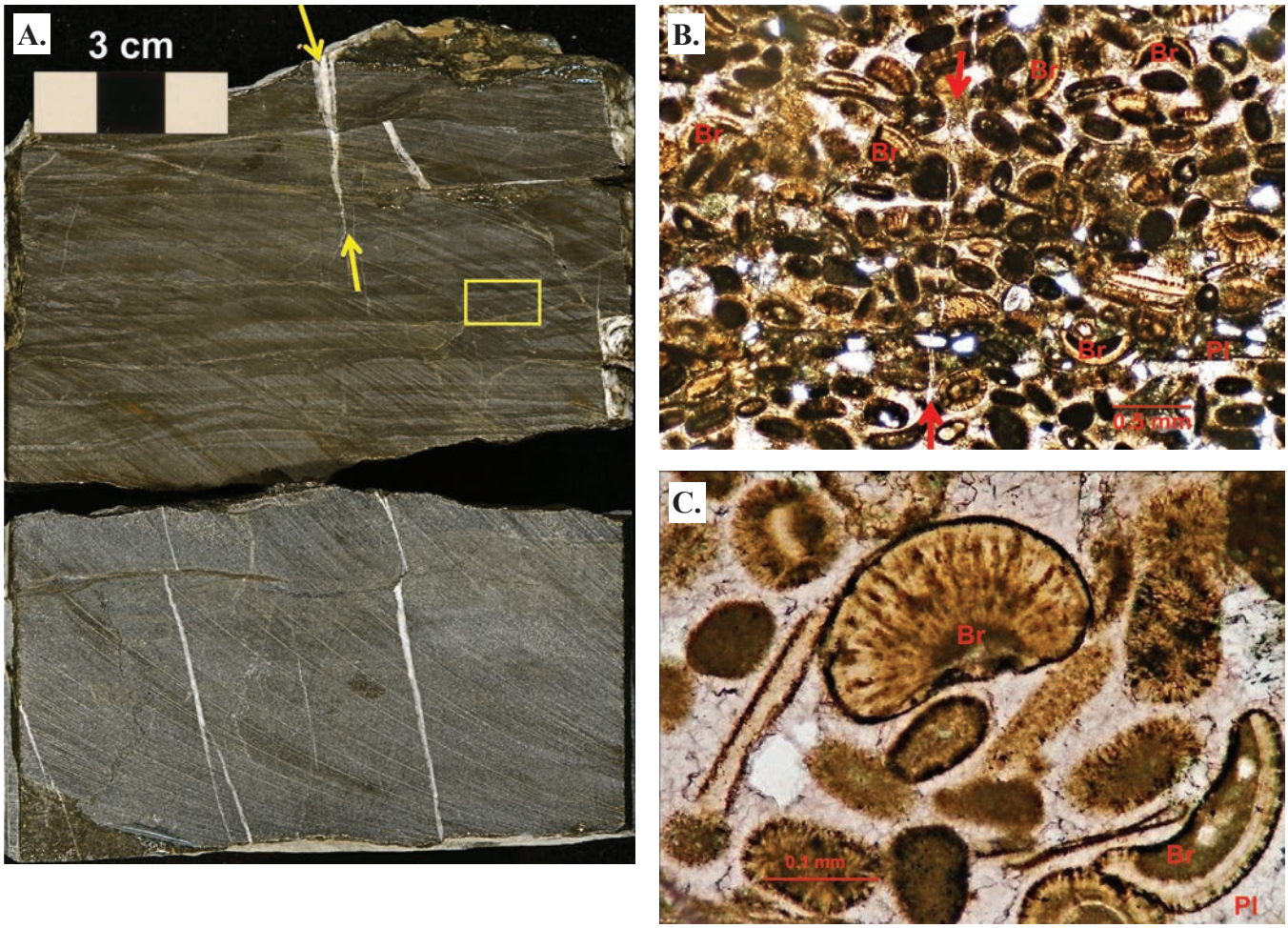

Figure 64. *Microbialites and associated grainstone, Rich Member, UPRR No. 3-3 core.* ***(A)*** *Oolitic grainstone bound by laminated microbial structures, 2745.6 meters (9008.0 ft); core plug analysis: porosity = 1.5%, permeability = 0.01 mD. Note the two types of fractures: (1) a tensional gash (between yellow arrows), and vertical tectonic fractures healed with white calcite. Yellow box indicates the location of photomicrographs in B and C.* ***(B)*** *Photomicrograph of oolitic/skeletal grainstone diluted with quartz silt grains (plane light). Note the abundance of broken ooids (Br) as well as the complex cementation that occluded all matrix pores. A microfracture (between red arrows) is healed with calcite.* ***(C)*** *Close-up photomicrograph of ooids, skeletal grains, peloids, and quartz grains completely surrounded by calcite cements (stained pink) (plane light). Note the broken ooids (Br), which are probably indicative of formation under elevated salinity.*

Rich Member: The Rich Member consists of light to medium gray, light brown-gray to yellow-brown, dense, finely crystalline to micritic or cryptocrystalline limestone (figure 68A). The total thickness of the Rich section at Peoa is 52.2 meters (171.3 ft). Laminated siltstone partings and sandy limestone are also found in several units of the Rich. Bedding is thin to thick to massive, with occasional planar cross-stratification and current ripples. Weathering along closely spaced rectilinear fractures within dense homogeneous limestone beds yields abundant pencils and plates. There is little to no primary porosity within the crystalline to micritic limestone units of the Rich in the Peoa section.

Microbialite beds thicken (up to a meter [3 ft]) and thin due to localized microbial growth activities. Upward thickening of the microbialites created undulatory upper bed surfaces (figure 68B). Small microbial heads can be closely spaced and may have "lumpy-bumpy" cores (figure 68C). Continuous horizontal stromatolitic laminae are composed of alternating lime muds and silty dolomites (figure 68D).

Boundary Ridge Member: The Boundary Ridge Member is composed of a basal dark, red-brown siltstone to claystone (figure 68A), light to medium gray finely crystalline limestone, and very fine to fine-grained, well-sorted, light brown-gray to yellow-gray sandstone and calcarenite. The total thickness of the Boundary Ridge section at Peoa is 23.2 meters (76.2 ft). Bedding is thin to thick, with some contorted bedding (within lensoidal-shaped bodies), cross-stratification, parallel laminae, and occasional ripples. The Rich forms slopes and ledges, which break into rectangular blocks.

We did not find microbialites within the Boundary Ridge Member. However, the limestone beds (grainstones) were rich in ooids that are worth noting (figure 69A). Thin sections show that a few grainstones contain microbial grains or articu-

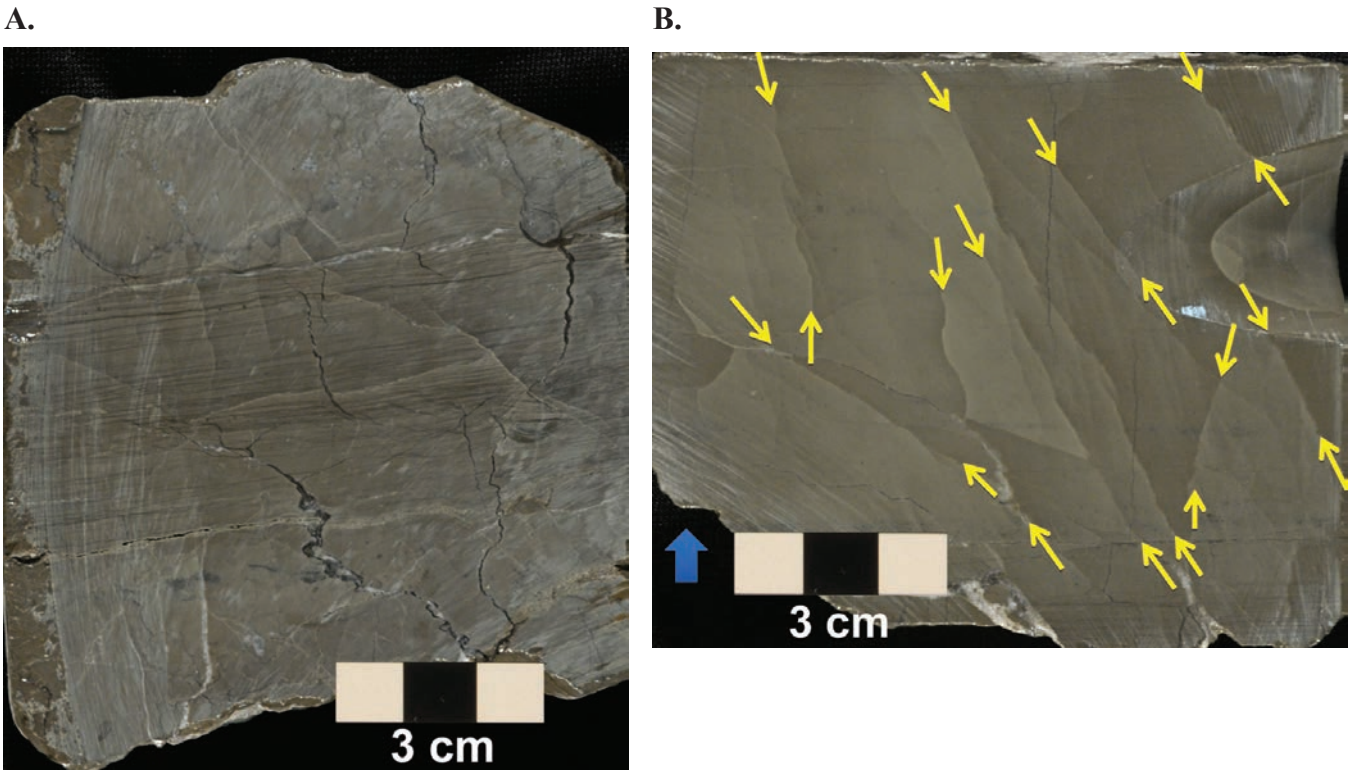

Figure 65. *Microbialites from the Watton Canyon Member of the Twin Creek Formation, UPRR No. 3-3 core.* ***(A)*** *Lime mudstone with millimeter-scale microbial laminations, 2669.7 meters (8759.0 ft). Note the vertical (bed normal) stylolites and the healed fractures.* ***(B)*** *Close-up photograph of a lime mudstone exhibiting microbial laminations. Oblique open fractures form conjugate sets (between yellow arrows). Fractures with other orientations are mineralized and healed with calcite. Core plug analysis from both intervals: porosity = 1.4%, permeability = 0.01 mD.*

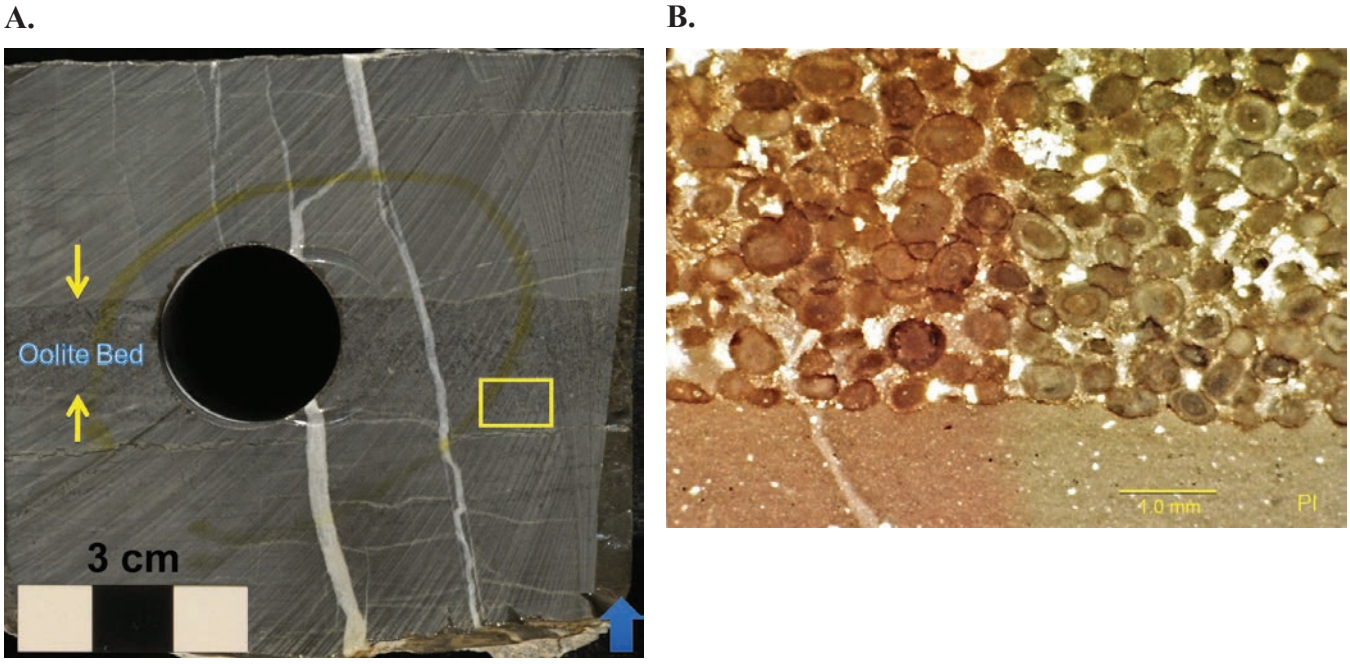

Figure 66. *Microbialites and assocated oolitic grainstone, Watton Canyon Member, UPRR No. 3-3 core, 2670.4 meters (8761.0 ft.).* ***(A)*** *Thin bed of ooids (between yellow arrows) within a massive lime mudstone exhibiting microbial laminae. Note the vertical fractures healed with white calcite. Yellow box indicates the location of photomicrograph in B.* ***(B)*** *Photomicrograph (plane light) showing contact between the oolitic grainstone bed and microbial lime mudstone. Note the rounded quartz silt grains (in white).*

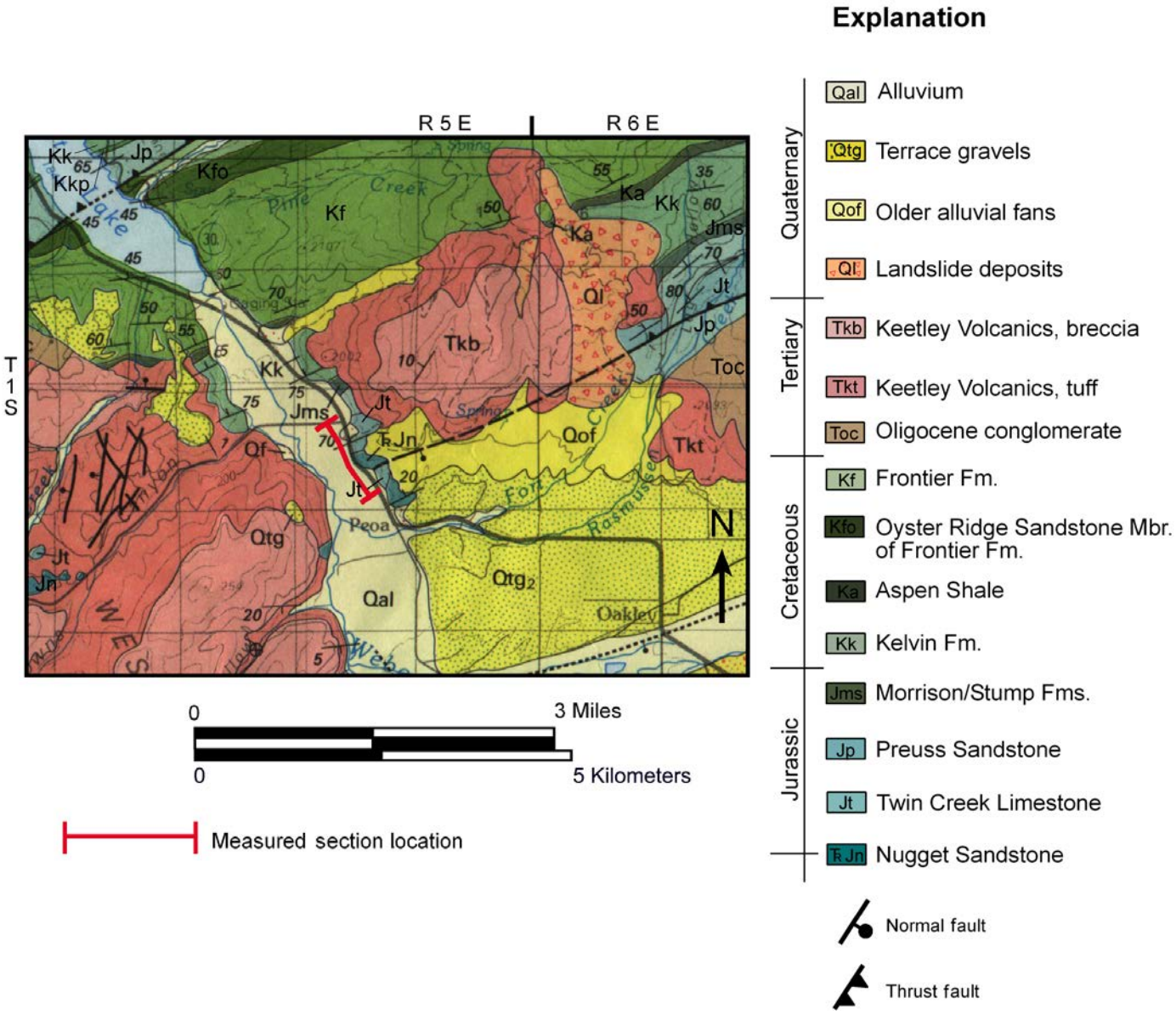

Figure 67. *Geologic map of the Peoa area, Summit County, Utah, showing the location of the stratigraphic measured section through the Twin Creek Limestone. Modified from Bryant (1990). See figure 56 for location of Peoa area.*

lated ostracods. Grainstones are well cemented having only minor isolated pores created by dissolution of ooids (moldic porosity) (figure 69B). Some ooids contain microposity; microfractures are typically healed. Early marine, isopachous calcite cement is present around some of the ooids whereas later spar has filled pores (figures 69C and 69D).

Watton Canyon Member: The Watton Canyon Member is composed of light to medium gray, dense, resistant, finely crystalline to micritic limestone (figure 70A); some beds are silty or sandy and composed of detrital quartz grains. The total thickness of the Watton Canyon section at Peoa is 73.4 meters (240.9 ft). Bedding is thin to thick, with large-scale current ripples and silty lamina or partings that exhibit cross-stratification in some units. Limestones locally contain stylolites, oolites, peloids, and fossils (primarily thin-shelled pelecypods such as *Styolina*). Bedding surfaces exhibit rectilinear fracturing, often calcite filled. Except for a few vugs, visible porosity is lacking in the outcrop. The Watton Canyon forms ledges and cliffs that weather into plates and blocks.

Microbialites in the Watton Canyon Member include stromatolites and thrombolites in the upper part of the section, found with some associated ooids. Outcrops display growth surfaces on top of microbialite beds and subtle "lumpy-bumpy" microbial mini-heads (figure 70B). Microbial heads, some domal or massive, may show synoptic relief along irregular top surfaces (figure 70C). Locally there is evidence of boring. Laterally linked hemispherical microbial laminae within stromatolites can have dolomitic compositions and hints of intercrystalline porosity (figure 70D). These features are most similar in ap-

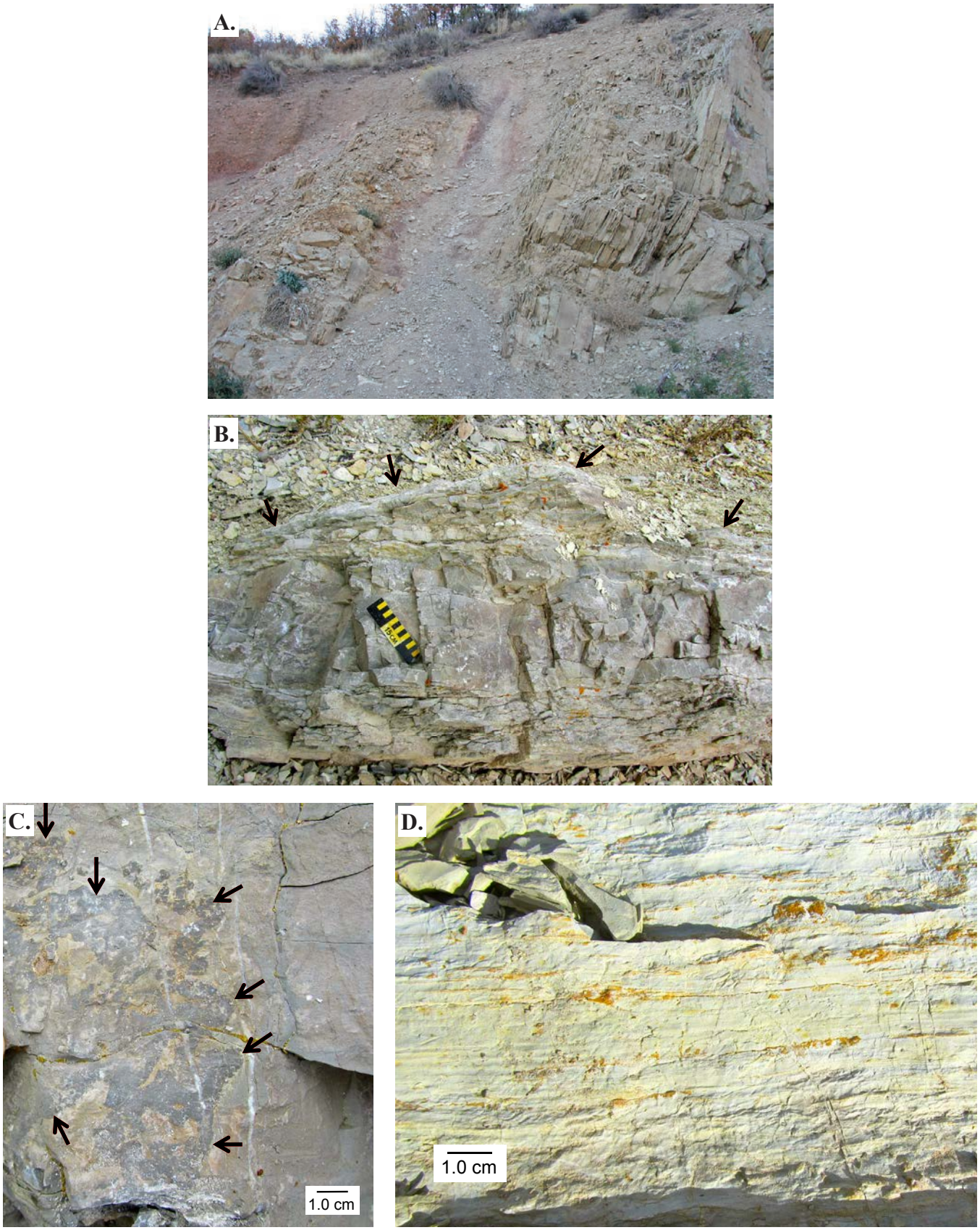

Figure 68. *Characteristics of the Rich Member of the Twin Creek Limestone, Peoa section.* ***(A)*** *Contact between fractured Rich Member limestone (right) and basal siltstone with sealed fractures of the overlying Boundary Ridge Member (left).* ***(B)*** *Undulatory upper surface (black arrows) of a typical microbial bed.* ***(C)*** *"Lumpy-bumpy" microbial head (black arrows) with internal sediment-fill cavities (tan).* ***(D)*** *Stromatolitic laminae composed of alternating lime muds and silty dolomites.*

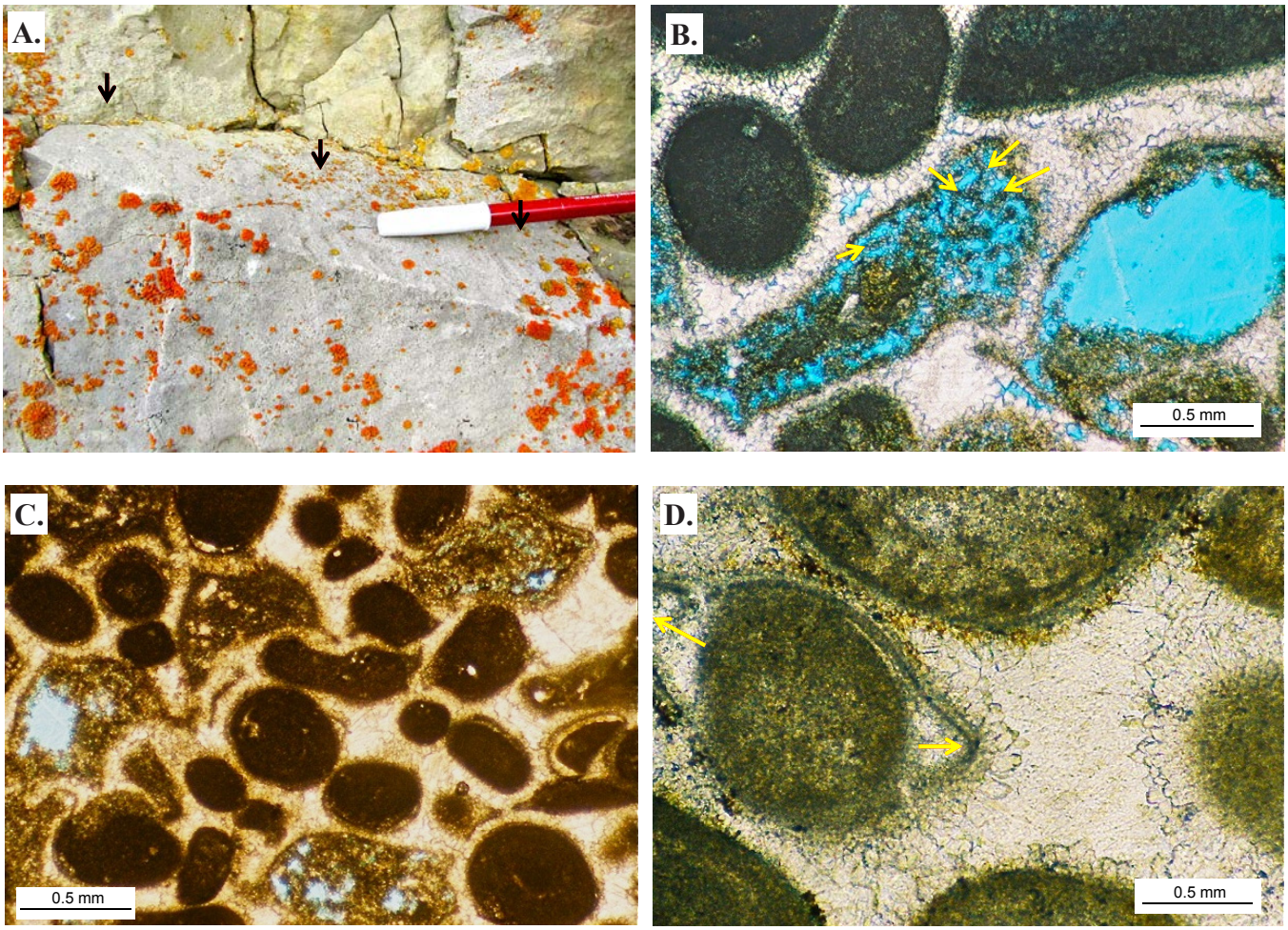

Figure 69. *Characteristics of the Boundary Ridge Member of the Twin Creek Limestone, Peoa section.* ***(A)*** *Inclined top of an oolitic grainstone bed (black arrows).* ***(B)*** *Photomicrograph (plane light) of moldic pores created from the dissolution of ooids or microbial grains. Yellow arrows show partially dissolved grain.* ***(C)*** *Well-cemented oolitic grainstone (plane light) showing hints of early marine isopachous calcite cements and later spar fillings. Note broken ooids, common in saline environments.* ***(D)*** *Close-up image (plane light) of cement generations around ooids, starting with marine cements at yellow arrows.*

pearance to those found in the Rich Member core from the UPRR No. 3-3 well at Pineview field (figure 63). Some examples show possible desiccation cracks filled with microbial material. Erosional trucation is also suggested on a few laterally linked hemispherical stromatolite heads.

The irregular margins of massive microbial heads are well displayed in thin section (figure 71A). Microbial heads can be surrounded by various generations of calcite cement including recrystallized calcite, mini-botryoids, and late calcite spar (figures 71B and 71C) whereas in other examples the microbial heads are surrounded by muddy sediment (figure 71D). Thin sections of the laterally linked hemispherical stromatolites show well-defined regular alternations between light-colored sediment (quartz silt- and lime mud-rich) and dark-colored laminae (figure 71E). Close-up images display vague "ghosts" of microbial filaments or intertwined microbial filaments (figure 71F). Significant microporosity typically is developed in the sediment-rich laminae during burial diagenesis.

Synopsis and Discussion

The marine microbialites that we have described from cores and outcrops of the Middle Jurassic Twin Creek Limestone are not unique. Numerous examples of Phanerozoic marine microbialites have been documented—the Upper Cambrian Notch Peak Formation (figure 72), Utah; the Middle Cambrian Carrara Formation, California; and the Upper Cambrian Bonanza King Formation, Nevada, to name a few (Shapiro and Awramik, 2009). These examples include thrombolites, stromatolites, and branching digitate forms (dendrolites) of various thicknesses and lengths. Associated carbonate grains include ooids and oncoids. The marine microbialites in the Twin Creek have many very similar characteristics to these Cambrian counterparts, although perhaps more subtle in their expression and scale.

Marine conditions were favorable for microbial development in the Twin Creek Limestone, such as the shallow, somewhat restricted embayment of the sea that extended into southern Utah from Canada during the Middle Jurassic. Eustatic fluctu-

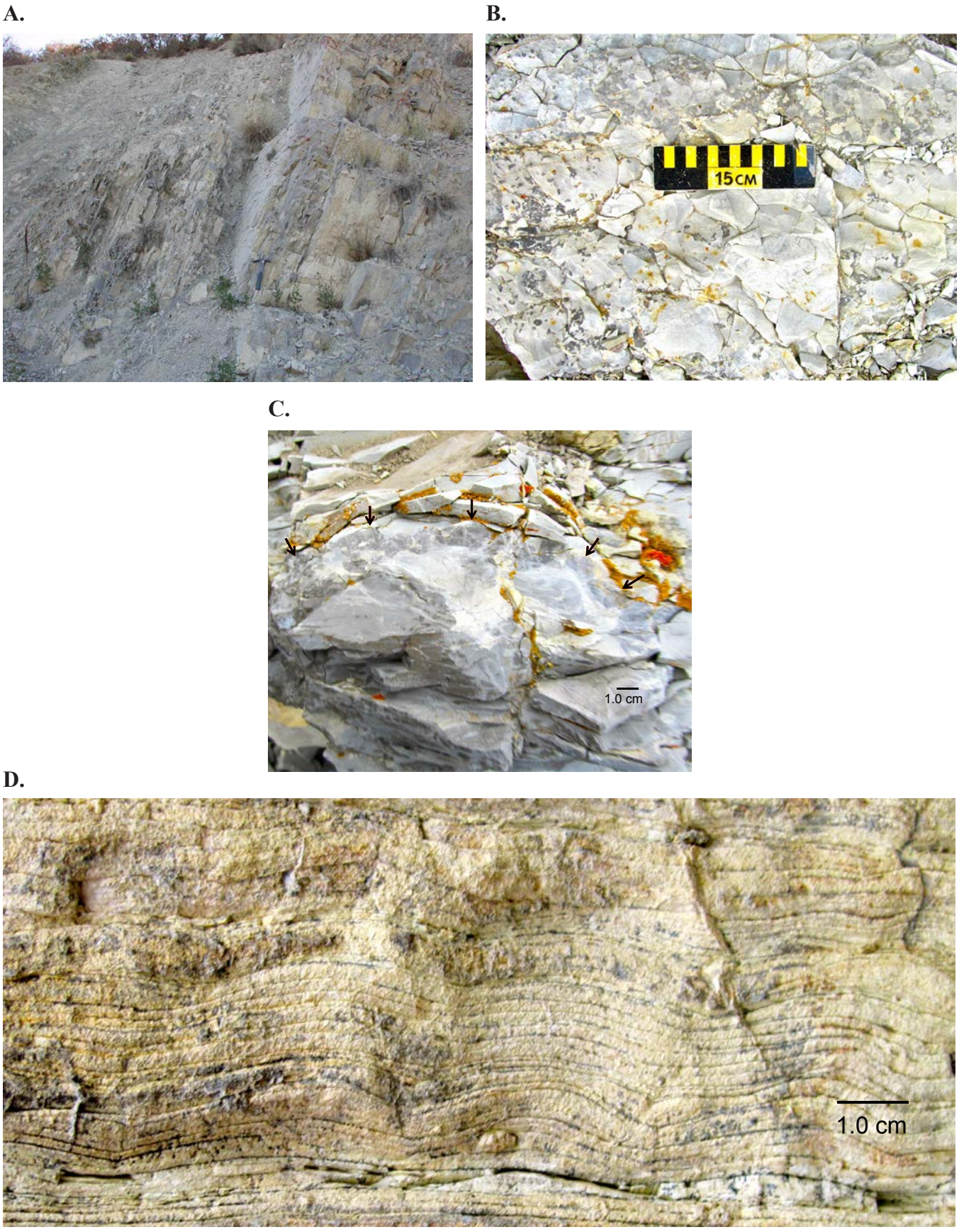

Figure 70. *Characteristics of the Watton Canyon Member of the Twin Creek Limestone, Peoa section.* ***(A)*** *Contact between fractured Watton Canyon Member limestone and the basal argillaceous unit of the overlying Leeds Creek Member.* ***(B)*** *"Lumpy-bumpy" microbial mini-heads (in dark gray).* ***(C)*** *Small domal microbial head (beneath black arrows).* ***(D)*** *Laterally linked hemispherical microbial laminae within stromatolites.*

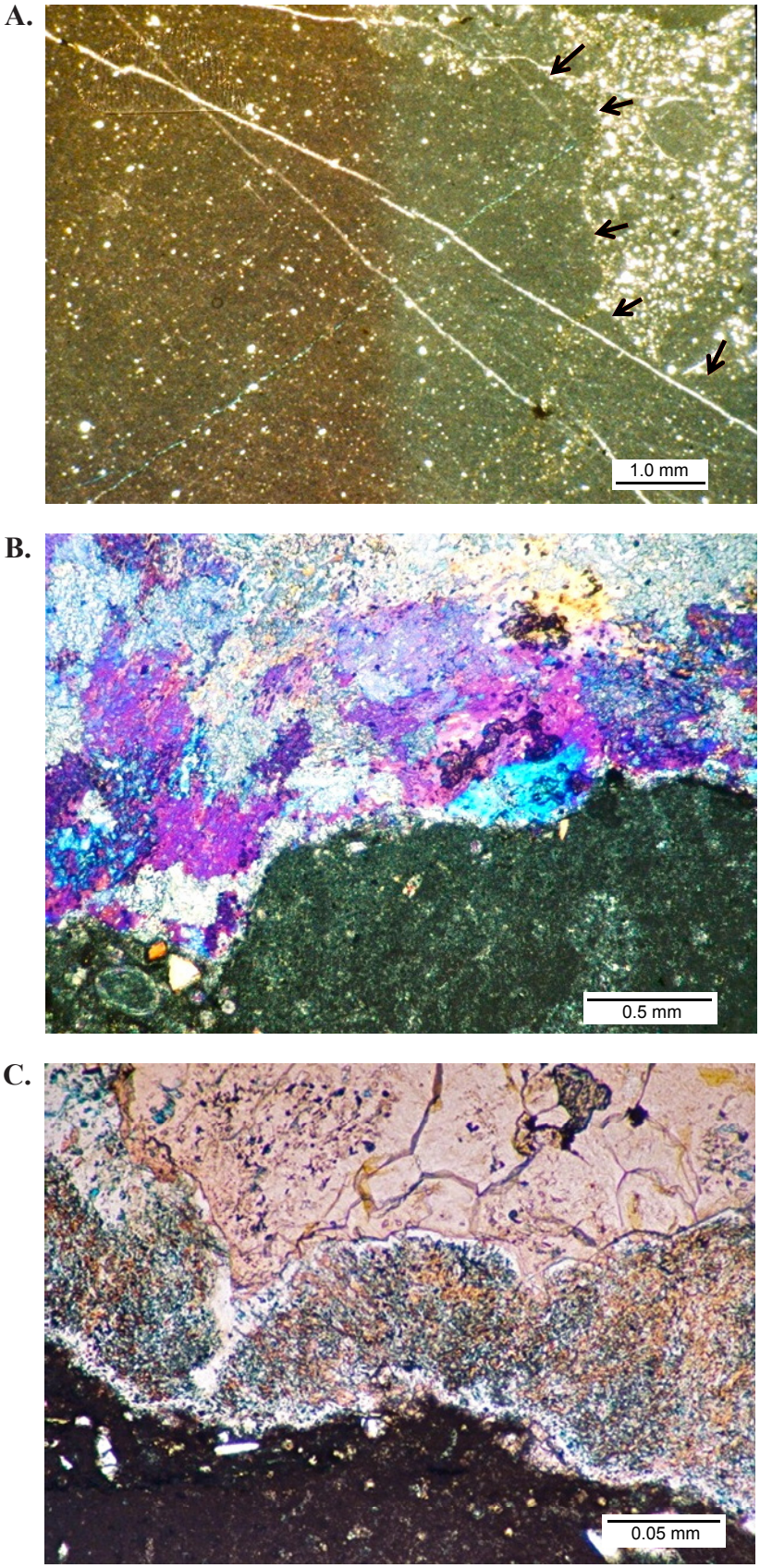

Figure 71. *Photomicrographs of microbialites from Watton Canyon Member outcrop samples, Peoa section.* ***(A)*** *Irregular margin of a massive, fractured microbialite head. Black arrows mark a few points along the margin of this "head" (plane light).* ***(B)*** *Irregular margin of a massive microbialite "head" surrounded by recrystallized calcite cement (crossed nicols with accessory plate).* ***(C)*** *Irregular margin of a massive microbialite "head" surrounded by mini-botyroids and then calcite spar cement (plane light, calcite stained with Alizarin Red-S solution).*

D.

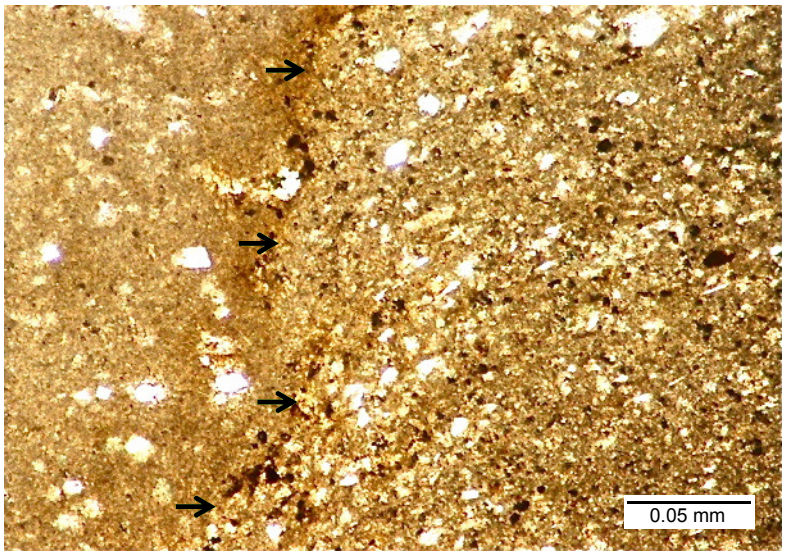

E.

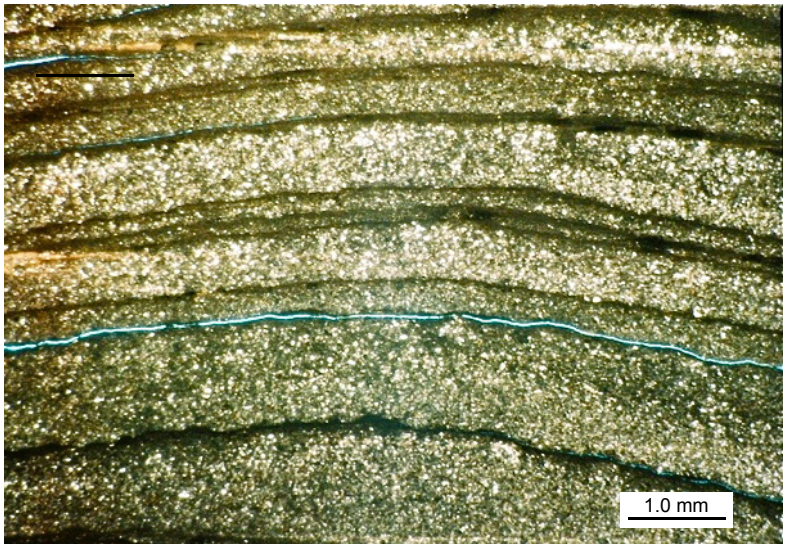

F.

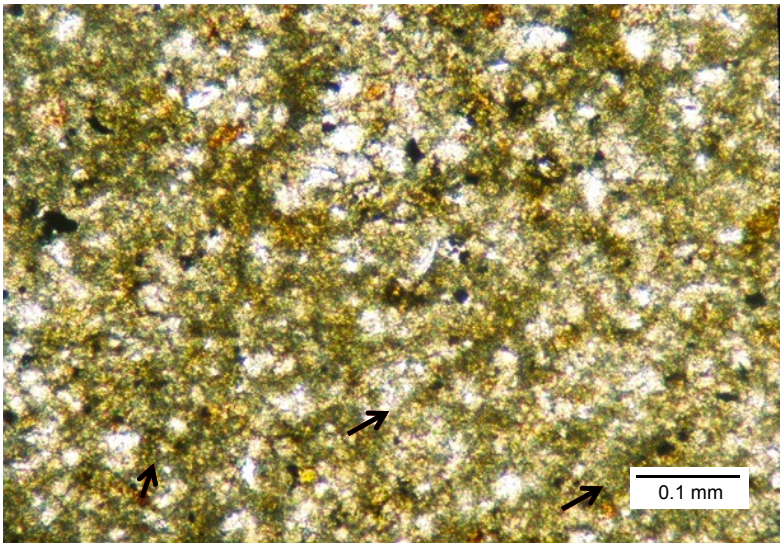

Figure 71 continued. *Photomicrographs of microbialites from Watton Canyon Member outcrop samples, Peoa section.* ***(D)*** *Muddy sediment surrounding the irregular margin of a massive microbialite head (black arrows) (plane light).* ***(E)*** *Well-defined laminae in linked hemispherical stromatolites (plane light). Outcrop shown on figure 70D.* ***(F)*** *Close-up image of E showing "ghosts" of microbial filaments (black arrows) (plane light).*

Figure 72. *Stromatolites in the marine Upper Cambrian Notch Peak Formation, Chalk Knolls, Tule Valley, Millard County, western Utah. Photograph by Stefan Kirby, Utah Geological Survey.*

ations caused numerous transgressions and regressions resulting in deposition of carbonates, fine-grained clastic red beds, and sabkha evaporites (Imlay, 1967, 1980; Kocurek and Dott, 1983; Hintze and Kowallis, 2009). The fact that large microbial domes and columns appear to be lacking in the Twin Creek supports our interpretation that the environments were supratidal to sabkha, tidal flat, and inner shelf lagoon. Common to these depositional environments is a quiet, shallow-water setting, with some areas of intermittent exposure. Today in Shark Bay (figure 58), large-scale microbial features are associated with areas of wave action whereas the smaller-scale microbialites (mats) grow in quiet-water environments (Noffke and Awramik, 2013).

Triassic Microbial Carbonates at Upper Valley Oil Field, Kaiparowits Basin

Upper Valley field produces oil from the Permian Kaibab Limestone and Triassic Moenkopi Formation in the Laramide-age Kaiparowits Basin in south-central Utah (figure 73). These formations were deposited in shallow-marine to tidal flat environments (figure 74). Upper Valley is the only field in the basin, much of which is within the Grand Staircase–Escalante National Monument, designated in 1996. The reservoir rocks in both formations are carbonates. We recognize microbialites in the productive Timpoweap Member of the Moenkopi Formation, which may have implications for future exploration opportunities in southern Utah.

Field Overview

Upper Valley is located on the flank of an elongate, north-northwest to south-southeast-trending surface anticline (figure 73). However, the oil has been hydrodynamically displaced to the western flank of the structure (figure 75). The seals for the reservoirs are provided by the low-permeability, mud-dominated carbonate units within the Kaibab Limestone and Timpoweap Member of the Moenkopi Formation and the siltstone and clastic mudstone in the lower red member of the Moenkopi. Oil analysis suggests two possible sources for the hydrocarbon production at Upper Valley: the Mississippian Chainman Shale or an unknown Permian source (Sprinkel and others, 1997). Upper Valley field and the potential of the Kaiparowits Basin area have been described in detail by Campbell (1969), Peterson (1973), Sharp (1976, 1978), Montgomery (1984), Goolsby and others (1988), Doelling and Davis (1989), Allin (1990, 1993), Gautier and others (1996), and Allison (1997).

Upper Valley field was discovered in April 1964 with the completion of the Tenneco Oil Company Unit No. 2 well (NW1/4NW1/4 section 13, T. 36 S., R. 1 E., SLBL&M, Garfield County) which had an IPF of 300 BOPD and no water. The initial reservoir pressures for the field ranged from 1250 to 1700 psi (Allin, 1993). The field currently has 19 producing wells and 6 abandoned producers. Cumulative production as of March 1, 2021, was 29,458,504 BO, 192,499 MCFG,

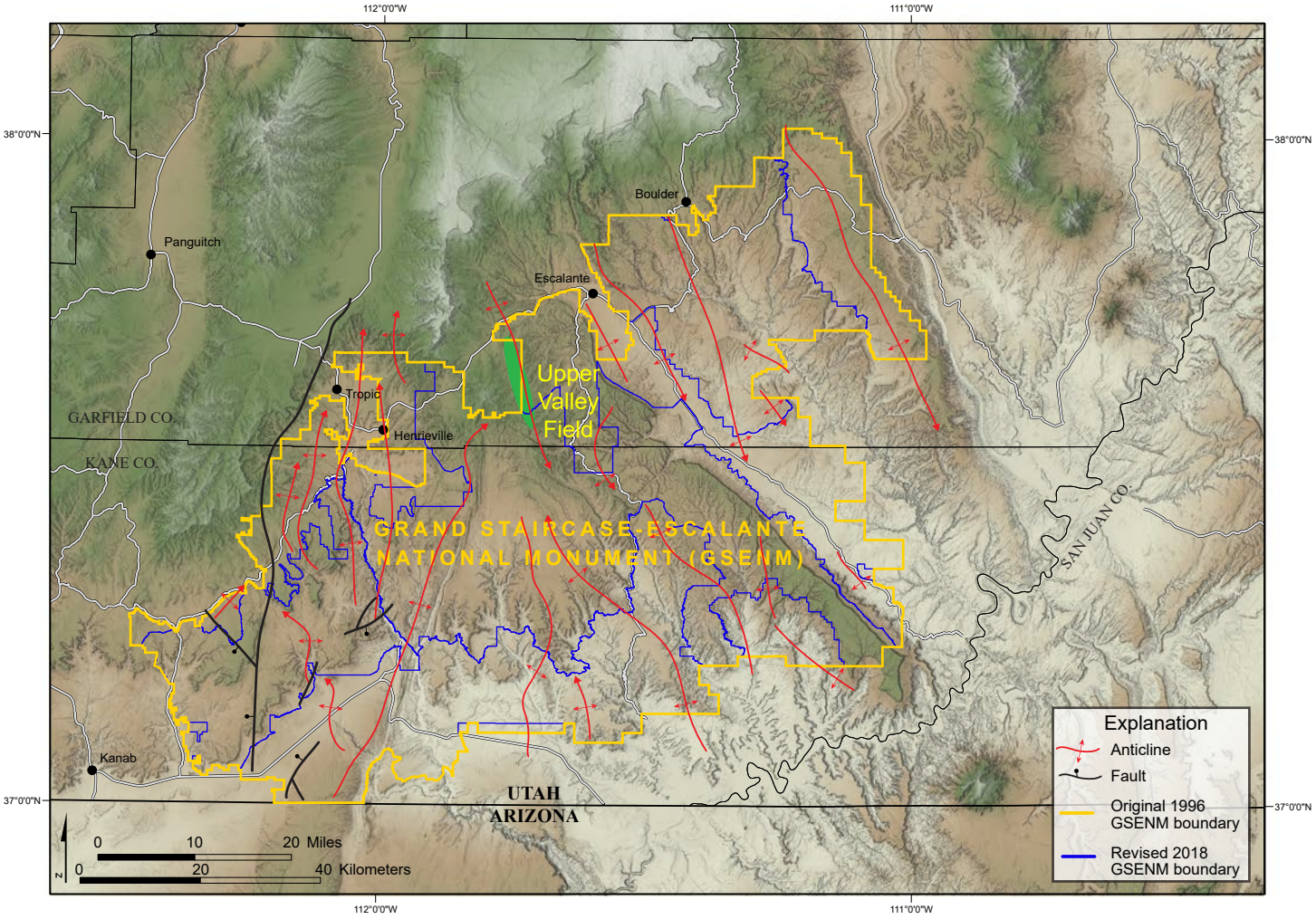

Figure 73. *Upper Valley oil field and structures in the Laramide-age Kaiparowits Basin, south-central Utah. After Sharp (1976).*

and 596,910,822 BW (Utah Division of Oil, Gas and Mining, 2021a). Estimated OOIP is 84 million BO (Goolsby and others, 1988); estimated original ultimate recovery was estimated at 25,000,000 BO, however, production exceeded that value many years ago. Peripheral updip water injection for pressure maintenance began in 1969. Currently a tertiary polymer flood is in place and there are 11 injection wells in the field.

Production at Upper Valley field is from marine carbonate zones in the Beta Member of the Kaibab Limestone (K-3 and K-4 porosity zone) and the Timpoweap Member (K-1 and K-2) of the Moenkopi Formation (figures 75 and 76). The net pay thickness for all perforated zones in the field is 23 meters (75 ft) over a 1360-hectare (3360 ac) area. The oil/water contact is curvilinear and ranges in elevation from 300 meters (986 ft) above mean sea level (AMSL) in the northern end of the structure to -11 meters (-35 ft) AMSL at the southern end. The K-4 porosity zone of the Beta Member exhibits pervasive interparticle porosity and is the main reservoir (figures 75 and 76). Porosity averages 18% in the K-4 porosity zone; porosity in the K-1, K-2, and K-3 zones is discontinuous (Allen, 1993). Permeability varies, with some units as high as 300 mD, and averaging 100 mD. The drive mechanism is water; water saturation averages 40%, but the most prolific wells in the field began with 25% to 32% (Allin, 1996). The BHT is 60°C (140°F).

Many wells were drilled both prior to and since the discovery of Upper Valley field targeting the crests of numerous surface structures in the Kaiparowits Basin rather than the more risky flanks. Therefore, remaining potential may be significant along those flanks but because a large part of the region is in the Grand Staircase–Escalante National Monument, it is unlikely that further exploration will occur there for similar structures.

General Core Evaluation

The core from the Upper Valley Unit No. 4 well (SE1/4SE1/4 section 24, T. 36 S., R. 1 E., SLBL&M) has been described and tied to geophysical well logs by Sharp (1976) (figure 76) and Goolby and others (1988). Their analyses show carbonate

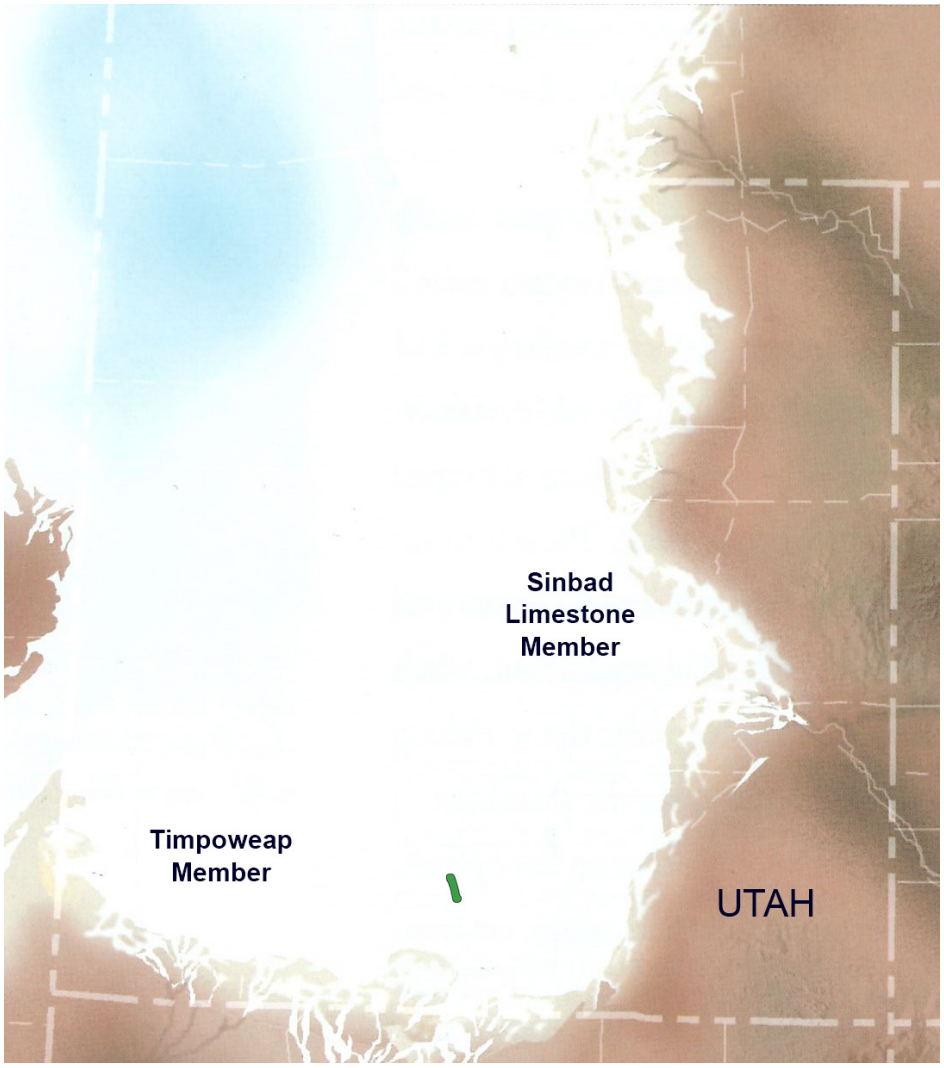

Figure 74. *Paleogeography of the Moenkopi Formation during the Early Triassic. The green oval represents the approximate position of Upper Valley field, Garfield County, Utah. Modified from Blakey and Ranney (2008).*

fabrics range from oolitic/skeletal grainstone to wackestone containing intergranular, vuggy, moldic, channel, intercrystalline, and fracture porosity types. Dolomitization has occurred in various degrees and forms. From these porous intervals, the Upper Valley Unit No. 4 well produced 1,270,442 BO, 9722 MCFG, and 20,042,889 BW as of March 1, 2021 (Utah Division of Oil, Gas and Mining, 2021b).

The Upper Valley Unit No. 4 cores display several exposure surfaces and associated breccia zones. Core interpretation, mapping, and correlation of field rock units indicate a variety of carbonate depositional environments (figure 77) including open marine subtidal, nearshore marine/intertidal, restricted marine/lagoon, and supratidal/microbial (algal mat). Our work builds on these studies and provides a more detailed description of the microbialites, including microbial laminates and stromatolites, well exhibited in the productive K-2 zone of the Timpoweap Member of the Moenkopi Formation (see the appendix for complete set of close-up photos from the Upper Valley No. 4 core).

Microbialites and Associated Grains

The best examples of microbialites are found in the K-2 zone of the Timpoweap Member; however, they are present in a few beds of the K-3 zone of the Kaibab Limestone. Microbialites in the K-2 zone include dolomitic stromatolites, thrombolites, and cryptalgal laminites. Stromatolites have small, low-relief heads formed over rip-clasts (figure 78A) or large, high-relief heads formed over either rip-up clasts or mini-teepee desiccation structures (figure 78B). These features have excellent visble porosity in the form of dissolution molds, vugs, and possible microbial construction or fenestral pores. Other large stromatolitic heads are associated with underlying mud-supported dolomite beds containing moldic pores from the dissolution of fossils (figure 78C). It is possible that minor relief on the shallow, muddy bottom provided the substrate for stromatolite growth. Thrombolites in the K-2 zone are generally small in size and have small, connected pores as indicated by oil staining (figure 79A). Flat cryptalgal (microbial mats) laminites are also common and display birdseye fenestral and lami-

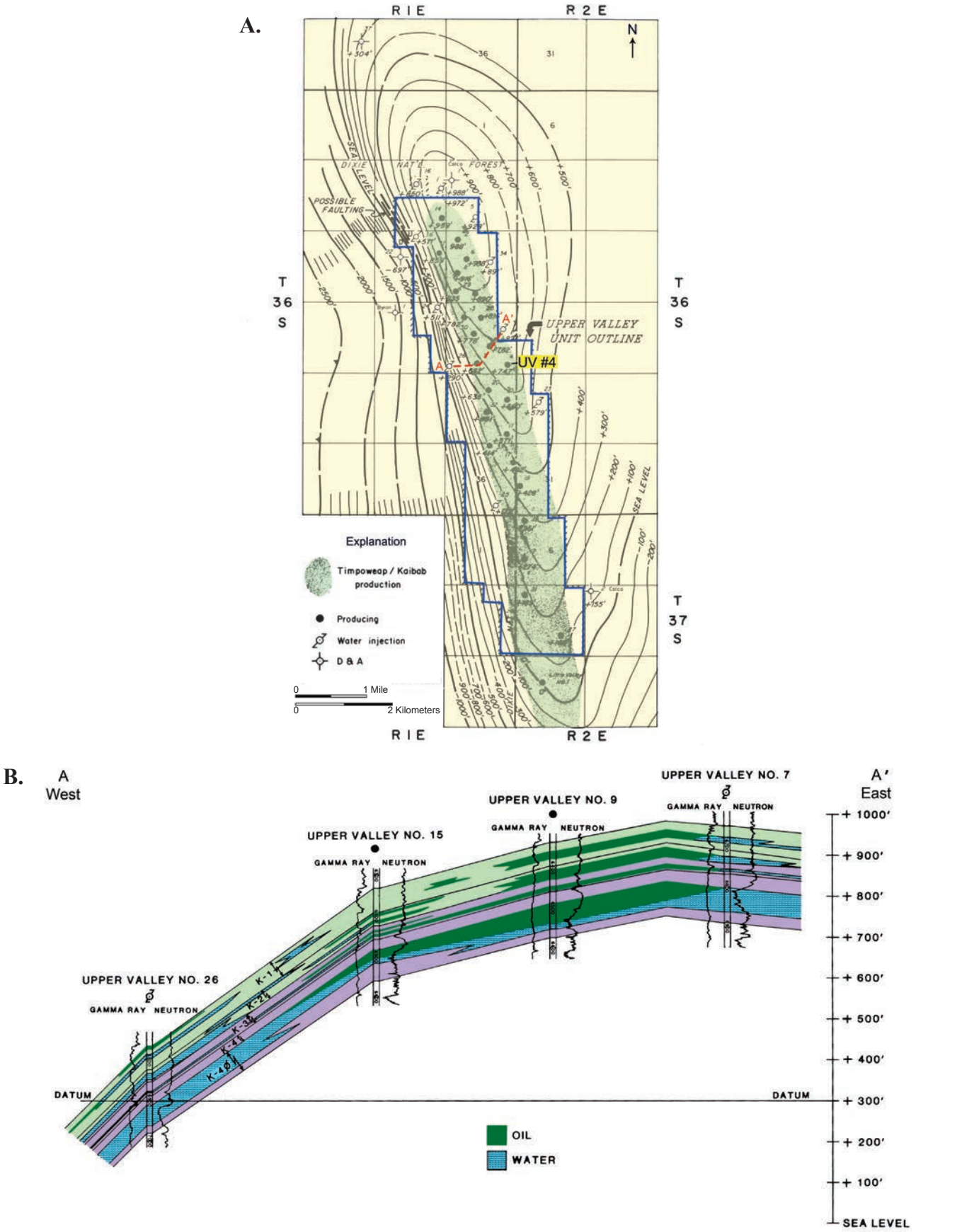

Figure 75. *Geology of Upper Valley field, Garfield County, Utah.* ***(A)*** *Structure on the top of the K-4 porosity zone, Permian Kaibab Limestone, Upper Valley field. Contour interval = 100 feet, datum = mean sea level. Note location of the Upper Valley Unit No. 4 (UV #4) well.* ***(B)*** *East-west structural cross section showing hydrodynamically displaced oil/water contact. After Sharp (1976).*

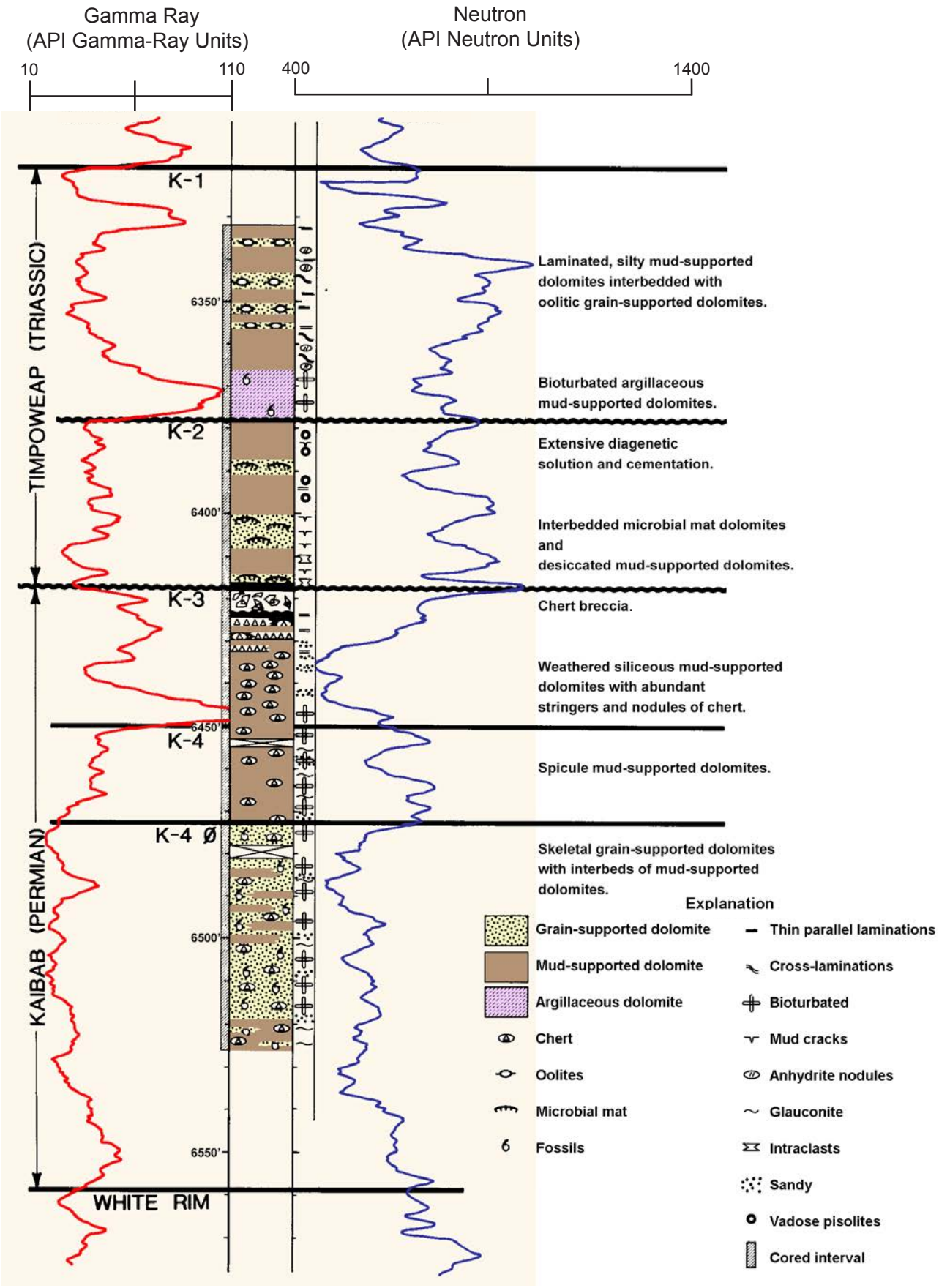

Figure 76. *Type gamma-ray and neutron log combined with core description of the K-1 through K-4 porosity zone in the Kaibab Limestone and the Timpoweap Member of the Moenkopi Formation, Upper Valley Unit No. 4 well, Upper Valley field. After Sharp (1976).*

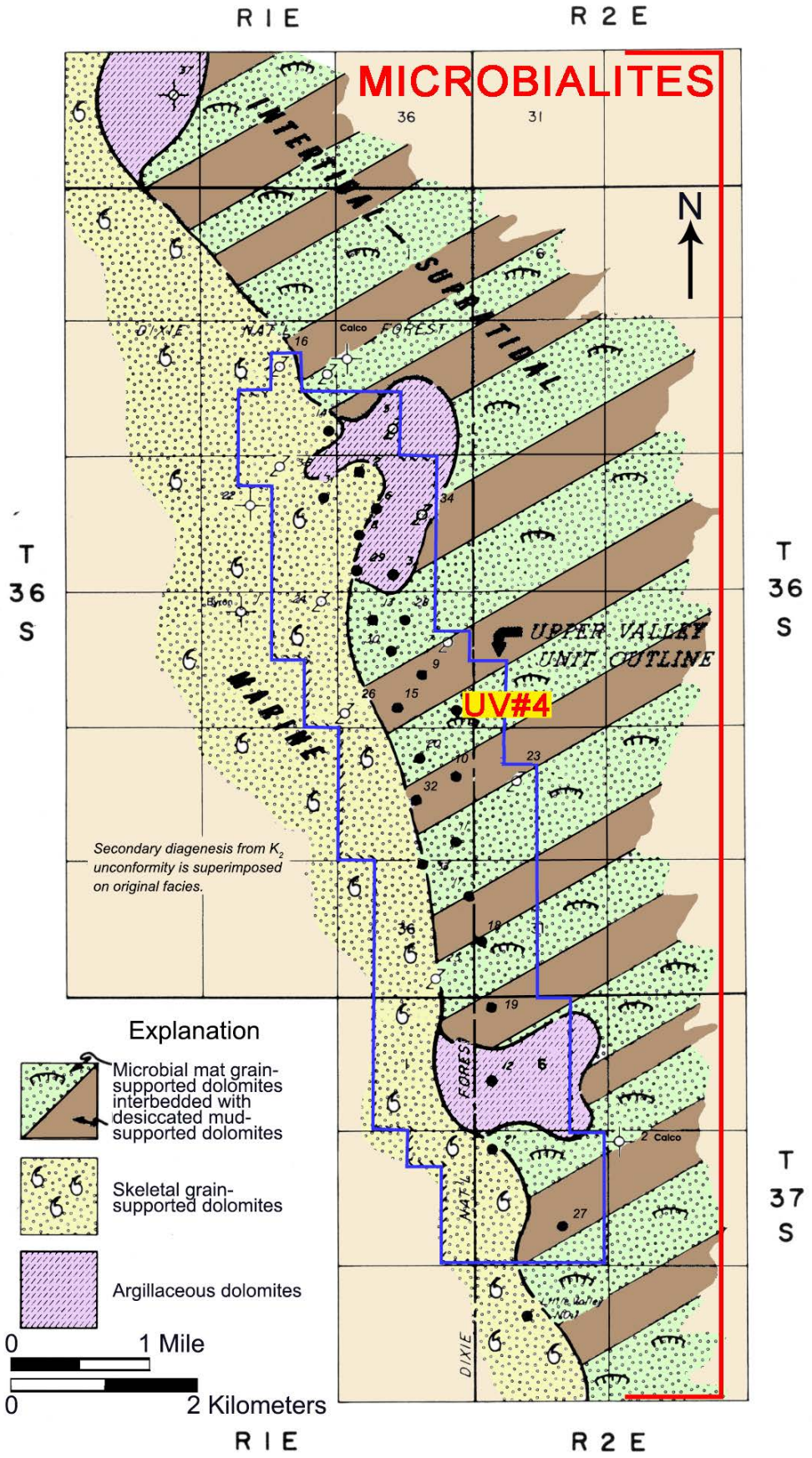

Figure 77. *Facies distribution within the K-2 zone of the Timpoweap Member, Upper Valley field. Note location of the Upper Valley Unit No. 4 (UV #4) well. After Sharp (1976).*

noid dissolution cavities, desiccation features, or vertical fractures (figure 79B). Sharp (1976) attributed these fractures to syndepositional exposure and drying. Maximum porosity and permeability measurements from core-plug data for cryptalgal laminites are 8.9% and 60 mD, respectively (Sharp, 1976). Pores are often partially filled with anhydrite and drusy dolomite cements. Stromatolites, thrombolites, and cryptalgal mats grew in the intertidal to supratidal environment (Sharp, 1976).

The K-3 zone of the Kaibab Limestone contains small cycles of microbial laminites and grainstone composed of peloids and coated grains. Nodular chert within a dolomitic matrix is also common. Maximum porosity and permeability measurements from core-plug data for the grainstones are 19.9% and 162 mD, respectively (Sharp, 1976). The microbial laminites and associated carbonate grains formed in a restricted marine environment (Sharp, 1976).

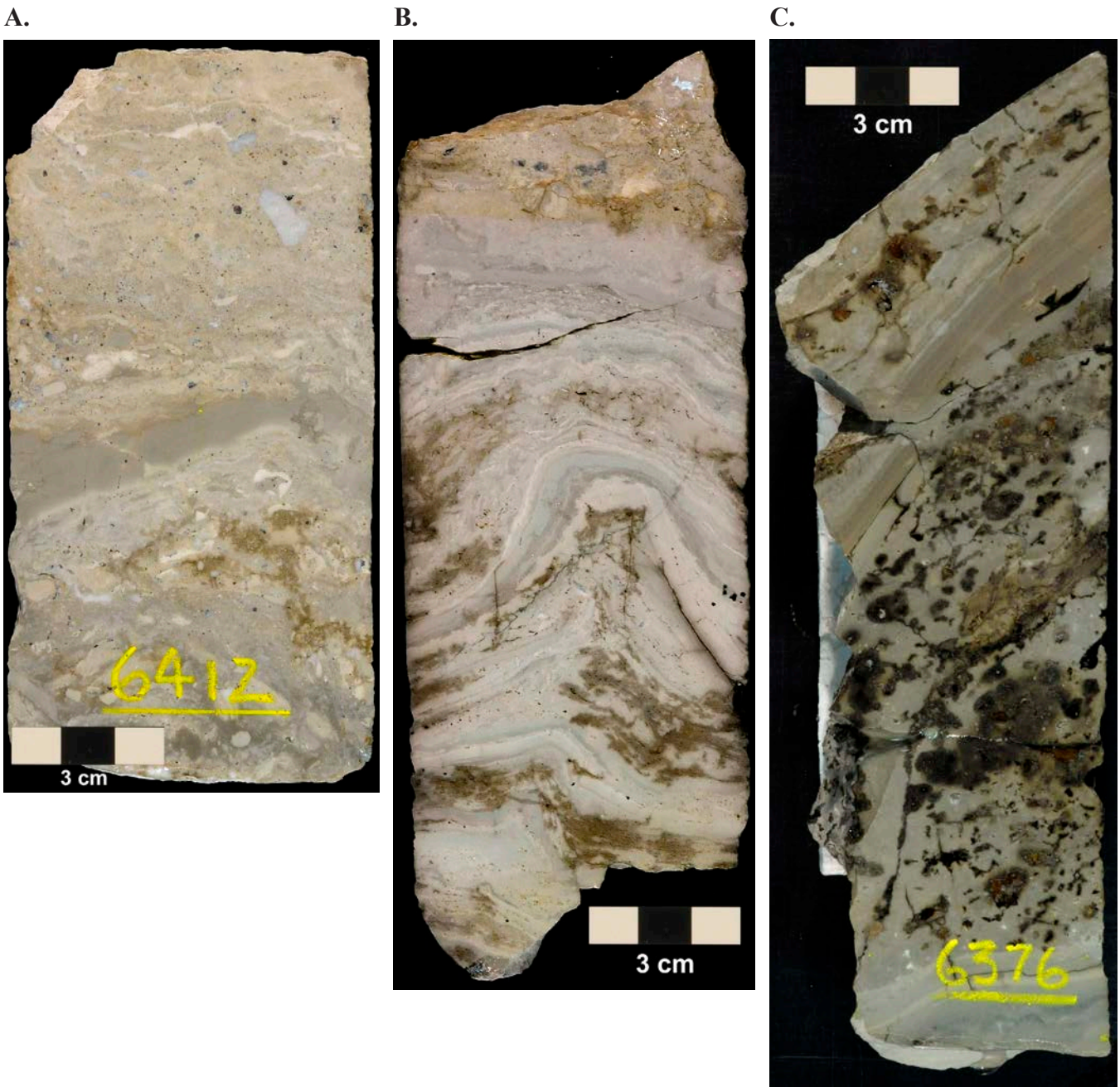

Figure 78. *Stromatolites in the K-2 zone of the Timpoweap Member from the Upper Valley Unit No. 4 core.* ***(A)*** *Low-relief stromatolite heads formed over rip-ups and clasts of white siltstone, sandstone, and black chert; 1954 meters (6412 ft).* ***(B)*** *Stromatolite over rip-ups or mini-teepee desiccation structure coated with microbial mats; 1952.7 meters (6406.5 ft).* ***(C)*** *Large stromatolitic head (partial) over a moldic dolomite (possible fossil molds); 1943 meters (6376 ft).*

Figure 79. *Thrombolites and cryptalgal laminites in the K-2 zone of the Timpoweap Member from the Upper Valley Unit No. 4 core.* ***(A)*** *Small thrombolite with oil staining; 1943.9 meters (6377.5 ft).* ***(B)*** *Flat cryptalgal (microbial) laminites with desiccation features, vertical fractures, and some minor anhydrite; 1953.6 meters (6409.5 ft).*

Synopsis and Discussion

As we observed in the Twin Creek Limestone and documented in the modern environment of Shark Bay, the smaller-scale stromatolites, thrombolites, and cryptalgal mats of the K-2 zone of the Timpoweap Member likely grew in very shallow, quiet-water, marine intertidal to supratidal environments. However, subaerial exposure and desiccation played a major role in microbial growth and characteristics during Timpoweap time. In addition to the desiccation-caused fractures mentioned in the previous section, we observed extensive solution collapse brecciation in the core. Recall that exposure of modern microbialites in Great Salt Lake caused bleaching and the death of the cyanobacteria within their domal buildups, and as the lake level decreased further, the inner structures of the domes would collapse. It is plausible that under the exposed conditions of the Timpoweap supratidal environment, that some of the collapse features observed in the core formed in the same way. Exposure of the Timpoweap microbialites could also account for the dissolution porosity observed in core, and much of the porosity identified on well logs throughout Upper Valley field.

A series of domal microbial buildups composed of boundstone, and associated oncoids and pisoids, is present in the Timpoweap Member outcrop near the Hurricane Cliffs south of the town of Hurricane, southwestern Utah (figure 80), about 150 kilometers (93 mi) west-southwest of Upper Valley field (first identified by Scott Ritter and Chris Perfili, Brigham Young University, in 2017). Oolitic beds are also present in Timpoweap Canyon, the type locality of the Timpoweap Member (Nielsen and Johnson, 1979). These microbialites and associated carbonate grains have similar characteristics to those we identified in the Upper Valley Unit No. 4 core, and thus likely had similar depositional environments. Furthermore, we speculate that Timpoweap microbialites in the subsurface between the Hurricane Cliffs outcrop and Upper Valley field represent a new drilling target for oil in stratigraphic, structural, or combination traps.

Pennsylvanian Paradox Formation Microbial Carbonates at Greater Aneth Oil Field, Paradox Basin

Greater Aneth is Utah's largest oil field and produces oil from the Pennyslvanian (Desmoinesian) Paradox Formation in the Paradox Basin of southeastern Utah, southwestern Colorado, and a small part of Arizona (figures 81 and 82) within the Colorado Plateau. The Paradox Formation is dominated by marine carbonate rocks (limestone and dolomite) and evaporites deposited in a warm shallow-shelf, often restricted sea (figure 83). In addition to Greater Aneth field, numerous smaller fields produce from the Paradox Formation throughout the basin (figure 81). We identified microbialites in the Paradox Formation within the Aneth Unit of Greater Aneth field, suggesting the potential for untested intervals in the field and elsewhere in the basin.

Field Overview

The Greater Aneth field is a stratigraphic trap producing primarily from the Desert Creek zone of the Paradox Formation, which is sealed and sourced by the organic-rich, overlying Gothic and underlying Chimney Rock shales, respectively

Figure 80. *Domal microbial buildup, approximately 2.3 meters (7.5 ft) in height in the Timpoweap Member near the Hurricane Cliffs, southwestern Utah; see inset map for location of outcrop and Upper Valley field. Photograph courtesy of Scott M. Ritter, Brigham Young University.*

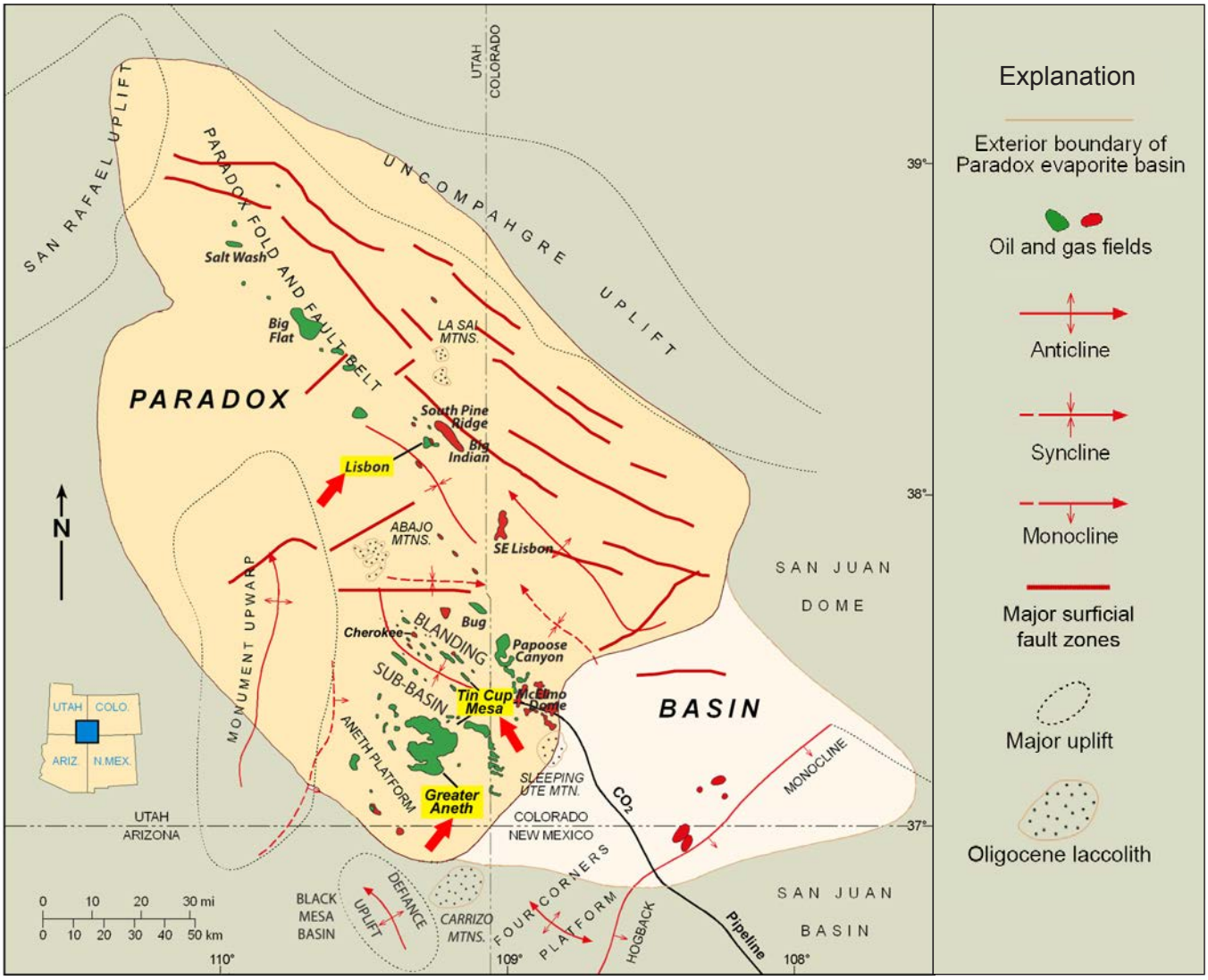

Figure 81. *Oil and gas fields in the Paradox Basin of Utah, Colorado, and Arizona. The play area for the Paradox Formation and Leadville Limestone are colored light orange; Greater Aneth, Tin Cup Mesa, and Lisbon fields are highlighted. Modified from Harr (1996) and Wood and Chidsey (2015).*

Age	Stratigraphic Unit		Thickness (m)	Lithology	Products
PENN	Hermosa Group	Paradox Fm.	0–4300		potash & salt
		Pinkerton Trail Fm.	0–46		
	Molas Formation		0–30		
M	Leadville Limestone		90–180		
DEV	Ouray Limestone		0–46		
	Elbert Formation		30–60		
		McCracken Ss. Mbr.	8–30		
€	"Lynch" Dolomite		240–300		

Oil and gas production; Condensate and oil production

Figure 82. *Stratigraphic column of part of the Paleozoic section determined from subsurface well data on the Paradox Basin. Modified from Hintze and Kowallis (2009).*

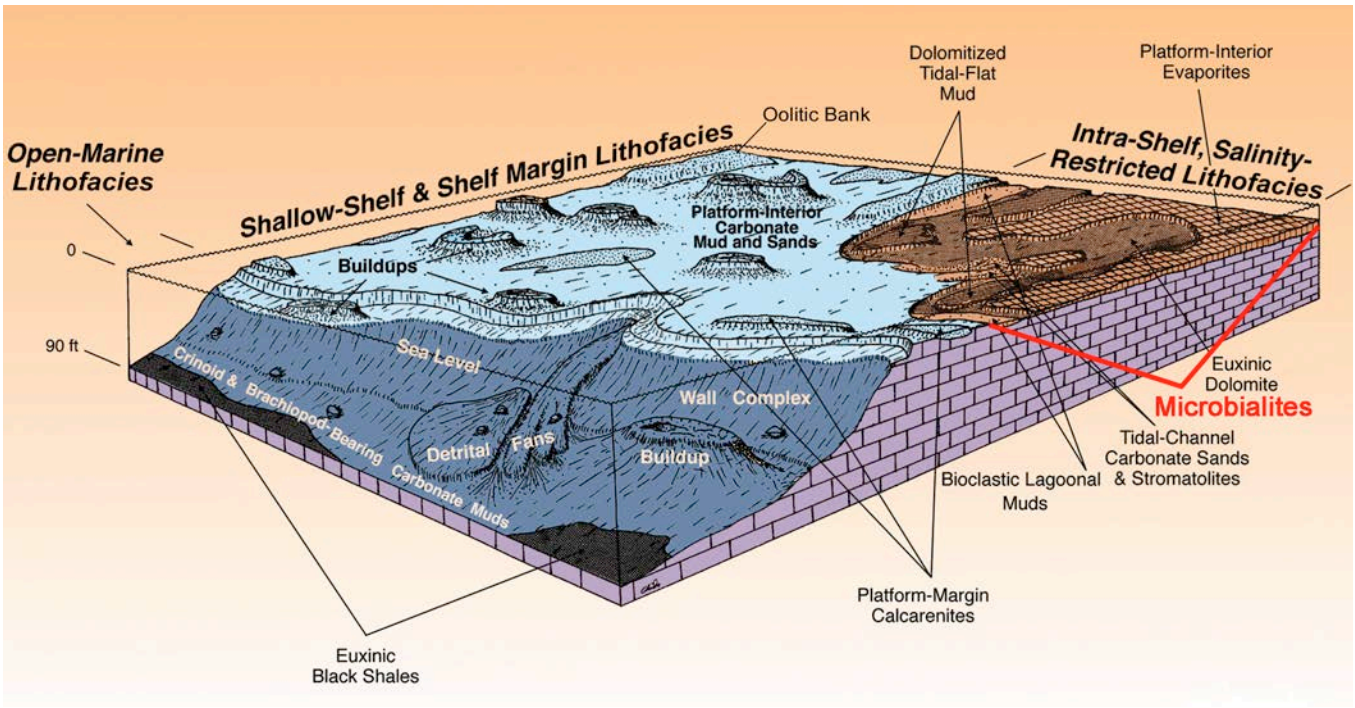

Figure 83. *Major depositional environments, as determined from cores, of the Desert Creek zone of the Pennsylvanian Paradox Formation within the Aneth platform, Utah. After Chidsey and others (1996).*

(figure 84). The Desert Creek zone creates an irregular west-northwest-trending reservoir buildup on the Aneth platform (figure 85). The trap was created by facies changes, including evaporites, that seal the reservoir laterally in addition to the seals above and below. Within the field, the Desert Creek is divided into three subzones: a relatively thin lower interval which represents a transition to the Chimney Rock shale, a middle interval composed predominantly of phylloid-algal buildup lithofacies, and an upper interval composed of oolitic-peloidal calcarenite lithofacies (Peterson and Ohlen, 1963; Babcock, 1978a, 1978b, 1978c, 1978d; Peterson, 1992; Moore and Hawks, 1993; Chidsey and Eby, 2014). The Desert Creek reservoir at Greater Aneth field consists of limestone (algal bafflestone and oolitic, peloidal, and skeletal grainstone and packstone) and finely crystalline dolomite. Fractures and small faults add to the reservoir heterogeneity.

Greater Aneth field was discovered in February 1956 with the completion of the Texaco No. 1 Navajo C well (NW1/4NE1/4 section 23, T. 40 S., R. 24 E., SLBL&M, San Juan County), which had an IPF of 568 BOPD and 4376 MCFGPD. The original reservoir field pressure was 2170 psi (Moore and Hawks, 1993). Currently, 443 producing (or shut-in) wells and 122 abandoned producers are in the field. Cumulative production as of March 1, 2021, was 498,011,587 BO, 472.1 BCFG, and 2,057,633,345 BW (Utah Division of Oil, Gas and Mining, 2021a). The OOIP for Greater Aneth field was estimated at 1100 million barrels (Babcock, 1978a, 1978b, 1978c, 1978d; Peterson, 1992). Greater Aneth's long and continued productive history is a result of secondary/tertiary recovery programs, which include waterflooding and carbon dioxide flooding, the largest and only in Utah, respectively. An extensive and successful horizontal drilling program has also been conducted in Greater Aneth field. As a result of these programs, more than 40% of the estimated OOIP has been recovered.

The net reservoir thickness of the Desert Creek zone at Greater Aneth is 15 meters (50 ft) over a 19,530-hectare (48,260 ac) area. Porosity averages 10% in interparticle, vuggy, moldic, and intercrystalline pore networks enhanced by fractures. Original carbonate fabrics are commonly overprinted by dolomitization, early marine cementation, dissolution, and late calcitic or anhydritic filling, among other diagenetic events. Thus, diagenesis further complicates the reservoir heterogeneity. Permeability averages 10 mD, ranging from 3 to 30 mD. The original drive mechanism is fluid expansion and solution gas; original water saturation was 24%. The BHT averages 52°C (125°F) (Peterson and Ohlen, 1963; Babcock, 1978a, 1978b, 1978c, 1978d; Peterson, 1992; Moore and Hawks, 1993; Chidsey and Eby, 2014).

General Core Evaluation

We described three cores from the Aneth Unit (one of four drilling units) in the northwestern part of Greater Aneth field (figure 86, plates 10 through 12, and the appendix): Aneth Unit (AU) No. F-317 (NW1/4SW1/4 section 17, T. 40 S., R. 24 E., SLBL&M), AU No. H-117 (NE1/4NE1/4 section 17, T. 40 S., R. 24 E., SLBL&M), and AU No. 27-C-3 (NW1/4SE1/4 section 27, T. 40 S., R. 24 E., SLBL&M). As of March 1, 2021, the AU No. F-317 well produced 866,953 BO, 1.23 BCFG,

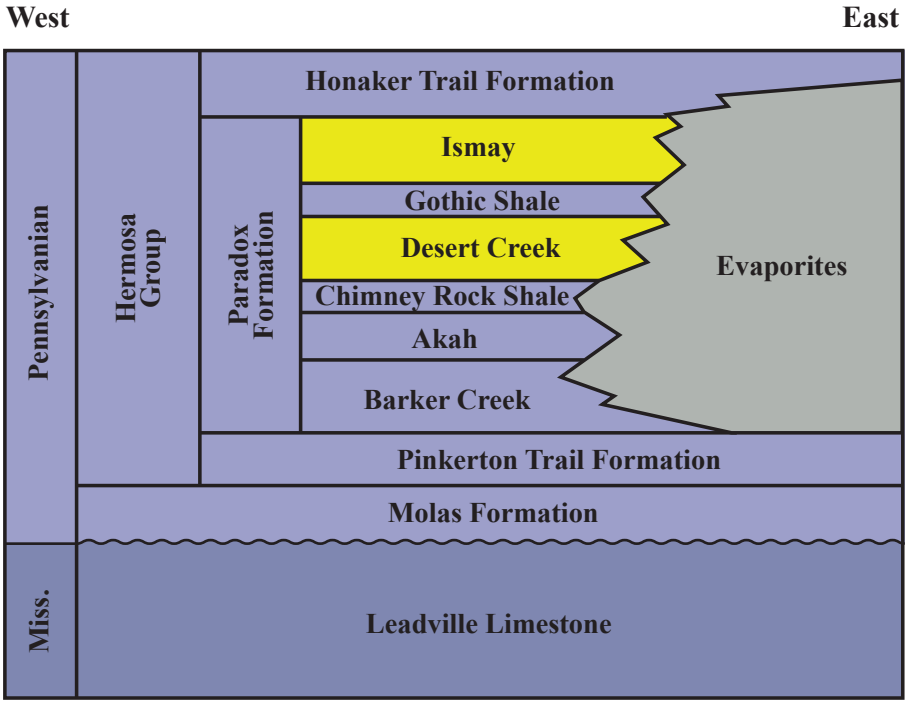

Figure 84. *Pennsylvanian stratigraphy of the Paradox Basin including informal zones of the Paradox Formation; the productive Ismay and Desert Creek zones are shown in yellow.*

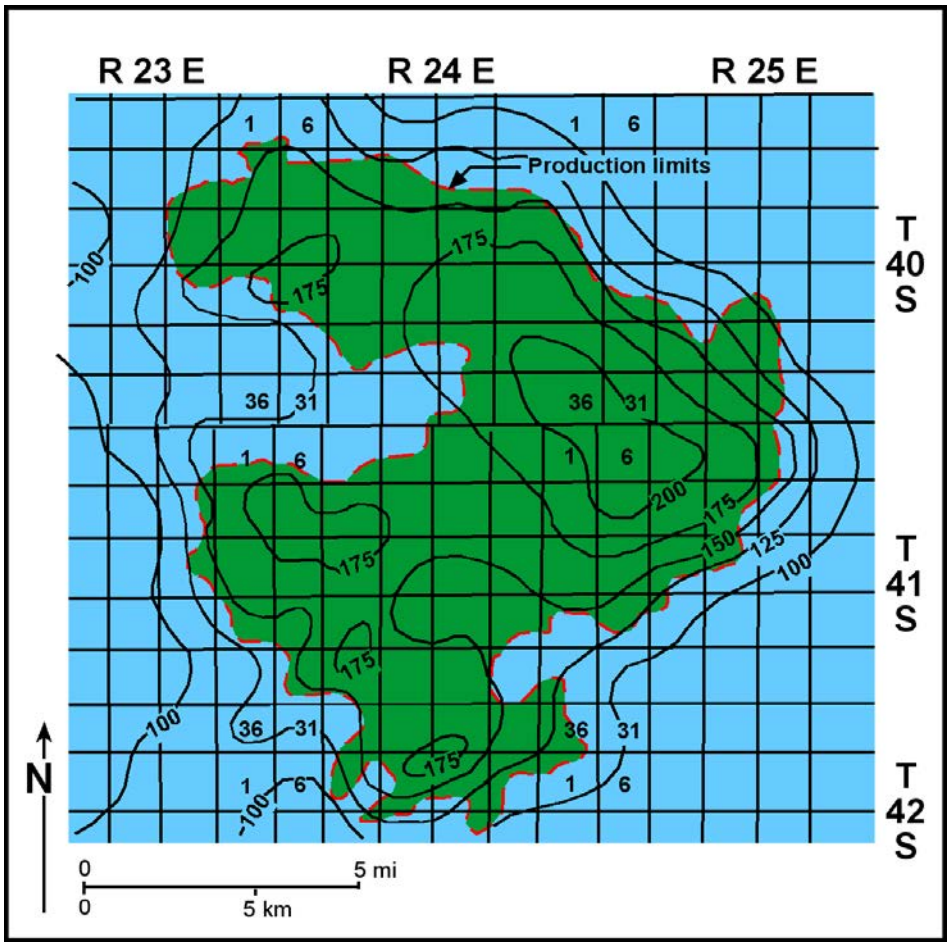

Figure 85. *Generalized thickness map of the Desert Creek zone, Greater Aneth field, San Juan County, Utah; contour interval = 25 feet. Modified from Peterson and Ohlen (1963).*

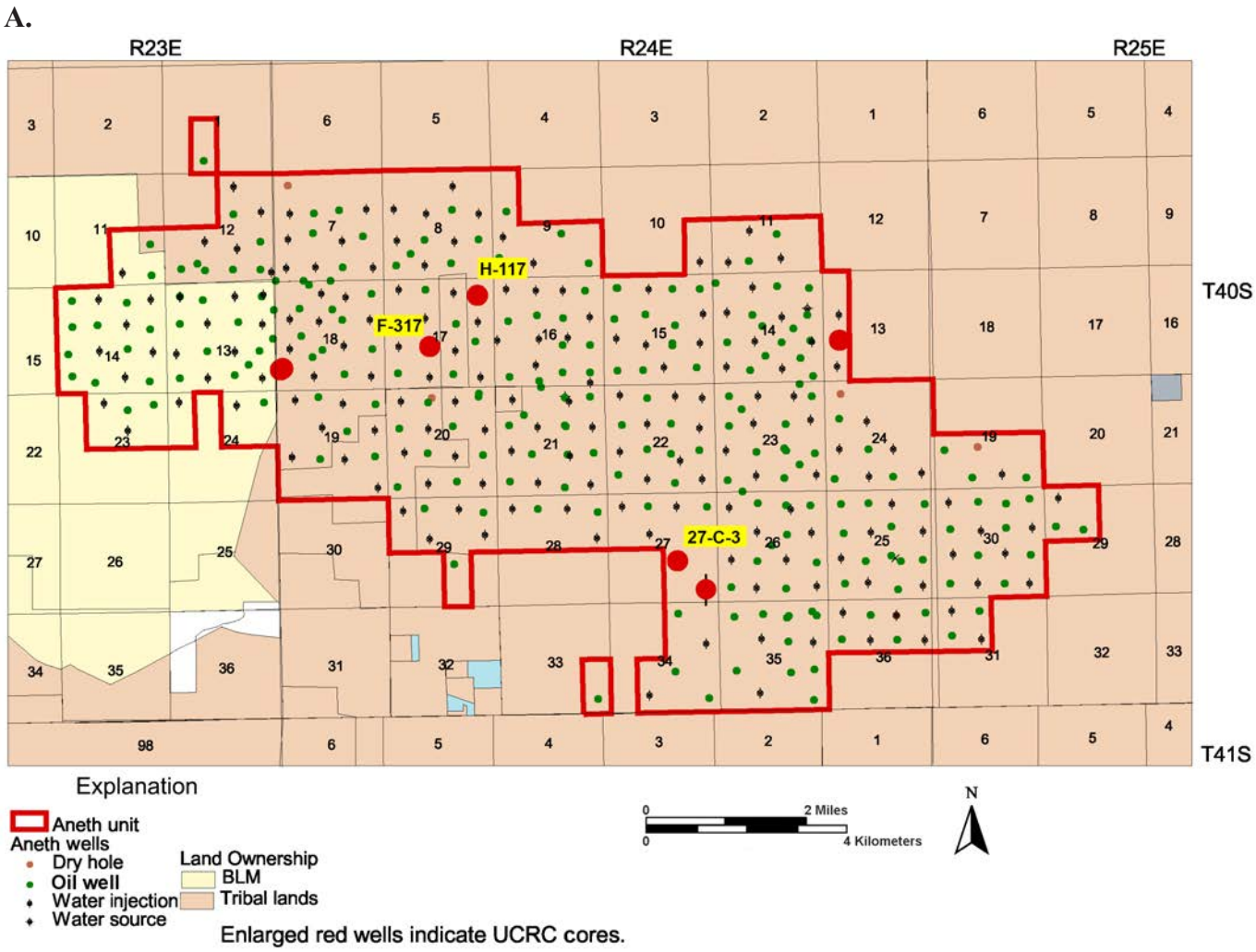

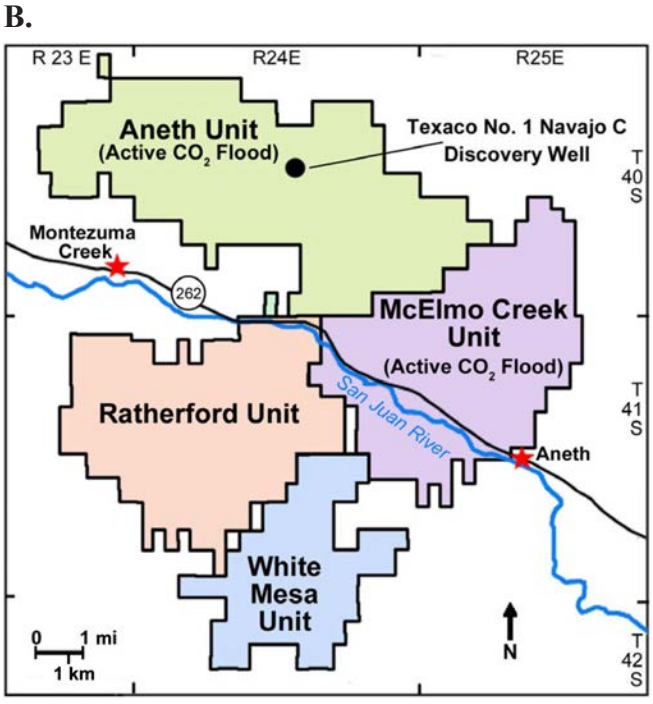

Figure 86. ***(A)*** *Land ownership and base map of wells in the Aneth Unit, Greater Aneth field. Wells with cores used in this study are highlighted.* ***(B)*** *Drilling units in Greater Aneth field.*

and 9,002,451 BW; the AU No. H-117 well produced 579,258 BO, 0.44 BCFG, and 2,405,675 BW; and the AU No. 27-C-3 well (currently shut-in) produced 227,470 BO, 1.23 BCFG, and 340,971 BW (Utah Division of Oil, Gas and Mining, 2021b). The general analysis of the cores from these wells indicates a complex Desert Creek reservoir representing a variety of depositional environments (high- and low-energy open-marine shelf, shallow-marine beach [foreshore] and shoals, phylloid-algal mounds, and low-energy, intra-shelf salinity-restricted mini-basins [figure 83]), which produce significant heterogeneity. Most carbonate fabrics are present: mudstone, wackestone, packstone, grainstone, bafflestone, boundstone, rudstone, and floatstone. Carbonate grains include peloids, ooids and oncoids, phylloid-algal plates, forams, and coated and skeletal grains. Pore types consist of fabric-selective shelter, moldic, interparticle, intraparticle, and intercrystalline, whereas nonfabric selective types include fracture and vuggy. Most of the Desert Creek units are composed of limestone but there are a few dolomite beds. A quartz siltstone is present near the top of the Desert Creek zone. There is evidence of hydrothermal dolomite, brecciation, and minor faults that may affect fluid flow. Some beds display burrows (tubular tempestites) and suggest subaerial exposure.

Intra-shelf salinity-restricted lithofacies, which include tidal flats, are found in the Desert Creek (figure 83) and other Paradox Formation zones as dolomitized packstone and grainstone. Megafossils and visible porosity are very rare in the tidal flat setting. Non-skeletal grainstone (calcarenite) composed of ooids, oncoids, coated grains, and "hard peloids" occurs as high-energy deposits in some tidal flat channel deposits. Remnants of interparticle and moldic pores may be present in this lithofacies. We identified microbialites in the cores that represent tidal flat environments and nearby phylloid-algal buildups.

Microbialites and Associated Grains

Several of the reservoir lithofacies described above contain good evidence of microbial activities including sediment bindings and dense lithification and structures with relief. The following lithofacies types have microbial components:

1. phylloid-algal bafflestones and buildups,
2. stromatolitic columns and domes associated with both ooids and skeletal grains (figure 87),
3. dolomitic muds associated within intra-shelf salinity-restricted mini-basins, and
4. possible tidal-flat caps to phylloid-algal mounds and grainstones.

Thrombolites (figures 88 and 89) are common in the intra-shelf salinity-restricted tidal-flat lithofacies. Digitate stromatolites are often found with thrombolites. Skeletal grains and ooids accumulated between microbial columns or as small lenses within the thrombolites and stromatolites (figure 89).

Figure 87. *Small digitate stromatolites encased in skeletal/oolitic grainstone with good reservoir quality. Aneth Unit No. F-317 core (figure 86), 1645.8 to 1646.6 meters (5401.5–5402.1 ft).*

Stromatolites are also found associated with tidal-channel carbonate sands in the tidal-flat lithofacies (figure 83) and there is evidence of erosion at the tops of some stromatolitic columns.

One other lithofacies seems to be associated with microbial development: saline oolite lithofacies consisting of broken and re-generated ooids, cerebroid ooids, and highly assymetrical ooids. The ooids in these types of grainstone beds resemble Great Salt Lake ooids (figure 24).

Reservoir quality of the Desert Creek microbialites is variable. Stromatolites and thrombolites encased in or associated with skeletal or oolitic grains combined show fair to good visible porosity (figures 87 and 89). Some examples appear oil saturated or the pores are lined with bitumen. Oncolitic rudstone and floatstone are well cemented and thus have poor reservoir quality (figure 90). The microbialite contribution to the total reservoir volume has yet to be determined.

Figure 88. *Porous thrombolitic grainstone. Note black bitumen lining pores. Aneth Unit No. H-117 core (figure 86), 1646.2 to 1646.4 meters (5400.8–5401.4 ft).*

Figure 89. *Oil-saturated thrombolitic/stromatolitic boundstone with skeletal grainstone lenses containing fair to good reservoir quality. Aneth Unit No. 27-C-3 core (figure 86), 1747.7 to 1747.9 meters (5734.0–5734.5 ft).*

Figure 90. *Oncolitic rudstone/floatstone with very poor reservoir quality. Aneth Unit No. H-117 core (figure 86), 1643.7 to 1644.6 meters (5392.8–5395.7 ft).*

Synopsis and Discussion

Paleozoic marine microbialites are not rare (figure 72) and thus their discovery in the Pennsylvanian Paradox Formation at Greater Aneth field should come as no surprise. The fact that we now recognize microbialites in the field implies that they are likely present elsewhere in the Paradox Formation in the Paradox Basin. We examined only a few cores; however, in 2016–17, the Utah Geological Survey received a major donation of cores from over 125 wells in Greater Aneth from the field operator, Resolute Energy Corporation (Chidsey, 2017). We recommend that these cores be evaluated as to the presence of micobialites and their reservoir potential.

The Blanding sub-basin lies north of the Aneth platform (figure 81). Many depositional environments in the Desert Creek and overlying Ismay zones of the Paradox Formation are similar to those on the Aneth platform—tidal flats within restricted inner shelf/platform interior, and intra-shelf basins (anhyrditic salinas) and phylloid-algal mounds on middle shelf/open platform interior settings (Chidsey and Eby, 2009). The restricted inner shelf/platform interior represents sediments deposited in shallow water (0 to approximately 14 meters [0–45 ft]), having generally low-energy and poor circulation conditions. This environment was conducive to microbial growth and stromatolites, thrombolites, and cryptalgal mats (laminations) are present in Blanding sub-basin Desert Creek and Ismay cores (Chidsey and Eby, 2009). Tidal flat lithofacies are found in the Upper Ismay zone as dolomitized packstone and grainstone. Clotted, lumpy, and poorly laminated microbial structures resembling small thrombolites and intraclasts are common (figure 91).

Porosity, if present, in microbial carbonates at Greater Aneth field as well as fields in the Blanding sub-basin, represents potential storage for new reserves. Extensive and successful horizontal drilling programs have been conducted for over 25 years at Greater Aneth field. Stacked, multiple horizontal laterals encounter porous and permeable intervals untouched by waterflooding (Amateis, 1995). This technique could target newly identified microbialites at Greater Aneth and other Paradox Formation fields in the basin.

Mississippian Leadville Limestone Microbial Carbonates at Lisbon Oil Field, Paradox Basin

Lisbon is a large oil and gas field located in the fold and fault belt of the northern Paradox Basin (figure 81). The field produces mainly from the Mississippian Leadville Limestone (figure 82), a shallow marine, carbonate-shelf deposit. Although there are seven other fields in the trend, several now abandoned, Lisbon accounts for most of the Leadville oil and gas production in the basin. The Leadville has extensive dolomitization, unusual brecciation, and massive amounts of bitumen. These characteristics combined with a variety of

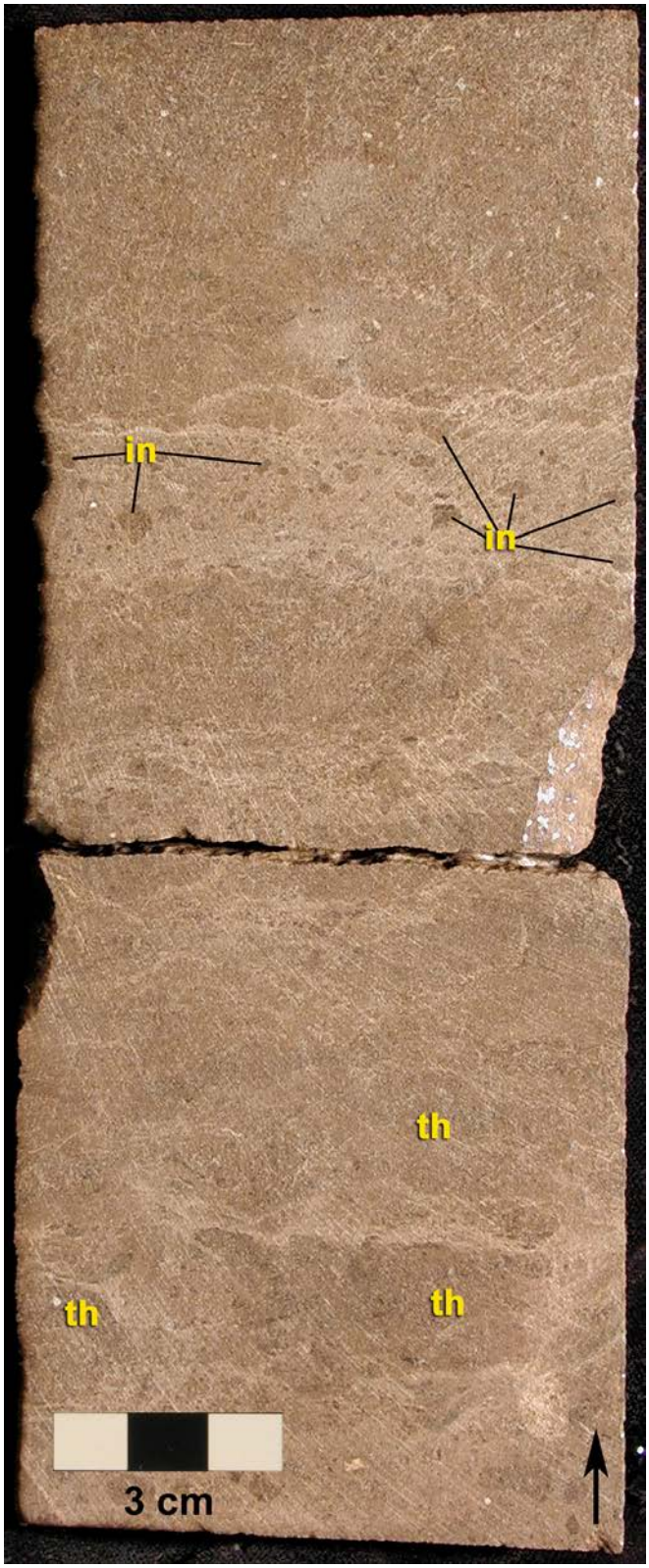

Figure 91. *Dolomitized lumpy microbial structures resembling small thrombolites (th) and intraclasts (in) composed of desiccated and redeposited thrombolitic fragments, tidal flat lithofacies, Ismay zone, Tin Cup Mesa field, Utah (figure 81). Tin Cup Mesa No. 2-23 well, section 23, T. 38 S., R. 25 E., SLBL&M; core from 1664.4 meters (5460.5 ft).*

carbonate depositional environments (figure 92) have created a unique reservoir hetergeneity. We have identified microbialites in Lisbon cores indicating that micribial communities lived in the marine shallow-shelf setting.

Field Overview

The Lisbon trap is an elongate, asymmetric, northwest-trending anticline, with nearly 600 meters (2000 ft) of structural closure and bounded on the northeastern flank by a major, basement-involved normal fault that has over 760 meters (2500 ft) of displacement (Smith and Prather, 1981) (figure 93). Several minor, northeast-trending normal faults divide the Lisbon Leadville reservoir into compartments. The seals for the Leadville producing zones are the overlying clastic beds of the Pennsylvanian Molas Formation (figure 82). Hydrocarbons in the Leadville are further sealed by evaporite (salt and anhydrite) beds within the overlying Pennsylvanian Paradox Formation. Hydrocarbons in Leadville reservoirs were also likely generated from source rocks in the Paradox.

Lisbon field was discovered in 1960 with the completion of the Pure Oil Company No. 1 NW Lisbon USA well (NE1/4NW1/4 section 10, T. 30 S., R. 24 E., SLBL&M, San Juan County) which had an IPF of 179 BOPD and 4376 MCFGPD. The original reservoir field pressure was 2982 psi (Clark, 1978). Currently, 18 producing (or shut-in) wells, 13 abandoned producers, 5 injection wells (4 gas injection wells and 1 water/gas injection well), and 4 dry holes are in the field. Cumulative production as of March 1, 2021, was 50,679,482 BO, 762 BCFG (cycled gas), and 50,511,202 BW (Utah Division of Oil, Gas and Mining, 2021a, 2021b). Original ultimate recovery was estimated at nearly 43,000,000 BO (Smouse, 1993); however, like Upper Valley field, production has surpassed that value. Hydrocarbon gas that was re-injected into the crest of the structure to control pressure decline is now being produced.

The net reservoir thickness is 69 meters (225 ft) over a 2072-hectare (5120 ac) area (Clark, 1978; Smouse, 1993). Reservoir quality is greatly improved by natural fracture systems associated with the Paradox fold and fault belt. Porosity averages 6% in intercrystalline and moldic networks enhanced by fractures; permeability averages 22 mD. The original drive mechanism is an expanding gas cap and gravity drainage; original water saturation was 39% (Clark, 1978; Smouse, 1993). The BHT ranges from 56° to 87°C (133°–189°F).

General Core Evaluation

We identified microbialites in two of the five cores from wells in Lisbon field (figure 93): Lisbon No. B-610 (NE1/4NW1/4 section 10, T. 30 S., R. 24 E., SLBL&M) and Lisbon No. B-816 (NE1/4SW1/4 section 16, T. 30 S., R. 24 E., SLBL&M). These wells are now gas injection wells, although the No. B-610 had produced 12,766 BO and 0.5 BCFG prior to its conversion to an injection well (Utah Division of Oil, Gas and Mining, 2017b).

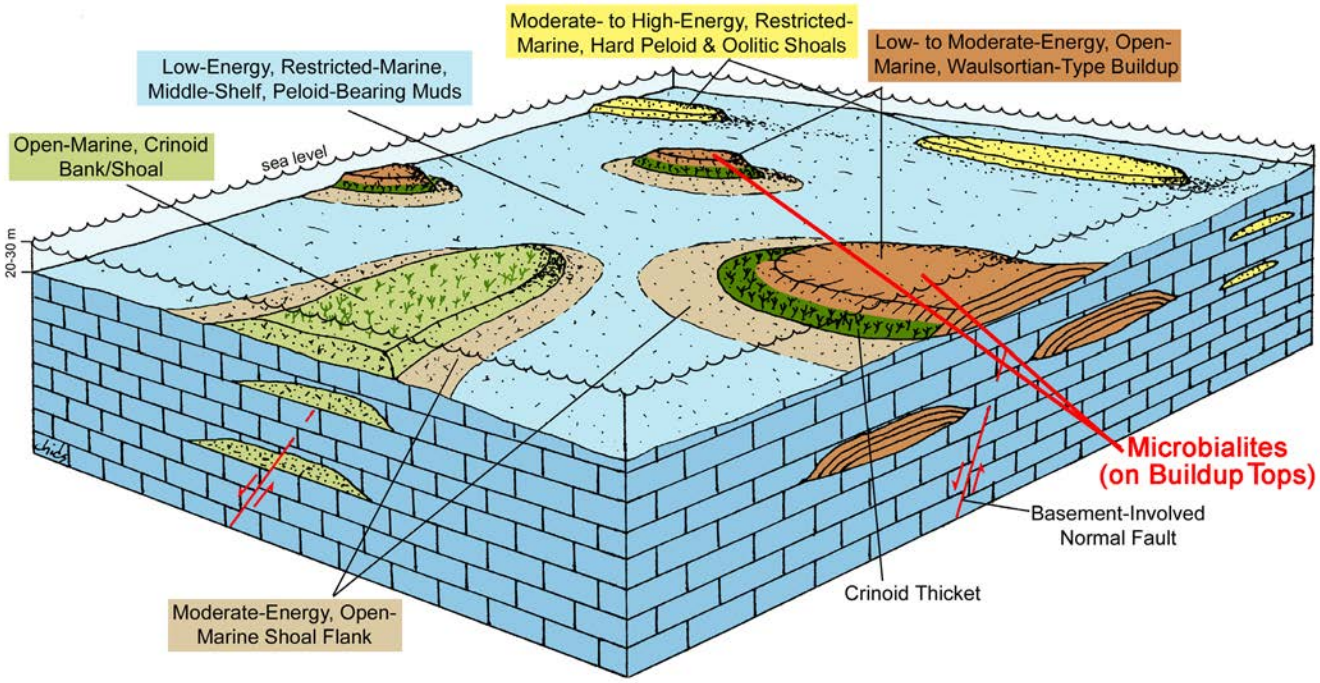

Figure 92. *Major depositional environments, as determined from cores, of the Mississippian Leadville Limestone, Lisbon field, Utah. After Chidsey and Eby (2016).*

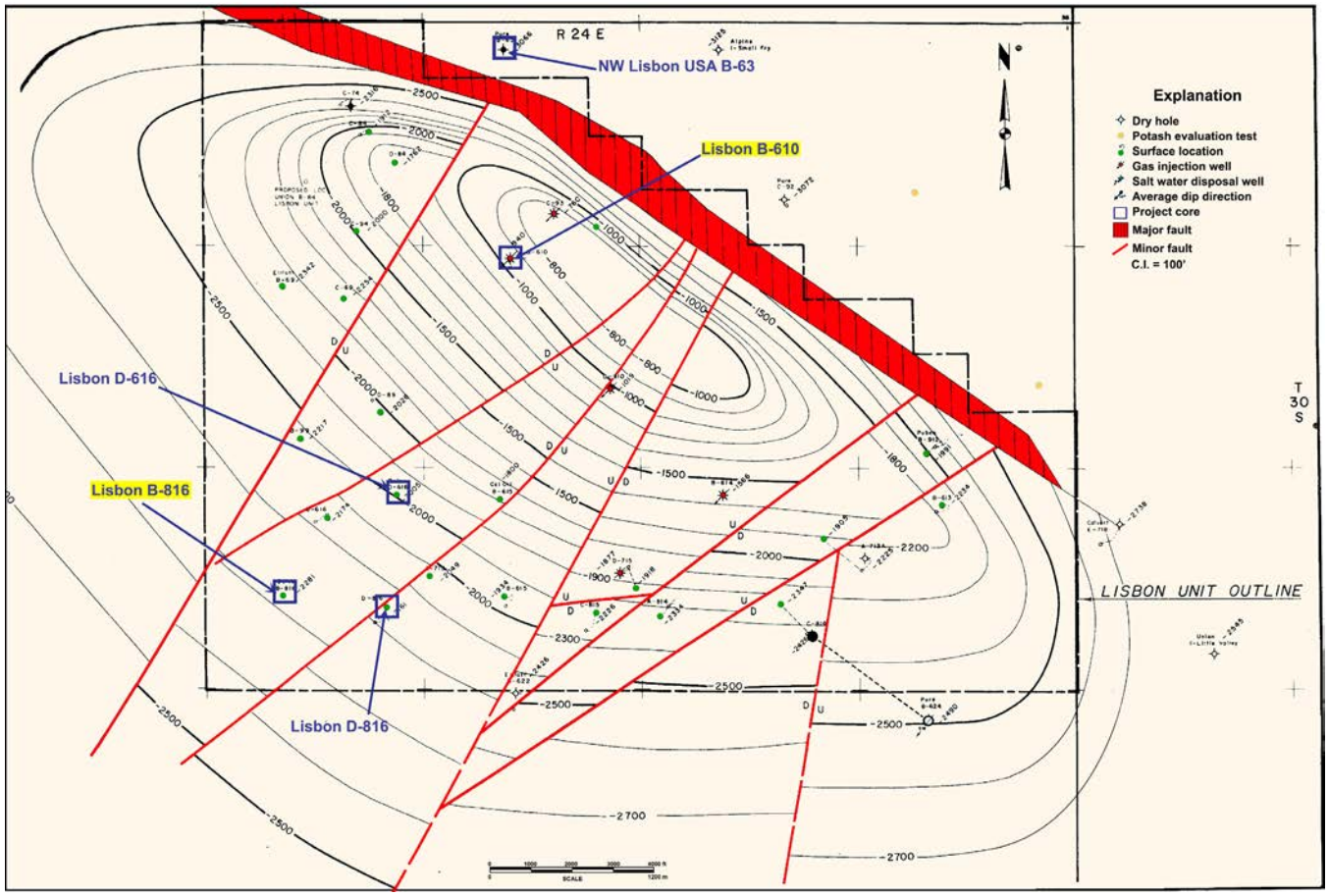

Figure 93. *Top of structure of the Leadville Limestone, Lisbon field, San Juan County, Utah. Also displayed are wells from which cores were examined in this study; those with microbialites are highlighted. Modified from C.F. Johnson, Union Oil Company of California files, 1970; courtesy of Tom Brown, Inc.*

The Leadville Limestone, as determined from cores (plates 13 and 14, and the appendix), was deposited in open-marine (crinoidal banks or shoals and Waulsortian-type buildups), oolitic and peloid shoal, and middle shelf depositional environments (figure 92). Producing units in Lisbon field contain dolomitized crinoidal/skeletal grainstone, packstone, and wackestone carbonate fabrics. Diagenesis includes fracturing, autobrecciation, karst development, hydrothermal dolomitization, and bitumen plugging. Two major types of diagenetic dolomite are observed in the Leadville Limestone at Lisbon field: (1) tight "early" dolomite consisting of very fine grained (<5 µm), interlocking crystals that preserve depositional fabrics; and (2) porous, coarser (>100–250 µm), rhombic and saddle crystals that discordantly replace limestone and earlier very fine grained dolomite. Pervasive leaching episodes that produced vugs and extensive microporosity predate or are concomitant with late dolomite formation. Rock units with open-marine and restricted-marine lithofacies constitute a significant reservoir potential, having both effective porosity and permeability when dissolution of skeletal grains, followed by dolomitization, has occurred.

Waulsortian buildups or mud mounds (leolites) developed exclusively during the Mississippian in many parts of the world (Wilson, 1975) and Waulsortian-type buildups were first described in Lisbon field by Fouret (1982). They are steep-sloped tabular, knoll, or sheet forms composed of several generations of mud deposited in a subtidal setting (Lees and Miller, 1995; Fouret, 1982, 1996) (figure 92). The lime mud was precipitated by bacteria and fungal/cyanobacterial filaments (Lees and Miller, 1995). Cyanobacteria were a likely precursor to the green algae *Ivanovia* responsible for Pennsylvanian buildups in the Paradox Basin (Fouret, 1982, 1996). Crinoids and sheet-like fenestrate byrozoans, in the form of thickets, are associated with the deeper parts of the mud mounds and are indicative of well-circulated, normal-marine salinity. Water depths ranged from 20 to 30 meters (60–90 ft). The thickets surrounded and helped to stabilize the mound. Burrowing organisms added a pelletal component to the mud and burrowing often destroyed laminations or made them discontinuous. Individual mounds range from less than a meter to tens of meters thick, and cover hundreds of meters in area with distinctive flank deposits. They form thick, extensive aggregates often located on paleotopographic highs associated with basement-involved faults (figure 92). This lithofacies represents a low- to moderate-energy environment. The depositional fabrics of the Waulsortian-type buildups include mud-supported boundstone, packstone, and wackestone (figure 94). Rocks representing Waulsortian-type buildups typically contain the following diagnostic constituents: peloids, crinoids, bryozoans, and associated skeletal debris, and *stromatactis* (cavities with curved or irregular tops and flat bases filled with calcite cement). Rock units having this lithofacies constitute a significant reservoir potential, having both effective porosity and permeability, especially after dolomitization. Waulsortian-type buildups are identified in several additional cores described by Fouret (1982, 1996). We recognized microbialites on the tops of these buildups (figure 92).

Microbialites

Although the quality of the Lisbon cores was generally poor, we identified stromatolites but no thrombolites or other types of microbialites. The environment where stromatolites grew was likely more open marine and slightly higher energy than the settings for the marine microbialites found in the Paradox, Moenkopi, and Twin Creek Formations described earlier. Leadville stromatolites are found in mud-dominated boundstone/bindstone; lime mud binds the stromatolitic laminations (figures 95 and 96). Possible subaerial exposure is indicated by eroded stromatolite heads and desiccation features (figure 96). Stromatolitic packages often alternate with rip-up clasts and eroded heads (figure 97). Not unexpected in mud-mound settings, associated carbonate grains are not present even though the surrounding low-energy, restricted-marine middle shelf is represented by peloid-bearing muds (figure 92).

Figure 94. *Typical peloidal/skeletal packstone/wackestone representing moderate- to low-energy, open-marine (and in places, middle shelf), Waulsortian-type buildup lithofacies. Lisbon No. B-816 core (figure 93), 2635 meters (8646 ft).*

Figure 95. *Stromatolitic boundstone/bindstone dominated by muddy fabrics. Note laminated rip-up clasts; the black areas are bitumen-lined pores. Lisbon No. B-610 core (figure 93), 2395 to 2396 meters (7858–7862 ft).*

Like the underlying mud-mound Waulsortian-type buildups, the microbial-bearing carbonates are dolomitized. Silicification of thin intervals can be seen in lighter rocks. Pores and fractures are lined with bitumen (figures 95 through 97); associated laminated rip-up clasts are common.

The pervasive dolomitization and extensive bitumen-lined porosity suggests that these micobialites may have moderate to good reservoir quality. The microbialite contribution to the total Leadville reservoir volume has yet to be determined and would be a difficult task given the condition and limited number of cores in this large, mature field.

Synopsis and Discussion

The Paradox fold and fault belt is a 19,400 square-kilometer (7500 mi^2) area that is relatively unexplored—only about 100 exploratory wells have penetrated the Leadville (less than one well per township). The presence of microbialites at Lisbon field suggests they may occur in other Leadville Limestone fields in the region (figure 81), as was implied from Paradox Formation cores at Greater Aneth field to the south. The key to finding microbialites in the Leadville is identifying the Waulsortian-type mud-mound buildups upon which they grew. Dolomitization of these mud mounds and associated microbialites has produced reservoir-quality rocks at Lisbon, especially late hydrothermal dolomitization recognized at Lisbon (Eby and others, 2005). We propose similar conditions could have created large, untested, diagenetic-type hydrocarbon traps (in most cases combined with basement-involved structures like Lisbon) in the Paradox fold and fault belt involving mud mounds and microbialites.

SUMMARY AND CONCLUSIONS

The potential of microbial carbonate reservoirs is now recognized in numerous emerging oil plays in many regions of the world. Petrographic analyses and pore type descriptions of both modern and ancient microbialites are extremely useful in determining reservoir characteristics in potential petroleum plays. Northern Utah's Great Salt Lake contains excellent examples of Holocene microbial carbonates and associated carbonate grains, especially in Bridger Bay at the northern tip of Antelop Island and at Rozel Point. Great Salt Lake's geometry and Holocene carbonate "factory" serve as an excellent analog to the Eocene lacustrine Green River Formation (Lake Uinta) of the Uinta Basin, northeast Utah. Many of the microbial features observed in the Green River cores are also well displayed in extensive nearby outcrops—stromatolites, thrombolites, oncolites, and travertine/tufa. In addition, examples of marine microbial carbonates and their associated carbonate grains are present in subsurface oil field cores from Mississippian, Pennsylvanian, Triassic, and Jurassic reservoirs in Utah. (These cores are available for detailed study at the UCRC.)

Figure 96. *Stromatolitic laminations bound by lime mud. Note desiccation features and microfractures. Black bitumen lines open pores and fractures. Lisbon No. B-610 core (figure 93), 2433 to 2435 meters (7983–7990 ft).*

Figure 97. *Stromatolitic packages alternating with rip-up clasts and eroded heads. Silicification of thin intervals can be seen in lighter rocks; bitumen lines some of the open pores and fractures. Lisbon No. B-816 core (figure 93), 2633 to 2636 meters (8637–8648 ft).*

Great Salt Lake is a hypersaline lake where microbialites and associated carbonate grains are widespread. The margin of the lake is a shallow ramp that creates a susceptibility to rapid and widespread shoreline changes. Petrographic analysis of Holocene microbialites shows that open constructional pores are common. Beaches and nearby dunes consist of abundant hypersaline ooids and coated grains, some of which are being lithified into crusts while retaining high interparticle porosity. Carbonate muds and unconsolidated ooids often provide an adequate substrate for microbialite formation.

The carbonate flat environment along the margin of ancient Lake Uinta was very similar to that of Great Salt Lake—relatively shallow water, subject to extensive rapid shoreline fluctuations, periods of high salinity, etc.—which resulted in microbial growth along with oolite, oncolite, and peloid formation, as observed in the Green River Formation in the Skyline 16 research core. The core displays (1) low-relief stomatolites and thrombolites, (2) excellent primary megascopic and microporosity within microbial fabrics, (3) grainstones composed with abundant interparticle and intraparticle porosity, (4) sharp contacts between grainstones and microbialites, (5) porous, lacy dolomite with possible evaporite crystal molds within dense, carbonate muds, and (6) silicification in some microbial intervals. Thrombolites preserve greater concentrations of megascopic porosity than stromatolites. Outcrops of the Green River Formation near the Skyline 16 well site display many of the microbial features observed in the core. Thrombolitic heads contain large (megascopic), open constructional pores. Well-developed laminations in stromatolitic heads have abundant primary porosity between microbial filaments. Pisoids, ooids, oncoids, ostracods, and peloids are frequently associated with the microbial facies.

West Willow Creek field produces oil from a small microbialite mound (E_2 carbonate bed) within the Green River Formation—the only such known field in the Uinta Basin. The microbial reservoir developed on sand near the southern shore of Lake Uinta during a very low lake-level cycle. However, the growth of this microbial mound was able to keep pace with the eventual rising lake level resulting in a general deepening cycle. Lake conditions were also conducive for microbialite, ooid, peloid, and especially oncoid development; ostracods and turretellid gastropods flourished. Stromatolitic and thrombolitic microbialites contain well-preserved primary interparticle and intraparticle porosity; dolomitization in the upper part created the best reservoir quality. Associated grainstones between laminated microbial fabrics also provide good to excellent interparticle porosity. Patches of microporosity are well developed within the oncolites, another significant component to the microbial system. Additional microbial mounds are likely in the Green River Formation but remain to be discovered in the Uinta Basin.

A survey of carbonate cores from other active Utah oil fields also reveals a variety of microbial fabrics, associated carbonate grains, pore types, and reservoir characteristics from marine rocks. The reservoirs, fields, and geologic locations, respectively, are the (1) Jurassic Twin Creek Limestone, Pineview field, thrust belt, (2) Triassic Moenkopi Formation (K-2 Zone, Timpoweap Member), Upper Valley field, Kaiparowits Basin, (3) Pennsylvanian Paradox Formation, Greater Aneth field, Paradox Basin, and (4) Mississippian Leadville Limestone, Lisbon field, Paradox Basin.

- Pineview field produces oil and gas from a subsidiary closure on a ramp anticline where the low-porosity carbonates of the Twin Creek Limestone are extensively fractured. Most production is from the Watton Canyon and Rich Members in which cores reveal complex reservoir heterogeneity due to a variety of carbonate facies, textures, structures, and diagenesis. Depositional environments include open marine, low- to high-energy middle shelf, marine sabkha, oolitic shoals, inner shelf microbial lagoon, and microbial tidal flat. The best analog for observing microbial lithofacies in outcrop of the Twin Creek is to the southwest of Pineview field. Microbialites and associated grains include microlaminated (stromatolitic) mudstone, thrombolites, small microbial heads, peloids, and oolites.

- Upper Valley field produces hydrodynamically displaced oil on the flank of an elongate, north-northwest to south-southeast-trending surface anticline. Production is from marine carbonate zones in the Permian Kaibab Limestone (K-3 and K-4 porosity zone) and the Timpoweap Member (K-1 and K-2) of the Moenkopi Formation. Depositional environments include open marine subtidal, nearshore marine/intertidal, restricted marine/lagoon, and supratidal/microbial (algal mat). Microbialites, some showing excellent visble porosity, are well exhibited in the productive K-2 zone of the Timpoweap and the K-3 zone of the Kaibab. Small-scale stromatolites, thrombolites, and cryptalgal mats of the K-2 zone of the Timpoweap Member likely grew in very shallow, quiet water, marine intertidal to supratidal environments. However, subaerial exposure and desiccation affected microbial growth and characteristics.

- Greater Aneth, Utah's largest oil field, produces primarily from the Desert Creek zone of the Paradox Formation on a giant carbonate buildup forming a stratigraphic trap. The Desert Creek reservoir represents a variety of depositional environments: open-marine shelf, shallow-marine beach and shoals, phylloid-algal mounds, and low-energy, intra-shelf salinity-restricted mini-basins. Thrombolites are common in the intra-shelf salinity-restricted tidal-flat lithofacies; digitate stromatolites are often found with thrombolites. Sediment bindings, dense lithification, and structures with relief are evidence of microbial activities associated with (1) phylloid-algal buildups, (2) ooids and skeletal grains (stromatolitic columns and domes), (3) dolomitic muds within saline intrashelf mini-basins, and (4) tidal flat caps to phylloid-algal mounds and grainstones. Clotted, lumpy, poorly laminated microbial structures resemble small thrombolites. Re-generated, cerebroid, and highly asymmetrical oolites are similar to Great Salt Lake ooids.

- Lisbon field, located in the fold and fault belt of the northern Paradox Basin, produces oil and gas from the shallow marine, carbonate-shelf Leadville Limestone. The Lisbon trap is an elongate, asymmetric, northwest-trending anticline, bounded on the northeastern flank by a major, basement-involved normal fault. The Leadville was deposited in open-marine (crinoidal banks or shoals and Waulsortian-type buildups), oolitic and peloid shoals, and middle shelf depositional environments. Microbialites (stromatolites only) grew on the tops of Waulsortian-type buildups; associated carbonate grains are not present. The Leadville reservoir, including the microbialites, is also characterized by pervasive dolomitization, extensive bitumen-lined porosity, and brecciation.

Porosity has developed in many marine microbial fabrics: intercrystalline, dissolution (moldic), interparticle, intraparticle/microbial construction, and extensive microporosity. Microbial dolomite/dolomitization have enhanced porosity and permeability development. Cores evaluated as part of this study can serve as production-scale analogs for comparison of marine microbialites to the more common freshwater lacustrine microbial reservoirs. Marine microbial carbonates represent potential new drilling targets within existing fields and hydrocarbon plays in Utah and the Rocky Mountain region.

ACKNOWLEDGMENTS

Support for this research was provided by Utah Geological Survey (UGS) and Eby Petrography & Consulting, Inc., under the UGS's "Characterization of Utah's Hydrocarbon Reservoirs, Metals, and Industrial Minerals" program. The Skyline 16 coring project was funded by the UGS and the University of Utah, Institute for Clean and Secure Energy, U.S. Department of Energy/National Energy Technology Laboratory grant DE-FE0001243. Evaluation of the Twin Creek Limestone core was conducted under the Preferred Upstream Management Program of the U.S. Department of Energy, National Energy Technology Laboratory, Tulsa, Oklahoma, contract number DE-FC26-02NT15133.

Jen Miller, Cheryl Gustin, Jay Hill, James Parker, Jeremy Gleason, and Stevie Emerson of the UGS drafted figures; Michael D. Laine, Thomas Dempster, and Brad Wolverton of the UCRC prepared samples and photographed cores. Gary Aho, Sage Geotech, was a consultant to the Skyline 16 drilling project; the coring company was Himes Drilling. Morgan Rosenberg, University of Utah Department of Geology and Geophysics M.Sc. student, under the direction of Lauren Birgenheier, measured and described the Green River Formation outcrop sections at the "Condo" and "Flash Flood" localities in Evacuation Creek. Birgenheier also co-described the Skyline 16 research core. Thin sections from the core and outcrops were prepared by Tulsa Sections, Inc.

We appreciate the encouragement and significant discussions with Stanley M. Awramik of the University of California Santa Barbara, the late H. Paul Buchheim of Loma Linda University, Scott M. Ritter of Brigham Young University (BYU), and V. Paul Wright of the BG Group. This study was carefully reviewed by David W. Bowen, Montana State University; Scott M. Ritter, BYU; Michael C. Pope, Texas A&M University; Kathryn Gibbons, Nexen; and Stephanie Carney, Mike Hylland, and Bill Keach of the UGS. Their suggestions and constructive criticism greatly improved the manuscript. Finally, we thank Jen Miller, John Good, and the UGS editorial production team for their efforts in producing this publication.

REFERENCES

Ahr, W.M., 2008, Geology of carbonate reservoirs—the identification, description, and characterization of hydrocarbon reservoirs in carbonate rocks: Hoboken, New Jersey, John Wiley and Sons, Inc., 296 p.

Ahr, W.M., 2009, Microbial carbonates as hydrocarbon reservoirs: American Association of Petroleum Geologists Search and Discovery Article #30106.

Ahr, W.M., Mancini, E.A., and Parcell, W.C., 2011, Pore characteristics in microbial carbonate reservoirs: American Association of Petroleum Geologists Search and Discovery Article #30167.

Aitken, J.D., 1967, Classification and environmental significance of cryptalgal limestone and dolomites, with illustrations from the Cambrian and Ordovician of southwestern Alberta: Journal of Sedimentary Petrology, v. 7, p. 1163–1178.

Allin, D.L., 1990, Colorado Plateau sub-surface water flow key: Oil and Gas Journal, v. 88, no. 30, p. 52–54.

Allin, D.L., 1993, Upper Valley, Garfield County, Utah, *in* Hill, B.G., and Bereskin, S.R., editors, Oil and gas fields of Utah: Utah Geological Association Publication 22, non-paginated.

Allison, M.L., 1997, A preliminary assessment of energy and mineral resources within the Grand Staircase-Escalante National Monument: Utah Geological Survey Circular 93, p. 13–25, https://doi.org/10.34191/C-93.

Amateis, L.J., 1995, Application of sequence stratigraphic modeling to integrated reservoir management at Aneth Unit, Greater Aneth field, Utah: Society of Petroleum Engineers, SPE Paper 030534, p. 35–49.

Awramik, S.M., and Buchheim, H.P., 2013, Microbialites of the Eocene Green River Formation as analogs to the South Atlantic pre-salt carbonate hydrocarbon reservoirs: American Association of Petroleum Geologists Search and Discovery Article #90169.

Awramik, S.M., and Buchheim, H.P., 2015, Giant stromatolites of the Eocene Green River Formation (Colorado, USA): Geology, v. 48, no. 8, p. 691–694.

Babcock, P.A., 1978a, Aneth (Aneth Unit), San Juan County, Utah, *in* Fassett, J.E., editor, Oil and gas fields in the Four Corners area: Four Corners Geological Society Guidebook, v. II, p. 577–579.

Babcock, P.A., 1978b, Aneth (McElmo Creek Unit), San Juan County, Utah, *in* Fassett, J.E., editor, Oil and gas fields in the Four Corners area: Four Corners Geological Society Guidebook, v. II, p. 580–583.

Babcock, P.A., 1978c, Aneth (Ratherford Unit), San Juan County, Utah, *in* Fassett, J.E., editor, Oil and gas fields in the Four Corners area: Four Corners Geological Society Guidebook, v. II, p. 584–586.

Babcock, P.A., 1978d, Aneth (White Mesa Unit), San Juan County, Utah, *in* Fassett, J.E., editor, Oil and gas fields in the Four Corners area: Four Corners Geological Society Guidebook, v. II, p. 587–590.

Baskin, R.L., 2014, Occurrence and spatial distribution of microbial bioherms in Great Salt Lake, Utah: Salt Lake City, University of Utah, Ph.D. dissertation, 190 p.

Baxter, B.K., 2018, Great Salt Lake microbiology—a historical perspective: International Microbiology 21, p. 79–95.

Baxter, B.K., and Butler, J.K., editors, 2020, Great Salt Lake biology—a terminal lake in a time of change: Heidelberg, Germany, Springer, 527 p.

Baxter, B.K., Litchfield, C.D., Sowers, K., Griffith, J.D., DasSarma, P.A., and DasSarma, S., 2005, Great Salt Lake microbial diversity, *in* Gunde-Cimerron, N., Oren, A., and Plemenita, A., editors, Adaptation to life in high salt concentrations in Archaea, Bacteria, and Eukarya: Springer, Cellular Origin, Life in Extreme Habitats and Astrobiology, v. 9, p. 9–95.

Bereskin, S.R., Morgan, C.D., and McClure, K.P., 2004, Descriptions, petrology, photographs, and photomicrographs of core from the Green River Formation, south-central Uinta Basin, Utah: Utah Geological Survey Miscellaneous Publication 04-2, 203 p., https://doi.org/10.34191/MP-04-2.

Blakey, R., and Ranney, W., 2008, Ancient landscapes of the Colorado Plateau: Grand Canyon, Grand Canyon Association, 156 p.

Blazzard, 1979, Pineview, Summit County, Utah, *in* Cardinal, D.F., and Steward, W.W., editors, Wyoming oil and gas fields symposium, Greater Green River Basin: Wyoming Geological Association, p. 286–288.

Borer, J.M., 2016, High-resolution stratigraphy of the lower portion of the Green River Formation at Raven Ridge and Red Wash field, NE Uinta Basin, Utah, Colorado, USA—facies and stratigraphic patterns in a high-gradient, high-energy lacustrine system: The Mountain Geologist, v. 53, no. 3, p. 119–223.

Bosence, D.W.J., Gibbons, K.A., Le Heron, D.P., Morgan, W.A., Pritchard, T., and Vining, B.A., 2015, Microbial carbonates in space and time—introduction, *in* Bosence, D.W.J., Gibbon, K.A., Le Heron, D.P., Morgan, W.A., Pritchard, T., and Vining, B.A., editors, Microbial carbonates in space and time—implications for global exploration and production: The Geological Society, London, Special Publication 418, p. 1–15.

Bouton, A., Vennin, E., Boulle, J., Pace, A., Bourillot, R., Thomazo, C., Brayard, A., Désaubliaux, G., Goslar, T., Yokoyama, Y., Dupraz, C., and Visscher, P.T., 2016a, Linking the distribution of microbial deposits from the Great Salt Lake (Utah, USA) to tectonic and climatic processes: Biogeosciences, v. 13, p. 5511–5526.

Bouton, A., Vennin, E., Mulder, T., Pace, A., Bourillot, R., Thomazo, C., Brayard, A., Goslar, T., Buoncristiani, J-F., Désaubliaux, G., and Visscher, P.T., 2016b, Enhanced development of lacustrine microbialites on gravity flow deposits, Great Salt Lake, Utah, USA: Sedimentary Geology, v. 341, p. 1–12.

Bradley, W.H., 1929, Algae reefs of the Green River Formation: U.S. Geological Survey Shorter Contributions to General Geology, 1928, p. 203–223.

Braga, J.C., Martin, J.M., and Riding, R., 1995, Controls on microbial dome fabric development along a carbonate-siliciclastic shelf-basin transect, Miocene, SE Spain: PALAIOS, v. 10, no. 4., p. 347–361.

Bruce, C.L., 1988, Jurassic Twin Creek Formation—a fractured limestone reservoir in the overthrust belt, Wyoming and Utah, *in* Goolsby, S.M., and Longman, M.W., editors, Occurrence and petrophysical properties of carbonate reservoirs in the Rocky Mountain region: Rocky Mountain Association of Geologists Guidebook, p. 105–120.

Bryant, B., 1990, Geologic map of the Salt Lake City 30' x 60' quadrangle, north-central Utah, and Uinta County, Wyoming: U.S. Geological Survey Miscellaneous Investigation Series Map I-1944, 1:100,000.

Buchheim, H.P., and Awramik, S.M., 2012, Predicting lacustrine microbialite distribution and facies associations—the Eocene Green River Formation analogue: American Association of Petroleum Geologists Search and Discovery Article #10428.

Buchheim, H.P., and Awramik, S.M., 2013, Microbialites of the Eocene Green River Formation as analogs to the South Atlantic pre-salt carbonate hydrocarbon reservoirs [abs.]: The Geological Society, Microbial Carbonates in Space and Time—Implications for Global Exploration and Production, Programme and Abstract Volume, p. 64–65.

Buchheim, H.P., Awramik, S.M., and Leggitt, V.L., 2010, Lacustrine stromatolites and microbialites as petroleum reservoirs: American Association of Petroleum Geologists Search & Discovery Article #90104.

Buchheim, H.P., Awramik, S.M., Leggitt, V.L., Demko, T.M., Lamb-Wozniak, K., and Bohacs, K.M., 2012, Large lacustrine microbialite bioherms from the Eocene Green River Formation—stratigraphic architecture, sequence stratigraphic relations, and depositional model: American Association of Petroleum Geologists Search and Discovery Article #90153.

Burne, R.V., and Moore, L.S., 1987, Microbialites—organosedimentary deposits of benthic microbial communities: Palaios, v. 2, p. 241–254.

Campbell, J.A., 1969, The Upper Valley oil field, Garfield County, Utah, *in* Geology and natural history of the Grand Canyon region: Four Corners Geological Society 5th Field Conference Guidebook, p. 195–200.

Carminatti, M., Wolff, B., and Gamboa, L., 2008, New exploratory frontiers in Brazil, Madrid, Spain, Proceedings of the 19th World Petroleum Congress, 11 p.

Carminatti, M., Dias J.L., and Wolff, B., 2009, From turbidites to carbonates—breaking paradigms in deep waters: Offshore Technology Conference, Houston, Texas, May 4–7, 2009, OTC 20124, 7 p.

Carozzi, A.V., 1962a, Observations on algal biostromes in the Great Salt Lake, Utah: Journal of Geology, v. 70, p. 246–252.

Carozzi, A.V., 1962b, Cerebroid oolites: Illinois Academy of Science Transactions, v. 55, p. 239–249.

Cashion, W.B., 1967, Geology and fuel resources of the Green River Formation, southeastern Uinta Basin, Utah and Colorado: U.S. Geological Survey Professional Paper 548, 48 p.

Cashion, W.B., and Donnell, J.R., 1972, Chart showing correlation of selected key units in the organic-rich sequence of the Green River Formation, Piceance Creek Basin, Colorado, and Uinta Basin, Utah: U.S. Geological Survey Oil and Gas Investigations, Chart OC 65.

Chafetz, H.S., and Guidry, S.A., 1999, Bacterial shrubs, crystal shrubs, and ray-crystal shrubs—bacterial vs. abiotic precipitation: Sedimentary Geology, v. 126, p. 57–74.

Chidsey, T.C., Jr., 2017, Utah Core Research Center receives a treasure trove donation of Greater Aneth oil field cores: Utah Geological Survey, Survey Notes, v. 49, no. 2, p. 6–7, https://doi.org/10.34191/SNT-49-2.

Chidsey, T.C., Jr., and Eby, D.E., 2009, Regional lithofacies trends in the upper Ismay and lower Desert Creek zones in the Blanding sub-basin of the Paradox Basin, Utah, *in* Houston, W.S., Wray, L.L., and Moreland, P.G., editors, The Paradox Basin revisited—new developments in petroleum systems and basin analysis: Rocky Mountain Association of Geologists Special Publication, p. 436–470.

Chidsey, T.C., Jr., and Eby, D.E., 2014, Reservoir properties and carbonate petrography of the Aneth Unit, Greater Aneth field, Paradox Basin, southeastern Utah, *in* MacLean, J.S., Biek, R.F., and Huntoon, J.E., editors, Geology of Utah's far south: Utah Geological Association Publication 43, p. 153–197, 2 appendices, 6 plates.

Chidsey, T.C., Jr., and Eby, D.E., 2016, Chapter 9—Mississippian Leadville Limestone Paradox Basin play, *in* Chidsey, T.C., Jr., editor, Major oil plays in Utah and vicinity: Utah Geological Survey Bulletin 137, p. 145–157, https://doi.org/10.34191/B-137.

Chidsey, T.C., Jr., Eby, D.E., and Lorenz, D.M., 1996, Geological and reservoir characterization of small shallow-shelf fields, southern Paradox Basin, Utah, *in* Huffman, A.C., Jr., Lund, W.R., and Godwin, L.H., editors, Geology and resources of the Paradox Basin: Utah Geological Association Publication 25, p. 39–56.

Chidsey, T.C., Jr., Vanden Berg, M.D., and Eby, D.E., 2015, Petrography and characterization of microbial carbonates and associated facies from modern Great Salt Lake and Uinta Basin's Eocene Green River Formation in Utah, USA, *in* Bosence, D.W.J., Gibbon, K.A., Le Heron, D.P., Morgan, W.A., Pritchard, T., and Vining, B.A., editors, Microbial carbonates in space and time—implications for global exploration and production: The Geological Society, London, Special Publication 418, p. 261–286, http://dx.doi.org/10.1144/SP418.6.

Choquette, P.W., and Pray, L.C., 1970, Geologic nomenclature and classification of porosity in sedimentary carbonates: American Association of Petroleum Geologists Bulletin, v. 54, no. 2, p. 207–250.

Clark, C.R., 1978, Lisbon, San Juan County, Utah, *in* Fassett, J.E., editor, Oil and gas fields of the Four Corners area: Four Corners Geological Society, v. II, p. 662–665.

Collister, J.W., and Schamel, S., 2002, Lipid composition of recent sediments from the Great Salt Lake, *in* Gwynn, J.W., editor, Great Salt Lake—an overview of change: Utah Department of Natural Resources Special Publication, p. 127–142.

Cook, C.W., and Dunleavy, J.R., 1996, Pineview, Summit County, Utah, *in* Hill, B.G., and Bereskin, S.R., editors, Oil and gas fields of Utah: Utah Geological Association Publication 22 (Addendum), non-paginated.

Della Porta, G., 2015, Carbonate build-ups in lacustrine, hydrothermal and fluvial settings—comparing depositional geometry, fabric types and geochemical signature, *in* Bosence, D.W.J., Gibbon, K.A., Le Heron, D.P., Morgan, W.A., Pritchard, T., and Vining, B.A., editors, Microbial carbonates in space and time—implications for global exploration and production: The Geological Society, London, Special Publication 418, p. 17–68, http://dx.doi.org/10.1144/SP418.6.

Doelling, H.H., and Davis, F.D., 1989, The geology of Kane County, Utah: Utah Geological and Mineral Survey Bulletin 124, 192 p., 10 plates, https://doi.org/10.34191/B-124.

Donnell, J.R., and Blair, R.W., Jr., 1970, Resource appraisal of three rich oil-shale zones in the Green River Forma-

tion, Piceance Creek Basin, Colorado: Colorado School of Mines Quarterly, v. 65, no. 4, p. 73–87.

Eardley, A.J., 1938, Sediments of the Great Salt Lake: American Association of Petroleum Geologists Bulletin, v. 22, p. 1305–1411.

Eby, D.E., Chidsey, T.C., Jr., Morgan, C.D., McClure, K., Humphrey, J.D., Moore, J.N., Taylor, L.H., and Weyland, V.H., 2005, Dolomitization of the Mississippian Leadville reservoir at Lisbon field, Utah [abs.]: American Association of Petroleum Geologists Annual Convention, Official Program with Abstracts, v. 14, p. A40.

Fouch, T.D., 1975, Lithofacies and related hydrocarbon accumulations in Tertiary strata of the western and central Uinta Basin, *in* Bolyard, D.W., editor, Symposium on deep drilling frontiers in the central Rocky Mountains: Rocky Mountain Association of Geologists Guidebook, p. 163–173.

Fouch, T.D., Nuccio, V.F., Anders, D.E., Rice, D.D., Pitman, J.K., and Mast, R.F., 1994, Green River (!) petroleum system, Uinta Basin, Utah, USA, *in* Magoon, L.B., and Dow, W.G., editors, The pet¬roleum system—from source to trap: American Association of Petroleum Geologists Memoir 60, p. 399–421.

Fouke, B.W., 2011, Hot-spring systems geobiology—abiotic and biotic influences on travertine formation at Mammoth Hot Springs, Yellowstone National Park, USA: Sedimentology, v. 58, p. 170–219.

Fouret, K.L., 1982, Depositional and diagenetic environment of the Mississippian Leadville Formation at Lisbon field, Utah: College Station, Texas A&M University, M.S. thesis, 119 p.

Fouret, K.L., 1996, Depositional and diagenetic environment of the Mississippian Leadville Limestone at Lisbon field, Utah, *in* Huffman, A.C., Jr., Lund, W.R., and Godwin, L.H., editors, Geology and resources of the Paradox Basin: Utah Geological Association Publication 25, p. 129–138.

Gautier, D.L., Dolton, G.L., Takahashi, K.I., and Varnes, K.L., editors, 1996, 1995 National assessment of United States oil and gas resources—results, methodology, and supporting data: U.S. Geological Survey Digital Data Series DDS-30, release 2.

Gebelein, C.D., and Hoffman, P., 1971, Algal origin of interlaminated limestone—dolomite sedimentary rocks, *in* Bricker, O.P., editor, Carbonate cements: Baltimore, Maryland, John Hopkins, p. 319–325.

Gilbert, G.K., 1890, Lake Bonneville: U.S. Geological Survey Monograph 1, 438 p.

Godsey, H.S., Oviatt, C.G., Miller, D., and Chan, M.A., 2011, Stratigraphy and chronology of officiated with the Provo shoreline, Pleistocene Lake Bonneville, Utah: Palaeogeography, Palaeoclimatology, and Palaeoecology, v. 310, p. 442–450.

Goolsby, S.M.L., Dwyff, L., and Fryt, M.S., 1988, Trapping mechanisms and petrophysical properties of the Permian Kaibab Formation, south-central Utah, *in* Goolsby, S.M.L., and Longman, M.W., editors, Occurrence and petro-physical properties of carbonate reservoirs in the Rocky Mountain region: Rocky Mountain Association of Geologists Guidebook, p. 193–210.

Grey, K., and Awramik, S.M., 2020, Handbook for the study and description of microbialites: Geological Survey of Western Australia, Bulletin 147, 278 p.

Grey, K., and Planavsky, N.J., 2009, Microbialites of Lake Thetis, Cervantes, Western Australia—a field guide: Geological Survey of Western Australia, Record 2009/11, 21 p.

Gwynn, J.W., 1996, Commonly asked questions about Utah's Great Salt Lake and ancient Lake Bonneville: Utah Geological Survey Public Information Series 39, 22 p., https://doi.org/10.34191/PI-39.

Halley, R.B., 1976, Ooid fabric and fracture in the Great Salt Lake: Journal of Sedimentary Petrology, v. 47, no. 3, p. 1099–1120.

Halley, R.B., 1977, Textural variation within Great Salt Lake algal mounds, *in* Walter, M.R., editor, Stromatolites, developments in sedimentology: Amsterdam, Elsevier, p. 435–446.

Handley, K., and Campbell, K., 2011, Character, analysis and preservation of biogenicity in terrestrial siliceous stromatolites from geothermal settings, *in* Tewari, V.C., and Seckback, J., editors, Stromatolites—interaction of microbes with sediments: Heidelberg, Springer Series Origin, Life in Extreme Habitats and Astrobiology, v. 18, p. 359–382, DOI: 10.1007/978-94-007-0397-1.

Harr, C.L., 1996, Paradox oil and gas potential of the Ute Mountain Ute Indian Reservation, *in* Huffman, A.C., Jr., Lund, W.R., and Godwin, L.H., editors, Geology of the Paradox Basin: Utah Geological Association Publication 25, p. 13–28.

Hintze, L.F., and Kowallis, B.J., 2009, Geologic history of Utah: Brigham Young University Geology Studies Special Publication 9, 225 p.

Homewood, P.W., Mettraux, M., Vanden Berg, M.D., Foubert, A., and Schaegis, J.C., 2018, Presalt reservoir analogs—lacustrine microbialites fed by shore zone hot springs, Lakeside, UT: American Association of Petroleum Geologists Datapages Search and Discovery.

Homewood, P.W., Mettraux, M., Vanden Berg, M.D., Foubert, A., Neumann, R., Newell, D., and Atwood, G., in press, Lakeside microbialites—the perplexing record of a transitional Great Salt Lake shoreline, *in* Della Porta, G., Rogerson, M., and Tagliasacchi, E., editors, Non-marine carbonates—from the geological record to present-day processes: The Depositional Record.

Imlay, R.W., 1967, Twin Creek Limestone (Jurassic) in the Western Interior of the United States: U.S. Geological Survey Professional Paper 540, 105 p.

Imlay, R.W., 1980, Jurassic paleobiogeography of the conterminous United States in its continental setting: U.S. Geological Survey Professional Paper 1062, 134 p.

Johnson, R.C., Mercier, T.J., Brownfield, M.E., and Self, J.G., 2010, Assessment of in-place oil shale resources in the Green River Formation, Uinta Basin, Utah and Colorado: U.S. Geological Survey Digital Data Series DDS-69-BB, chap. 1, 153 p.

Johnson, R.C., Nichols, D.J., and Hanley, J.H., 1988, Stratigraphic sections of lower Tertiary strata and charts showing palynomorphs and mollusk assemblages, Douglas Creek arch area, Colorado and Utah: U.S. Geological Survey Miscellaneous Field Studies MF-1997, 2 plates, scale 1:125,000.

Kahle, C.F., 1974, Ooids from Great Salt Lake, Utah, as an analogue for the genesis and diagenesis of ooids in marine limestones: Journal of Sedimentary Research, v. 44, p. 30–39.

Kanik, M., Munro-Ehrlich, M., Fernandes-Martins, M.C., Payne, D., Gianoulias, K., Keller, L., Kubacki, A., Lindsay, M.R., Baxter, B.K., Vanden Berg, M.D., Colman, D.R., Boyd, E.S., 2020, Unexpected abundance and diversity of phototrophs in mats from morphologically variable microbialites in Great Salt Lake, Utah: Applied Environmental Microbiology, v. 86, p. 165–220, https://doi.org/10.1128/AEM.00165-20.

Kennard, J.M., and James, N.P., 1986, Thrombolites and stromatolites—two distinct types of microbial structures: Palaios, v. 1, p. 492–503.

Kocurek, G., and Dott, R.H., Jr., 1983, Jurassic paleogeography and paleoclimate of the central and southern Rocky Mountains region, *in* Reynolds, M.W., and Dolly, E.D., editors, Symposium on Mesozoic paleogeography of west-central U.S.: Society for Sedimentary Geology (SEPM), Rocky Mountain Section, p. 101–116.

Lees, A., and Miller, J., 1995, Waulsortian banks, *in* Monty, C.L.V., Bosencce, D.W.J., Bridges, P.H., and Pratt, B.R., editors, Carbonate mud-mounds—their origin and evolution: International Association of Sedimentologists Special Publication No. 23, p. 191–271.

Leggitt, V.L., Biaggi, R.E., and Buchheim, H.P., 2007, Paleoenvironments associated with caddisfly-dominated microbial-carbonate mounds from the Tipton Shale Member of the Green River Formation—Eocene Lake Gosiute: Sedimentology, v. 53, no. 3, p. 661–699.

Lindsay, M.R., Anderson, C., Fox, N., Scofield, G., Allen, J., Anderson, E., Bueter, L., Poudel, S., Sutherland, K., Munson-McGee, J.H., Nostrand, J.D., Zhou, J., Spear, J.R., Baxter, B.K., Lageson, D.R., and Boyd, E.S., 2017, Microbialite response to an anthopogenic salinity gradient in Great Salt Lake, Utah: Geobiology, v. 15, issue 1, p. 131–145.

Madison, M.J., Martinko, J.M., Stahl, D.A., and Clark, D.P., 2012, Brock biology of microorganisms (13th edition): San Franscico, California, Pearson Education, Inc., publishing as Benjamin Cummings, 1155 p.

Margolis, L., 1998, Symbiotic planet—a new look at evolution: New York, Basic Books, 146 p.

Matthews, A.A.L., 1930, Origin and growth of the Great Salt Lake oolites: Journal of Geology, v. 38, p. 633–642.

Miller, S.E., 2011, Evaluation of biogenicity and branching in stromatolites from the Tipton Member, Green River Formation [abs.]: Geological Society of America Abstracts with Programs, v. 43, no. 5, p. 585.

Montgomery, S.L., 1984, Kaiparowits Basin—an old frontier with new potential: Petroleum Frontiers, v. 1, no. 2, p. 4–25.

Moore, T.R., and Hawks, R.L., 1993, Greater Aneth, *in* Hill, B.G., and Bereskin, S.R., editors, Oil and gas fields of Utah: Utah Geological Association Publication 22 (Addendum), non-paginated.

Morgan, C.D., 2003, Geologic guide and road logs of the Willow Creek, Indian Canyon, Soldier Creek, Nine Mile, Gate and Desolation Canyons, Uinta Basin, Utah: Utah Geological Survey Open-File Report 407, 58 p., 2 appendices, https://doi.org/10.34191/OFR-407.

Morgan, C.D., Chidsey, T.C., Jr., McClure, K.P., Bereskin, S.R., and Deo, M.D., 2003, Reservoir characterization of the lower Green River Formation, southwest Uinta Basin, Utah: Utah Geological Survey Open-File Report 411, 140 p., https://doi.org/10.34191/OFR-411.

Murray, R.C., 1960, Origin of porosity in carbonate rocks: Journal of Sedimentary Research, v. 30, no. 1, p. 59–84.

Nakano, C.M.F., Pinto, A.C.C., Marcusso, J.L., and Minami, K., 2009, Pre-salt Santos Basin—extended well test and production pilot in the Tupi area—the planning phase: Offshore Technology Conference, Houston, Texas, May 4–7, 2009, OTC 19886, 8 p.

Neuendorf, K.K.E., Mehl, J.P., Jr., and Jackson, J.A., 2011, Gossary of geology (5th edition) revised: Alexandria, Virginia, 783 p.

Newell, D.L., Jensen, J.L., Frantz, C.M., and Vanden Berg, M.D., 2017, Great Salt Lake (Utah) microbialite $\delta^{13}C$, $\delta^{18}O$, and $\delta^{15}N$ record fluctuations in lake biogeochemistry since the late Pleistocene: Geochemistry, Geophysics, Geosystems, v. 18, p. 3631–3645.

Nielson, R.L., and Johnson, J.L., 1979, The Timpoweap Member of the Moenkopi Formation, Timpoweap Canyon, Utah: Utah Geology, v. 6, no. 1, p. 17–28.

Noffke, N., and Awramik, S.M., 2013, Stromatolites and MISS—differences between relatives: GSA Today, v. 23, no. 9, p. 4–9, doi: 10.1130/GSATG187A.1.

Osmond, J.C., 2000, West Willow Creek field—first productive lacustrine stromatolite mound in the Eocene Green

River Formation, Uinta Basin, Utah: The Mountain Geologist, v. 37, no. 3, p. 157–170.

Oviatt, C.G., 2014, The Gilbert episode in the Great Salt Lake Basin, Utah: Utah Geological Survey Miscellaneous Publication 14-3, 20 p., https://doi.org/10.34191/MP-14-3.

Oviatt, C.G., 2015, Chronology of Lake Bonneville, 30,000 to 10,000 yr B.P.: Quaterary Science Reviews, v. 110, p. 166–171.

Pace, A., Bourillot, R., Vennin, E., Galaup, S., Bundeleva, I., Patrier, P., Dupraz, C., Thomazo, C., Sansjofre, P., Yokoyama, Y., Franceschi, M., Anguy, Y., Pigot, L., Virgone, A., and Visscher, P., 2016, Microbial and diagenetic steps leading to the mineralization of Great Salt Lake microbialites: Scientific Reports, v. 6 (31495), 12 p.

Paradis, O.P., 2019, Great Salt Lake ooids—insights into rate of formation, potential as paleoenvironmental archives, and biochemistry: Los Angelos, University of Southern California, Ph.D dissertation, 181 p.

Parcell, W.C., 2002, Sequence stratigraphic controls on the development of microbial fabrics and growth forms—implication for reservoir quality distribution in the Upper Jurassic (Oxfordian) Smackover Formation, eastern Gulf Coast, USA: Carbonates and Evaporites, v. 17, p. 166–181.

Pedley, H.M., 1990, Classification and environmental models of cool freshwater tufas: Sedimentary Geology, v. 68, p. 143–154.

Pedley, M., Rogerson, M., and Middleton, R., 2009, Freshwater calcite precipitates from in vitro mesocosm flume experiments—a case study for biomediation of tufas: Sedimentology, v. 56, no. 2, p. 511–527.

Pedone, V.A., and Folk, R.L., 1996, Formation of aragonite cement by nannobacteria in the Great Salt Lake, Utah: Geology, v. 24, p. 763–765.

Pedone, V.A., and Norgauer, C.H., 2002, Petrography and geochemistry of recent ooids from the Great Salt Lake, Utah, *in* Gwynn, J.W., editor, Great Salt Lake—an overview of change: Utah Department of Natural Resources Special Publication, p. 33–41.

Peixoto Filho, F.T., and de Souza Neto, I.S., 2010, Brazilian pre-salt—the challenges of coring at a new frontier: Society of Petroleum Engineers Paper 139195, 7 p.

Pentecost, A., 2005, Travertine: Springer, Berlin, 445 p.

Peterson, J.A., 1992, Aneth field – U.S.A., Paradox Basin, Utah, *in* Foster, N.H., and Beaumont, E.A., editors, Stratigraphic traps III: American Association of Petroleum Geologists Treatise of Petroleum Geology—Atlas of Oil and Gas Fields, p. 41–82.

Peterson, J.A., and Ohlen, H.R., 1963, Pennsylvanian shelf carbonates, Paradox Basin, *in* Bass, R.O., editor, Shelf carbonates of the Paradox Basin: Four Corners Geological Society Symposium, 4th Field Conference, p. 65–79.

Peterson, P.R., 1973, Upper Valley field: Utah Geological and Mineralogical Survey Oil and Gas Field Studies, no. 7, 4 p.

Petroleum Information, 1984, Overthrust belt field summaries: Petroleum Information Corporation, Denver, Colorado, 99 p.

Platt, N.H., and Wright, V.P., 1991, Lacustrine carbonate facies, models, facies distributions and hydrocarbon aspects, *in* Anadon, P., and Kelts, K., editors, Lacustrine facies analysis: International Association of Sedimentologists Special Publication 13, p. 57–74.

Post, F.J., 1980, Biology of the North Arm, *in* Gwynn J.W., editor, Great Salt Lake—a scientific, historical and economic overview: Utah Geological and Mineral Survey Bulletin 116, p. 313–321, https://doi.org/10.34191/B-116.

Remy, R.R., 1992, Stratigraphy of the Eocene part of the Green River Formation in the south-central part of the Uinta Basin, Utah: U.S. Geological Survey Bulletin 1787, Chapter BB, p. 1–79.

Riding, R., 2000, Microbial carbonates—the geological record of calcified bacterial-algal mats and biofilms: Sedimentology, v. 47, p. 179–214.

Riding R., 2011, Microbialites, stromatolites, and thrombolites, *in* Reitner J., and Thiel V., editors, Encyclopedia of geobiology: Springer, Dordrecht, Encyclopedia of Earth Sciences Series, p. 635–654, https://doi.org/10.1007/978-1-4020-9212-1_196.

Rosenberg, M.J., 2013, Facies, stratigraphic architechure, and lake evolution of the oil shale bearing Green River Formation, eastern Uinta Basin, Utah: Salt Lake City, University of Utah, M.S. thesis, 141 p.

Rosenberg, M.J., Birgenheier, L.P., and Vanden Berg, M.D., 2015, Facies, stratigraphic architechure, and lake evolution of the oil shale bearing Green River Formation, eastern Uinta Basin, Utah, *in* Smith, M.E., and Carroll, A.R., Stratigraphy and paleolimnology of the Green River Formation, western USA: Syntheses in Limnogeology, v. 1, Springer Dordrecht, p. 211–249, https://doi.org/10.1007/978-94-017-9906-5_9.

Ryder, R.T., Fouch, T.D., and Elison, J.H., 1976, Early Tertiary sedimentation in the western Uinta Basin, Utah: Geological Society of America Bulletin, v. 87, p. 496–512.

Saller, A.H., 2004, Paleozoic dolomite reservoirs in the Permian Basin, SW USA—stratigraphic, distribution, porosity, permeability, and production, *in* Braithwaite, C.J.R., Rizzi, G., and Dorke, G., editors, The geometry and petrogenesis of dolomite hydrocarbon reservoirs: The Geologic Society (London) Special Publication 235, p. 309–323.

Saller, A.H., and Henderson, N., 1998, Distribution of porosity and permeability in platform dolomites—insight from the Permian Basin of West Texas: American Association of Petroleum Geologists Bulletin 82, p. 1528–1550.

Saller, A., Rushton, S., Buambua, L., Inman, K., McNeil, R., and Dickson, J.T., 2016, Presalt stratigraphy and depositional systems in the Kwanza Basin, offshore Angola: American Association of Petroleum Geologists Bulletin, v. 100, p. 1135–1164.

Sandberg, P.A., 1975, New interpretations of Great Salt Lake ooids and of ancient non-skeletal carbonate mineralogy: Sedimentology, v. 22, p. 497–537.

Sarg, J.F., Huang, S., Tänavsuu-Milkeviciene, K., and Humphrey, J.D., 2013, Lithofacies, stable isotope composition, and stratigraphic evolution of microbial and associated carbonates, Green River Formation (Eocene), Piceance Basin, Colorado: American Association of Petroleum Geologists Bulletin, v. 97, no. 11, p. 1937–1966.

Shapiro, R.S., and Awramik, S.M., 2009, Atlas of microbialites: Microbial Workshop, Houston, Texas, March 26, 2009, 25 p.

Sharp, G.C., 1976, Reservoir variations at Upper Valley field, Garfield County, Utah, *in* Hill, J.G., editor, Symposium on the geology of the Cordilleran Hingeline: Rocky Mountain Association of Geologists Guidebook, p. 325–344.

Sharp, G.C., 1978, Upper Valley, Garfield County, Utah, *in* Fossett, J.E., editor, Oil and gas fields of the Four Corners area: Four Corners Geological Society Guidebook, v. II, p. 709–711.

Smith, K.T., and Prather, O.E., 1981, Lisbon field—lessons in exploration, *in* Wiegand, D.L., editor, Geology of the Paradox Basin: Rocky Mountain Association of Geologists Guidebook, p. 55–59.

Smith, M.E., Carroll, A.R., and Singer, B.S., 2008, Synoptic reconstruction of a major ancient lake system—Eocene Green River Formation, western United States: Geological Society of America Bulletin, v. 120, no. 1/2, p. 54–84, doi:10.1130/B26073.1.

Smouse, D., 1993, Lisbon, San Juan County, Utah, *in* Hill, B.G., and Bereskin, S.R., editors, Oil and gas fields of Utah: Utah Geological Association Publication 22, nonpaginated.

Sprinkel, D.A., 2009, Interim geologic map of the Seep Ridge 30' x 60' quadrangle, Uintah, Duchesne, and Carbon Counties, Utah, and Rio Blanco and Garfield Counties, Colorado: Utah Geological Survey Open-File Report 549, GIS data, 3 plates, scale 1:100,000, https://doi.org/10.34191/OFR-549dm.

Sprinkel, D.A., 2018, Interim geologic map of the east part of the Duchesne 30' x 60' quadrangle, Duchesne and Wasatch Counties, Utah: Utah Geological Survey Open-File Report 689, 38 p., 2 plate, scale 1:62,500, https://doi.org/10.34191/OFR-689.

Sprinkel, D.A., Castaño, J.R., and Roth, G.W., 1997, Emerging plays in central Utah based on a regional geochemical, structural, and stratigraphic evaluation [abs.]: American Association of Petroleum Geologists Bulletin Annual Convention, Official Program with Abstracts, v. 6, p. A110.

Sprinkel, D.A., and Chidsey, T.C., Jr., 1993, Jurassic Twin Creek Limestone, *in* Hjellming, C.A., editor, Atlas of major Rocky Mountain gas reservoirs: New Mexico Bureau of Mines and Mineral Resources, p. 76.

Surdam, R.C., and Wray, J.L., 1976, Lacustrine stromatolites, Eocene Green River Formation, Wyoming, *in* Walter, M.R., editor, Stromatolites: Amsterdam, Elsevier, p. 535–541.

Swierenga, M., Sarg, J.F., and Tänavsuu-Milkeviciene, K., 2015, Depositional history and lateral variability of a microbial carbonate in the middle Green River Formation, Three Mile Canyon, eastern Uinta Basin, Utah, *in* Vanden Berg, M.D., Ressetar, R., and Birgenheier, L.P., editors, Geology of Utah's Uinta Basin and Uinta Mountains: Utah Geological Association Publication 44, p. 69–89.

Tänavsuu-Milkeviciene, K., and Sarg, F.J., 2012, Evolution of an organic-rich lake basin—stratigraphy, climate and tectonics: Piceance Creek Basin, Eocene Green River Formation: Sedimentology, v. 59, no. 6, p. 1735–1768.

Töro, B., and Pratt, B.R., 2015, Characteristics and implications of sedimentary deformation features in the Green River Formation (Eocene) in Utah and Colorado, *in* Vanden Berg, M.D., Ressetar, R., and Birgenheier, L.P., 2015, editors, Geology of Utah's Uinta Basin and Uinta Mountains: Utah Geological Association Publication 44, p. 371–422.

U.S. Geological Survey Oil Shale Assessment Team, 2010, Oil shale resources of the Uinta Basin, Utah and Colorado: U.S. Geological Survey Digital Data Series DDS–69–BB, 7 chapters, CD.

U.S. Geological Survey, 2020, Great Salt Lake—lake elevations and elevation changes: https://www.usgs.gov/centers/ut-water/science/great-salt-lake-elevations?qt-science_center_objects=0#qt-science_center_objects.

Utah Division of Oil, Gas and Mining, 1994, PG&E West Willow Creek field hearing: Cause No. 233-01, Docket No. 94-016, Exhibits 9 and 11.

Utah Division of Oil, Gas and Mining, 1997a, Structure map of top Watton Canyon, Pineview field: Cause No. 167-8, Exhibit No. P-5.

Utah Division of Oil, Gas and Mining, 1997b, Structural cross section, Pineview field: Cause No. 167-8, Exhibit No. P-6.

Utah Division of Oil, Gas and Mining, 2021a, Oil and gas summary production report by field, February 2021, Online, https://oilgas.ogm.utah.gov/oilgasweb/publications/monthly-rpts-by-fld.xhtml, accessed May 2021.

Utah Division of Oil, Gas and Mining, 2021b, Oil and gas summary production report by well, February 2021: Online, https://oilgas.ogm.utah.gov/oilgasweb/publications/monthly-rpts-by-well.xhtml, accessed May 2021.

Vanden Berg, M.D., 2011, Exploring Utah's other great lake: Utah Geological Survey, Survey Notes, v. 43, no. 2, p. 1–2, https://doi.org/10.34191/SNT-43-2.

Vanden Berg, M.D., 2019, Domes, rings, ridges, and polygons—characteristics of microbialites from Utah's Great Salt Lake: Sedimentary Record, v. 17, no. 1, p. 4–10.

Vanden Berg, M.D., and Birgenheier, L.P., 2016, Evaluation of the upper Green River Formation's oil shale resource in the Uinta Basin, Utah, *in* Spinti, J., and Smith, P., editors, Utah oil shale: Science, Technology, and Policy Perspectives: CRC Press/Taylor & Francis Group, p. 59–85.

Vanden Berg, M.D., Lehle, D.R., Carney, S.M., and Morgan, C.D., 2013, Geological characterization of the Birds Nest aquifer, Uinta Basin, Utah—assessment of the aquifer's potential as a saline water disposal zone: Utah Geological Survey Special Study 147, 53 p., https://doi.org/10.34191/SS-147.

Vennin, E., Bouton, A., Bourillot, R., Pace, A., Roche, A., Brayard, A., Thomazo, C., Virgone, A., Gaucher, E.C., Desaubliaux, G., and Visscher, P.T., 2019, The lacustrine microbial carbonate factory of the successive Lake Bonneville and Great Salt Lake, Utah, USA: Sedimentology, v. 66, no. 1, p. 65–204.

Wasson, M.S., Saller, A., Andres, M., Self, D., and Lomando, A., 2012, Lacustrine microbial carbonate facies in core from the lower Cretaceous Toca Formation, Block 0, offshore Angola [abs.]: American Association of Petroleum Geologists Hedberg Conference, Microbial Carbonate Reservoir Characterization, June 4–8, 2012, Houston, Texas, p. 4.

Wilson, J.L., 1975, Carbonate facies in geologic history: New York, Springer-Verlag, 471 p.

Wood, R.E., and Chidsey, T.C., Jr., 2015, Oil and gas fields map of Utah: Utah Geological Survey Circular 119, scale 1:700,000, https://doi.org/10.34191/C-119.

Wright, V.P., and Barnett, A.J., 2015, An abiotic model for the development of textures in some South Atlantic Early Cretaceous lacustrine carbonates, *in* Bosence, D.W.J., Gibbon, K.A., Le Heron, D.P., Morgan, W.A., Pritchard, T., and Vining, B.A., editors, Microbial carbonates in space and time—implications for global exploration and production: The Geological Society, London, Special Publication 418, p. 209–219, http://dx.doi.org/10.1144/SP418.6.

Wyoming Oil and Gas Conservation Commission, 2021, Yellow Creek field: Online, http://pipeline.wyo.gov/productioncountyyear.cfm, accessed May 2021.

Yingst, R.A., Bartley, J.K., Chidsey, T.C., Jr., Cohen, B.A., Hynek, B.M., Kah, L.C., Minitti, M.E., Vanden Berg, M.D., Williams, R.M.E., Adams, M., Black, S., El-Maary, M.R., Gemperline, J., Kronyak, R., and Lotto, M., 2020, Is a linear or a walkabout protocol more efficient when using a rover to choose biologically relevant samples in a small region of interest?: Astrobiology, v. 20, no. 3, 42 p.

APPENDIX:

CORE PHOTOGRAPHS

Link to supplemental data download:
https://ugspub.nr.utah.gov/publications/special_studies/ss-168/ss-168-a.pdf

UTAH GEOLOGICAL SURVEY
a division of
Utah Department of Natural Resources

Plate 1
Utah Geological Survey Special Study 168
Microbial Carbonate Reservoirs and Analogs from Utah

CORE DESCRIPTION – GREEN RIVER FORMATION, SKYLINE 16 RESEARCH CORE

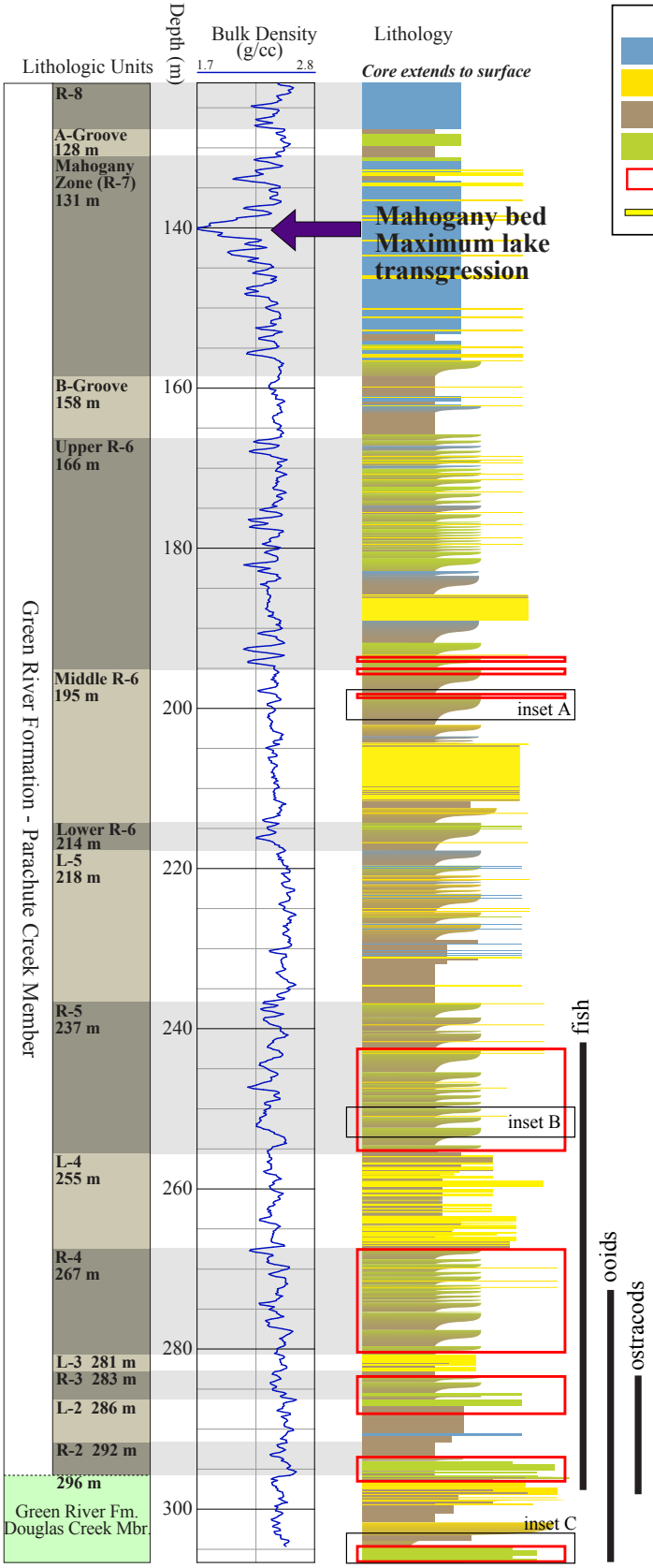

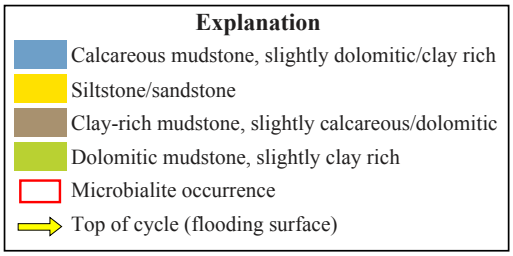

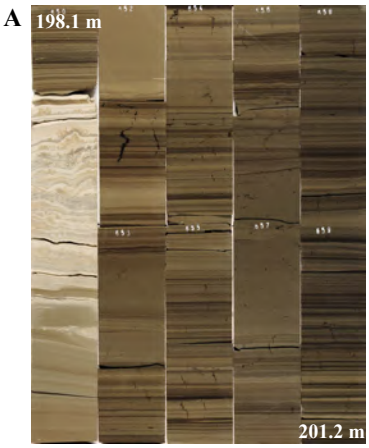

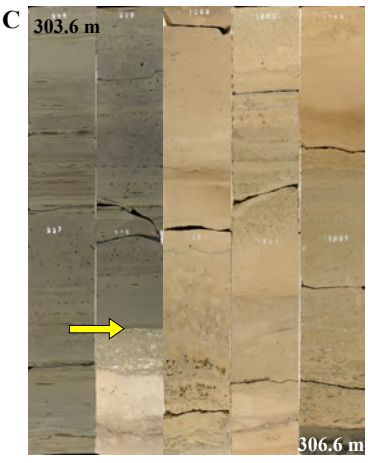

UTAH GEOLOGICAL SURVEY
a division of
Utah Department of Natural Resources

Plate 2
Utah Geological Survey Special Study 168
Microbial Carbonate Reservoirs and Analogs from Utah

CONDO MEASURED SECTION, GREEN RIVER FORMATION

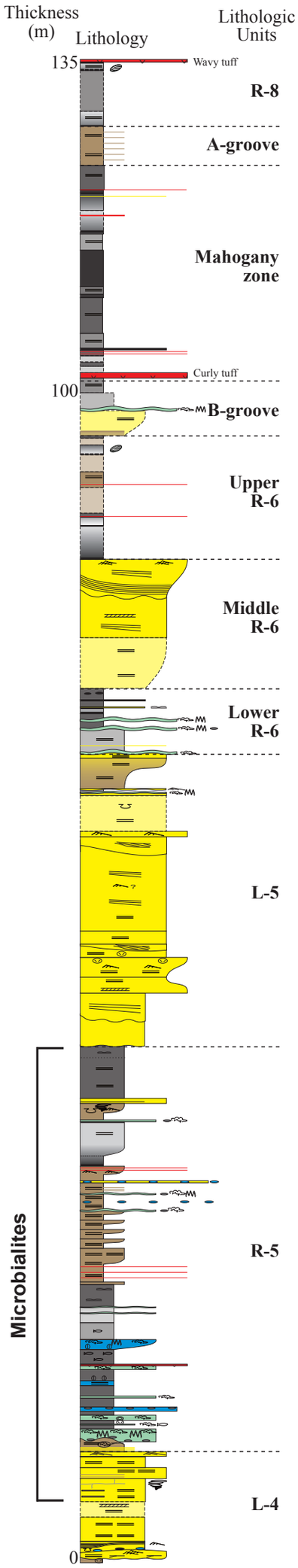

Explanation

Lithology:

- Claystone/siltstone
- Sandstone
- Carbonate
- Microbiolite
- Tuff
- Organic rich
- Covered section

Symbols:

- Horizontal, planar lamination
- Low-angle planar lamination
- Trough cross-bedding
- Low angle planar dipping surfaces
- Accretionary surfaces
- Siltstone and/or heterolithic rip-up clast
- Carbonate rip-up clast
- Organic-rich clast
- Current ripple cross-lamination
- Combined flow ripple cross-lamination
- Climbing ripple cross-lamination
- Wavy bedding
- Convolute bedding
- Load casting
- Concretion
- Shell material
- Gar fish scales
- Botfly larvae
- Ooids
- Ostracods
- Thrombolites
- Stromatolites
- De-watering structures

Modified from Rosenberg (2013) and Rosenberg and others (2015)

UTAH GEOLOGICAL SURVEY
a division of
Utah Department of Natural Resources

Plate 3
Utah Geological Survey Special Study 168
Microbial Carbonate Reservoirs and Analogs from Utah

FLASH FLOOD MEASURED SECTION, GREEN RIVER FORMATION

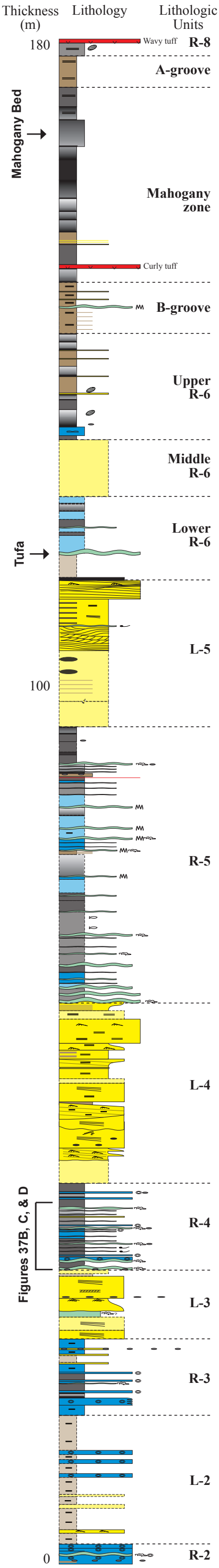

Explanation

Lithology:

- Claystone/siltstone
- Sandstone
- Carbonate
- Microbiolite
- Tuff
- Organic rich
- Covered section

Symbols:

- Horizontal, planar lamination
- Low-angle planar lamination
- Trough cross-bedding
- Low angle planar dipping surfaces
- Accretionary surfaces
- Siltstone and/or heterolithic rip-up clast
- Carbonate rip-up clast
- Organic-rich clast
- Current ripple cross-lamination
- Combined flow ripple cross-lamination
- Climbing ripple cross-lamination
- Wavy bedding
- Convolute bedding
- Load casting
- Concretion
- Shell material
- Gar fish scales
- Botfly larvae
- Ooids
- Ostracods
- Thrombolites
- Stromatolites
- De-watering structures

Modified from Rosenberg (2013) and Rosenberg and others (2015)

UTAH GEOLOGICAL SURVEY
a division of
Utah Department of Natural Resources

Plate 4
Utah Geological Survey Special Study 168
Microbial Carbonate Reservoirs and Analogs from Utah

CORE DESCRIPTION A – E_2 CARBONATE BED, GREEN RIVER FORMATION, FEDERAL NO. 15-24B WELL, WEST WILLOW CREEK FIELD

Compensated Neutron-Formation Density and Gamma-Ray Log, Federal No. 15-24B Well

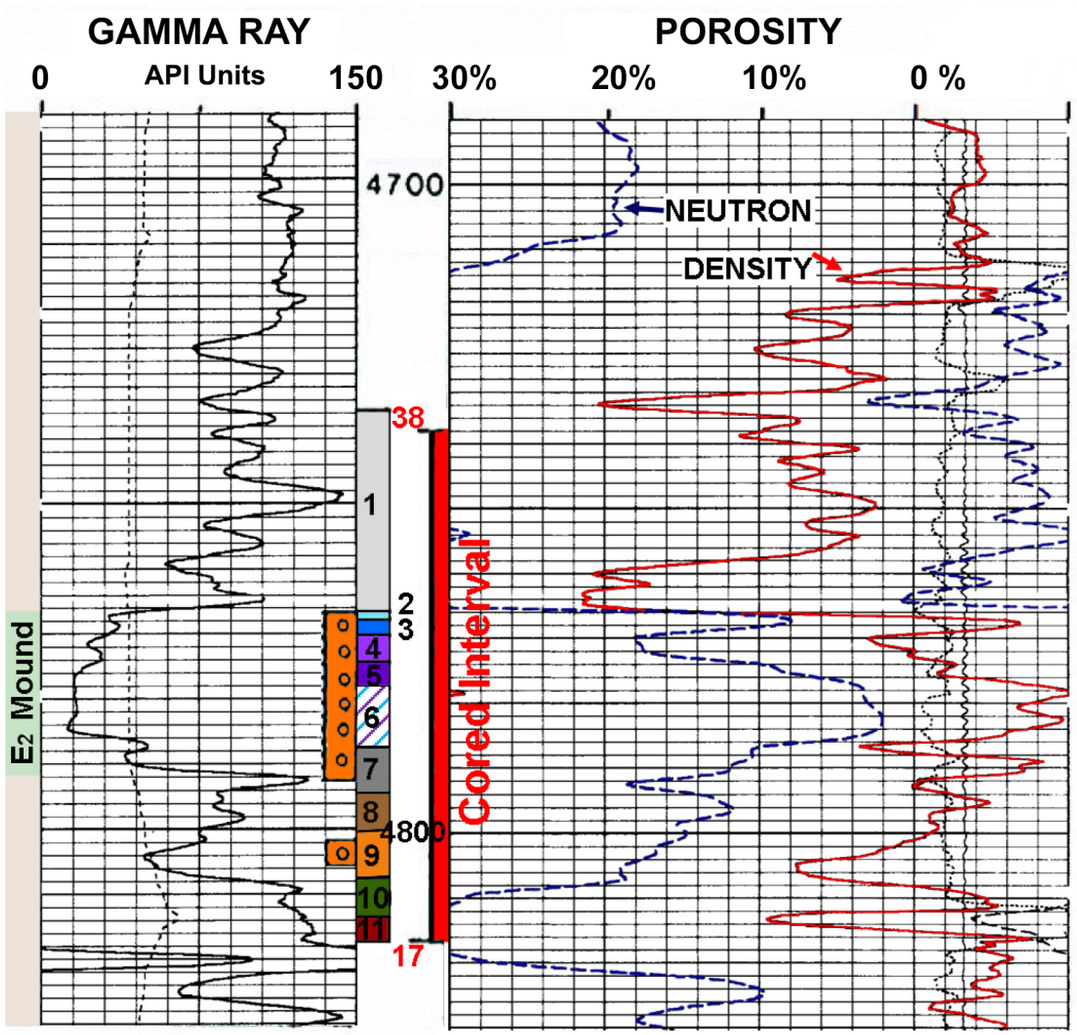

The numbered/color-coded stratigraphic units are described in the adjacent table; the perforated interval is indicated by circles on the outside left of the center column.

Major Characteristics of the E_2 Carbonate Bed, Federal No. 15-24B Core

UNIT	DEPTH (ft)	THICKNESS (ft)	DESCRIPTION
1	4738–69	31	SHALE, black, fissile to blocky, very fine laminations with fish scales and pyritized ostracods and very thin pyritized laminations; very thin, (algal?) coal laminations and lacey coal patterns on lamination surfaces; chert nodules up to 2 inches long and up to 1-1/4 inches thick on bedding; irregular chert nodule piercing overlying laminations; few thin, oil-saturated tuff laminations up to 2 inches thick.
2	4769–69.9	0.9	LIMESTONE, ostracodal in laminations that thicken upward, base is oil-stained tuff with ostracods.
3	4769.9–72.5	2.6	LIMESTONE, light gray, upper part contains gastropods up to 3/4 inch in diameter with calcite crystal-lined vugs in chambers; lower part, oncolites up to 3/4 inch in diameter; tubes of light gray limestone on bedding; 50° dip on bedding; vertical fracture partially filled with white calcite; horizontal stylolite at base.
4	4772.5–77.25	4.75	DOLOMITE, brown, fine crystalline, oncolites and irregular vertical tubes, oil stained, stromatolites in lower part.
5	4777.25–78.4	1.15	DOLOMITE, gray, very fine crystalline, oncolites up to 2 inches in diameter, vertical and horizontal fractures, 1/32 inch, white calcite filling, horizontal stylolites.
6	4778.4–90.7	12.3	DOLOMITE, brown, fine crystalline; oncolites with dolomite crystal-lined vugs In centers, grades down into dolomite, gray, with abundant gastropods with white calcite filling upper parts of chambers, middle part, vertical fracture, 1/4 inch, white calcite filled, with slickensides; lower middle part, oncolites 1 inch in diameter; lower 3.6 feet, turritellid gastropods with white calcite filling chambers; flatened thin-shelled pelecypod, oncolites; vertical fracture, 1/32 inch, with white calcite filling; color changes from brown, oil stained, at top to gray, non-oil stained at base.
7	4790.7–90.9	0.1 0.1	COAL, black, vitreous, hard, possibly alginite. SILTSTONE, light gray, no roots.
8	4790.9–96.5	5.6	SHALE, black, interbedded with black limestone; abundant rotund and turretellid gastropods to 2-1 /2 inches, pelecypods, white calcite filling gastropod chambers, flat shale pebbles at base.
9	4796.5–03	6.5	SILTSTONE, gray, unlaminated, calcareous, bioturba ted(?); black oblique, organic marks, 4 inches by 1/4 inch, smoo th on one edge, serated on the other edge; ghosts of oncolites.
10	4803–16.5	13.5	SHALE, gray-green, dip of bedding is horizontal at top, 10° in middle and 20° at the base. Possible effect of fault(?).
11	4816.5–17	0.5	SHALE, mottled maroon and gray, wavey laminations.

Modified from Osmond (2000)

UTAH GEOLOGICAL SURVEY
a division of
Utah Department of Natural Resources

CORE DESCRIPTION B – E_2 CARBONATE BED, GREEN RIVER FORMATION, FEDERAL NO. 15-24B WELL, WEST WILLOW CREEK FIELD

Plate 5
Utah Geological Survey Special Study 168
Microbial Carbonate Reservoirs and Analogs from Utah

Geophysical Logs

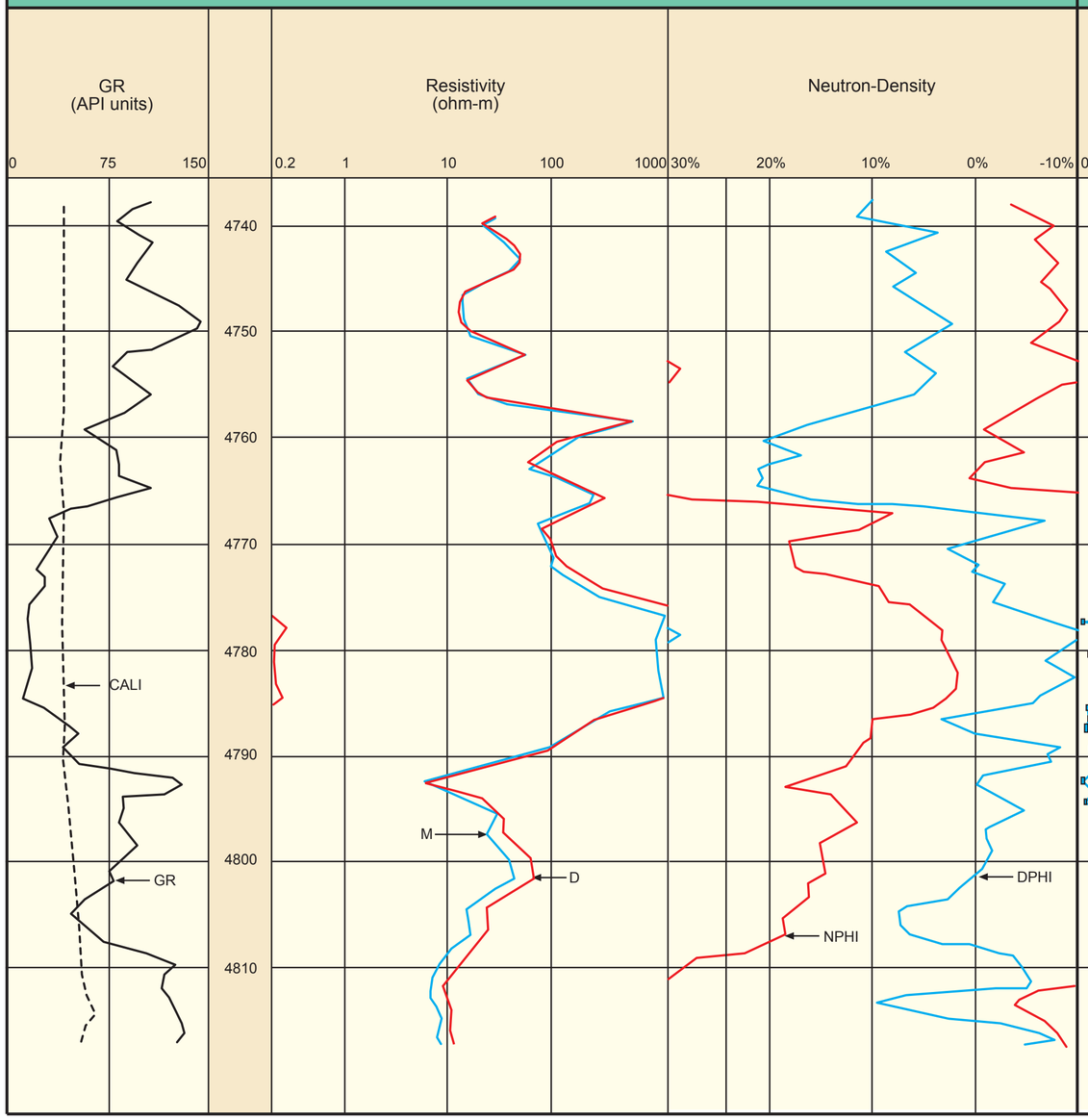

Core-Plug Analysis

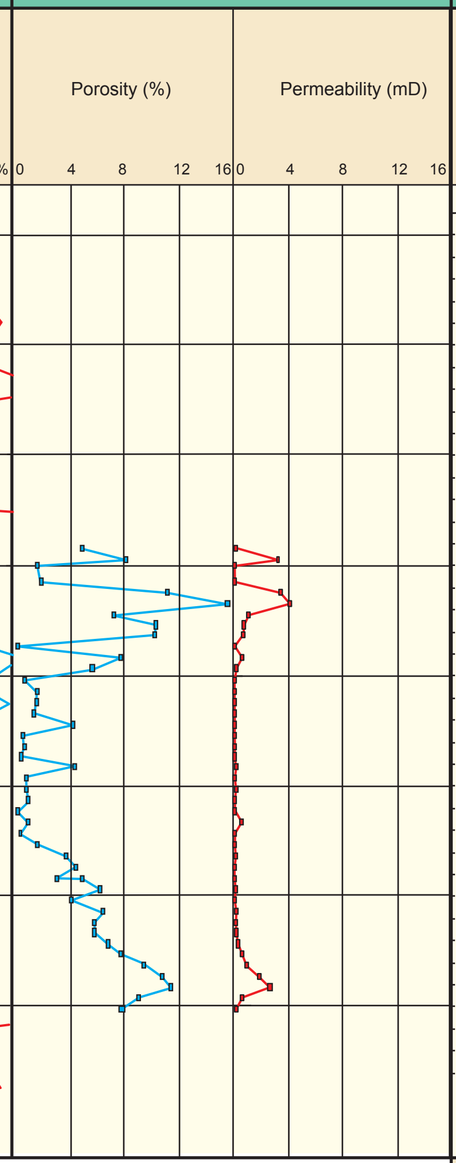

Conventional Core

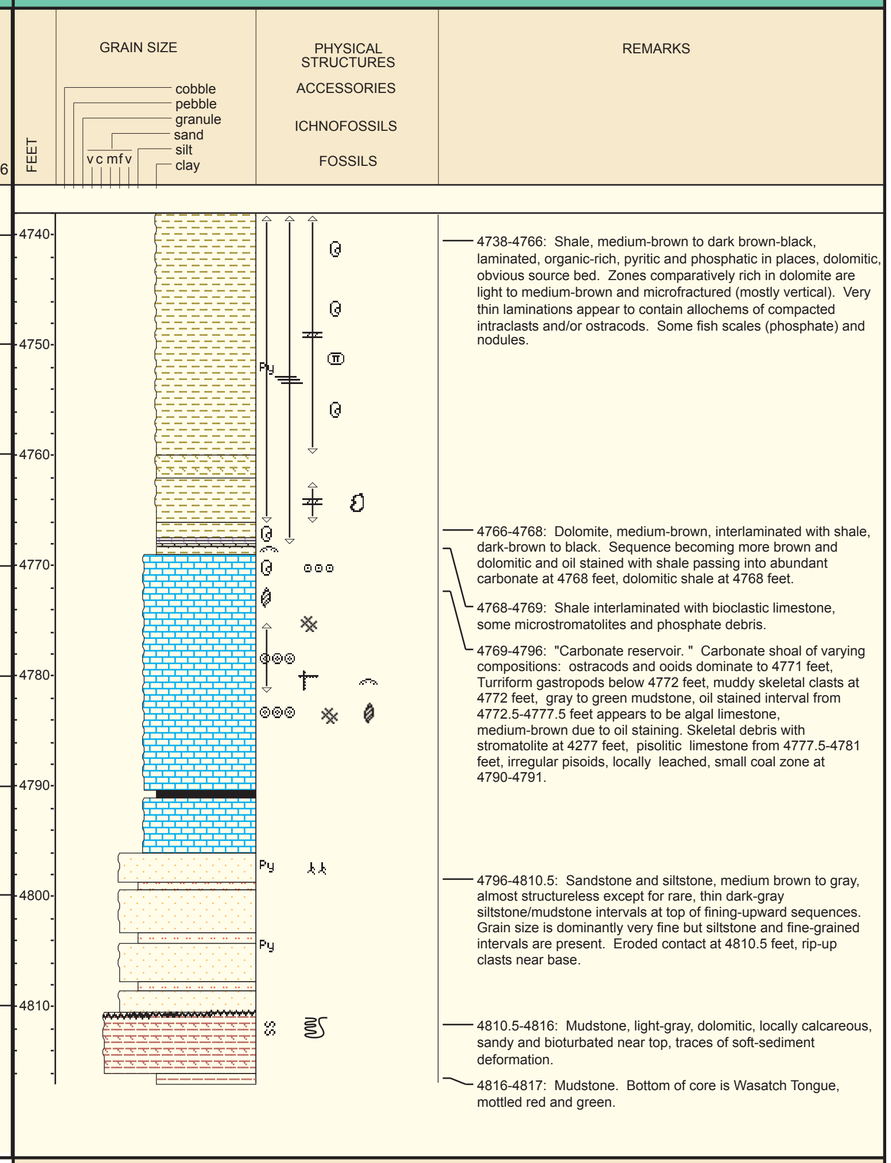

West Willow Creek Field
Federal 15-24B
SW1/4SE1/4 section 24,
T. 9 S., R. 19 E., SLBL&M

API: 43-047–32420
Depth: 4738–4817 feet
Interval: Carbonate marker unit
(Castle Peak interval)

Cumulative Production: 15,639 BO, 5025 MCFG, and 8674 BW (abandoned in 2007). Utah Division of Oil, Gas and Mining well records.

Abbreviations

GR – Gamma ray
CALI – Caliper
M – Resistivity medium
D – Resistivity deep
NPHI – Neutron porosity
DPHI – Density porosity
mD – Millidarcies
SLBL&M – Salt Lake Base Line and Meridian
API – American Petroleum Institute well number

Explanation

Lithology
Sandstone, Siltstone, Shale, Mudstone, Coal, Dolomitic mudstone, Dolomitic shale, Limestone, Dolomite

Contact
- Scour

Physical Structures
- Planar Lamination
- Fractures
- Soft-sediment deformation

Lithologic Accessories
- Dolomitic
- Pyrite
- Oolites
- Pisolites
- Concretion/nodule

Ichnofossils
- Rootlets
- Bioturbation

Fossils
- Algal stromatolite
- Gastropods
- Ostracods
- Fish scales (phosphate)
- Algal organic framework

After Bereskin and others (2004)

GEOGHYSICAL WELL LOG OF THE TWIN CREEK LIMESTONE, UPRR NO. 3-3 WELL, PINEVIEW FIELD

UPRR No. 3-3 Well
API No. 43-043-30019
NW1/4SE1/4 section 3, T. 2 N., R. 7 E., SLBL&M
Summit County, Utah
KB: 6689 ft

Cumulative Production (Twin Creek & Nugget):
315,581 BO, 0.65 BCFG

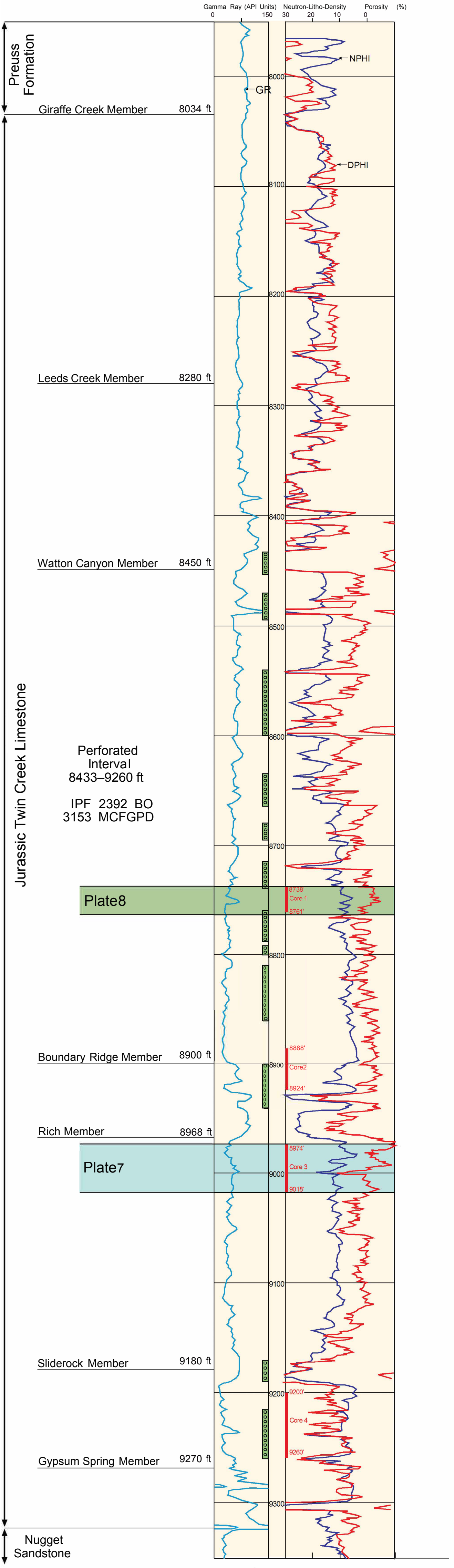

TD: 10,300 ft
Completed: 07/21/76
P&A: 06/20/92
Note: cores described on plates 7 and 8.

UTAH GEOLOGICAL SURVEY
a division of
Utah Department of Natural Resources

CORE DESCRIPTION – RICH MEMBER, TWIN CREEK LIMESTONE, UPRR NO. 3-3 WELL, PINEVIEW FIELD

Plate 7
Utah Geological Survey Special Study 168
Microbial Carbonate Reservoirs and Analogs from Utah

Geophysical Logs

Gamma Ray API Units: 0 – 75 – 150

Neutron – Litho-Density Porosity: 30% – 20% – 10% – 0%

Curves: NPHI, DPHI

Porosity (%): 0 – 2 – 4 – 6

Permeability (mD): 0.010 – 0.100 – 1.000 – 10 – 100

Feet: 8975, 8980, 8985, 8990, 8995, 9000, 9005, 9010, 9015

Conventional Core

Grain: cobble, pebble, granule, very coarse, coarse, medium, fine, very fine, silt, clay

Fabric: boundstone, grainstone, packstone, wackestone, mudstone

Pore Types: FR

Physical Structures

Texture (%): Dolomitic and Anhydritic Shale; Shale; m p s

Framework Constituents: Fos; ooo

Fractures

Cement: Cal, Anh

Facies	Remarks
Terrestrial to marine sabka.	
Low-energy, peritidal (microbial mats/tidal flat).	Exposure surface.
Terrestrial to marine sabka.	Microbial mats.
Thrombolic buildups in a salinity restricted inner shelf.	Microbialite with “clotted” fabric (thrombolitic).
Supratidal to sabka.	Laminated microbial mats (stromatolites) with variable amounts of nodular anhydrite.
Silt and lime mud tidal flat with intermittant exposure.	Laminated and rippled siltstones alternating with microlaminated (microbial) lime mud. Mud cracks filled with quartz silt. Occasional flame structures, flaser bedding (?) and soft sediment deformation.

UPRR 3-3

NW1/4SE1/4 section 3,
T. 2 N., R. 7 E., SLBL&M
KB: 6689 ft

TD: 10,294 f
Completed: 5-24-76

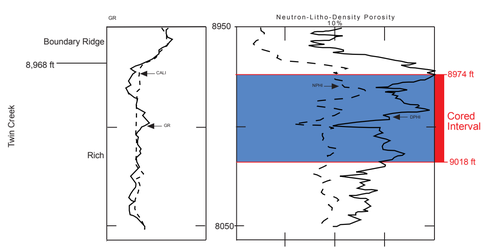

Abbreviations

KB – Elevation of kelly bushing
GR – Gamma ray
CALI – Caliper
NPHI – Neutron porosity
DPHI – Density porosity
SLBL&M – Salt Lake Base Line and Meridian
TD – Total depth

Explanation

Lithologic Composition
- Limestone
- Dolomite
- Silty limestone
- Shale

Texture
- s – Skeletal grains
- a – Phylloid-algal plates
- m – Micrite
- p – Peloid
- o – Ooid
- Siltstone

Contacts
- Sharp

Physical Structures
- Anhydritic
- Fractures
- Laminae
- Cross-bedding
- Mud cracks
- Rip-up clasts
- Current ripples

Framework Constituents
- ooo – Oolitic
- ⊖⊖⊖ – Coated grains
- Q – Ostracods
- ◆◆◆ – Peloids
- Fos – Unidentified fossils

Pore Types
- Mo – Moldic
- BC – Intercrystal
- BP – Interparticle
- WP – Intraparticle
- Vug – Vug
- SH – Shelter
- FR – Fracture

Cement
- Dol – Dolomite
- Cal – Calcite
- Anh – Anhydrite
- Hal – Halite

Abundance
- Pervasive
- Abundant

UTAH GEOLOGICAL SURVEY
a division of
Utah Department of Natural Resources

CORE DESCRIPTION – WATTON CANYON MEMBER, TWIN CREEK LIMESTONE, UPRR NO. 3-3 WELL, PINEVIEW FIELD

Plate 8
Utah Geological Survey Special Study 168
Microbial Carbonate Reservoirs and Analogs from Utah

Geophysical Logs

Conventional Core

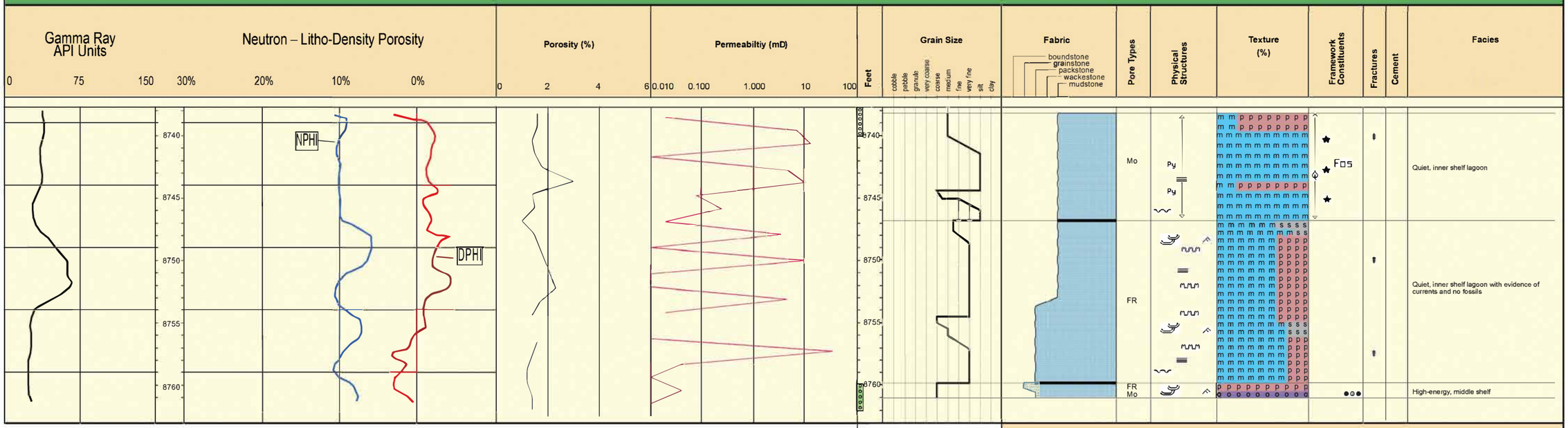

UPRR 3-3

NW1/4SE1/4 section 3,
T. 2 N., R. 7 E., SLBL&M
KB: 6689 ft

TD: 10,294 ft
Completed : 5-24-76

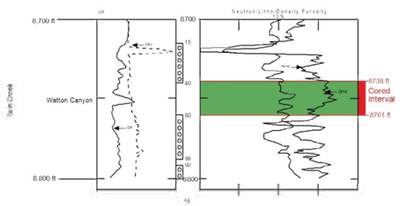

Abbreviations

KB – Elevation of kelly bushing
GR – Gamma ray
CALI – Caliper
NPHI – Neutron porosity
DPHI – Density porosity
SLBL&M – Salt Lake Base Line and Meridian
TD – Total depth

Explanation

Lithologic Composition
- Limestone

Framework Constituents
- ooo – Oolitic
- ★ – Crinoids
- Plant remains
- Fos – Unidentified fossils

Texture
- s – Skeletal grains
- a – Phylloid-algal plates
- m – Micrite
- p – Peloid
- Ooid
- Siltstone

Pore Types
- Mo – Moldic
- BC – Intercrystal
- BP – Interparticle
- WP – Intraparticle
- Vug – Vug
- SH – Shelter
- FR – Fracture

Contacts
- Sharp

Cement
- Dol – Dolomite
- Cal – Calcite
- Anh – Anhydrite
- Hal – Halite

Abundance
- Pervasive
- Abundant

Physical Structures
- Stylolites
- Current ripples
- Fractures
- Laminae
- Mud cracks
- Cross-bedding
- Py – Pyrite

PEOA MEASURED SECTION, JURASSIC TWIN CREEK LIMESTONE

section 14, T. 1 S., R. 5 E., Summit County, Utah

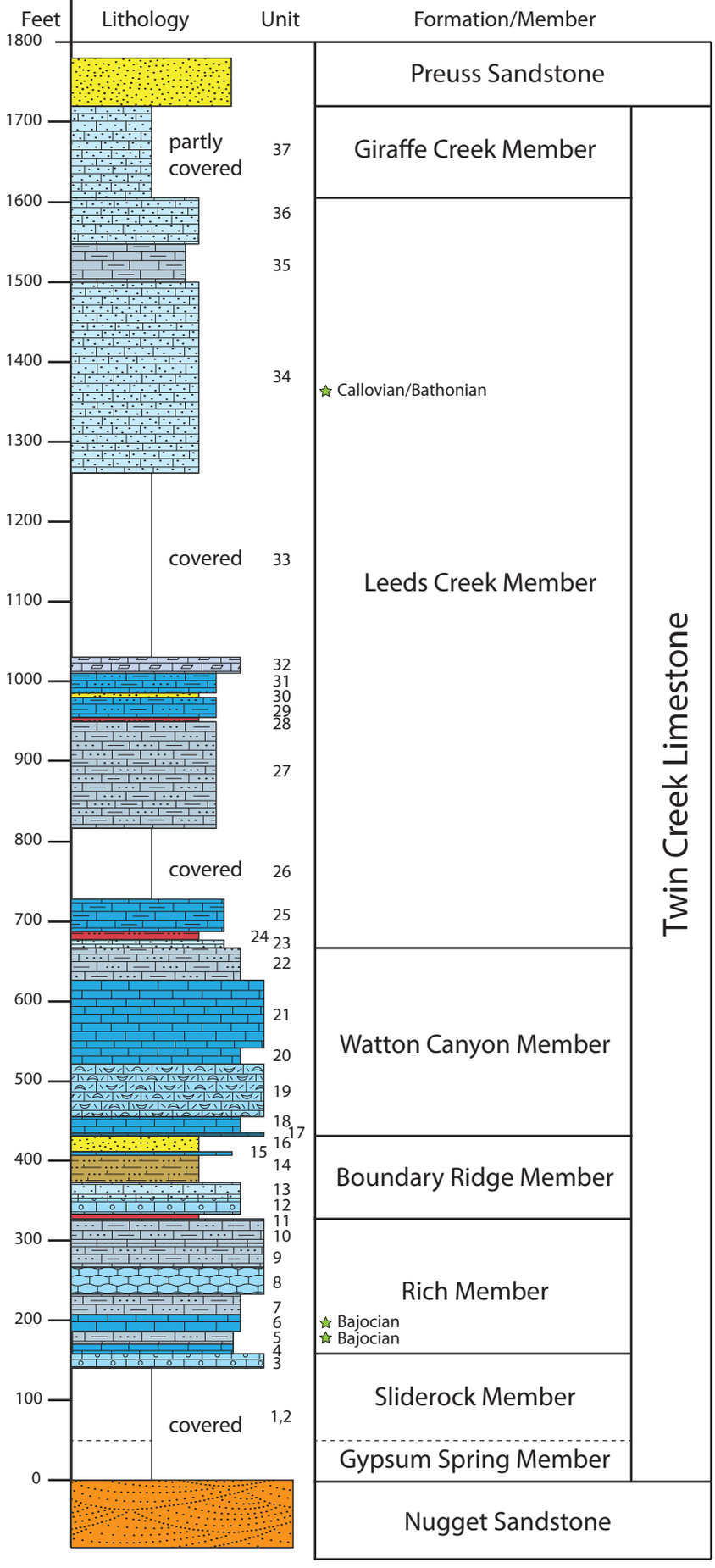

Explanation

- Palynology
- Limestone
- Argillaceous limestone
- Sandy limestone
- Silty limestone
- Oolitic limestone
- Fossiliferous limestone
- Vuggy limestone
- Brecciated limestone
- Siltstone
- Sandstone
- Eolian sandstone

Unpublished data from by D.A. Sprinkel and H.H. Doelling, Utah Geological Survey

UTAH GEOLOGICAL SURVEY
a division of
Utah Department of Natural Resources

CORE DESCRIPTION – DESERT CREEK ZONE, PARADOX FORMATION, ANETH UNIT NO. F-317 WELL, GREATER ANETH FIELD

Plate 10
Utah Geological Survey Special Study 168
Microbial Carbonate Reservoirs and Analogs from Utah

Geophysical Logs

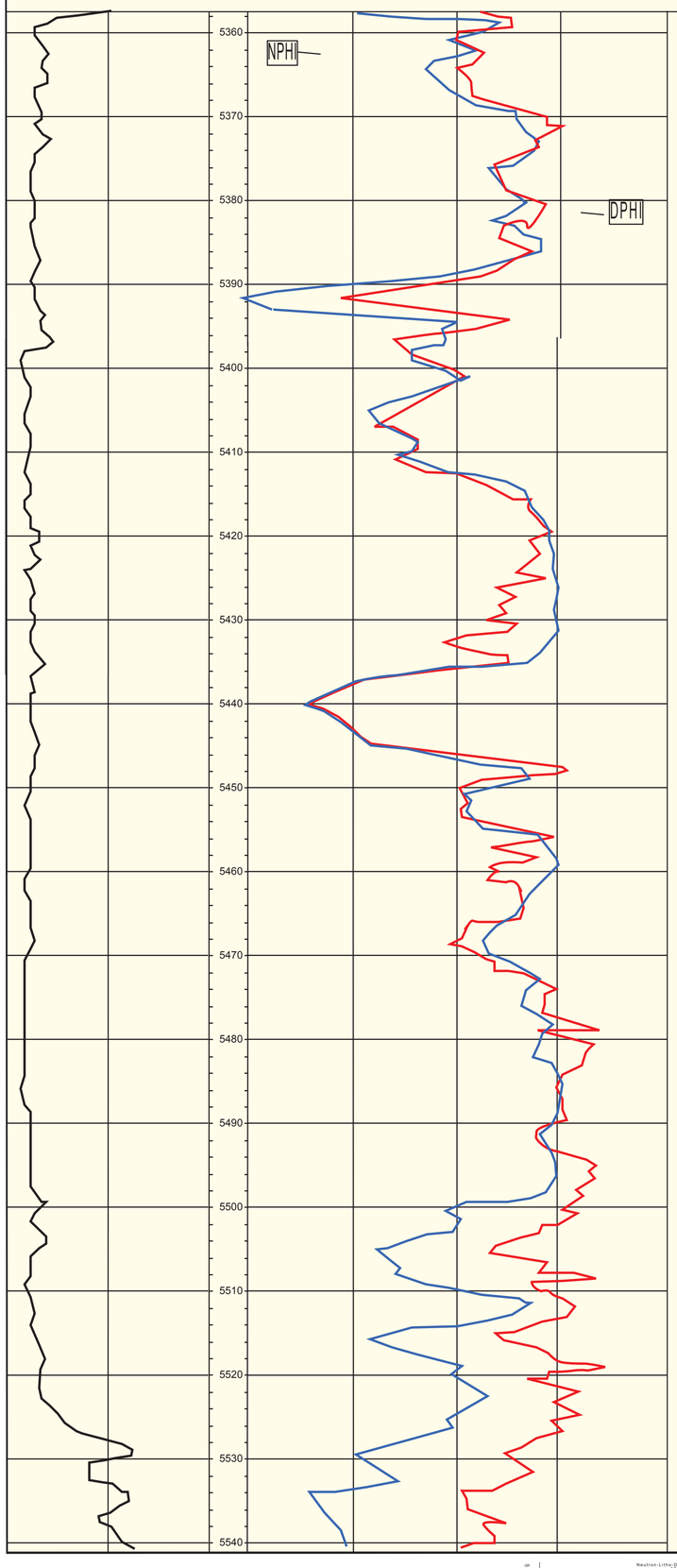

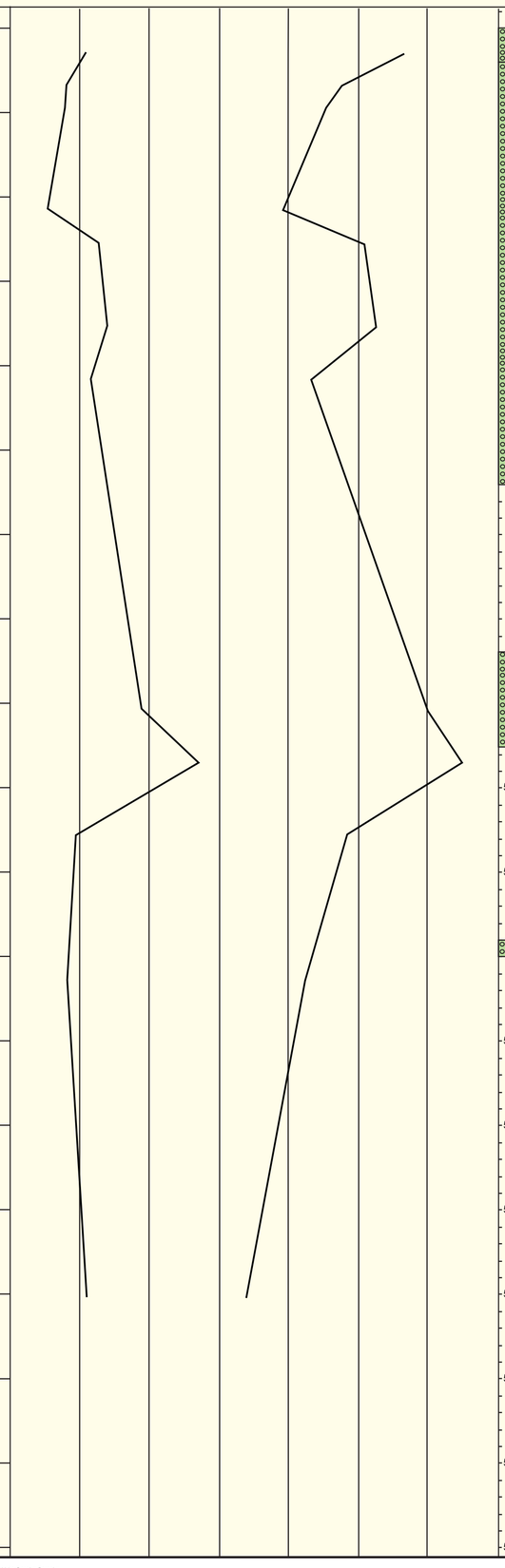

Conventional Core

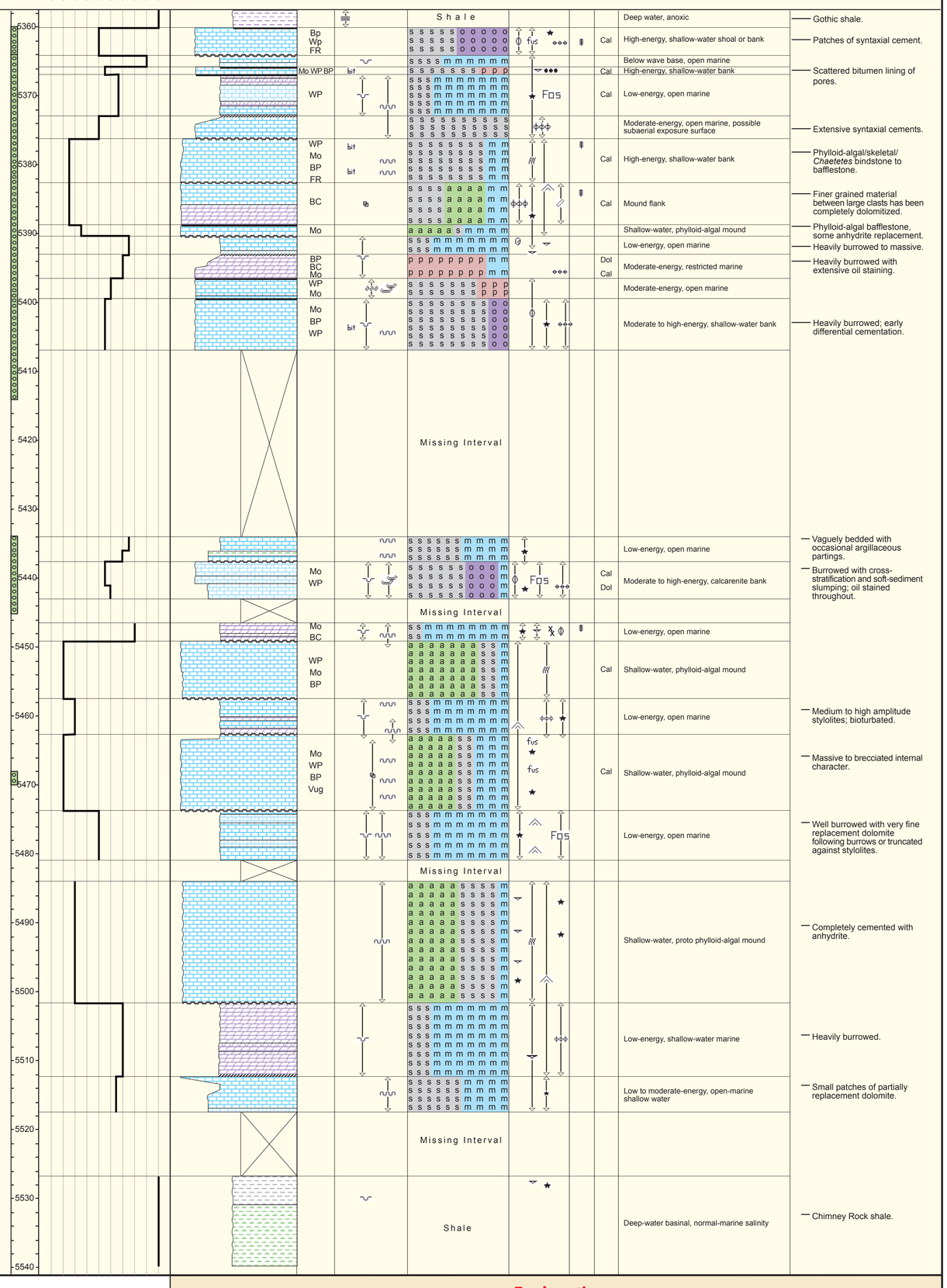

Aneth Unit No. F-317

NE1/4SW1/4 section 17,
T. 40 S., R. 24 E., SLBL&M
KB: 4564 ft

TD: 5598 ft
IPF: 394 BOPD, 759 MCFPD, 22 BWPD
Completed: 2-23-74

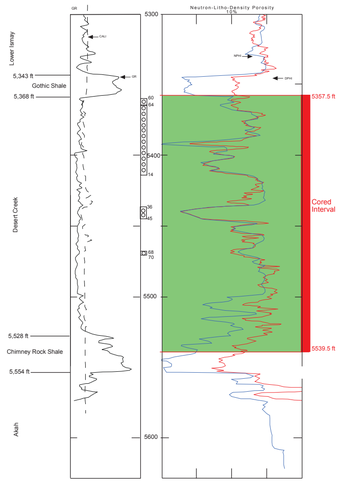

Abbreviations

KB – Elevation of kelly bushing
GR – Gamma ray
CALI – Caliper
NPHI – Neutron porosity
DPHI – Density porosity
SLBL&M – Salt Lake Base Line and Meridian
TD – Total depth

Explanation

Lithologic Composition
- Limestone
- Dolomite
- Calcareous shale
- Shale
- Dolomitic limestone
- Siltstone
- Shaley limestone
- Calcareous dolostone

Texture
- s – Skeletal grains
- a – Phylloid-algal plates
- m – Micrite
- p – Peloid
- o – Ooid
- Siltstone

Framework Constituents
- Brachiopods
- Ostracods
- Crinoids
- Coated grains
- Chaetetes
- Sponge spicules
- Intraclasts
- Foraminifera (benthonic)
- Fusulinids
- Phylloid-algal plates
- Fos – Unidentified fossils
- Peloids

Pore Types
- Mo – Moldic
- BC – Intercrystal
- BP – Interparticle
- WP – Intraparticle
- Vug – Vug
- SH – Shelter
- FR – Fracture

Contacts
- Sharp
- Gradational
- Stylolite

Cement
- Dol – Dolomite
- Cal – Calcite
- Anh – Anhydrite
- Hal – Halite

Abundance
- Pervasive
- Abundant

Physical Structures
- Stylolites
- Burrows
- Fractures
- Laminae
- Breccia
- Cross-bedding
- Bit – Bitumen
- Clasts
- Shell fragments

UTAH GEOLOGICAL SURVEY
a division of
Utah Department of Natural Resources

CORE DESCRIPTION – DESERT CREEK ZONE, PARADOX FORMATION, ANETH UNIT NO. H-117 WELL, GREATER ANETH FIELD

Plate 11
Utah Geological Survey Special Study 168
Microbial Carbonate Reservoirs and Analogs from Utah

Geophysical Logs

Conventional Core

Gamma Ray API Units: 0 – 100 – 200
Neutron – Litho-Density Porosity: 30% – 20% – 10% – 0%
Porosity (%): 0 – 10 – 20 – 30
Permeabiltiy (mD): 0.010 – 0.100 – 1.000 – 10 – 100
Feet
Grain Size: cobble, pebble, granule, very coarse, coarse, medium, fine, very fine, silt, clay
Fabric: bafflestone, grainstone, packstone, wackestone, mudstone
Pore Types
Physical Structures
Texture (%)
Framework Constituents
Fractures
Cement
Lithofacies
Remarks

Feet	Pore Types	Texture	Cement	Lithofacies	Remarks
5380		Shale		Deep water, anoxic setting	
5390			Cal	Moderate-energy, shallow marine	Well-developed oncolitles & rhodolites.
			Cal	Lower foreshore	
5400	BP, Mo		Cal	High-energy, shallow-water shoal	
				Low- to moderate-energy, open-marine shelf	
5410	BC			Low- to moderate-energy, open marine	Upper 6 inches contains vertical cracks (microkarst) filled with coarse, overlying crinoidal grainstone fillings.
	Mo		Cal	High-energy, shallow-water shoal	
5420	BP		Dol	Moderate-energy, shallow-water bank	Upper surface marked with soil or microkarst features.
					Cryptalgal limestone.
	Mo		Cal	Moderate-energy, shallow-marine bank	Some black bitumen lining ineffective pores.
	BC, Mo			Low-energy, open-marine shelf	Entirely oil stained except uppermost 6 inches.
5430				Very low-energy, deep-marine shelf	
5440		Missing Interval			
	Mo, BP		Cal		Differential early marine cementation.
5450	BP, WP, MO		Cal	Moderate-energy, shallow-water bank	Lite oil staining.
	BC, Mo			Low-energy, below wave base, open-marine shelf	
5460				Very low-energy, open marine	Possible soil-related nodules.
	BC, BC			High-energy, open-marine bank	
5470	BC			Low-energy, deeper water open marine	
				Low-energy, deeper water, open marine	
5480	WP, BC, Mo		Cal	Moderate-energy, open-marine bank	
	Mo, WP, BP, FR		Cal	Moderate-energy, algal buildup	
5490		Missing Interval			
	BC			Low-energy, open-marine shelf	
5500	BC, Mo, Sh			Moderately high-energy, phylloid-algal buildup	
5510					
5520		Missing Core		Moderately high-energy algal/cement buildup	
5530					
5540				Low-energy, open-marine shelf	
5550				Moderate- to low-energy, algal buildup	
5560	BC			Low-energy, shallow-water buildup	
5570		Shale		Deep water anoxic setting	

Aneth Unit No. H-117

NE1/4NE1/4 section 17,
T. 40 S., R. 24 E., SLBL&M
KB: 4553 ft

TD: 5590 ft
IPF: 612 BOPD, 1487 MCFPD, 108 BWPD
Completed: 05-05-74

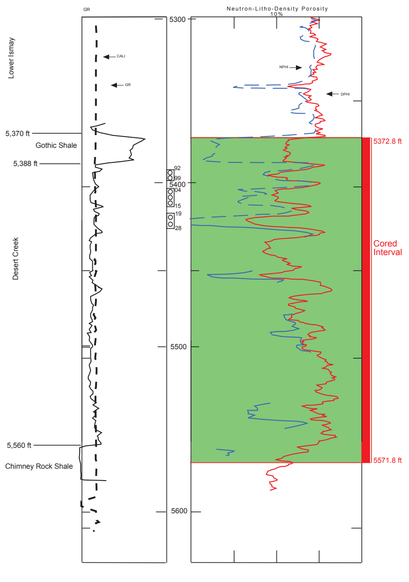

Abbreviations

KB – Elevation of kelly bushing
GR – Gamma ray
CALI – Caliper
NPHI – Neutron porosity
DPHI – Density porosity
SLBL&M – Salt Lake Base Line and Meridian
TD – Total depth

Explanation

Lithologic Composition
- Limestone
- Dolomite
- Calcareous shale
- Shale
- Dolomitic limestone
- Siltstone
- Calcareous dolomite

Texture
- s – Skeletal grains
- a – Phylloid-algal plates
- m – Micrite
- p – Peloid
- o – Ooid
- Siltstone

Contacts
- Sharp
- Gradational
- Stylolite

Physical Structures
- Stylolites
- Burrows
- Fractures
- Laminae
- Breccia
- Cross-bedding
- Rip-up clasts
- Bitumen

Framework Constituents
- Algal stromatolite
- Ostracods
- Crinoids
- Coated grains
- Peloids
- Chaetetes
- Intraclasts
- Oolitic
- Brachiopods
- Gastropods
- Foraminifera (benthonic)
- Fusulinids
- Phylloid-algal plates
- Unidentified fossils
- Coated grains
- Bryozoa

Pore Types
- Mo – Moldic
- BC – Intercrystal
- BP – Interparticle
- WP – Intraparticle
- Vug – Vug
- SH – Shelter

Cement
- Dol – Dolomite
- Cal – Calcite
- Anh – Anhydrite
- Hal – Halite

Abundance
- Pervasive
- Abundant

UTAH GEOLOGICAL SURVEY
a division of
Utah Department of Natural Resources

CORE DESCRIPTION – DESERT CREEK ZONE, PARADOX FORMATION, ANETH UNIT NO. 27-C-3 WELL, GREATER ANETH FIELD

Plate 12
Utah Geological Survey Special Study 168
Microbial Carbonate Reservoirs and Analogs from Utah

Geophysical Logs

Conventional Core

Gamma Ray API Units (0 – 12.5)
Sonic Log Interval transit time (microseconds/foot) (86 – 66 – 46)
Porosity (%) (0 – 10 – 20 – 30)
Permeabiltiy (mD) (0.010 – 0.100 – 1.000 – 10 – 100)
Feet
Grain Size (cobble, pebble, granule, very coarse, coarse, medium, fine, very fine, silt, clay)
Fabric (bafflestone, grainstone, packstone, wackestone, mudstone)
Pore Types
Physical Structures
Texture (%)
Framework Constituents
Fractures
Cement
Lithofacies
Remarks

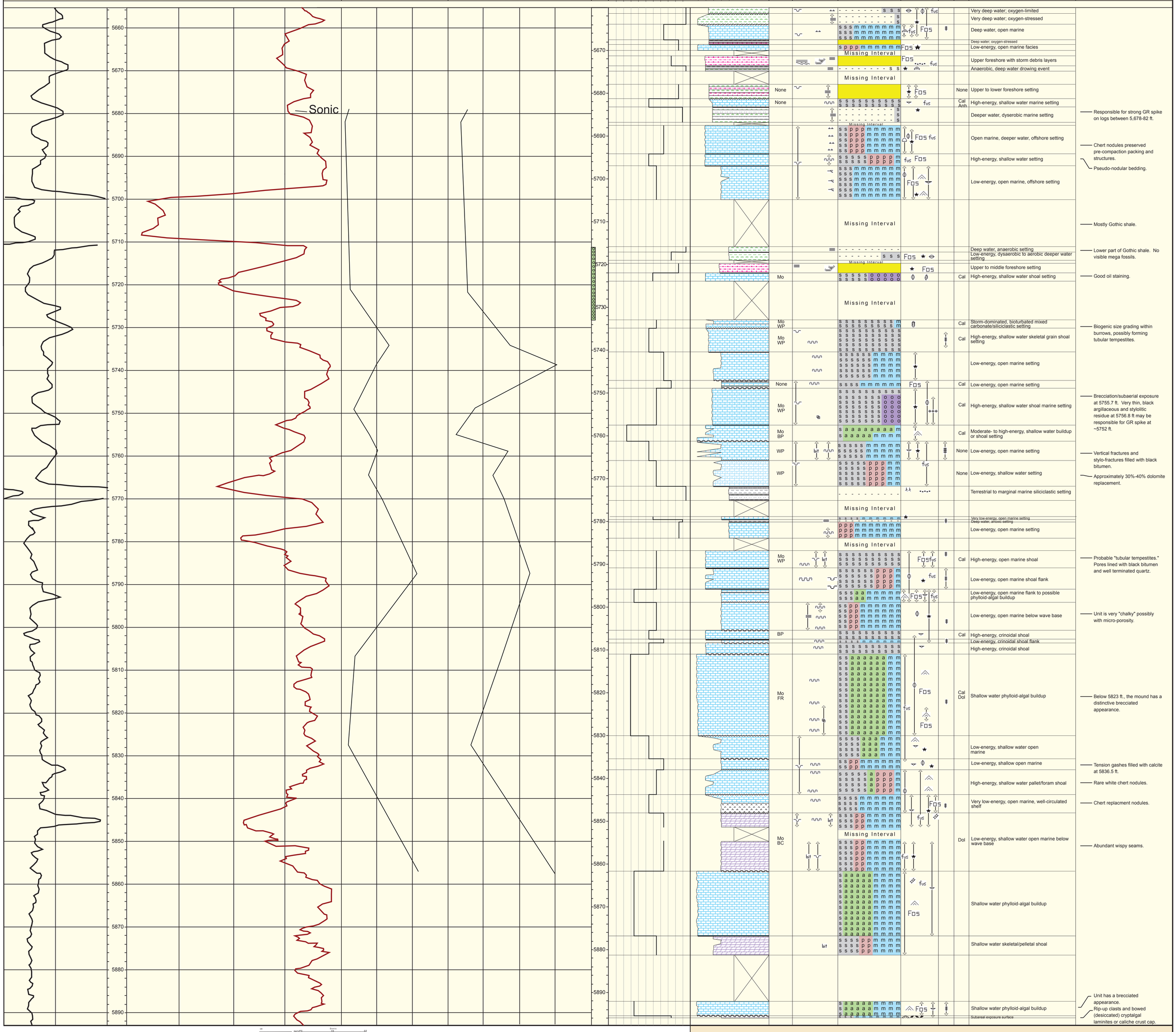

Aneth Unit No. 27-C-3

NW1/4SE1/4 section 27,
T. 40 S., R. 24 E., SLBL&M
KB: 4553 ft

TD: 5915 ft
IPF: 144 BOPD, 61 MCFPD
Completed: 09-30-60

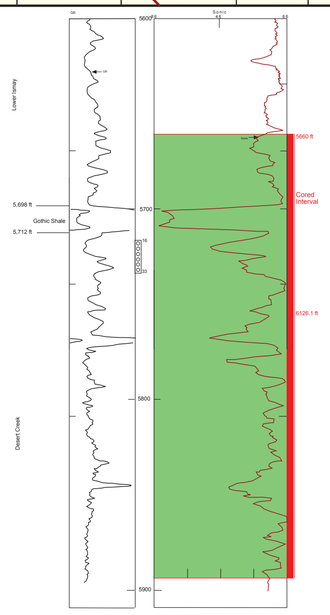

Abbreviations

KB – Elevation of kelly bushing
GR – Gamma ray
SLBL&M – Salt Lake Base Line and Meridian
TD – Total depth

Explanation

Lithologic Composition
- Siltstone
- Calcareous siltstone
- Silty calcareous shale
- Calcareous shale
- Limestone
- Dolomitic limestone
- Silty limestone
- Calcareous dolomitic limestone
- Cherty
- Dolomite
- Calcareous dolomite
- Shale
- Silty shale

Texture
- s – Skeletal grains
- a – Phylloid-algal plates
- m – Micrite
- p – Peloid
- o – Ooid
- Siltstone

Contacts
- Sharp
- Gradational
- Stylolite

Cement
- Dol – Dolomite
- Cal – Calcite
- Anh – Anhydrite
- Hal – Halite

Physical Structures
- Stylolites
- Burrows
- Fractures
- Laminae
- Breccia
- Cross-bedding
- Rip-up clasts
- Bitumen
- Graded bedding
- Cherty
- Wispy laminations

Framework Constituents
- Algal stromatolite
- Foraminifera (benthonic)
- Crinoids
- Coated grains
- Trilobites
- Phylloid-algal plates
- Sponges
- Ophiomorpha
- Rootlets
- Brachiopods
- Gastropods
- Foraminifera (benthonic)
- Fusulinids
- Algae, (undifferentiated)
- Unidentified fossils
- Coated grains
- Molluscs (undifferentiated)
- Coal fragments

Pore Types
- Mo – Moldic
- BC – Intercrystal
- BP – Interparticle
- WP – Intraparticle
- Vug – Vug
- SH – Shelter

Abundance
- Pervasive
- Abundant

UTAH GEOLOGICAL SURVEY
a division of
Utah Department of Natural Resources

CORE DESCRIPTION – LEADVILLE LIMESTONE, LISBON NO. B-610 WELL, LISBON FIELD

Plate 13
Utah Geological Survey Special Study 168
Microbial Carbonate Reservoirs and Analogs from Utah

Remarks

7590-7601: Medium to dark grayish brown to medium to dark brown dolomite with slightly limey intervals in two places. Generally mudstone and barren, in places massive with several brittle brecciated intervals at top, 7591.5, 7592.5-7595.5 and 7599.5 feet. No porosity associated with fractures, all fractures filled with white calcite, most porosity is micro intercrystalline.

7601-7603.3: Light to medium gray dolomite, fossiliferious packstone to wackestone with visible open moldic porosity and swarms of open vertical fractures. Muddier at base with faint laminae and possible early fractures.

7603.3-7610: Medium to dark gray to brownish gray dolomite, interbedded cryptalgal laminated mudstone and skeletal packstone/grainstone. Generally medium bedded with modest skeletal moldic porosity in calcarenites and synsedy's breccia in laminated mudstone. Note: 7606.5-7607.7 is all rubble and unslabbed.

7610-7610.5: Light gray limestone with bitumen staining, crinoidal and bryozoan grainstone with modest moldic and intercrystalline porosity. Massive calcarenite dolomite solution front seen with vertical contact.

7610.5-7611.0: Alternating dark to light gray dolomite and dolomitic shale, thin bedded and delicately laminated. Dark areas may be dolomitic mudstone. No burrows or fauna, stained with bitumen along micro porosity.

7611-7616: Light to medium gray dolomite. Burrowed and churned skeletal grainstone to wackestone with vague bedding. Fossils include mostly lags of poorly sorted crinoids, fenestrate bryozoans. Poor to no visible porosity, no fractures open, stylolites with scattered black clasts in breccia (depositional).

7616-7623.5: Light gray to medium dark gray limestone, packstone to wackestone, massive, probably due to bioturbation. Skeletal components mostly crinoids and bryozoan fragments. Some brecciation and fractures filled with gray shale.

7623.3-7626: Light gray dolomite, crinoidal and bryozoan wackestone to packstone, heavily brecciated with black shale and insoluable residue within cracks. No visible porosity, massive.

7626-7628.5: Limestone and dolomitic limestone, light gray to dark gray, crinoidal wackestone to packstone, with black shale or insoluable residue between crinoids.

7628.5-7633.5: Light gray to dark gray dolomite, fossiliferous wackestone to packstone, with mostly crinoids "floating" in dark colored lime muds.

7633.5-7636: Missing Interval.

7636-7637.5: Limestone, wackestone with dark gray staining, crinoidal grainstone to packstone. Massive with healed microfractures and stylofractures.

7637.5-7645: Light to medium gray dolomite with dark gray bitumen staining. Medium bedded alternating mudstone with vague laminae and skeletal with trace moldic porosity. Some local breccia with dark colored insoluable residue.

7645-7655.7: Light and dark gray limestone. Crinoidal/skeletal packstone with some grainstone and wackestone. Some local pockets of brecciation and cracks filled with gray clays. Local patches of replacement chert especially at 7655 feet where calcite sponges occur.

7655.7-7656.5: White to light gray dolomite, crinoidal wackestone, tight.

7656.5-7684.3: Dark gray to dark brownish gray limestone to slightly dolomitic limestone. Crinoidal and fossiliferious wackestone to some packstone. Very tight, no visible porosity, some vertical fractures, generally healed.

7684.3-7693: Light to medium gray dolomite, skeletal hard pelletal grainstone to packstone. Fair to good moldic and intercrystalline porosity, massive, no apparent bedding, black bitumen staining. Moldic crinoids, bryozoans and brachiopods. Core resembles cinder blocks in terms of pores and weight. Short vertical fractures and fracture swarms at 7689.5-7691 feet, medium to coarse grained, dolomite rhombs lining pores, large elongate intraclasts with orientation of 20-25 degrees to vertical at 7692 feet. Isolated small rugose coral at 7687 feet. Few minor blebs of white replacement chert. Bryozoans are probably fenestrate.

7693-7703: Dark to medium gray dolomite. Mudstone/wackestone alternating with wackestone/packstone, thin interbeds. Several thin intervals with good open fracture swarms(vertical). Some patches of skeletal molds in addition to open fractures. Generally very poor matrix permeability, only fracture permeability. In some intervals the fracturing is so intense to form 'tectonic' breccias. Fossils and fossil molds are mostly small to medium crinoids, solitary coral in mud at 7702 feet.

7703-7706.5: Dark gray limestone and dolomitic limestone, thin bedded mudstone and crinoidal packstone/wackestone. Low-amplitude stylolites along bedding planes. Tension gash-style fracture filled with white calcite. Mostly rubble or missing core, depth may not be accurate.

7706.5-7710.5: Light to medium gray dolomite with abundant black bitumen lining pores and fractures. Skeletal packstone to wackestone, mostly crinoids. Open, short, vertical fractures and stylofractures at 7710.5 feet. Scattered moldic porosity, tectonic breccia/fracture swarm at 7708-7709 feet.

7710.5-7711: Limestone, same as above, but no moldic porosity and healed micro fractures.

7711-7719: Light to medium dark gray dolomite, mostly crinoidal grainstone/packstone with patchy moldic porosity. A few vertical hairline fractures; No large open megafractures. A few scattered fenestrate bryozoans, white patches are tight over dolomitized areas, post dating moldic phase, stylolite with thick insoluable residue. Bitumen lining porosity.

7719-7720: Limestone to dolomitic limestone, mostly crinoidal grainstone/packstone. Mostly fills in crinoid/fossil mold and vertical fractures. Patches of moldic pores lined with bitumen.

7720-7731: Light gray to medium dark gray dolomite with bitumen. Mostly crinoidal/skeletal fragments with calcite, patches of over dolomitized rock (after moldic phase). Large rugose coral at 7727 feet, swarms of open vertical fractures at 7728-7729 feet.

7731-7732: Limestone, mostly secondary after dolomite and calcite filling of molds. Crinoidal grainstone/packstone, high amplitude stylolites, remnant molds (without calcite) filled with abundant bitumen.

7732-7739.8: Dolomite, crinoidal wackestone/packstone, with small bryozoans within mud. Brecciation due to fracture and tectonic brecciation. Lower 1.5 feet is rubble.

7739.8-7744.5: No recovery.

7744.5-7745: Limestone, mostly crinoidal grainstone, originally white, some fractures lined with black bitumen, but no matrix porosity, slightly dolomitic.

7745-7747: Dolomite and argillaceous mudstone, wackestone and packstone, mostly crinoidal. Highly fractured and stylofractured. Two inches of gray shale or dolomitized shale at 7746 feet.

7747-7748: Limestone, crinoidal grainstone/packstone, mostly secondary limestone after dolomite and moldic porosity. Now tight, except for fractures lined with bitumen.

7748-7750.5: Light to medium gray dolomite, grainstone/packstone, crinoidal with occasional bryozoan fragments. Only scattered moldic porosity, but intense fracturing with solution enlargement.

7750.5-7751.5: Medium gray brown dolomite, mudstone. Millimeter and centimeter scale laminations with scattered grainstone/packstone skeletal lenses. Moldic porosity in grains, small microfractures.

7751.5-7752.7: Light gray brown limestone and dolomitic limestone, crinoidal packstone with intense microfractures, lined with black bitumen.

7752.7-7777: Light to medium gray dolomite, almost entirely mudstone, medium bedded with occasional laminae, but not much cryptalgal laminae. Swarm brecciation throughout resembling karst, but may be subcutaneous. Some fractures and space between clasts filled with white calcite. Some of the clasts are black. No matrix porosity exept for rare small fossil molds. Most fractures healed or filled with clays and residue.

7777-7777.5: Dolomite, coarse grained, fossiliferous grainstone/packstone to rudestone with lime mud intervals. Scattered moldic porosity only in bryozoan and under skeletal molds.

7777.5-7795.5: Light medium gray to medium gray brown dolomite, medium to thick bedded, alternations between packstone/grainstone and mudstone/wackestone. Calcarenites are mostly skeletal/intraclast composition with scattered moldic porosity, including crinoid columnals and bryozoan molds. No moldic porosity in mudstone/wackestone intervals; occasional open vertical microfractures. Sparse to moderate fractures, white band of chert at 7788.5 feet. Very little bioturbation at thin chert interval.

7795.5-7799: Medium gray to medium gray brown dolomite, brecciated mudstone, becoming limy in lower 1 foot. Barren of fossils, solid breccia under cover, vertical stylolites and stylofractures lined with insoluable residue and white late calcite. White to light gray chert (3 inches thick) just above limy interval at 7798 feet. All fractures filled with white calcite.

7799-7812: Medium gray to medium brown gray dolomite, generally thin to medium bedded alternating between grainstone/packstone and laminated (cryptalgal) mudstone (rarely wackestone). Slightly limy in calcarenites, some black staining (with bitumen). Vertical and oblique fractures, mostly filled with white calcite. Small amount of brecciation, with rare white chert replacement, except for solution collapse breccia at 7806-7807 feet. Some 3-6 inch beds have good visible WP, moldic and BP porosity, but may have vertical porosity barriers due to interbedding with dolomitic muds.

7812-7833: Missing Interval.

7833-7848: White to light gray dolomite, brecciated extensively with brittle soution collapse character. Angular clast within a grossly bedded framework of alternating mudstone/wackestone and packstone/grainstone layers on the order of 4 to 6 inches thick. Extensive vertical fractures, mostly open and lined with bitumen. Scattered moldic porosity.

7848-7848.5: Missing Interval.

7848.5-7852: Medium grayish brown dolomite, mostly mudstone with sparse wackestone, some moldic porosity, mostly small crinoids. Thin to medium bedding, sparse evidence of burrows. Tight with healed fractures.

7852-7855: Medium grayish brown dolomite, grainstone/packstone to rudestone with crude bedding and fair to good moldic porosity lined with bitumen.

7855-7857.5: Medium gray dolomite, mostly massive mudstone/wackestone with thin white chert band at 7855.3 feet.

7857.5-7880: Light to medium gray dolomite with some bitumen staining around molds. Generally medium to coarse grainstone/packstone with moldic porosity and mixed skeletal grains, including crinoids and fenestrate bryozoans. Some intraclasts, fragmented rugose coral at 7869.5 feet, crudely bedded. Modest amount of vertical fractures, most of which are partially to completely healed with white calcite. Mostly rubble between 7871.5-7875 feet.

7880-7882.5: Light brown gray to dark brown dolomite, brecciated clasts of dolomitic grainstone/packstone and mudstone, with good moldic micro porosity (hydrokarst?). Distinct dark-color due to bitumen staining.

7882.5-7885: Light gray dolomite with black bitumen staining, coarse skeletal grainstone/packstone to rudstone.

7885-7886.5: Medium gray to medium brown gray dolomite, mudstone, barren of fossils, cracked breccia with black shaley fillings and white calcite cement between brittle clasts. No matrix porosity.

7886.5-7891.5: White to light gray dolomite, except for black bitumen staining. Coarse grainstone/packstone and rudstone with some depositional clasts and skeletal molds, mostly crinoids and bryozoans. Large scale cross-bedding, short segment open fractures.

7891.5-7905: Dark gray to dark grayish brown, appearance of mudstone/wackestone, but may have been a very fine grainstone/packstone in parts. Microporous dolomite, possible hydrokarst (Wabaman), completely stained with bitumen.

7905-7940.5: Medium gray to medium to dark gray brown dolomite, mostly laminated and bedded mudstone with depositional and karstic brecciation, vertical stylolites. No matrix porosity, some open fractures. Mostly a laminated to thin bedded tidal flat sequence with some rip-up and mud crack breccias. Also some probable tectonic breccias between 7912.5-7914 feet. Cross-bedded peloidal and intraclast grainstone between 7930-7931 feet. Mud cracks at 7928 feet. Three inches of laminated black shale with angular rip-ups of dolomite at base.

7940.5-7944: Medium gray dolomite, mudstone, laminated and thin bedded with some rip-up breccia and calcite healed fractures.

7944-7951.2: White to light gray dolomite with some dark gray bitumen in molds. Medium skeletal/peletal grainstone/packstone with inclined bedding and cross-bedding. Well bedded, no burrows, possible micro porosity, stylofractures, small moldic porosity.

7951.2-7955: Light and dark gray dolomite, alternating mudstone (dark) and fine peletal/skeletal grainstone/packstone (light) with minor small moldic porosity. Well bedded, thin to medium scale, calcerenites have sharp bases, eroded at base. Swarm of fractures with basal one foot.

7955-7957.8: Light to dark brown gray dolomite, laminated mudstone with brecciation, both deposition rounded clasts in lower one foot as well as crackle/tectonic in upper foot.

7957.8-7967.5: Light to medium gray dolomite, well bedded and cross-bedded, large skeletal/peletal grainstone/packstone with bedding defined by grain size. Abundant moldic porosity, some open fracture swarms.

7967.5-7997: Light gray brown to medium gray dolomite, almost entirely mudstone, with laminated (cryptalgal) intervals with some thin peletal/skeletal grainstone/packstone. No significant burrows or brecciation. Most vertical fractures are filled with white dolomite.

7997-8001.5: Light gray to dark gray dolomite, interbedded peletal grainstone/packstone and mudstone. Bedded and laminated. No visible matrix porosity, vertical fractures filled with dolomitic black shale becoming limy in lowermost foot. Base is an eroded soil zone, green shale with light colored dolomitic clasts.

8001.5-8004: Limy shale and siltstone, gray green with white to light gray clasts. Residuum is soil zone of shale/silt with light colored limestone clasts. Weathered soil zone. Top of Ouray.

8004-8030: White to light gray limestone, mostly mudstone with birdseye and fractures.

Lisbon B-610
NE1/4NW1/4 section 10
T. 30 S., R. 24 E., SLBL&M
KB: 6588 feet

TD: 8440 feet
IPF: 587 BPD, 4376 MCFD, no water
Completed: 3-11-1961

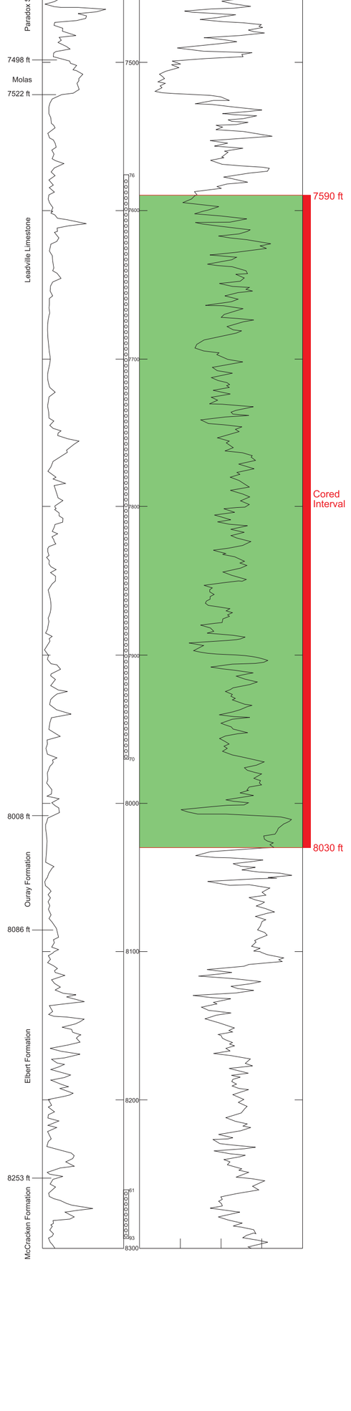

Abbreviations
KB – Elevation of kelly bushing
mD – Millidarcies
GR – Gamma ray
IPF – Initial potential flow
SLBL&M – Salt Lake Base Line and Meridian
TD – Total depth

Explanation

Lithologic Composition
- Limestone
- Dolomite
- Dolomitic limestone
- Siltstone
- Shale

Framework Constituents
- Crinoids
- Fos - Unidentified fossils
- Bryozoans
- Brachiopods
- Corals

Texture
- s — Skeletal grains
- m — Micrite
- p — Peloid

Pore Types
- Mo — Moldic
- BC — Intercrystal
- Vug — Vug
- Mi — Microporosity
- Fr — Fracture

Abundance
- Pervasive
- Abundant
- Rare

Physical Structures
- Stylolites
- Fractures
- Sulfide minerals
- Slickensides
- Anhydrite, mosaic
- bit - Bitumen
- Mudcracks
- Cross-bedding
- Calcareous
- Dolomitic
- Breccia
- Clasts
- Rip-up clasts
- Cherty
- Burrows

UTAH GEOLOGICAL SURVEY
a division of
Utah Department of Natural Resources

CORE DESCRIPTION – LEADVILLE LIMESTONE, LISBON NO. B-816 WELL, LISBON FIELD

Plate 14
Utah Geological Survey Special Study 168
Microbial Carbonate Reservoirs and Analogs from Utah

Geophysical Logs

Gamma Ray API Units: 0 – 82.5 – 165
Perforated Interval
Depth (feet)
Resistivity (OHM-M): 0 – 100 – ∞
Conductivity (MILLIMHOS/M): 200 – 100 – 0

Core Plug Analysis

Permeability (mD): 0.01 – .1 – 1 – 10 – 100 – 1000
Porosity (%): 0 – 40 – 80 – 120 – 160

Conventional Core

Feet
Fabric: boundstone, grainstone, packstone, wackestone, mudstone
Pore Type
Physical Structures
Texture (%)
Framework Constituents
Fractures
Cement
Color
Facies
Remarks

Pore Type	Color	Facies	Remarks
BC	med GY	Moderate-energy, restricted-marine shelf facies-"hard" peloid shoals	**8463-8465.4:** Medium gray to brown gray dolomite; peloidal grainstone to packstone. Some black bitumen within patches of micro-intercrystalline space. Burrowed with coarser sediment fillings. Disseminated sulfides (mostly pyrite) within matrix as well as fracture fillings.
Mi	med gy BR	Low-energy, restricted-marine, middle shelf facies	**8465.4-8470.5:** Medium gray brown dolomite, slightly calcareous. Massive, microporous groundmass (mudstone?) without bitumen (water wet?), containing clasts of microporous dark gray dolomite impregnated with bitumen. Displays a brecciated appearance, with microfractures. Some of the clasts are bounded by white, pearly masses of baroque dolomite.
BC	mdk GY med gy BR	Low- to moderate-energy, open-marine middle shelf facies	**8470.5-8483.0:** Medium to dark gray and medium gray brown dolomite; peloidal/skeletal wackestone to packstone. Micro-inter-crystalline porosity with bitumen linings. Extensive micro-fractures, some lined with calcite and bitumen. Minor chert replacement of matrix, resulting in areas that resemble clasts, especially at 8473.3 feet. Possible disseminated sulfide minerals. Possible bed-normal stylo-fractures.
Mi	med GY	High-energy, open-marine shoal facies	**8483.0-8489.3:** Medium to dark gray dolomite; skeletal/peloidal grainstone to packstone, with 3 inches of breccia at top of interval. Dolomite is microporous and impregnated with black bitumen. Clasts in breccia at top also have microporosity lined with bitumen such that the clasts appear black. Large coral (*Syringipora*) head at 8485.2 feet. Coral is white, but completely dolomitized.
	WH	Moderate-energy, open-marine shoal flank facies	**8489.3-8496.2:** White limestone; crinoidal/skeletal packstone to wackestone, with some brachiopods and bryozoans near top of unit. Abundant wispy seams and low-amplitude stylolites. Some bed normal stylolites, and swarms of vertical fractures, most of which are lined with bitumen. Scattered pockets and halos near fractures display leaching with minor dolomite and bitumen.
	mdk GY	Possible subaerial surface	**8496.2-8497.0:** Medium to dark gray dolomite, slightly calcareous, especially toward base. Dense, microdolomitic (muddy) matrix with breccia - either subaerial exposure or hydrothermal origin. Clasts are fractured dolomite, chert and limestone, generally angular and poorly size-sorted.
	WH	Moderate- to high-energy middle shelf, open-marine shoal facies	**8497.0-8502.0:** White limestone; crinoidal grainstone to packstone. Massive to bedded with low- to medium-amplitude stylolites. Some vertical (bed-normal) stylolites and vertical fractures and stylo-fractures. Occasional wispy seam stylolites. No visible matrix porosity.
Mi	WH BK	High-energy, open-marine shoal facies	**8502.0-8512.3:** White to black limestone; crinoidal/skeletal grainstone to packstone, with occasional rugose corals (two types). Highly altered by leaching and corrosion of grains with bitumen impregnating pores. Some of the limestone is completely altered to microporosity.
	mlt GY	High-energy, open-marine shoal facies	**8512.3-8519.0:** Light to medium gray limestone; crinoidal/skeletal grainstone to packstone. Some brachiopods at 8518 feet. Generally unaltered, well preserved unit with no visible matrix porosity. Some low- to medium-amplitude stylolites, vertical (bed-normal) stylolites, and vertical fractures lined with bitumen.
BC	mdk GY	Moderate-energy, open-marine, shoal flank facies	**8519.0-8523.0:** Medium to dark gray dolomite, slightly calcareous. Peloidal/skeletal packstone to wackestone. Displays extensive micro-intercrystalline porosity lined with bitumen. Most of the unit displays isolated molds of crinoids and other small fossils surrounded by a micro-crystalline dolomite matrix. Some patches of late white calcite.
		High-energy, open-marine shoal facies	**8523.0-8535.6:** White to dark gray limestone, crinoidal/skeletal grainstone to packstone, and occasional wackestone. Massive, and generally unaltered to only slightly altered. Patches of dissolution, especially along vertical fractures which are lined with bitumen. Low- to moderate-amplitude stylolites. Minor etched patches of limesotne matrix with some bitumen staining.
	WH dk GY	High-energy, open-marine shoal facies	**8535.6-8576.4:** White to dark gray limestone, crinoidal/skeletal grainstone to packstone, with occasional small rugose corals and brachiopod shells. Burrowed in upper half; cross-bedded (low- to medium-angle) in lower half. Highly altered by dissolution and corrosion (late?), with black bitumen impregnation. Becomes slightly dolomitic in lowermost two feet. Probable white kaolinite (dickite?) clay masses at 8553 and 8562 feet.
BC Mi	dk GY BK	High-energy, open-marine shoal facies	**8576.4-8579.3:** Dark gray to black dolomite, slightly calcareous; crinoidal/skeletal packstone to grainstone, with small rugose corals. Highly altered due to dissolution and corrosion, leading to microporosity impregnated with black bitumen. Some small white patches of relatively unaltered crinoidal limestone. Mostly micro-intercrystalline porosity throughout, with scattered small dissolution vugs. Minor moldic porosity near base.
			8579.3-8637.0: Missing Interval (Core #3).
BC Mi	lt br GY mdk GY	Low to moderate-energy, open-marine, middle shelf facies	**8637.0-8642.7:** Light brown gray and medium to dark gray limestone, pelodial/skeletal packstone to wackestone, and rarely grainstone. Moderate alteration and leaching, with bitumen plugging. Becomes lightly dolomitic in basal one foot. Very fine, micro-intercrysalline porosity, with some fossil molds. Swarms of vertical fractures filled with calcite. Early complete chert replacement at 8637.0-8637.3 feet (but highly brecciated), and at 8641.0-8641.3 feet. Possible minor soil zone or exposure surface at 8639.5 feet.
	med GY BK	Moderate- to low-energy, open-marine buildup facies; possible "Waulsortian facies"	**8648.0-8662.0:** Light to dark gray and black dolomite, occasionally cherty; peloidal/skeletal packstone to wackestone and some mudstone with "soft" peloidal matrix. Crinoids and sheet-like fenestrate bryozoans.
	lt GY BK	Low-energy, restricted-marine, middle shelf facies	**8648.0-8662.0:** Light gray to black dolomite; skeletal/"soft" peloidal wackestone to mudstone. In places laminated with small crinoids "floating" in the dolomitic mud matrix. Some vertical fractures lined with bitumen and white calcite. Scattered crinoid molds.
Mo Mi	WH mdk GY	High-energy, open-marine shoal facies	**8662.0-8674.5:** White and medium to dark gray dolomite; crinoidal grainstone to packstone, with some crinoidal wackestone. Variable degrees of alteration from massive white dolmitic calcarenites, to moldic and corroded crinoidal calcarenites lined with bitumen, to completely altered "false black shales" (which are microporous dolomites impregnated with black bitumen). Low- to high-amplitude stylolites. Some molds contain pearly white saddle dolomite, calcite and bitumen.
Mo BC Mi		High- to moderate-energy, open-marine shoal and shoal flank facies	**8674.5-8681.5:** Medium to dark gray limestone and dolomite, crinoidal/skeletal packstone to grainstone, and wackestone. Highly altered, corroded and microcrystalline unit with visible moldic and intercrystalline porosity that is extensively lined with bitumen. Vertical fractures lined with white calcite. Several thin (1 inch) chert layers at 8675.8, 8676.7, 8680 feet and at base.
BC Mi	mdk GY	High-energy, open-marine shoal facies	**8681.5-8697.0:** Medium to dark gray dolomite, calcareous in part; mostly crinoidal grainstone to packstone with some horizontal stratification. Moderately to highly altered by leaching and corrosion. Fine, micro-intercrystalline porosity lined with bitumen. Some high-amplitude stylolites. Vertical fractures lined with bitumen and white calcite.

Explanation

Lithologic Composition
- Limestone
- Dolomite

Texture
- s – Skeletal grains
- m – Micrite
- p – Peloid

Pore Types
- Mo – Moldic
- BC – Intercrystal
- Vug – Vug
- Mi – Microporosity
- Fr – Fracture

Abundance
- I – Pervasive
- Abundant
- Rare

Framework Constituents
- Crinoids
- Bryozoans
- Brachiopods
- Corals
- Fos – Unidentified fossils

Physical Structures
- Stylolites
- Fractures
- $ – Sulfide minerals
- Slickensides
- Anhydrite, mosaic
- bit – Bitumen
- Calcareous
- Dolomitic
- Burrows
- Cross-bedding
- Chert
- Breccia
- Py – Pyrite

Lisbon B-816

NE1/4SW1/4 section 16,
T. 30 S., R 24 E., SLBL&M
KB: 6095 feet

TD: 8730 feet
IPF: 554 BPD, 869 MCFD, no water
Completed: 12-7-1962

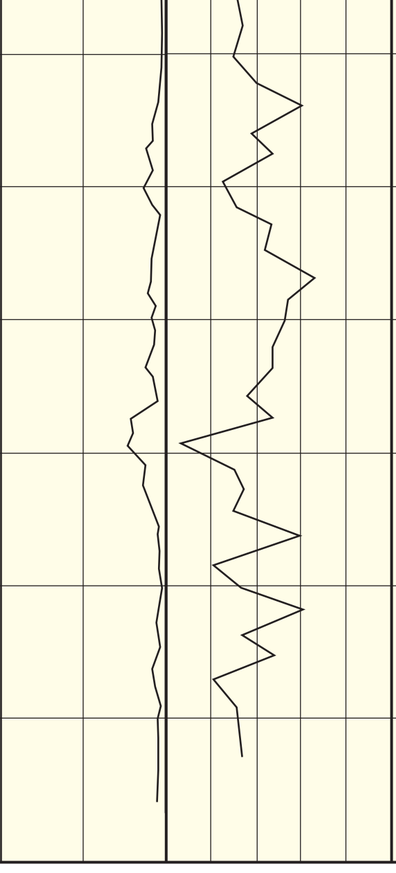

Abbreviations

KB – Elevation of kelly bushing
mD – Millidarcies
GR – Gamma ray
IPF – Initial potential flow
SLBL&M – Salt Lake Base Line and Meridian
TD – Total depth